AN ABSTRACT OF THE THESIS OF

Dah-Cheng Lin for the degree of Doctor of Philosophy in Chemical Engineering

presented on November 8, 1995

Title: Kinetic Study on the Synthesis of Si_3N_4 via the Ammonization of SiO Vapor

Abstract approved: _____

Shoichi Kimura

Silicon monoxide (SiO) vapor generated from Si/SiO_2 mixed-powder compacts was used with NH_3 to synthesize silicon nitride (Si_3N_4) in a 38.1 mm I.D. tubular-flow reactor, operated at temperatures in the range of 1300-1400 °C. The generation rate of SiO vapor at a given temperature was controlled by changing the pressure to prepare the compacts. The supply of NH_3 was adjusted so that the molar ratio of NH_3/SiO in the reacting zone covered a range from 0 to about 6000. NH_3 was also replaced by N_2 or an N_2/H_2 mixture for studying the mechanism of the SiO-NH_3 reaction.

The reaction of SiO with NH_3 was instantaneous when NH_3 was in excess, yielding three different types of silicon nitride at different longitudinal locations in the reactor: amorphous nanophase powder of an average size of about 20 nm, amorphous whiskers (0.5-4 μm in diameter), and α-polycrystals. The most favored product in the system was in the form of crystals, followed by either nanophase powder or whiskers. The yield of nanophase Si_3N_4 varied from 13 % to 43 %, based on SiO generated, depending on operating conditions.

NH_3 was essential for converting SiO into Si_3N_4, and SiO did not react with N_2 even in the presence of H_2. When NH_3 was fully decomposed into N_2 and H_2 before contacting with SiO, a small amount of Si_3N_4 whiskers and crystals were formed. However, no nanophase Si_3N_4 powder was synthesized in the reaction.

The amorphous products were crystallized at temperatures between 1300 and 1560 °C in a stream of dissociated NH_3, N_2, or N_2/H_2 mixture-gas. When dissociated NH_3 was used, nanophase Si_3N_4 powder was crystallized at 1300 °C in 5 hours while whiskers were crystallized at 1350 °C in 8 hours. The crystallization of whiskers and nanophase powder in N_2 progressed when they were heated at 1560 °C for 2 hours. Dissociated NH_3 showed a more enhanced effect on the crystallization than pure N_2 and N_2/H_2 mixture-gas.

An attempt was also made to test the feasibility of SiC synthesis from the SiO-CH_4 reaction at temperatures in the same range of 1300-1400 °C. Experiments showed that the synthesis of SiC via the SiO-CH_4 reaction was feasible, yielding two different types of SiC product: crystalline whiskers ($\approx$ 0.2 μm) and poly-crystal aggregates. The most favored product in the reaction was in the form of SiC crystals.

Kinetic Study on the Synthesis of Si_3N_4 via the Ammonization of SiO Vapor

by

Dah-Cheng Lin

A THESIS

submitted to

Oregon State University

in partial fulfillment of
the requirements for the
degree of

Doctor of Philosophy

Completed November 8, 1995

Commencement June 1996

Doctor of Philosophy thesis of Dah-Cheng Lin presented on November 8, 1995

APPROVED:

Redacted for Privacy

Major Professor, representing Chemical Engineering

Redacted for Privacy

Chair of Department of Chemical Engineering

Redacted for Privacy

Dean of Graduate School

I understand that my thesis will become part of the permanent collection of Oregon State University libraries. My signature below authorizes release of my thesis to any reader upon request.

Redacted for Privacy

Dah-Cheng Lin, Author

ACKNOWLEDGMENT

There has been much help and encouragement from others to make this study successful. Therefore, I would like to express my sincere appreciation to the following:

My advisor, Dr. Kimura, for his advice and guidance throughout this study. The opportunity to carry on this project will not be forgotten.

My committee members, Dr. Levien, Dr. Nelson, Dr. Reistad, and Dr. Rorrer, for their valuable time and suggestions regarding this research.

Dr. Keszler and Dr. Pastorek in the Chemistry Department at O.S.U., for their permission to use the X-ray diffraction and FT-IR equipment.

Dr. James C. Rawers from the U.S. Bureau of Mines, Albany research center, OR, for his assistance with taking SEM pictures and conducting oxygen analysis.

Dr. Akira Yato, Kyocera Industrial Ceramics Corp., Vancouver, WA, for help on the oxygen analysis.

Dr. Jun-ichi Koike, Tohoku University, Sendai, Japan, for taking the TEM picture.

Nick Wannenmacher, not only for his technical assistance on the experimental set-up, but also for his help with the computers.

My colleagues, Yao-Dian Liu, Tsai-Chen Wang, and Chia-Chang Hsu, for their help during the period of this study.

My wife, Whey-Juang Song, for her extremely good care of our two daughters during this study. Also, my family in Taiwan, especially for my brothers' encouragement and financial support.

TABLE OF CONTENTS

CHAPTER 1 INTRODUCTION 1

CHAPTER 2 THEORETICAL ASPECTS AND LITERATURE SURVEY 3

2.1 Synthesis Routes of Silicon Nitride 3

2.1.1 Direct Nitridation 3
2.1.2 Carbothermic Reduction and Nitridation of SiO_2 4
2.1.3 Ammonolysis of Silicon Tetrachloride 5
2.1.4 Gas Phase Reactions 6

2.2 Nitridation of Silicon Monoxide 7

2.3 Generation of Silicon Monoxide 8

2.4 Thermodynamic Considerations 8

2.4.1 Gibbs Free Energy Changes 9
2.4.2 Equilibrium Calculations 11

CHAPTER 3 EXPERIMENTAL APPARATUS AND PROCEDURES 14

3.1 Characteristics of Raw Materials 14

3.2 Experimental Apparatus 14

3.2.1 Preliminary Experiments 16
3.2.2 Thermal Gravity Analysis (TGA) 16
3.2.3 Ammonia Dissociation 18
3.2.4 Tubular Reactor 21

3.3 Experimental Conditions and Procedures 23

3.3.1 Sample Preparation 23
3.3.2 Preliminary Experiments 24
3.3.3 SiO Generation in TGA and SiO Generator 24
3.3.4 Ammonia Dissociation in Alumina Tube 26
3.3.5 SiO-NH_3 Reaction in Tubular Reactor 29

CHAPTER 4 EXPERIMENTAL RESULTS AND DISCUSSIONS 33

4.1 Preliminary Experiments 33

4.2 Generation of Silicon Monoxide 43

TABLE OF CONTENTS (Continued)

4.2.1 Generation in TGA 43
4.2.2 Generation in SiO Generator 46

4.3 Ammonia Dissociation 59

4.3.1 Derivation of Ammonia Dissociation Rate 59
4.3.2 Experimental Results 63

4.4 Silicon Nitride Formation via SiO-NH_3 Reaction 70

4.4.1 Qualitative Experiments in Tubular Reactor 70
4.4.2 Quantitative Studies of SiO-NH_3 Reaction 75

4.4.2.1 Mass Distribution of Product in Reactor 75
4.4.2.2 Product Morphology 86
4.4.2.3 Product Composition 94
4.4.2.4 Rate of SiO-NH_3 Reaction 96
4.4.2.5 Effect of $(dM_{SiO}/dt)_{Ave}$ on Product Distribution 96
4.4.2.6 Effect of NH_3 Inlet Pattern 98

4.5 Crystallization of Amorphous Product 98

4.5.1 Crystallization of Nanophase Powder 102
4.5.2 Crystallization of Whiskers 107
4.5.3 Effect of Gaseous Environment 107

CHAPTER 5 MATHEMATICAL MODELING OF SiO GENERATION: SOLID-SOLID REACTION 120

5.1 Model Derivations 121

5.2 Pseudo Steady State Approach 123

5.3 Model Inspection 126

5.3.1 Effect of Pellet Porosity (ε) 126
5.3.2 Effect of Pellet Thickness ($\delta_{initial}$ or $W_{initial}$) 130

CHAPTER 6 FORMATION MECHANISM OF SILICON NITRIDE 135

6.1 Reactant Effect 135

6.1.1 Product Distributions 137

TABLE OF CONTENTS (Continued)

6.1.2 Transformation of Product Based on IR Analysis 137

6.2 NH and NH_2 Effect on Si_3N_4 Formation 144

6.2.1 Product Distribution 146
6.2.2 Transformation of Product Based on IR Analysis 151
6.2.3 Residual NH_3 in Feeding Stream 151

CHAPTER 7 CONCLUSIONS AND RECOMMENDATIONS OF FUTURE WORK FOR Si_3N_4 SYNTHESIS VIA SiO-NH_3 REACTION 163

7.1 Conclusions 163

7.1.1 Generation of SiO Vapor 163
7.1.2 Ammonia Dissociation 164
7.1.3 Formation of Silicon Nitride 165
7.1.4 Crystallization of Amorphous Product 166

7.2 Recommendations for Future Work 167

CHAPTER 8 SIC SYNTHESIS VIA SiO-CH_4 REACTION 169

8.1 Introduction 169

8.2 Thermodynamic Considerations 170

8.3 Experiments 174

8.4 Results and Discussion 174

8.4.1 Product Distribution 177
8.4.2 Product Characterization 177
8.4.3 Heat Treatment of Carbon Elimination 180
8.4.4 Product Morphology 183
8.4.5 Product Yields 190

8.5 Conclusions 197

8.6 Recommendations for Future Work 199

CHAPTER 9 SUMMARY 200

TABLE OF CONTENTS (Continued)

BIBLIOGRAPHY	201
APPENDIX A	208
APPENDIX B	222
APPENDIX C	223

LIST OF FIGURES

Figure		Page
2.1	Gibbs free energy changes of Reactions (2.3), (2.13) and (2.14)	10
3.1	Experimental apparatus used for preliminary experiments	17
3.2	Flow diagram of Omnitherm TGA/1500	19
3.3	Experimental apparatus for determining NH_3 dissociation	20
3.4	Schematic diagram of tubular reactor for SiO-NH_3 reaction	22
4.1	Distributions of product via SiO-NH_3 reaction in preliminary experiments	34
4.2	IR spectra of whiskers produced from two different runs in preliminary experiments	35
4.3	IR spectra of standard Si_3N_4: (a) dominant α-form, (b) dominant β-form	36
4.4	IR spectrum of wall deposits, formed at locations 2 and 3, in preliminary experiments	39
4.5	IR spectrum of standard SiO_2	40
4.6	X-ray diffraction of nitridized sample powder in preliminary experiments	41
4.7	IR spectrum of nitridized sample powder in preliminary experiments	42
4.8	SiO generation curves obtained by TGA	45
4.9	Temperature effect on initial rates of SiO generation	48
4.10	$(dX/dt)_o$ decreasing with $W_{initial}$ at 1400 °C	50
4.11	$(dX/dt)_o$ decreasing with $W_{initial}$ at 1294 °C	52
4.12	Effect of compacting pressure on initial SiO generation rate at 1294 °C, using unsealed pellets	54
4.13	Effect of pellet porosity on initial SiO generation rate at 1294 °C, using unsealed pellets	55

LIST OF FIGURES (Continued)

Figure		Page
4.14	SiO generation curve in SiO generator at 1398 °C	56
4.15	SEM images of reacted pellets, compacted at 526.6 MPa	57
4.16	Notations for differential flow analysis	59
4.17	Differential flow analysis for determining reaction order of NH_3 dissociation	65
4.18	Time dependence of NH_3 dissociation rate in Al_2O_3 tube	66
4.19	Arrhenius-type relationship between rate constant k and temperature	69
4.20	Product distributions via SiO-NH_3 reaction in tubular reactor	73
4.21	IR spectra of products formed in qualitative experiments at 1400 °C: (a) whiskers, (b) crystals, (c) filter-collected powder	74
4.22(a)	IR spectra of products formed at 1400 °C: (a) whiskers, (b) crystals, (c) fine powder	78
4.22(b)	IR spectra of products formed at 1350 °C: (a) whiskers, (b) crystals, (c) fine powder	79
4.22(c)	IR spectra of products formed at 1300 °C: (a) whiskers, (b) crystals, (c) fine powder	80
4.23(a)	Mass distribution of products in tubular reactor at 1400 °C, using a bent NH_3 feeder	81
4.23(b)	Mass distribution of products in tubular reactor at 1400 °C, using a straight NH_3 feeder	82
4.23(c)	Mass distribution of products in tubular reactor at 1350 °C, using a bent NH_3 feeder	83
4.23(d)	Mass distribution of products in tubular reactor at 1350 °C, using a straight NH_3 feeder	84

LIST OF FIGURES (Continued)

Figure		Page
4.23(e)	Mass distribution of products in tubular reactor at 1300 °C, using a straight NH_3 feeder	85
4.24(a)	SEM images of whiskers	87
4.24(b)	SEM images of crystals	88
4.24(c)	TEM images of filter-collected powder	89
4.24(d)	SEM images of crystallized whiskers	90
4.24(e)	SEM images of crystallized nanophase powder	91
4.24(f)	SEM images of crystallized nanophase powder	92
4.25	XRD charts of unheated products formed at 1400 °C: (a) whiskers, (b) crystals, (c) nanophase powder	93
4.26	IR spectra of crystallized products, not exposed to air before the crystallization: (a) whiskers, (b) nanophase powder	95
4.27	Comparison between SiO generation rate and product formation rate	97
4.28	XRD charts of crystals formed at location 2, using: (a) bent NH_3 feeder at 1400 °C, (b) straight NH_3 feeder at 1400 °C, (c) bent NH_3 feeder at 1350 °C, (d) straight NH_3 feeder at 1350 °C	101
4.29	IR spectra of nanophase powder, heated for different lengths of time at 1300 °C in dissociated NH_3	103
4.30	XRD charts of nanophase powder, heated for different lengths of time at 1300 °C in dissociated NH_3	104
4.31	XRD charts of nanophase powder, heated in N_2: (a) at 1560 °C for 2 hours, (b) at 1300 °C for 5 hours	105
4.32	IR spectra of nanophase powder, heated in N_2: (a) at 1560 °C for 2 hours, (b) at 1300 °C for 5 hours	106

LIST OF FIGURES (Continued)

Figure		Page
4.33(a)	IR spectra of whiskers, heated for different lengths of time at 1300 °C in dissociated NH_3	108
4.33(b)	IR spectra of whiskers, heated for different lengths of time at 1350 °C in dissociated NH_3	109
4.33(c)	IR spectra of whiskers, heated for different lengths of time at 1400 °C in dissociated NH_3	110
4.34(a)	XRD charts of whiskers, heated for different lengths of time at 1300 °C in dissociated NH_3	111
4.34(b)	XRD charts of whiskers, heated for different lengths of time at 1350 °C in dissociated NH_3	112
4.34(c)	XRD charts of whiskers, heated for different lengths of time at 1400 °C in dissociated NH_3	113
4.35	XRD charts of whiskers, heated in N_2: (a) at 1560 °C for 2 hours, (b) at 1350 °C for 8 hours	114
4.36	IR spectra of whiskers, heated at 1350 °C for 8 hours: (a) in dissociated NH_3, (b) in N_2 (40 vol%) and H_2 (60 vol%), (c) in pure N_2	115
4.37	XRD charts of whiskers, heated at 1350 °C for 8 hours: (a) in dissociated NH_3, (b) in N_2 (40 vol%) and H_2 (60 vol%), (c) in pure N_2	116
4.38	IR spectra of nanophase powder, heated at 1300 °C for 5 hours: (a) in dissociated NH_3, (b) in pure N_2.	118
4.39	XRD charts of nanophase powder, heated at 1300 °C for 5 hours: (a) in dissociated NH_3, (b) in pure N_2.	119
5.1	Notations for SiO generation process	120
5.2	Porosity effect of pellet on SiO generation rate	128
5.3	Thickness effect of pellet on SiO generation	131
6.1(a)	Reactant effect on product distribution at 1400 °C	138

LIST OF FIGURES (Continued)

Figure		Page
6.1(b)	Reactant effect on product distribution at 1350 °C	139
6.1(c)	Reactant effect on product distribution at 1300 °C	140
6.2(a)	IR spectra of filter-collected powder formed at 1400 °C in different gaseous environments	141
6.2(b)	IR spectra of filter-collected powder formed at 1350 °C in different gaseous environments	142
6.2(c)	IR spectra of filter-collected powder formed at 1300 °C in different gaseous environments	143
6.3	Modified experimental set-up of NH_3 feeding system	145
6.4(a)	Radical effect on product distribution at 1400 °C	148
6.4(b)	Radical effect on product distribution at 1350 °C	149
6.4(c)	Radical effect on product distribution at 1300 °C	150
6.5(a)	IR spectra of unheated whiskers formed at 1400 °C under different conditions of NH_3 dissociation	152
6.5(b)	IR spectra of unheated whiskers formed at 1350 °C under different conditions of NH_3 dissociation	153
6.5(c)	IR spectra of unheated whiskers formed at 1300 °C under different conditions of NH_3 dissociation	154
6.6(a)	IR spectra of unheated crystals formed at 1400 °C under different conditions of NH_3 dissociation	155
6.6(b)	IR spectra of unheated crystals formed at 1350 °C under different conditions of NH_3 dissociation	156
6.6(c)	IR spectra of unheated crystals formed at 1300 °C under different conditions of NH_3 dissociation	157

LIST OF FIGURES (Continued)

Figure		Page
6.7(a)	IR spectra of unheated powder formed at 1400 °C under different conditions of NH_3 dissociation	158
6.7(b)	IR spectra of unheated powder formed at 1350 °C under different conditions of NH_3 dissociation	159
8.1	Gibbs free energy changes of Reaction (8.4) [JANAF, 1985]	171
8.2	Effect of adding H_2 on CH_4 decomposition	172
8.3	Equilibrium conversion of SiO into SiC via SiO-CH_4 reaction at 1600 K	173
8.4	Experimental apparatus for SiO-CH_4 reaction	175
8.5	XRD charts of unheated products formed at 1300 °C: (a) crystals in sampling tube #1, (b) deposits in sampling tube #2, (c) deposits in sampling tube #5	178
8.6	XRD charts of unheated products formed at different locations at 1400 °C: (a) crystals in sampling tube #1, (b) whiskers in sampling tube #1, (c) sampling tube #2, (d) sampling tube #4, (e) sampling tube #6	179
8.7	IR spectra of unheated products formed at different locations at 1400 °C: (a) crystals in sampling tube #1, (b) whiskers in sampling tube #1, (c) sampling tube #2, (d) sampling tube #4, (e) sampling tube #6	181
8.8	XRD charts of crystals formed at 1300 °C: (a) unheated, (b) heated in air at 1100 °C	182
8.9	XRD charts of heated products formed at 1400 °C: (a) whiskers, (b) crystals, (c) crystals deposited on the external sampling-tube wall around the clearance between sampling tubes (#1 through #4)	184
8.10	IR spectra of crystals formed at 1300 °C: (a) unheated, (b) heated in air at 1100 °C	185
8.11	IR spectra of heated products formed at 1400 °C: (a) whiskers, (b) crystals, (c) crystals deposited on the external sampling-tube wall around the clearance between sampling tubes (#1 through #4)	186

LIST OF FIGURES (Continued)

Figure		Page
8.12	IR spectra of crystals, heated at different temperatures for one hour	187
8.13(a)	SEM images of unheated crystals, formed at 1400 °C	188
8.13(b)	SEM images of unheated whiskers, formed at 1400 °C	189
8.13(c)	SEM images of crystals, heated at 700 °C in air/Ar mixture gas	191
8.13(d)	SEM images of crystals, heated at 1100 °C in air	192
8.13(e)	SEM images of whiskers, heated at 1100 °C in air	193
8.13(f)	SEM images of fine-black powder, heated at 1100 °C in air	194
8.14	IR spectra of heated fine powder, deposited in: (a) sampling tube #4, (b) sampling tube #6	195
8.15	Linear relationship between SiC yield and molar feed ratio of CH_4/SiO at 1400 °C	198

LIST OF TABLES

Table		Page
2.1	Equilibrium conversion of SiO into Si_3N_4 in Reaction (2.14)	12
3.1	Physical properties of raw material Si and SiO_2	15
3.2	Physical properties of compacted pellets	25
3.3	Operating conditions for SiO generation experiments	27
3.4	Operating conditions for differential analysis of NH_3 dissociation	30
3.5	A summary of operating conditions for SiO-NH_3 reaction in tubular reactor	32
4.1	Element analysis of fibrous whiskers formed at location 1	37
4.2	Experimental results of SiO generation in TGA analysis	44
4.3	Generation rates of SiO vapor in SiO generator	47
4.4	Effect of pellet thickness on SiO generation	49
4.5	Porosity effect on SiO generation at temperatures between 1294 and 1400 °C	53
4.6	Differential flow analysis of NH_3 dissociation	64
4.7	Calculated k values on the basis of pure NH_3 inlets ($\varepsilon_A = 1$)	68
4.8	Qualitative experiments with new tubular reactor at 1400 °C	71
4.9	Si_3N_4 synthesis and its distribution via SiO-NH_3 reaction in tubular reactor	76
4.10	Physical properties of gas flow in reactor system	99
5.1	Calculations for determining parameter α in Equation (5.24)	129
5.2	Calculated results of SiO generation rate using Equation (5.24)	133
6.1	Experimental conditions of runs for studying reactant effect on Si_3N_4 formation	136

LIST OF TABLES (Continued)

Table		Page
6.2	Experimental conditions of runs for studying radical effect on Si_3N_4 formation	147
6.3	Equilibrium calculations of NH_3 dissociation	161
8.1	Experimental conditions of SiO-CH_4 reaction in tubular reactor	176
8.2	SiC formation and its distribution within tubular reactor	196

NOMENCLATURE

C	gas concentration
C.P.	compacting pressure
d	inside diameter of tube
D	diffusion coefficient
$(dM_{SiO}/dt)_{Ave}$	average generation rate of SiO vapor
$(dM_{prd}/dt)_{Ave}$	average formation rate of product
d_p	particle size
dX/dt	conversion rate
F	flow rate of NH_3
G	Gibbs free energy
J	molecule diffusive flux
k	rate constant of NH_3 dissociation
K	calibration constant of X-ray diffraction
m	power of porosity effect in Equation (5.25)
M	molar mass, or solution concentration
n	reaction order of NH_3 dissociation
N	molecular fluxes
N_o	Avogadro constant
O.D., I.D.	outside and inside diameter of tube
P	gas pressure
$-r$	dissociation rate of NH_3
R	ideal gas constant
R^2	coefficient of multiple determination
T	temperature
TC	thermocouple
υ	velocity of gas flow
V	volume of reactor

X	conversion
y	molar fraction
W	mass of sample pellet

Greek symbols

Δ	difference of two specific states
α	crystalline form of silicon nitride, or parameter in Equation (5.25)
β	crystalline form of silicon nitride
δ	thickness of compacted pellet
ε	porosity of compacted pellet, or fractional change in volume
τ	tortuosity of compacted pellet
θ	X-ray diffraction angle
μ	gas viscosity
ρ	gas density
Φ	parameter in Equation (5.22)
κ	parameter in Equation (5.29)

subscript

ave or Ave	averaged value
A	noted as NH_3 during the derivation of rate equation
B	bulk stream of gas flow
f	final state
K	Knudsen diffusion
eq	equilibrium state
o	initial state, or standard state
pore	pore of compacted pellet
prd	product

S	surface of compacted pellet
SiO	silicon monoxide (SiO) vapor

KINETIC STUDY ON THE SYNTHESIS OF Si_3N_4 VIA THE AMMONIZATION OF SiO VAPOR

CHAPTER 1
INTRODUCTION

Silicon nitride (Si_3N_4) has become a promising material for use in coatings and other high-temperature structural applications because of its superior oxidation resistance, mechanical strength, and extreme hardness. It exists in both crystalline (α and β) and amorphous forms. Crystalline α-Si_3N_4 is an essential raw material for the sintering process, and will transform into β form at the final stage.

Several factors have limited the practical applications of Si_3N_4 though it has excellent properties at high temperatures. Producing low cost α-Si_3N_4 powder with high quality is the most critical factor for commercial applications. Further grinding will be necessary if raw α-Si_3N_4 powder is not small enough for fabricating β-Si_3N_4 parts. The brittle nature with a low toughness is also a key problem which needs to be solved.

According to the literature, the strength and toughness of sintered parts can be increased significantly with the addition of amorphous Si_3N_4-whisker into α-Si_3N_4 crystals during the sintering process, or by reducing particle sizes to nanometer levels. Nanophase Si_3N_4 can be sintered at lower temperatures, and has better plasticity and processability of sintered products. Considering all the factors mentioned above, fine-high-quality α-Si_3N_4 powder at low cost is the final goal for commercial production.

In this study, most effort has been made to investigate the Si_3N_4 synthesis from the reaction of SiO vapor with NH_3 under a variety of operating conditions. The kinetics of SiO-NH_3 reaction is studied systematically at temperatures between 1300 and 1400 °C. In addition, an attempt is also made to test the feasibility of the SiC formation via the SiO-CH_4 reaction at temperatures in the same range as an application of SiO vapor to the synthesis of Si-based ceramics.

This thesis is divided into nine chapters, where kinetic studies of the Si_3N_4 synthesis via the SiO-NH_3 reaction are included in Chapters 2-7. The SiC synthesis from the SiO-CH_4 reaction will be discussed independently in Chapter 8. A brief summary of these two reactions are given in Chapter 9.

Chapter 2 is a literature review of the relevant work reported in the field of Si_3N_4 synthesis. An evaluation of the current production processes of Si_3N_4 is also presented in this chapter. Chapter 3 describes the experimental set-up and procedures which are designed to study the nitridation kinetics of SiO vapor with NH_3 under a variety of operating conditions. Besides, the experimental apparatus used for the study of NH_3 dissociation is explained in this chapter.

The experimental results of SiO generation, NH_3 dissociation, and Si_3N_4 formation are discussed in Chapter 4. A kinetic equation has been derived to predict the dissociation of NH_3 in an Al_2O_3 tube used in the system. The product distribution and morphology are shown in this chapter. Important factors such as the kinetic rate of SiO-NH_3 reaction, the pattern of NH_3 feeding, and the crystallization of amorphous Si_3N_4, are also investigated.

In Chapter 5, a mathematical model is derived to predict the rate of SiO generation from Si/SiO_2 compacts, whose pellet porosity and thickness are correlated in the model. Systematic studies on the mechanism of SiO-NH_3 reaction are presented in Chapter 6. The reactant effects of N_2, N_2/H_2, and NH_3 on the Si_3N_4 formation are discussed in this chapter. The conclusions of the SiO-NH_3 reaction are given in Chapter 7. Recommendations for future work of the SiO-NH_3 reaction are also included in this chapter.

Chapter 8 discusses the experimental results regarding the synthesis of SiC from the SiO-CH_4 reaction. This chapter describes experimental findings that the SiO-CH_4 reaction is feasible to produce SiC at temperatures between 1300 and 1400 °C. Recommendations for future work of this reaction are given in this chapter.

Finally, Chapter 9 presents the summary of this study. The application of SiO vapor to the synthesis of Si-based ceramics will be mentioned in this chapter.

CHAPTER 2
THEORETICAL ASPECTS AND LITERATURE SURVEY

Since 1960's, silicon nitride (Si_3N_4) has been proposed to be a potential material in high-temperature applications, especially for advanced heat engines. After remarkable progress in developing reliable structural ceramics in the past decade, producing cost-effective products has become a key factor in facilitating commercial applications of Si_3N_4 [Sheppard, 1991; Winslow, 1993; Morgan, 1993].

2.1 Synthesis Routes of Silicon Nitride

Silicon nitride synthesis has been extensively investigated since 1970's. Different synthetic paths and methods have been reported in the literature. The most common processes are: direct silicon nitridation, carbothermic reduction and nitridation of SiO_2, ammonolysis of silicon tetrachloride, and gas phase reactions [Messier and Croft, 1982; Yamada, 1993]. Among these processes, only direct silicon nitridation and ammonolysis of silicon tetrachloride have been commercialized for the mass production of Si_3N_4.

2.1.1 Direct Silicon Nitridation

The direct nitridation of Si is one of the most prospected methods for the mass-production of high-quality Si_3N_4 powder at reasonable cost. The overall reaction is given as

$$\mathbf{3\ Si(s) + 2\ N_2(g) \rightarrow\ Si_3N_4(s)} \qquad \mathbf{(2.1)}$$

The investigation of the direct nitridation process has been more systematic since

1970's, but mechanisms proposed in the literature have not been consistent. However, the first stage of the process is believed to be the removal of native SiO_2 on Si powder surface. A certain amount of hydrogen is added into N_2 to enhance the reaction at this stage. The reaction is expressed as

$$\mathbf{Si(s) + SiO_2(s) \rightarrow 2\ SiO(g)} \qquad \textbf{(2.2)}$$

Barsoum *et al.* [1989 and 1991] have assumed that SiO can react with N_2 to form either Si_3N_4 or Si_2N_2O.

$$\mathbf{3\ SiO(g) + 2\ N_2(g) \rightarrow Si_3N_4(s) + 1.5\ O_2(g)} \qquad \textbf{(2.3)}$$

or

$$\mathbf{2\ SiO(g) + N_2(g) \rightarrow Si_2N_2O(s) + 0.5\ O_2(g)} \qquad \textbf{(2.4)}$$

After the first stage, the process can be characterized by a gas-solid reaction in which N_2 reacts with Si as given in Reaction (2.1). The reaction is generally carried out at temperatures between 1200 and 1400 °C. It should be noted that both α and β forms are produced in the process.

Si_3N_4 powder can be obtained at low production-cost from the direct nitridation process, but further grinding and acid leaching processes are required for the sintering process that follows. Also, the process has a slow reaction rate due to the resistance to nitrogen diffusing through Si_3N_4 layers formed on Si particles. Hence, it usually takes a long time to convert all Si into Si_3N_4. Since both α and β crystals are formed in the reaction, producing high α-content Si_3N_4 powder is also an important factor in the process.

2.1.2 Carbothermic Reduction and Nitridation of SiO_2

The carbothermic reduction process shows an alternative method to produce high-quality Si_3N_4 powders at low cost because of the availability of high-grade,

inexpensive SiO_2 and carbon (C) raw materials. The overall reaction for this process is

$$\mathbf{3\ SiO_2(s) + 6\ C(s) + 2\ N_2(g) \rightarrow Si_3N_4(s) + 6\ CO(g)} \qquad \mathbf{(2.5)}$$

It is believed that a process in two steps is involved in Reaction (2.5), which are the generation of SiO as an intermediate and formation of Si_3N_4.

$$\mathbf{3\ SiO_2(s) + 3\ C(s) \rightarrow 3\ SiO(g) + 3\ CO(g)} \qquad \mathbf{(2.6)}$$

and

$$\mathbf{3\ SiO(g) + 3\ C(s) + 2\ N_2(g) \rightarrow Si_3N_4(s) + 3\ CO(g)} \qquad \mathbf{(2.7)}$$

The reaction temperatures have been proposed to be in the range of 1350-1550 °C. In addition to Si_3N_4, β-SiC powder is obtained in the reaction at high temperatures around 1550 °C or higher. Also, an excess of carbon is required in the reaction on the basis of two considerations: reducing the partial pressure of O_2 in the process [Durham *et al.*, 1988], and the difficulty of mixing SiO_2 and C powders ideally [Durham *et al.*, 1991].

The carbothermic reduction process produces Si_3N_4 powder of high quality. Since excess carbon is used in the reaction, the product contains carbon at a high content and the removal of the residual carbon becomes a critical problem which needs to be solved in the process. Residual carbon in the product is typically burned out by O_2 at high temperatures. However, controlling oxygen contents in the product after burning carbon becomes a new problem for the process.

2.1.3 Ammonolysis of Silicon Tetrachloride

The formation of amorphous Si_3N_4 by the ammonolysis of silicon tetrachloride is complex, but can generally be expressed as three major steps: formation of silicon diimide ($Si(NH)_2$), calcination and crystallization [Yamada, 1993].

$$SiCl_4(\ell) + 6\ NH_3(\ell) \rightarrow Si(NH)_2(s) + 4\ NH_4Cl(s) \quad (2.8)$$

$$3\ Si(NH)_2(s) \rightarrow \text{amorphous } Si_3N_4(s) + 2NH_3(g) \quad (2.9)$$

Silicon diimide, $Si(NH)_2$, is formed at the interface of liquid NH_3 and $SiCl_4$ at room temperature, and the impurity (NH_4Cl) is washed out by an excess of NH_3. Purified $Si(NH)_2$ proceeds sequential decompositions to form amorphous Si_3N_4 powder with an average size less than 10 nm by the calcination at a temperature of about 1000 °C. Finally, the amorphous product is crystallized into submicron average sized Si_3N_4 powder at high temperatures around 1500 °C.

From a point of view of quality, the process produces high purity, extra-fine and high α-content Si_3N_4 powder. However, the production cost is very high because of the multi-step processes and a large amount of liquid NH_3 required for refining the intermediate product of $Si(NH)_2$.

2.1.4 Gas Phase Reactions

The process is generally characterized by a gas-phase reaction of silicon halide or silane with NH_3. The overall reaction is as follows:

$$3\ SiX_4(g) + 16\ NH_3(g) \rightarrow Si_3N_4(s) + 12\ NH_4X(s) \quad (2.10)$$

or

$$3\ SiH_4(g) + 4\ NH_3(g) \rightarrow Si_3N_4(s) + 12\ H_2(g) \quad (2.11)$$

where X represents F, Cl, or Br [Aboaf,1969; Allaire and Dallire, 1991; Lee *et al.*, 1992; Larson, 1993]. In these reactions, $Si(NH)_2$ is the intermediate product, and decomposes to form amorphous Si_3N_4 at high temperatures. Impurity NH_4X will be removed simultaneously during the calcination process. The Si_3N_4 powder produced by the gas phase reaction exhibits a high-quality amorphous form, but also has a high halogen content.

Producing fine-high-quality powder at low cost is the final goal for Si_3N_4 synthesis. However, each process mentioned above has several disadvantages though much effort has been made to meet the requirements. A simple chemical process would produce fine silicon nitride at more reduced cost, leading to a variety of applications of this material.

Reactions (2.3) and (2.7) suggest potential chemical reactions that would possibly yield fine Si_3N_4 via vapor-phase reactions involving SiO. After being generated form Si/SiO_2 mixtures, SiO may react with N_2, N_2/H_2 mixture, or NH_3 to form Si_3N_4. Since no carbon is used in the process, the impurity effect appearing in the carbothermic reduction nitridation of SiO_2 may be avoided.

2.2 Nitridation of Silicon Monoxide

As mentioned in the previous section, Si_3N_4 may be synthesized from the direct nitridation of SiO vapor. There are several processes reported in the literature regarding the nitridation of SiO. The processes are typically characterized by the nitridation of SiO_2 under NH_3 or N_2/H_2 gaseous environment in which SiO vapor can also be generated by the reduction of SiO_2 with H_2 or NH_3 at high temperatures in the system.

According to Cunningham and Davies [1969], amorphous Si_3N_4 whiskers were formed in the nitridation of SiO_2 at temperatures between 1426 and 1483 °C. The authors concluded that SiO vapor was generated from the reduction of commercial SiO_2 by H_2 and Si; then, SiO reacted with a mixture of NH_3 (50 %), H_2 (30 %), and N_2 (20 %) to form the product. The fibers obtained in their study exhibited lengths up to 38.1 cm, and diameters within a range of 5-30 μm.

Similar results were also reported by Sjöberg *et al.* [1987] for the reaction of amorphous SiO_2 and NH_3 at temperatures between 1050 and 1230 °C. It was believed that the reduction of SiO_2 also proceeded to generate SiO vapor due to the presence of NH_3 and H_2 in the process. In addition to Si_3N_4 whiskers, silicon oxynitride (Si_2N_2O) crystals were obtained in their study.

However, no direct evidence supports the nitridation of SiO vapor to synthesize Si_3N_4 in the processes mentioned above. Thus, further study on the direct nitridation of SiO is necessary for clarifying the role of SiO on the Si_3N_4 formation.

2.3 Generation of Silicon Monoxide

Generating SiO vapor is the first step to study the Si_3N_4 synthesis via the nitridation of SiO. The generation of SiO from the reduction of SiO_2 has been reported in the literature, in which SiO_2 is mostly reduced by Si, C, or H_2. A number of investigators studied the formation of SiO extensively in 1950's. A detailed review of this process was presented by Toropov and Barzakovskii [1966].

Kubaschewski and Chart [1974] used silicon (d_P<36 μm) and crystalline silicon dioxide (d_P<15 μm) powders to generate SiO vapor at temperatures between 1270 and 1600 K. The powders were well mixed at an equivalent molar ratio and compressed into pellets under a pressure of about 600 MPa in a steel die. They showed that the measured data of SiO vapor pressure could be represented by the following equation:

$$\log P_{SiO} = 13.613 - 17850 / T \qquad (2.12)$$

where P_{SiO} is the vapor pressure of SiO in Pa and T is the system temperature in K.

It is difficult to characterize SiO vapor because of its instability at low temperatures. However, "SiO" is believed to be a stoichiometric mixture of Si and SiO_2. The vapor condenses back to an amorphous mixture of Si and SiO_2 when temperatures are reduced [Brady, 1959; Lin and Joshi, 1969].

2.4 Thermodynamic Considerations

As mentioned earlier, it is believed that SiO plays an important role in the formation of Si_3N_4 in the carbothermic reduction and nitridation of silica. It is also

suspected in the direct nitridation of silicon that SiO generated from surface oxides is involved in the formation of silicon nitride. SiO is believed to be involved in the synthesis of Si_3N_4 via the nitridation of SiO_2 in ammonia. These reactions may be summarized into the following three overall equations:

$$\mathbf{3\ SiO(g) + 2\ N_2(g) \rightarrow Si_3N_4(s) + 1.5\ O_2(g)} \quad \textbf{(2.3)}$$

$$\mathbf{2\ SiO(g) + 2\ N2(g) + 3\ H_2(g) \rightarrow Si_3N_4(s) + 3\ H_2O(g)} \quad \textbf{(2.13)}$$

$$\mathbf{3\ SiO(g) + 4\ NH_3(g) \rightarrow Si_3N_4(s) + 3\ H_2O(g) + 3\ H_2(g)} \quad \textbf{(2.14)}$$

The intrinsic role of SiO in the process of Si_3N_4 formation in these reactions still remains unclear. Thus, thermodynamic calculations are essential and helpful before further study is conducted.

2.4.1 Gibbs Free Energy Changes

A reaction is favored if its Gibbs free energy change (ΔG^o) under the condition considered is negative because the ΔG^o value shows the potential for the reaction to proceed. At temperatures between 1400 and 1800 K, the Gibbs free energy changes of these reactions are shown in Figure 2.1. The Gibbs free energies of formation of relevant compounds used in the calculations were cited from the literature [JANAF, 1985].

Reaction (2.3) is not thermodynamically favored because of the positive free energy changes at given temperatures though it is frequently reported in the literature. Reaction (2.13) may be favored because its ΔG^o changes from negative to positive as the temperature increases around 1600 K. Reaction (2.14) has large negative values of ΔG^o at any given temperature, implying that it could be a potential reaction to produce Si_3N_4.

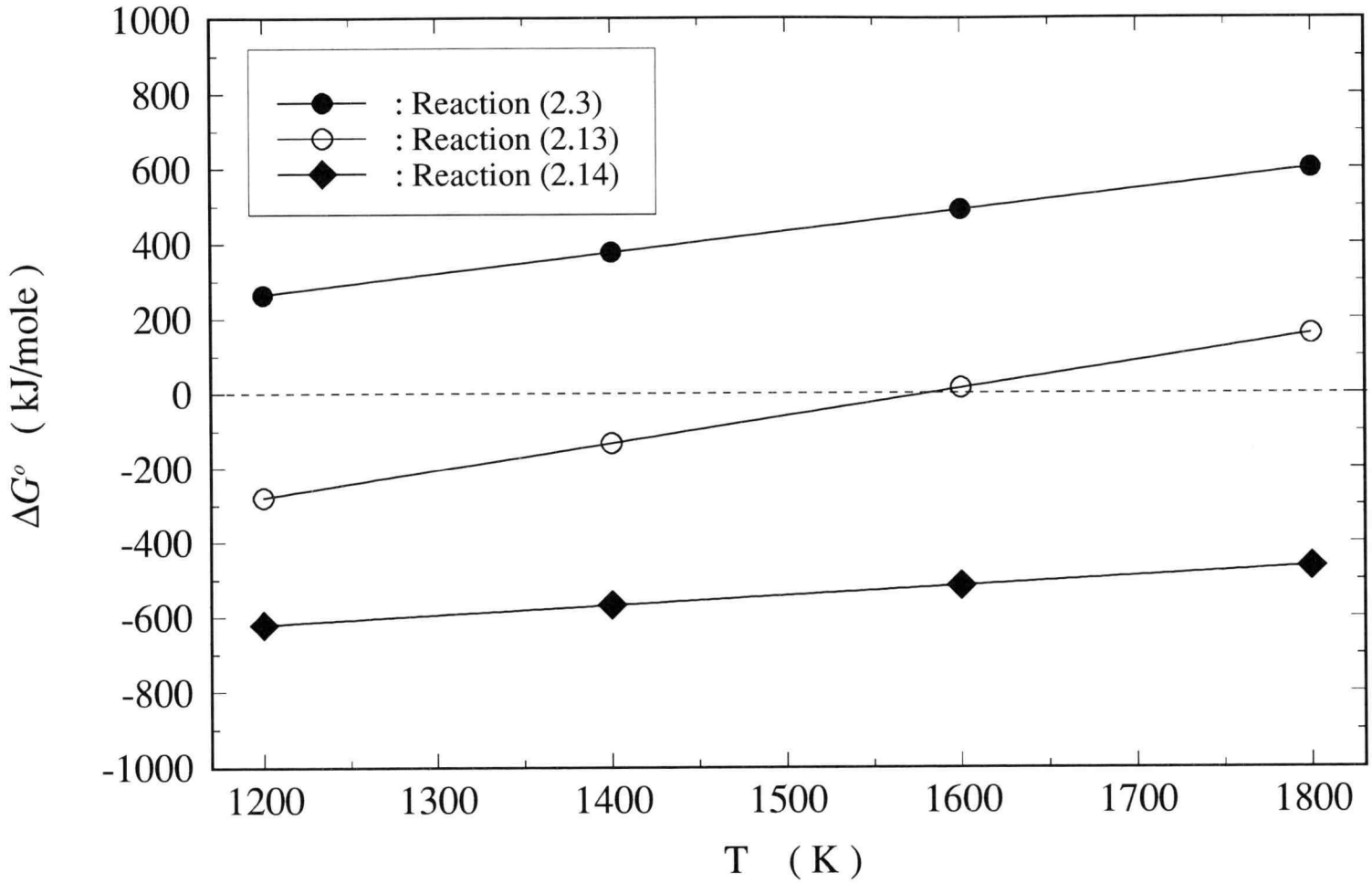

Figure 2.1 Gibbs free energy changes of Reactions (2.3), (2.13), and (2.14)

2.4.2 Equilibrium Calculations

Since Reaction (2.14) is thermodynamically favored at temperatures in the range studied, the extent of reactants converted into Si_3N_4 is of interest. A computer program, GIBBS, has been developed to calculate the equilibrium compositions using the Gibbs Free Energy Minimization method. This program is written in Fortran language and shown in Appendix A. It should be mentioned that the concept and procedure used in the GIBBS program follow the work by Eriksson [1971].

At temperatures in the range of 1400-1800 K, the equilibrium conversion of SiO in Reaction (2.14) is summarized in Table 2.1. The calculated results clearly indicate that SiO vapor can be completely converted into Si_3N_4 when NH_3 is in excess of the stoichiometry. However, the calculations only show the maximum conversion of SiO into Si_3N_4 that may be formed at the equilibrium conditions. A reaction could take a long time to reach the equilibrium conditions because of a slow reaction rate. Thus, Si_3N_4 may not be obtained in the process due to the limited reaction time even though the calculations indicate that Reaction (2.14) is favored. Kinetic studies are necessary for characterizing the Si_3N_4 formation via Reaction (2.14).

In addition to the formation of Si_3N_4, NH_3 dissociation should also be taken into consideration in Reaction (2.14). As indicated by Harrison and Kobe [1953], NH_3 fully decomposes into N_2 and H_2 toward equilibrium at temperatures above 1000 K.

$$\mathbf{2\ NH_3(g) \rightarrow N_2(g) + 3\ H_2(g)} \qquad \textbf{(2.15)}$$

If NH_3 has completely decomposed before it reacts with SiO vapor, Reaction (2.14) may be changed back to Reaction (2.13). Thus, determining the NH_3 dissociation becomes essential for further study of the SiO-NH_3 reaction.

Catalytic dissociation of NH_3 has been investigated extensively in the literature. However, no kinetic equation is available to describe the thermal dissociation of NH_3 in an Al_2O_3 tube in the temperature range between 1300 and 1400 °C. In this case, determining the dissociation rate of NH_3 needs to be made prior to the investigation of Reaction (2.14).

Table 2.1 Equilibrium conversion of SiO into Si_3N_4 in Reaction (2.14)

Molar Ratio (NH_3 /SiO)	**Temperature (K)**			
	1200	1400	1600	1800
4/3	99.99	99.91	99.63	98.90
2	100	100	100	99.99
10	100	100	100	100
30	100	100	100	100
100	100	100	100	100
1000	100	100	100	100

In this study, an attempt has been made to synthesize Si_3N_4 from the direct nitridation of SiO vapor with NH_3 under a variety of operating conditions. SiO vapor was firstly generated from the reduction of SiO_2 with elemental Si, and then carried by Ar gas into a separated zone to react with NH_3 for the formation of Si_3N_4 at temperatures in the range of 1300-1400 °C. The role of NH_3 in the formation of Si_3N_4 from SiO vapor is also investigated. In addition, the crystallization of amorphous Si_3N_4 was studied under different gaseous environments (dissociated NH_3, N_2, or N_2/H_2) at temperatures between 1300 and 1560 °C.

CHAPTER 3
EXPERIMENTAL APPARATUS AND PROCEDURES

3.1 Characteristics of Raw Materials

Silicon and silicon dioxide powders are the raw materials used for generating SiO vapor in this study. Essentially, the SiO generation is characterized by a solid-solid reaction. Solid-solid reactions can be divided into three types: simple addition, addition by elimination, and exchange. The reactions occurring in a mixed-powder system are complex because important factors, such as geometry, particle size distribution, sintering, are involved in the process. However, it is believed that reactions through species in contact with each other or through gaseous intermediates generally play an important role in the process [Sohn and Szekely, 1973; Tamhankar and Doraiswamy, 1979].

In the Si-SiO_2 reaction, it is difficult to identify the mechanism because the product SiO vapor is stable only at high temperatures. The physical contact between particles is expected to be important though the exact mechanism is unclear. If gas phase intermediates are involved in the process, either Si or SiO_2 particle surface area may also affect the overall reaction rate. With considering these two factors, fine particles (on the order of a few microns) are of interest in this study because of higher surface area and better contact between Si and SiO_2. The physical properties of raw Si and SiO_2 powders are given in Table 3.1.

3.2 Experimental Apparatus

This study is divided into four major sections: preliminary experiment, SiO generation, NH_3 dissociation and Si_3N_4 formation. Since the preliminary experiments were designed for testing the feasibility of Reactions (2.13) and (2.14), the results

Table 3.1 Physical properties of raw material Si and SiO_2

Properties	**Si**†		**SiO_2**‡	
Average size (μm)	3.7		3.0	
BET surface area (m^2/g)	2.5		700	
Vapor pressure★ (Pa)	0.036 at 1412 °C		0.0256 at 1728 °C	
Impurity (wt %)	Fe	0.08	Na	0.045
	Al	0.10	Al	0.016
	Ca	0.02	Fe	0.007
	C	0.02	Pb	0.0002
	O	0.51	Cu	0.00005

† : the powder and information are provided by the ShinEtsu, Japan

‡ : the powder and information are provided by the Fuji Silysia Chemical Ltd, Japan

★ : cited from Thermochemical Properties of Inorganic Substance [Knacke *et al.*, 1991]

were mainly used for qualitative analysis. In further quantitative study, feeding NH_3 and generating SiO vapor have been carried out at separated locations in the reactor to avoid NH_3 or N_2 from reacting with Si powder. The experimental design is presented in more detail in the following sections.

3.2.1 Preliminary Experiments

Several qualitative experiments were conducted to test the feasibility of Reactions (2.13) and (2.14). Figure 3.1 illustrates the experimental apparatus used for qualitative purposes. Experiments were accomplished in a silicon carbide furnace with a 30.48 cm long heating zone. A mullite tube (34.93 mm I.D., 914.4 mm long) was used as a reactor. The reaction temperature was measured by an external thermocouple and fixed at about 1350 °C.

3.2.2 Thermal Gravimetric Analysis (TGA)

As mentioned in Chapter 2, SiO vapor easily condenses back into a mixture of Si and SiO_2 when temperature is reduced. Under this circumstance, characterizing the generation rate of SiO in Reaction (2.2) is not an easy task. According to Table 3.1, vapor pressures of Si and SiO_2 powders are negligibly low at 1400 °C; thus, the mass loss of Si/SiO_2 mixtures should result from the SiO vaporization at temperatures in the range of 1300-1400 °C. On the basis of this assumption, the generation rate of SiO vapor was determined directly by measuring the change in sample mass during reaction experiments.

The structural properties of samples are supposed to change with the SiO generation. It is anticipated to have less physical contact between particles after SiO vapor escapes from the Si/SiO_2 mixture into the bulk gas. The generation rate of SiO is expected to decrease with reaction time. Thus, a continuous observation of the sample mass should be helpful to figure out the rate of reaction. Based on this

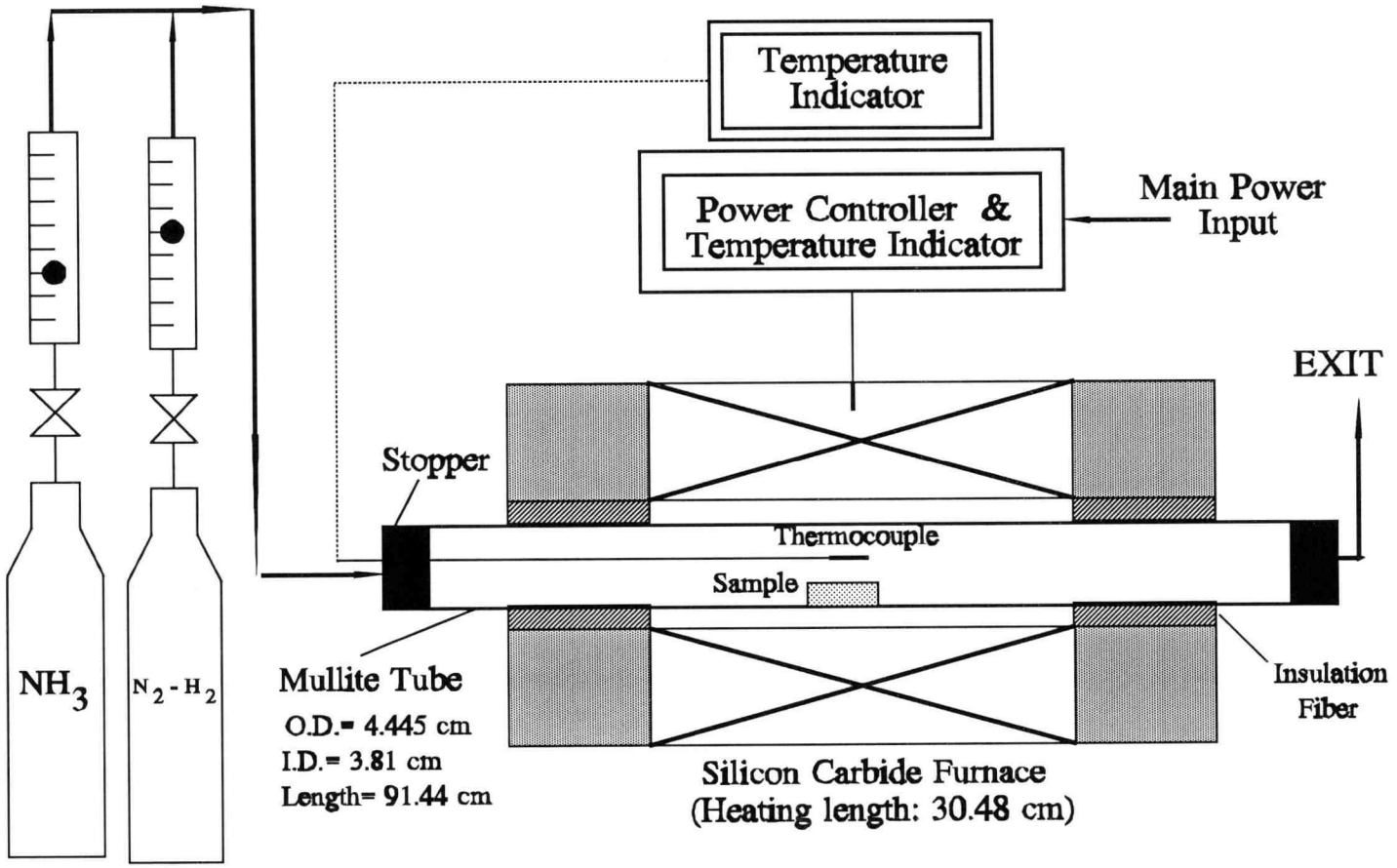

Figure 3.1 Experimental apparatus used for preliminary experiments

consideration, a thermal gravimetric analyzer (TGA/1500, Omnitherm Corp, Illinois) was used in this study.

The Omnitherm TGA/1500 system (Figure 3.2) consists of four units: an electronic balance, a programming controller, a data acquisition system, and a furnace. The maximum reachable temperature of the furnace is 1500 °C. A sample of solids was placed in the holder and was heated up to desired temperatures with Ar flow. The data acquisition system recorded the sample mass and temperature at specified intervals after the system was initiated. Further quantitative analysis was accomplished with the aid of a software installed in the computer.

3.2.3 Ammonia Dissociation

According to the thermodynamic calculations described in Chapter 2, NH_3 highly decomposes into N_2 and H_2 at temperatures above 1000 K. It is expected that a certain amount of NH_3 has decomposed before it reacts with SiO vapor to form Si_3N_4. Thus, the rate of NH_3 dissociation in an Al_2O_3 tube, used as a reactor part, should be determined prior to investigate the Si_3N_4 formation in Reaction (2.14).

A differential flow reactor (Figure 3.3) is designed for studying the dissociation rate of NH_3 at prescribed temperatures. The furnace (Lindberg, Wisconsin; model: 54454-2Z; length = 91.44 cm) consists of two heating zones, each of which is 30.48 cm long. The furnace temperature, controlled and measured separately in each zone, can reach temperatures up to 1800 °C with heating elements of molybdenum disilicide. An Al_2O_3 tube (O.D. = 6.35 mm; I.D. = 3.96 mm; length = 1.524 m) was used to feed NH_3 or Ar-NH_3 mixed gas. A mullite tube (8.89 cm-dia. × 0.9144 m), placed between the furnace and the Al_2O_3 tube, was used to protect the heating elements and thermo-couples inside the furnace. In order to measure the reaction temperature, an external thermocouple was placed at the center of each heating zone beside the Al_2O_3 tube.

A high concentration aqueous solution of hydrochloric acid (HCl) was used for absorbing NH_3 remaining undissociated in the exit stream. The exit gas was bubbled through two flasks, each of which contained two liters of the HCl solution. A

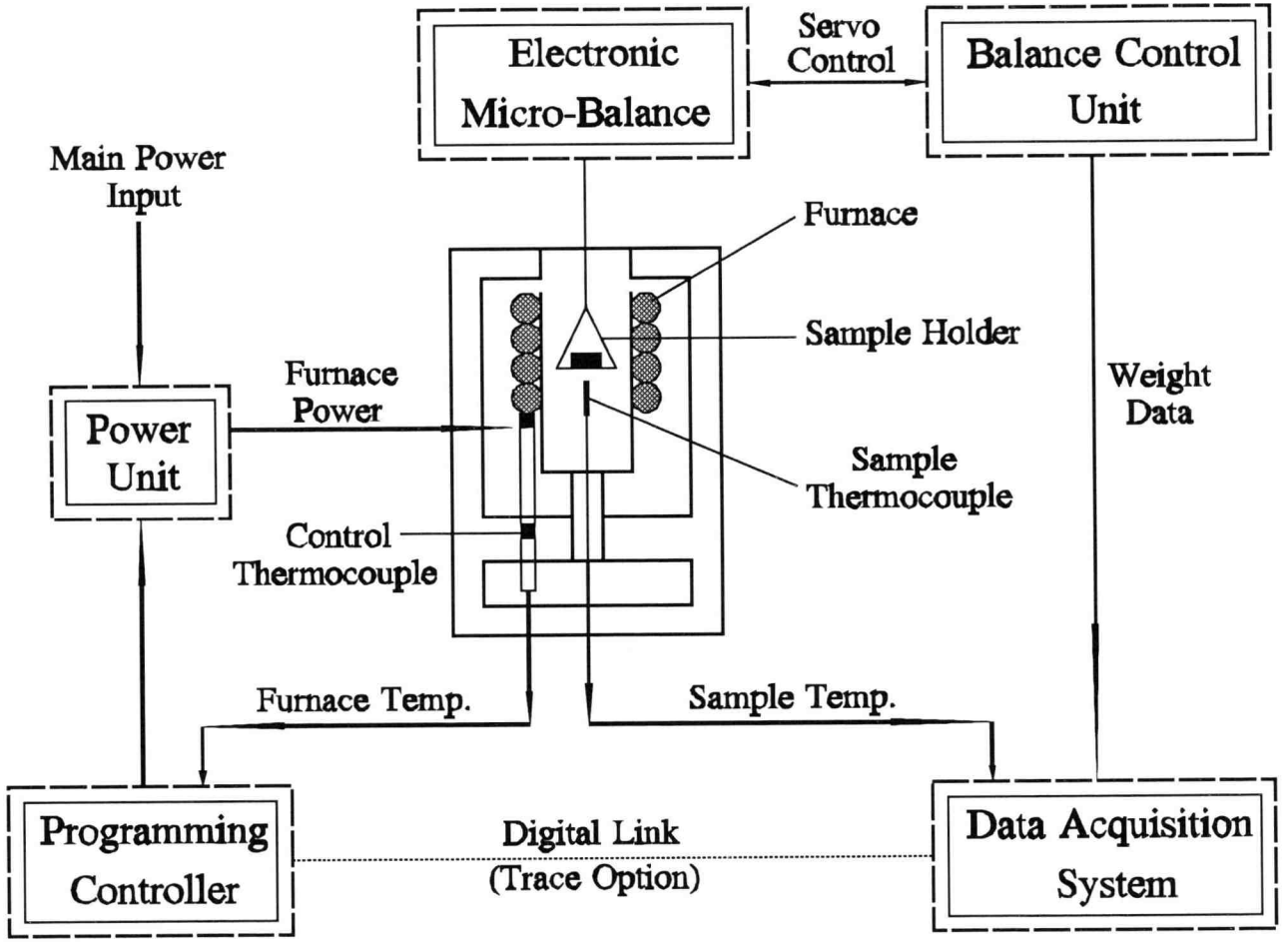

Figure 3.2 Flow Diagram of Omnitherm TGA/1500

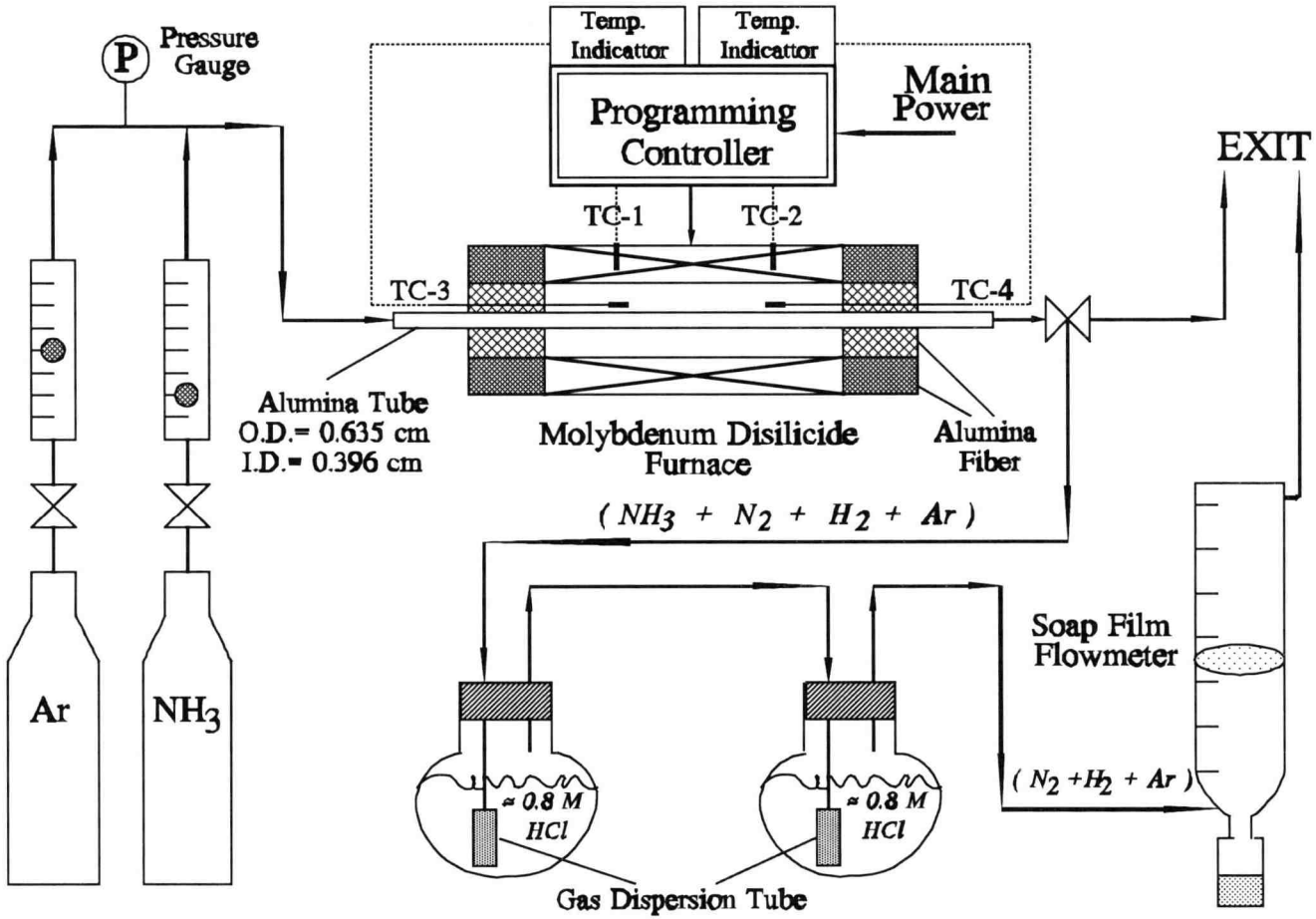

Figure 3.3 Experimental apparatus for determining NH_3 dissociation

dispersion-glass tube was placed in each flask to improve the absorption efficiency of the HCl solution. The total amount of N_2 and H_2, generated from the dissociation of NH_3, was measured directly by a soap-film flow meter, placed downstream the two flasks.

3.2.4 Tubular Reactor

Producing Si_3N_4 powder is the major goal of this study. Therefore, a well-designed reactor is essential for characterizing the SiO-NH_3 reaction. A detailed experimental setup for the Si_3N_4 formation is shown in Figure 3.4. Owing to the complexity of the reaction, the reactor is separated into three parts: an SiO generator, an NH_3 feeder and a tubular reactor for Si_3N_4 production. The furnace is the same one as mentioned previously in the section of NH_3 dissociation. In addition to the furnace thermocouple, two external thermocouples were directly applied to measure the temperatures of SiO generation and Si_3N_4 formation.

The SiO generator is made of a 13 cm long mullite tube, 1.91 cm O.D. and 1.43 cm I.D. The sample powders or pellets were placed at 1 cm upstream the exit of the SiO generator. As shown in Figure 3.4, SiO vapor produced inside the generator is carried by the Ar flow downstream to react with NH_3 at operating conditions.

A certain period of time is required for NH_3 to reach the reacting zone. However, the residence time of NH_3 in the feeder can be reduced by increasing the NH_3 feeding velocity. Thus, a small Al_2O_3 tube of 3.96 mm I.D. was used to feed NH_3 directly into reacting zone. In this fashion, NH_3 could reach the reacting zone in a short time before being highly decomposed. Two different types were employed to supply NH_3 into the reacting zone: a straight tube and a bent tube. The bent tube, shown in Figure 3.4, has a nozzle 30° tilted downward from the horizonal direction. The main purpose of this device is to improve the contact between NH_3 and SiO vapor. Besides, the NH_3 outlet was placed at the position of 6 cm downstream the SiO generator to avoid NH_3 from reacting with sample pellets in the SiO generator.

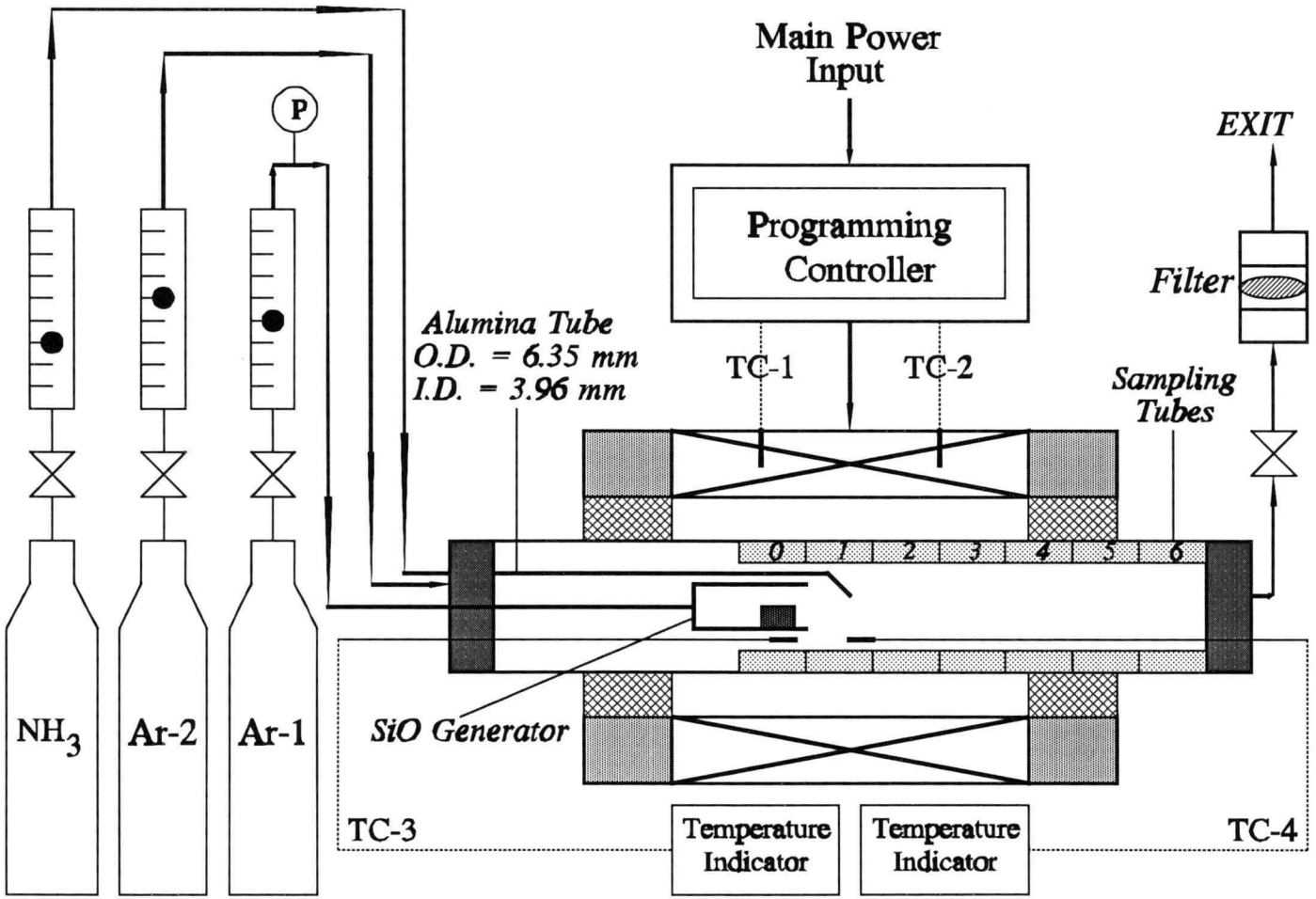

Figure 3.4 Schematic diagram of tubular reactor for SiO-NH_3 reaction

In general, products produced in a gas phase reaction are distributed widely in the reactor. Due to the low rate of SiO generation, a small amount of product was obtained in each run. Seven short Al_2O_3 tubes (34.9 mm O.D., 28.6 mm I.D., 101.6 mm long) were inserted into the reactor tube (44.45 mm O.D., 38.1 mm I.D., 1524 mm long) for collecting products precipitating at different locations.

With using the sampling tubes, it was easier to measure and collect the product because of their short length. SiO vapor was carried by the Ar flow downstream to react with NH_3, forming the product that deposited inside the sampling tubes. A certain amount of product was also carried out of the reactor by the gas flow. The carry over of any product material from the reactor was collected by a paper filter mounted downstream outside the reactor tube.

3.3 Experimental Conditions and Procedures

In order to increase the SiO generation rate, the reaction temperature should be set as high as possible. Experiments were operated at temperatures in the range of 1300-1400 °C. The system pressure was slightly higher than the atmospheric pressure.

3.3.1 Sample Preparation

Si and SiO_2 powders shown in Table 3.1 were well mixed at an equal-molar ratio in a mortar. To reduce moisture, both the powders were dried in an oven at 150 °C for a few hours, and weighed in a short time when they were taken out of the oven.

To obtain high physical contact between Si and SiO_2 particles, a stainless steel die (1.27 cm-dia.) was used to compress mixed powders into pellets at pressures up to 702.3 MPa. In order to control the thickness of pellets, a fixed amount ($\approx$ 0.5 gram) was used to make each pellet. The uncompressed well-mixed powder was also used to control the SiO generation rate in the process. The uncompressed powder has a higher

porosity and poor physical contact between Si and SiO_2 particles. The physical properties of compacted pellets are given in Table 3.2.

3.3.2 Preliminary Experiments

In order to reduce the resistance to intra-particle diffusion of SiO vapor, some pellets (dia. = 25.4 mm; C.P. = 140 Mpa) were crushed into small pieces of about 2 mm in size. A sample of about 2 grams was held in either an alumina tray or a quartz tray in each run. The system was purged by a reactant gas stream (NH_3 or N_2/H_2) to eliminate impure gases possibly remaining in the reactor before each run was initiated. Differently from the tubular reactor (Figure 3.4), NH_3 gas was directly fed into the reactor through the stopper without using the NH_3 feeder.

After each run for about 15 hours, products were cooled in the stream of reactant gas down to room temperature. Products collected from several locations in the reactor tube were analyzed by IR spectroscopy and X-ray diffractometry. The IR spectra presented by Wada *et al.* [1981] and the X-ray diffractions presented by Ito [1990] were used as the reference of Si_3N_4. Electron microprobe analysis was used for identifying the compositions of product.

3.3.3 SiO Generation in TGA and SiO Generator

The generation of SiO vapor was conducted using two different set-ups: the Omnitherm TGA/1500 and SiO generator. The TGA was operated at temperatures in the range of 1250-1350 °C. A maximum temperature of 1400 °C was used to generate SiO vapor in the SiO generator.

In the TGA analysis, a compacted pellet (25.4 mm-dia) was broken into small pieces because of the dimensional limitation. The average diameter and thickness of the broken pieces were 3.5 mm and 1.2 mm, respectively. The sample mass was measured directly by the electronic balance at any reaction time. Before the

Table 3.2 Physical properties of compacted pellets

Compacting pressure (MPa)	70.2	175.6	351.1	526.6	702.3
Average pore diameter (Å)	2575	2021	1350	991	871
Porosity (vol%)	48	43	38	34	32
Pore volume (cm^3/g)	0.38	0.32	0.27	0.18	0.17

experiment was initiated, the system was purged by Ar gas until the weight reading became stable. During the purging process, a certain amount of moisture was removed from the sample by the gas flow. Ar gas was also used to carry SiO vapor out of the reactor during the reaction. The data acquisition system recorded the reaction temperature and sample mass every 10 seconds since the heating operation was initiated. The rates of SiO generation were determined on the basis of the slopes of sample mass versus reaction time plots.

Similar to the TGA analysis, experiments were conducted in the SiO generator. Compacted pellets were dried in an oven at 150 °C for a few hours to reduce moisture content. Each pellet was weighed in a short time to avoid the pellet from reabsorbing ambient moisture. One pellet was placed and heated in the SiO generator without any Ar flow during the heating process. Ar was supplied into the SiO generator to remove SiO vapor downstream when the furnace reached a prescribed temperature. The generation rates were evaluated based on the loss of sample mass divided by the reaction time. Operating conditions of the SiO generation in the TGA and SiO generator are summarized in Table 3.3.

The effects of pellet porosity and thickness on the SiO generation were also investigated in the SiO generator. The bottom and radial sides of each pellet were sealed by ceramic glue, so that SiO vapor would diffuse through the pellet only in the axial direction. With a fixed amount of mixed powder, the pellet thickness was controlled to be roughly uniform while the pellet porosity was changed from 0.32 to 0.48. Thus, the effect of pellet porosity was studied under the uniform thickness-condition. For the thickness effect, the pellet porosity was fixed using a constant compacting pressure.

3.3.4 Ammonia Dissociation in Alumina Tube

In the differential flow analysis of NH_3 dissociation, the flow meter for feeding NH_3 was calibrated by the titration method to meet the required accuracy. Four liters of hydrochloric acid (HCl $\approx$ 0.8 M) in two flasks (two liters in each) were used to

Table 3.3 Operating conditions for SiO generation experiments

Reactor Type	TGA	SiO Generator
Sample compacting pressure (MPa)	175.6	526.6
Sample size (cm)	diameter: 0.35 thickness: 0.12	diameter: 1.27 thickness: 0.071 - 0.516
Ar flow velocity* (cm/sec)	0.19 - 0.52	15.05
Furnace temperature (°C)	1250 - 1350	1250 - 1400
Reaction temperature (°C)	1250 - 1358	1250 - 1393

★ : referred to room temperature

absorb NH_3 during the calibration. In order to maintain the absorbing efficiency, the final HCl concentration was controlled to remain around 0.2 M in each run. A standard sodium hydroxide (NaOH) solution was used for determining the HCl concentration with methyl orange as an indicator. The flow rate of NH_3 was determined on the basis of the concentration difference in the HCl solution.

A standard NaOH solution cannot be prepared by weighing solid NaOH due to the impurity and hygroscopic characteristics. Besides, NaOH easily dissolves carbon dioxide to precipitate as a carbonate. Potassium hydrogen phthalate (KHP) was hence used as the primary standard in the preparation of standard NaOH solution.

KHP contains one titratable acid functional group and reacts with NaOH as

$$\mathbf{HOOCC_6H_4COOK + NaOH \rightarrow H_2O + NaOOCC_6H_4COOK} \qquad \textbf{(3.1)}$$

KHP was dried in an oven to eliminate its moisture, and the sample mass was weighed in a short time after it was taken out of the oven. Phenolphthalein was used as an indicator in the preparation of standard NaOH solution.

With considering the possible catalytic behavior of alumina (Al_2O_3) at high temperatures, the reactor tube was heated at 1400 °C (a maximum temperature in this study) for one hour. After this preheating process, the reactor was cooled down to a desired temperature and the analysis was carried out at this temperature.

When a prescribed temperature was reached, NH_3 or Ar-NH_3 mixture gas was fed into the system and the exiting stream was introduced into the HCl solution. Thus, NH_3 remaining in the stream was absorbed and neutralized by HCl in the two flasks. The remaining amount of NH_3 was determined based on the concentration difference of the HCl solution. The dissociated amount of NH_3 was determined by the flow rate of N_2 and H_2 mixture gas passing through a soap-film flow meter, for which a correction of water vapor at room temperature was made.

The variation of NH_3 dissociation with time was recorded at each temperature. During the waiting period of two measurements, NH_3 was continuously fed into the

reactor but bypassed the HCl solution to an exit. Experimental conditions regarding the study of NH_3 dissociation are summarized in Table 3.4.

The rate of NH_3 dissociation was determined on the basis of the differential flow analysis at 1185 °C. Thus, the inlet NH_3 concentration was adjusted using Ar as inert balance and the order, n, of NH_3 dissociation with respect to its concentration was determined at this temperature. Another series of runs were also made at 1235 °C. Due to the high conversion of NH_3 dissociation, the data obtained in this series were used for reference to compare the dissociation order (n) with that determined at 1185 °C. However, the rate constant was finally determined based on the integral analysis using the rate equation obtained in the differential flow analysis at 1185 °C.

3.3.5 SiO-NH_3 Reaction in Tubular Reactor

Measuring sample mass accurately is a key factor in determining the SiO generation rate. Well-mixed powder or compacted pellets were dried in an oven at 150 °C. When a sample was taken out of the oven, the sample mass was measured in a short time. In addition, the sampling tubes, used for collecting the product, were washed after each run and dried at 150 °C. Each sampling tube was weighed by a balance with reading accuracy of 0.00001 gram before it was inserted into the reactor.

Before each run was initiated, the reactor system was purged by Ar gas at a flow rate of 2770 cm^3/min for 30 minutes to eliminate possible impure gases remaining in the system. A fixed ramp rate of 10 °C/min was used in all the experiments. It was expected that a certain amount of SiO vapor could escape from the sample though the preheating time was short compared to the total reaction time. In order to reduce the SiO vaporization, the reactor was filled with stagnant Ar gas during the heating process.

As soon as the system reached a prescribed reaction temperature, Ar and NH_3 were fed into the reactor to carry out the SiO-NH_3 reaction. SiO vapor was carried by the Ar flow (defined as Ar-1) downstream to the reacting zone. In addition to the Ar-1 stream entering into the SiO generator, another Ar gas stream (indicated as Ar-2)

Table 3.4 Operating conditions for differential analysis of NH_3 dissociation

Conditions	**Experiments of NH_3 dissociation**
Furnace temperatures (°C)	1200 - 1400
Reaction temperatures (°C)	1185 - 1382
***NH_3* flow rates*** (cm^3/min)	333 - 2032
***Ar* flow rates*** (cm^3/min)	0 - 1358
***HCl* concentration** (M)	0.2 - 0.8

$\star$: referred to room temperature

was directly introduced into the reactor from the stopper to avoid the back flow of the reactant gas or products.

Because the rate of SiO generation varied with temperature, different times were selected depending on reaction temperature: 4 hours at 1300 °C, 2 hours at 1350 °C, and 1 hour at 1400 °C. Preliminary experiments were made to confirm that these time periods of reaction were appropriate for further kinetic studies. An average SiO generation rate, $(dM_{SiO}/dt)_{Ave}$, was then calculated based on the loss of sample mass, M_{SiO}, divided by the reaction time. The amount of product, M_{prd}, was determined from the total mass gain of all the sampling tubes. The average rate of product formation, $(dM_{prd}/dt)_{Ave}$, was evaluated as the total mass of product divided by the reaction time. The experimental conditions of the SiO-NH_3 reaction are given in Table 3.5.

Products collected by scraping individual sampling-tubes were used for further analysis. For the characterization of products, IR spectroscopy, X-ray diffractometry, scanning electron microprobe analysis, scanning electron microscopy (SEM), and transmission electron microscopy (TEM) were used.

Amorphous products were also heated to higher temperatures, without being exposed to the atmosphere, for their crystallization. Product powder collected with a filter was handled in a glove box to avoid its contact with ambient moisture before heating for its crystallization. The α-/β-ratios in Si_3N_4 were quantitatively analyzed by XRD, using a calibration constant of $K_{\alpha/\beta} = 0.647$ with integrated intensities of the (102) and (210) peaks of α-Si_3N_4 and the (101) and (210) peaks of β-Si_3N_4 [Gazzara and Messier, 1973; Jovanovic and Kimura, 1994; Jovanovic *et al.*, 1994].

Table 3.5 A summary of operating conditions for SiO-NH_3 reaction in tubular reactor

Conditions	***SiO-NH₃* gas phase reaction**
***Ar-1* flow velocity** (cm/sec) ***Ar-1* flow rate** (cm^3/min)	14.4 (76.3 - 80.42)* 1387 (7345 - 7750)*
***Ar-2* flow rate** (cm^3/min)	1383 (7323 - 7727)*
***NH_3* feeding rate** (cm^3/min)	1382 (7318 - 7722)*
Furnace temperatures (°C)	1310 - 1410
***SiO* generation temperatures** (°C)	1301 - 1392
***SiO-NH_3* reaction temperatures** (°C)	1305 - 1395

★ : the values in the parenthesis are referred to reaction temperatures

CHAPTER 4
EXPERIMENTAL RESULTS AND DISCUSSIONS

4.1 Preliminary Experiments

In the set-up for preliminary experiments, NH_3 could react with either Si in the Si/SiO_2 mixture or SiO vapor generated by the reaction of Si and SiO_2. Also, NH_3 highly decomposed into N_2 and H_2 because of a longer residence time for NH_3 to stay before reaching the reacting zone. Thus, Si_3N_4 was produced by the direct nitridation (Si with NH_3 or N_2) as well as the gas phase reaction (SiO with NH_3 or N_2/H_2).

Product was not uniformly distributed in the reactor tube. The deposition of product was rather discrete, as shown in Figure 4.1 in relation to the temperature profile. Fibrous whiskers always formed right behind the reactant mixture sample (location 1) in the direction of flow when NH_3 was used as a reactant gas. Wall deposits were found at the exit of heating zone (location 2) where the temperature sharply dropped from 1350 °C to around 1000 °C. In addition, fluffy deposits were found at location 3 around the outlet of reactor. It should be mentioned that no whiskers at location 1 was obtained when N_2 was mixed with H_2 as a reactant gas. The products obtained by supplying a mixture of N_2 and H_2 were only wall deposits at location 2 and fluffy material at location 3.

Infra-red (IR) and electron microprobe analysis were used to identify the composition of product. The IR spectra of all the whiskers formed at location 1 were almost identical or very similar to that of Si_3N_4. The IR spectra of the whiskers and standard Si_3N_4 are shown in Figures 4.2 and 4.3, respectively. A comparison of these two figures shows the resemblance between these two spectra. As shown in Figure 4.2, the whiskers produced from two different runs were used for electron microprobe analysis, and the results are summarized in Table 4.1. According to the element analysis, one may write the whiskers as $Si_{40.26}N_{58.06}O_{1.68} \sim Si_{42.85}N_{54.80}O_{2.34}$. The compositions of whiskers are closed to that of α-Si_3N_4, $Si_{11.5}N_{15}O_{0.5}$, proposed by Wild

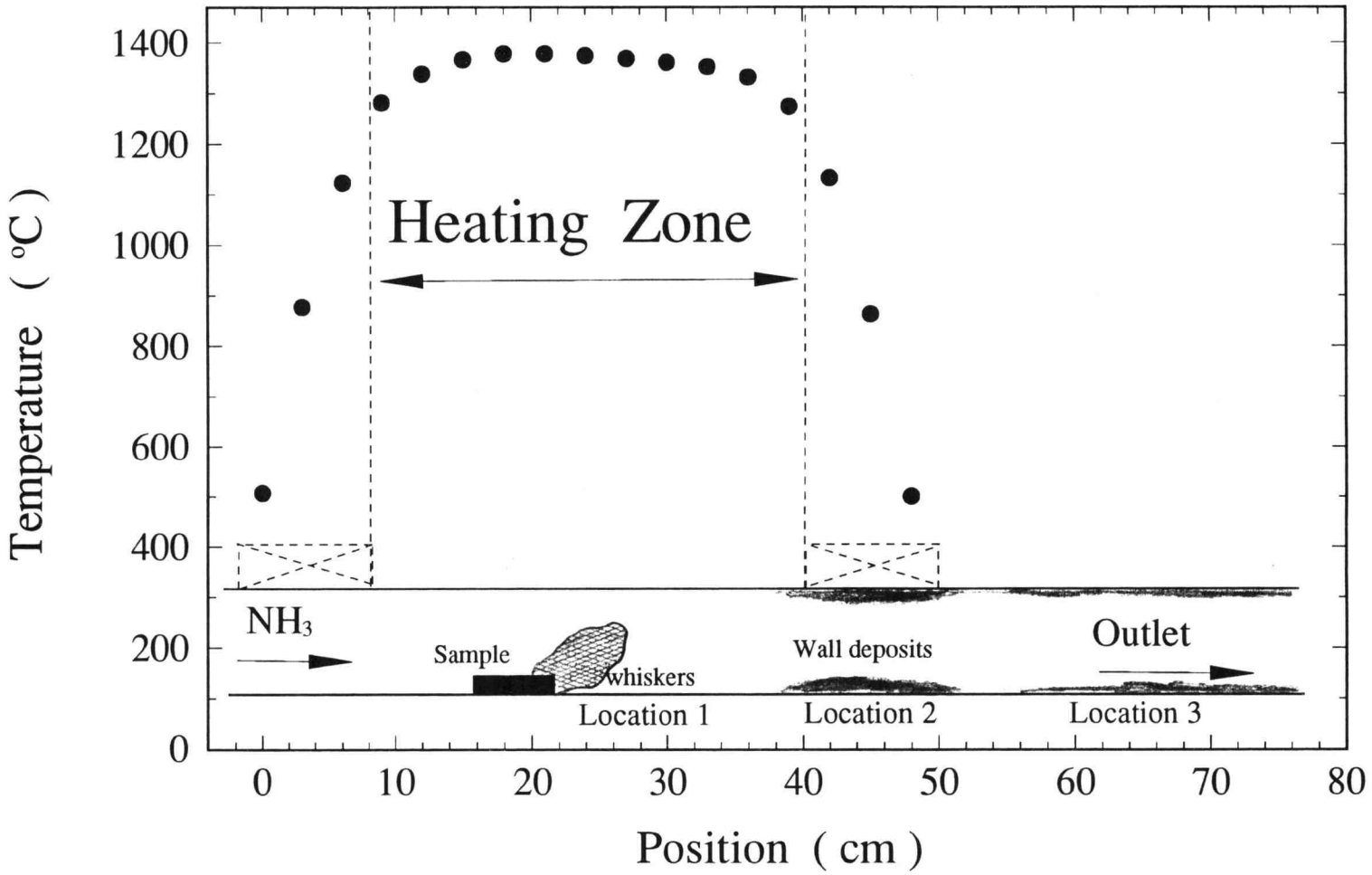

Figure 4.1 Distributions of product via $SiO\text{-}NH_3$ reaction in preliminary experiments

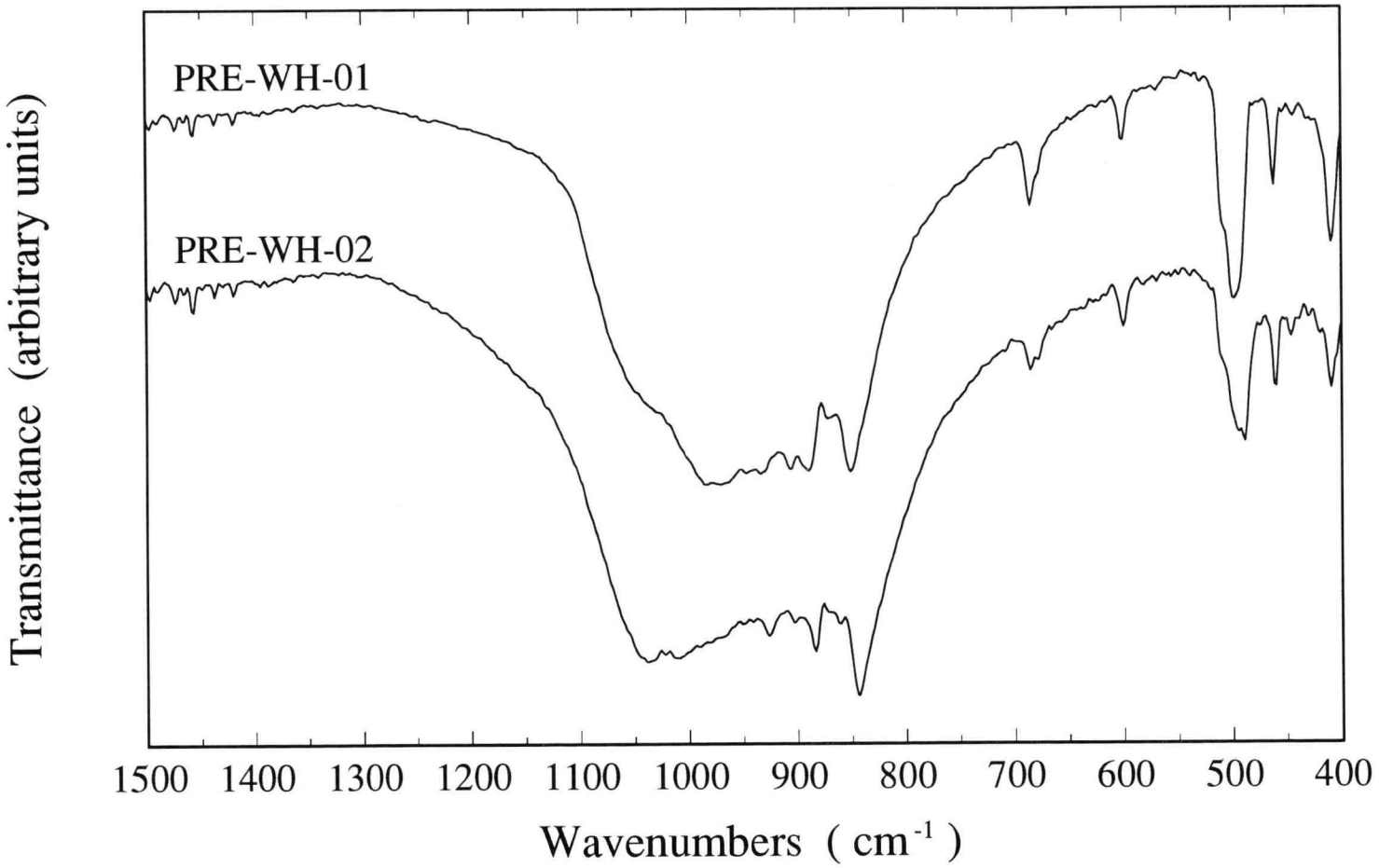

Figure 4.2 IR spectra of whiskers produced from two different runs in preliminary experiments

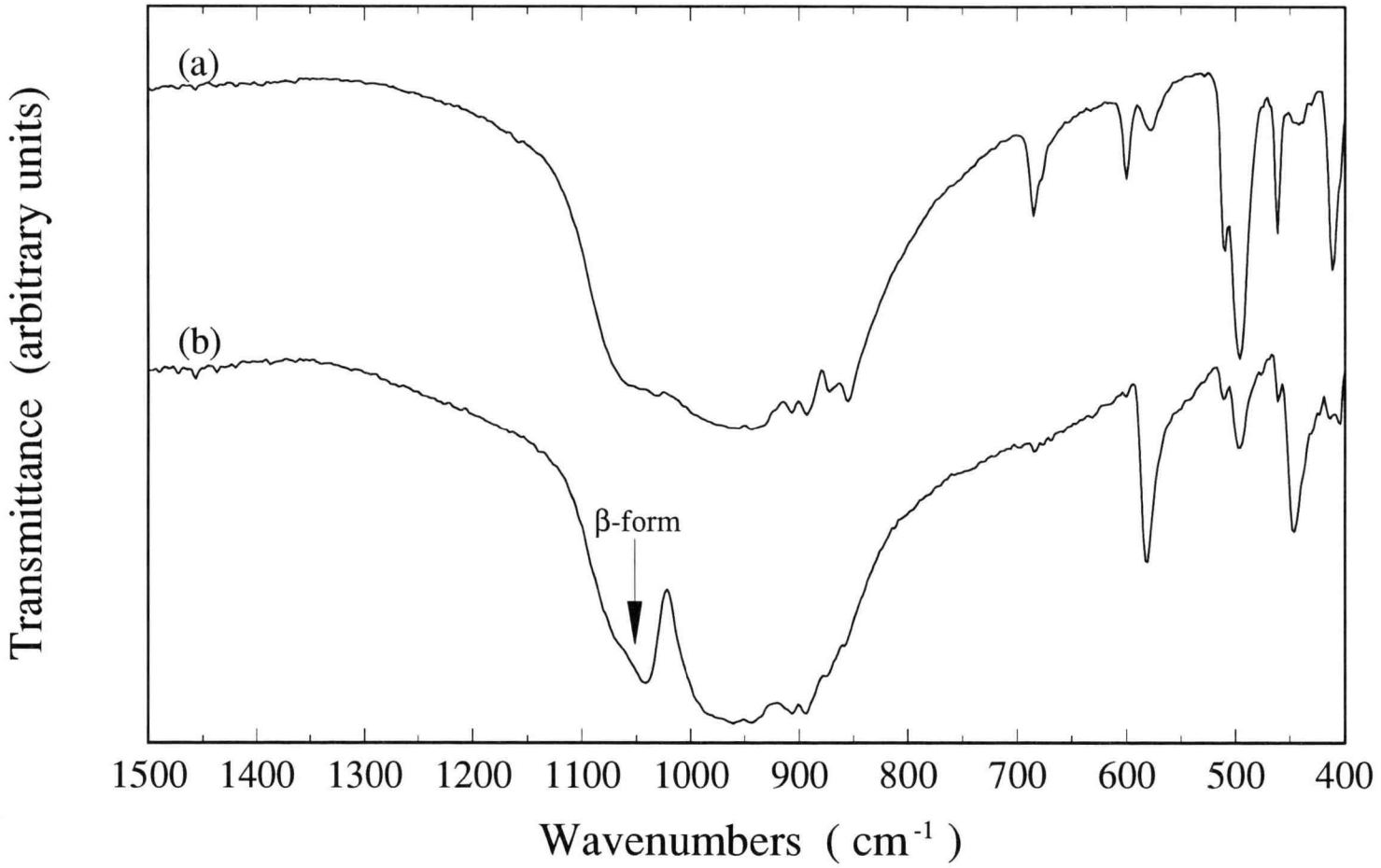

Figure 4.3 IR spectra of standard Si_3N_4: (a) dominant α-form, (b) dominant β-form

Table 4.1 Element analysis of fabrious whiskers formed at location 1

Fibrous Whiskers	**Element**	**I.X./I.STD**	**K Ratio**	**Concentration** (weight %)	**Atomic Coefficient** (mole %)
PRE-WH-01	*Si*	2.9169	0.5274	58.071	40.26
	N	1.1630	0.1082	41.771	58.06
	O	0.0337	0.0024	1.382	1.68
PRE-WH-02	*Si*	2.9686	0.5367	58.983	42.85
	N	0.9960	0.0927	37.618	54.80
	O	0.0464	0.0033	1.838	2.34

et al. [1972]. Based on the IR and element analysis, it is concluded that the whiskers formed at location 1 are Si_3N_4.

IR and X-ray analyses indicate that the wall deposits at location 2 and the fluffy material at location 3 are amorphous and not Si_3N_4 (Figure 4.4). Compared to Figure 4.5, showing the IR spectrum of standard SiO_2, it is believed that the product is a mixture of Si and SiO_2 (characterized as "SiO"). It is suspected, on the basis of thermodynamic calculations, that un-reacted SiO vapor has condensed back to Si and SiO_2 due to the temperature drop toward the reactor exit.

The quantities of the wall deposit and fluffy material at locations 2 and 3 were relatively small whenever the amount of whiskers at location 1 was large. If NH_3 feeding was sufficient and the reaction time was long enough, SiO vapor may have been completely converted into Si_3N_4 before exiting the reactor and condensing back to Si/SiO_2 mixture. It is hence suggested that feeding NH_3 and the residence time for $SiO\text{-}NH_3$ reaction may be two critical factors in the process.

Solids remaining in the sample tray were also analyzed by IR and X-ray methods. Part of sample solids was Si_3N_4 crystals, the majority of which was identified to be of α form as shown in Figure 4.6. It should be noted that no Si peak was detected in the X-ray diffraction. As seen in Figure 4.7, a certain amount of un-reacted SiO_2 is left in the sample. The results imply that Si powder was consumed by two reactions: the direct nitridation with NH_3 or N_2, and the reaction with SiO_2 to form SiO.

The preliminary experiments identify that Si_3N_4 can be produced from the reaction of SiO and NH_3 though "SiO" deposits are also obtained in the process. NH_3 highly decomposes into N_2 and H_2 owing to a long residence time. All SiO vapor may have a chance of being converted into Si_3N_4 only when NH_3 feeding is sufficient in the reactor. In this light, further systematic study on Reaction (2.14) was conducted in a new reactor with a longer reacting zone. Also, an Al_2O_3 tube with a small inside diameter (3.96 mm) was used to feed NH_3. Only the gas phase reaction of SiO and NH_3 is of interest in the further study.

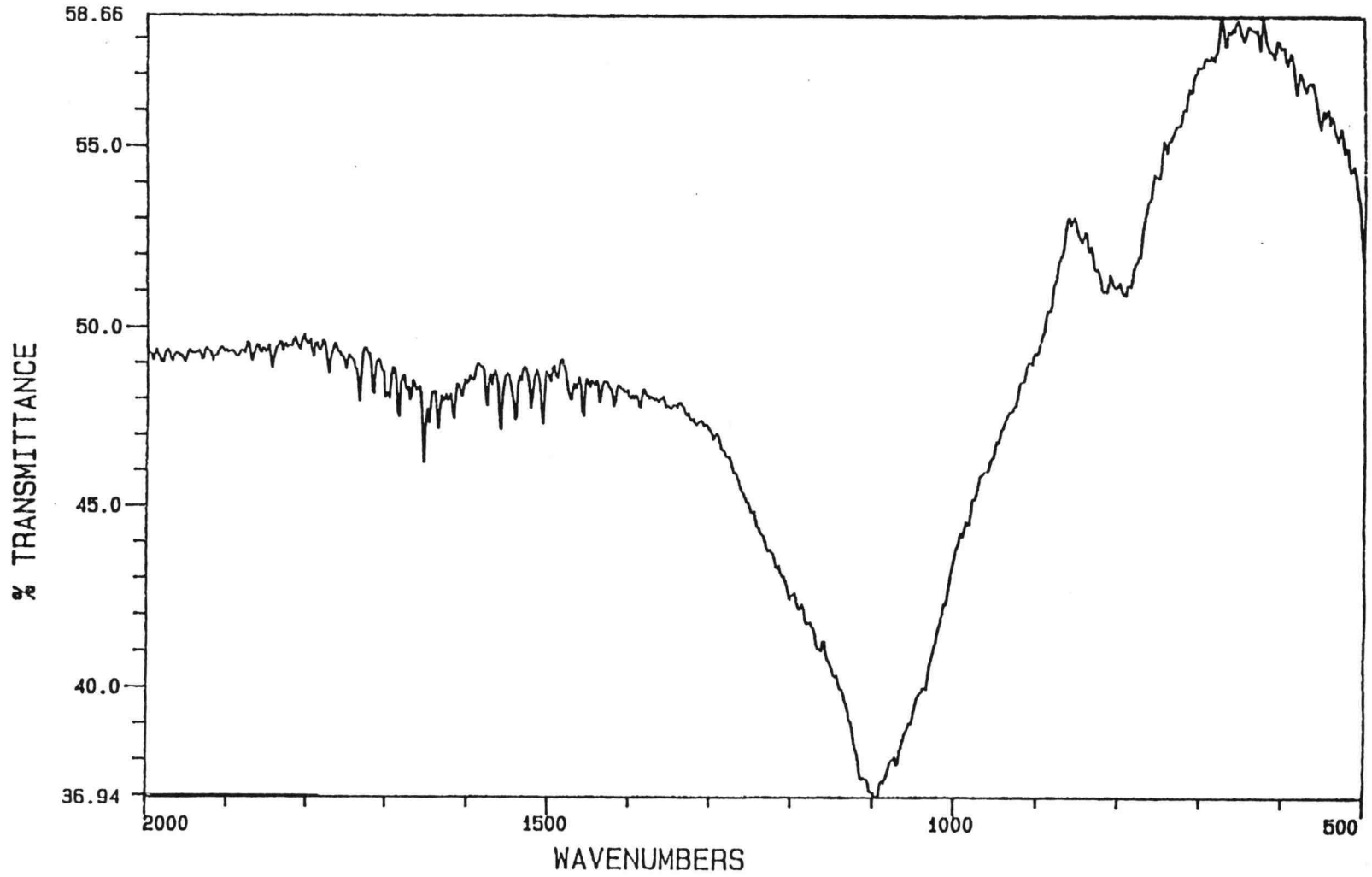

Figure 4.4 IR spectrum of wall deposits, formed at locations 2 and 3, in preliminary experiments

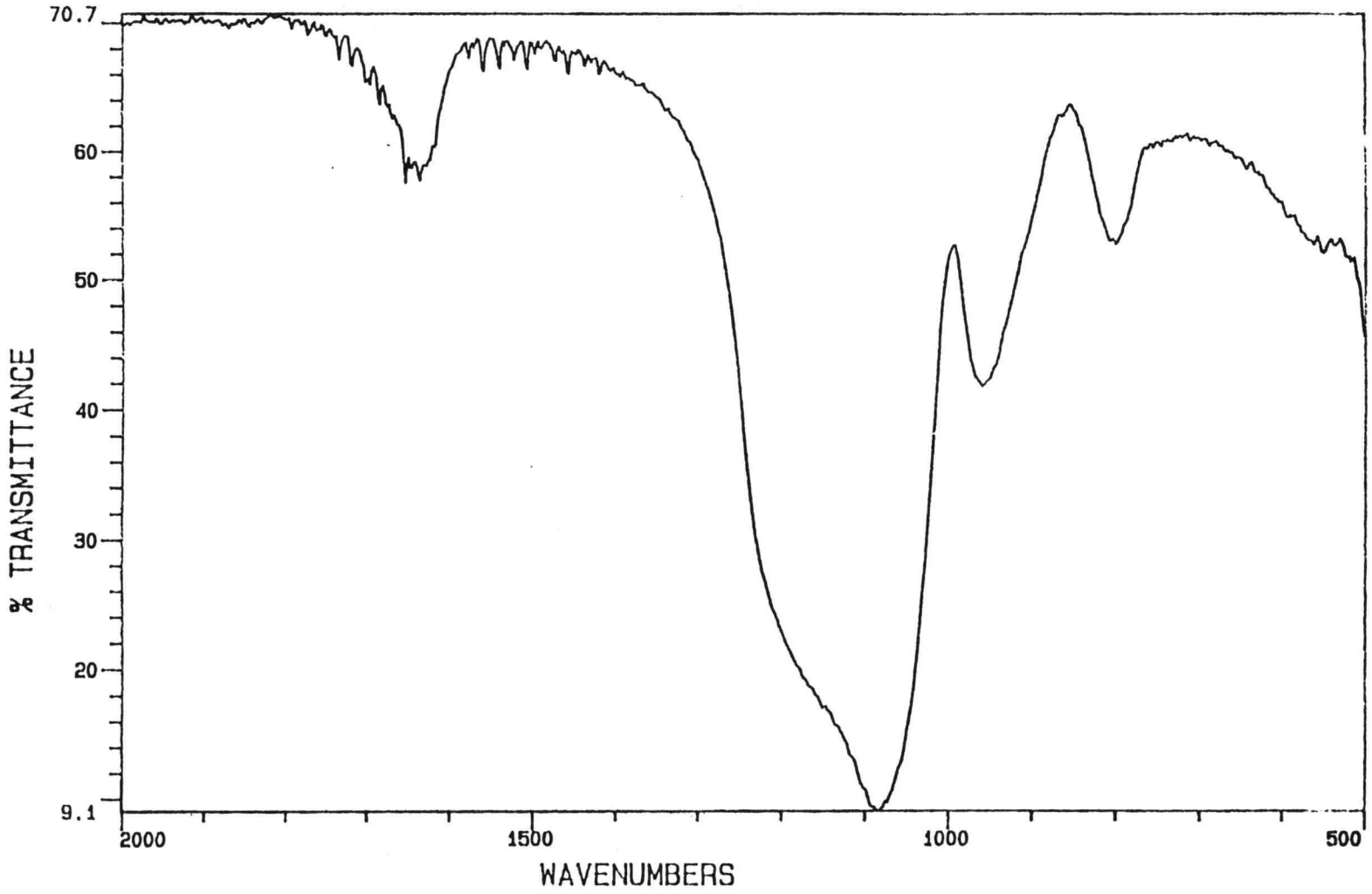

Figure 4.5 IR spectrum of standard SiO_2

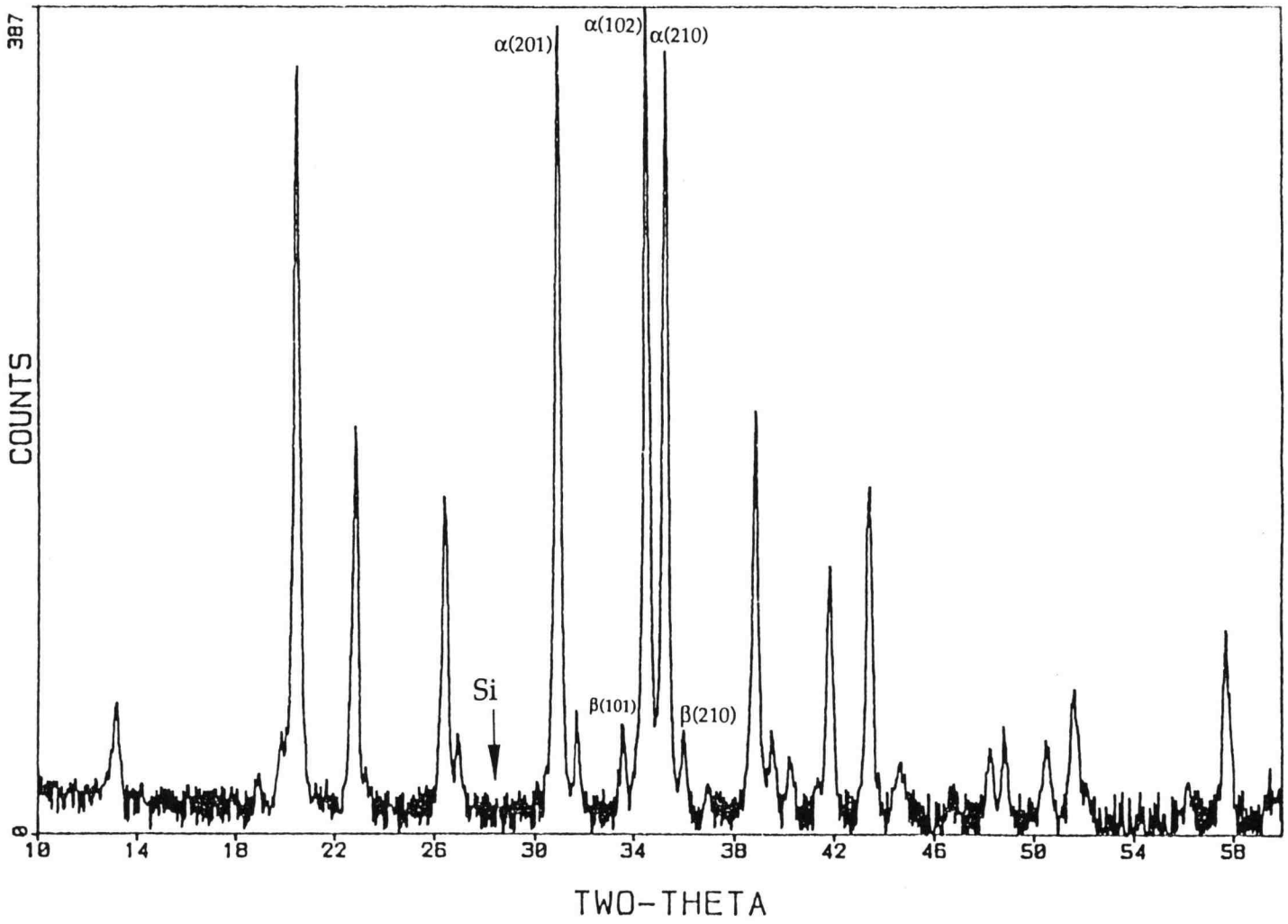

Figure 4.6 X-ray diffraction of nitridized sample powder in preliminary experiments

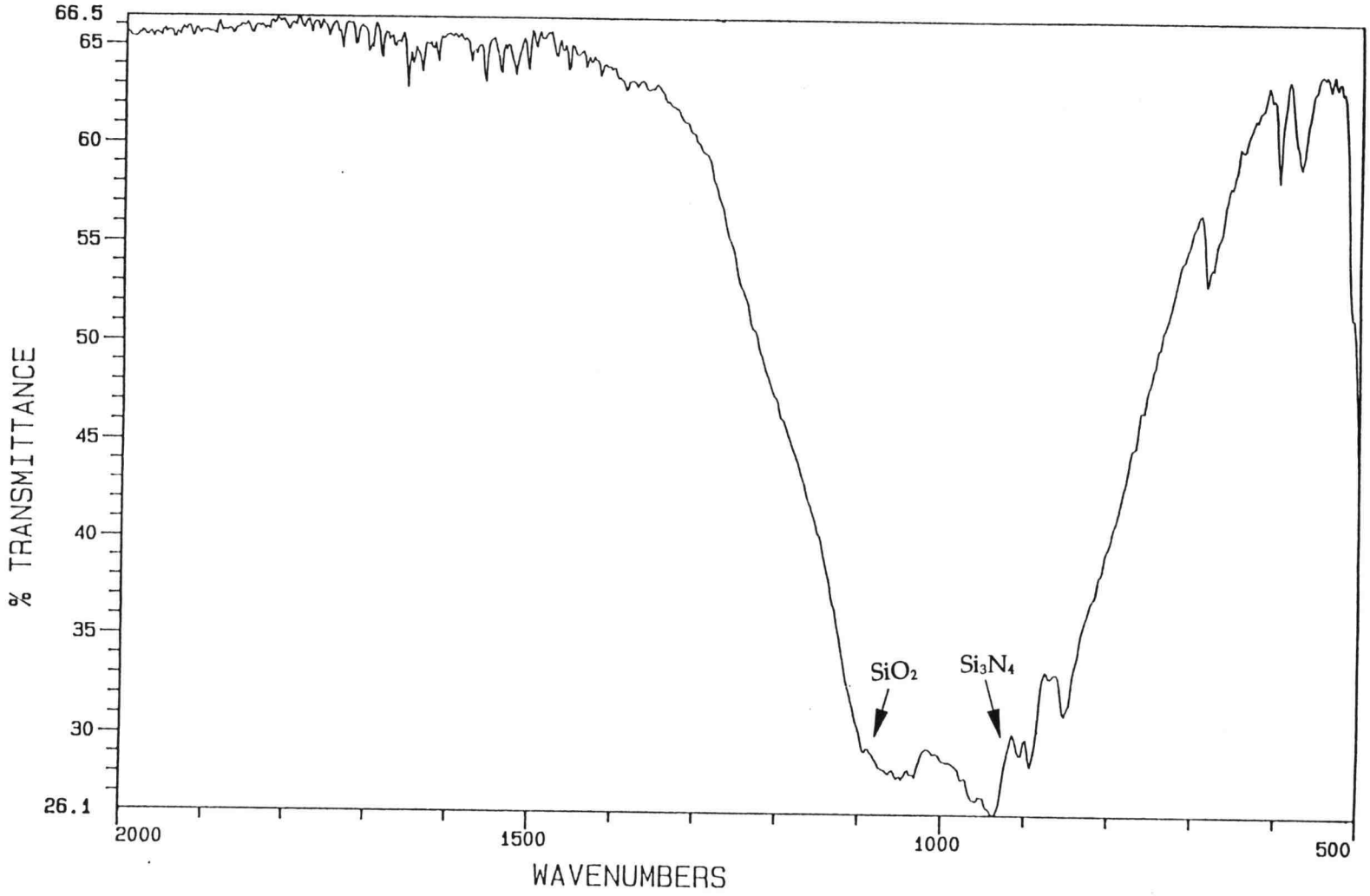

Figure 4.7 IR spectrum of nitridized sample powder in preliminary experiments

4.2 Generation of Silicon Monoxide

The preliminary experiments show a feasible way to produce Si_3N_4 by the reaction of SiO and NH_3. Generating SiO vapor as a raw material is the first step for the reaction to proceed. Thus, controlling and determining the generation rate of SiO are necessary before investigating the SiO-NH_3 reaction.

4.2.1 Generation in TGA

The SiO generation rate may be determined from the loss of sample mass during the reaction. Measuring the sample mass precisely is the most important factor in such an experiment. Thus, a thermal gravimetric analyzer was used for continuous observation of sample mass during the reaction. The experimental results are shown in Table 4.2 and Figure 4.8.

As seen in Figure 4.8, the SiO generation rate, evaluated as the slope of sample mass changing with time, decreases with an increase in time. The SiO generation curves are roughly linear during the initial stage at all the temperatures. The initial rates, $(dX/dt)_o$, shown in Table 4.2 are calculated on the basis of the initial slopes in Figure 4.8.

In the TGA analysis, the pellet was compressed at a rather low pressure of 175.6 MPa, leading to a high porosity. It is anticipated that both the pore diffusion and film mass transfer may be involved in the process. Three runs (TGA-05 through -07) were made to identify the external mass transfer resistance in the process. However, the initial rates did not change significantly though Ar velocity was increased from 1.037 to 2.843 cm/sec. On the basis of this finding, it is concluded that the process of SiO generation is limited by the pore diffusion step.

Table 4.2 Experimental results of SiO generation in TGA analysis

Run No.	SiO Generation Temperature (°C)	Ar velocity† (cm/sec)	Pellet‡ weight (mg)	$(dX/dt)_o \times 10^5$ (sec^{-1})
TGA-01	1250	0.971	6.83	3.083
TGA-02	1277	0.988	6.94	3.833
TGA-03	1305	1.006	15.41	8.100
TGA-04	1329	1.021	7.99	11.667
TGA-05	1354	1.037	8.65	16.167
TGA-06	1358	1.762	8.94	17.500
TGA-07	1356	2.843	8.61	17.000

† : referred to reaction temperature

‡ : compacting pressure = 175.6 MPa

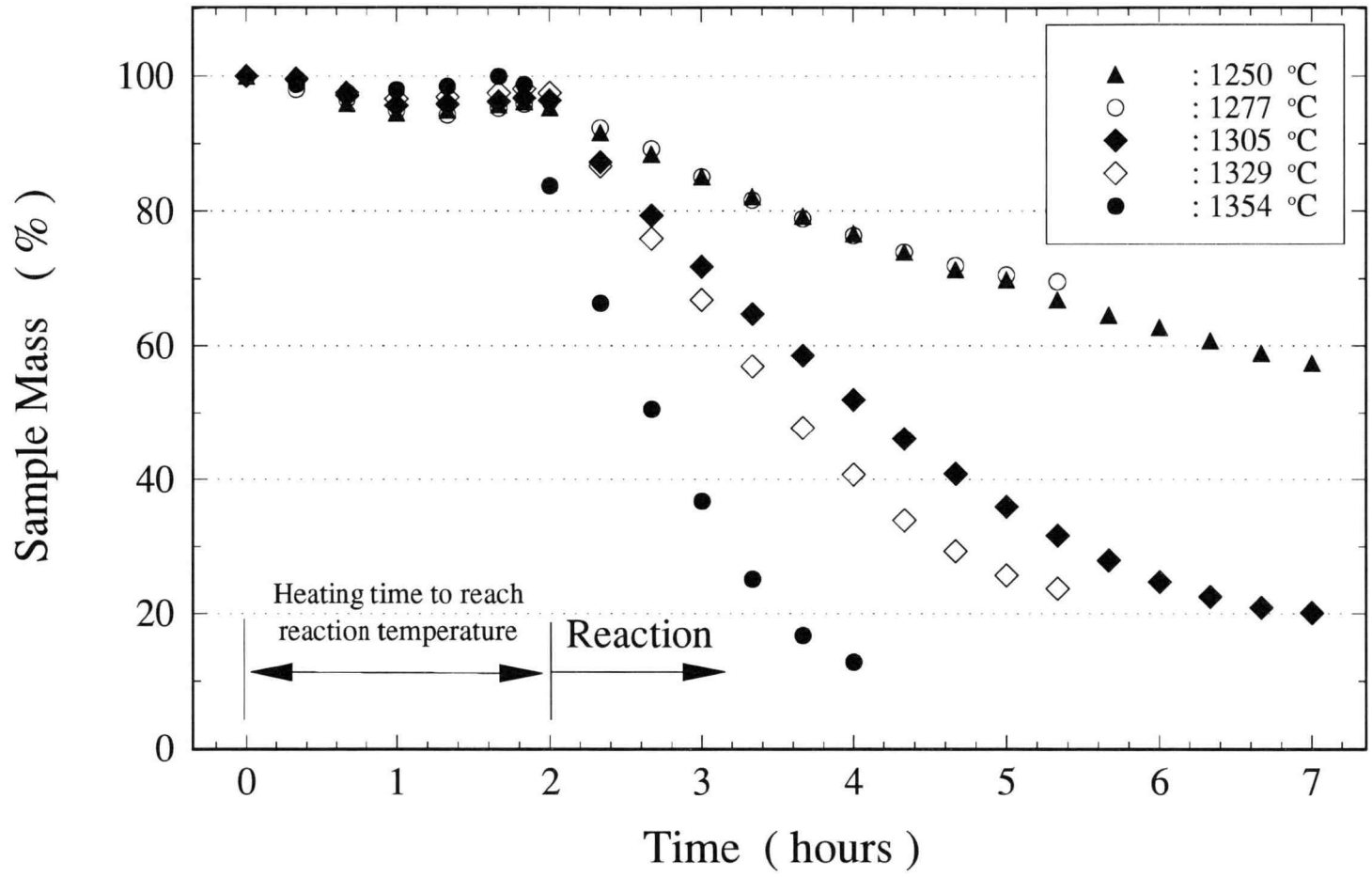

Figure 4.8 SiO generation curves obtained by TGA

4.2.2 Generation in SiO Generator

The TGA analysis gives a brief picture about the SiO generation at given temperatures. However, the generation rates obtained from the TGA analysis may not be appropriate for compacted pellets owing to more diffusion resistance in larger pellets. In order to determine the rates of SiO generation from compacted pellets, several runs were made using larger compacted pellets (12.7 mm-dia.) in the SiO generator. The initial rate was determined based on the loss of pellet mass during the beginning stage in each run. The experiments conducted in the SiO generator are summarized in Table 4.3.

According to Table 4.2 and 4.3, an Arrhenius-type plot between the initial rates and reaction temperatures is shown in Figure 4.9, which gives apparent activation energies of 347 (TGA) and 310 (SiO generator) kJ/mole, respectively. The values of SiO generation rate obtained from the SiO generator are smaller than those by the TGA equipment because the external surface area per unit mass of pellets used for the SiO generator is smaller than that for particles used for the TGA experiments. Also, a longer reaction time used for evaluating SiO generating rates rather than using the initial slope may have affected the overall-conversion rate values. The difference becomes more pronounced at higher temperatures, 1350 and 1400 °C. This leads to a slight decrease in the slope of the plot in Figure 4.9.

As mentioned earlier, the process of SiO generation is limited by the pore diffusion. For further study on this effect, several runs were made at a fixed temperature, using compacted pellets with different thickness ($\delta_{initial}$) but the same pellet porosity. In order to have diffusion fixed in the axial direction only, the radial and bottom sides of pellets were sealed by ceramic glue. Experimental results are shown in Table 4.4.

If the pellet apparent density is kept constant, the pellet size should be proportional to pellet mass $W_{initial}$. Since the pellet cross-sectional area and porosity were fixed, pellet thickness $\delta_{initial}$ was proportional to pellet mass $W_{initial}$. Thus, $W_{initial}$ is used instead of $\delta_{initial}$ in further discussions. As shown in Figure 4.10, $(dX/dt)_o$ decreases as $W_{initial}$ increases at 1400 °C, suggesting that a diffusion control mechanism

Table 4.3 Generation rates of SiO vapor in SiO generator

Run No.	**SiO Generation Temperature** (°C)	**Ar velocity** (m/sec)★	**Sample** (C.P. = 526.6 MPa)	$(dX/dt)_o \times 10^5$ (sec^{-1})
SIO-01	1250	0.771	1.27 cm-dia. pellet	1.333
SIO-02	1294	0.793	1.27 cm-dia. pellet	2.533
SIO-03	1343	0.818	1.27 cm-dia. pellet	4.633
SIO-04	1393	0.843	1.27 cm-dia. pellet	11.333

★ : referred to reaction temperature

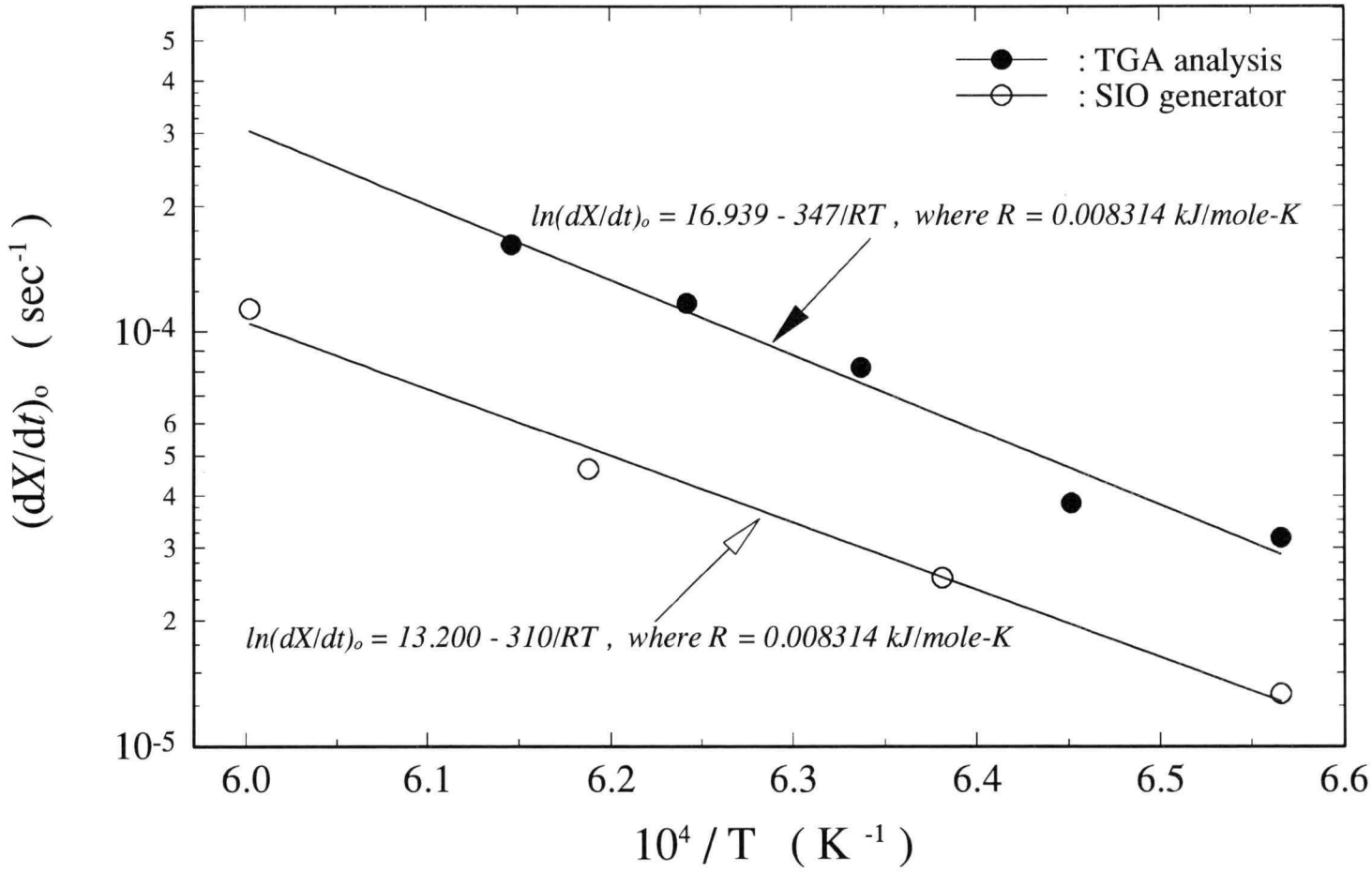

Figure 4.9 Temperature effect on initial rates of SiO generation

Table 4.4 Effect of pellet thickness on SiO generation

Pellet pretreatment	1294 °C		1400 °C	
	$W^{\dagger}_{initial}$ (g)	$(dX/dt)_o \times 10^5$ (1/sec)	$W^{\ddagger}_{initial}$ (g)	$(dX/dt)_o \times 10^5$ (1/sec)
the radial and bottom sides of pellets were sealed by ceramic glue	0.12560	3.258	0.18110	11.110
	0.23132	1.382	0.27360	8.352
	0.46355	1.230	0.36330	7.586
	0.69940	0.892	0.54330	5.540
	0.87150	1.058	0.63575	4.462
un-sealed pellet	0.04383	9.150		
	0.09302	5.917		
	0.22320	4.483		
	0.48230	2.267		

† : compacting pressure of pellet = 526.6 MPa

‡ : compacting pressure of pellet = 70.2 MPa

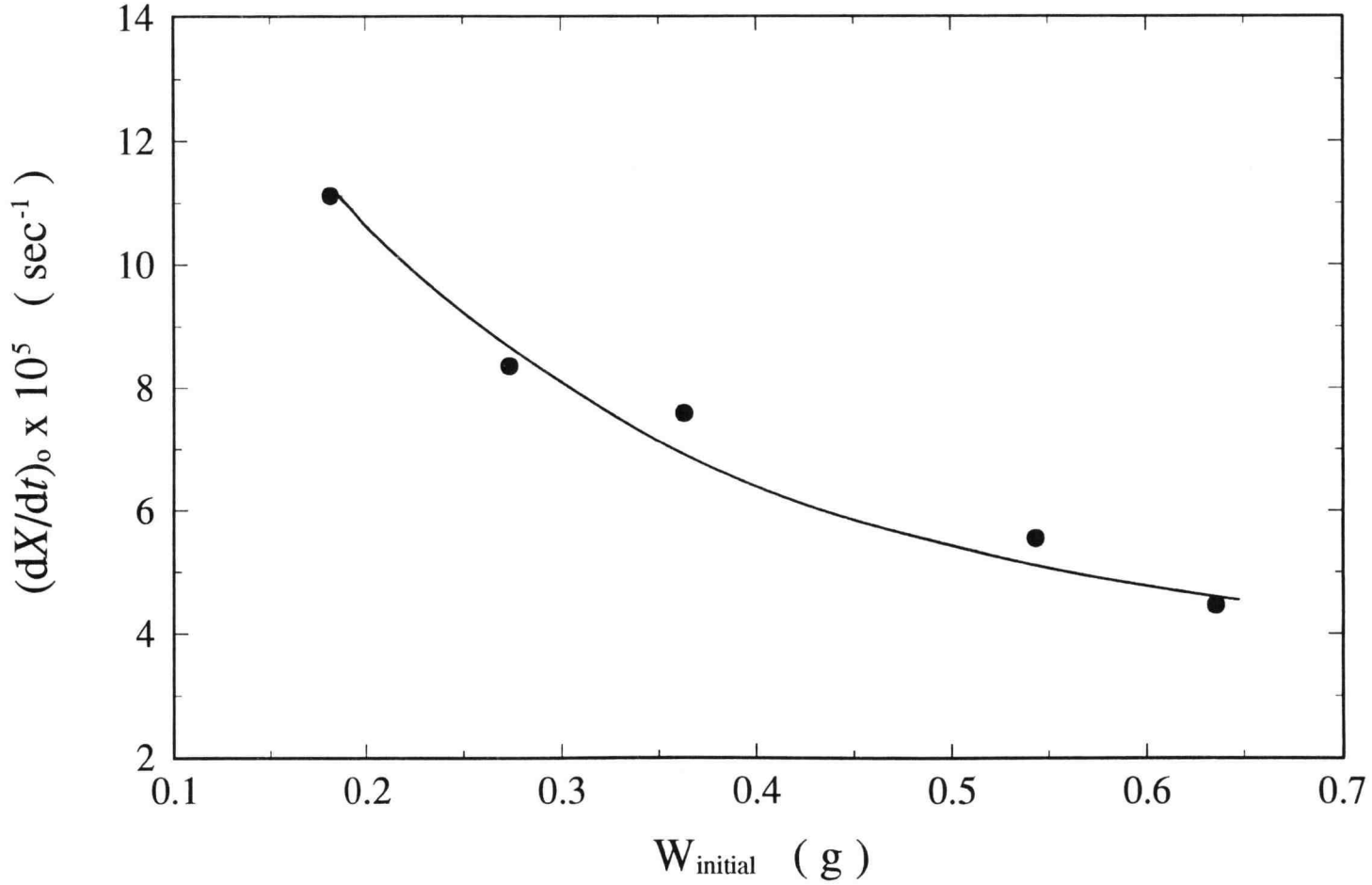

Figure 4.10 $(dX/dt)_o$ decreasing with $W_{initial}$ at 1400 °C

is involved in the process. Similar results were obtained at 1294 °C, shown in Figure 4.11. It should be mentioned that the generation rates of the un-sealed pellets are higher than those of the sealed pellets. It is believed that radial diffusion may be involved in the un-sealed pellets, leading to an increase in the overall generation rate.

Since the process is dominated by the pore diffusion of SiO, compacting pressure of pellets becomes important in the SiO generation (Table 4.5). A higher compacting pressure reduces the porosity and increases the diffusion resistance though it provides better physical contact between Si and SiO_2. Figure 4.12 indicates that the generation rate decreases with an increase in the compacting pressure. In correlation to the pellet porosity, the higher the pellet porosity the higher the SiO initial rate, shown in Figure 4.13.

It has been shown that the SiO generation rate decreases with reaction time and increases with the porosity of pellets. A series of preliminary experiments were made to confirm that the reaction time period set for each temperature was appropriate for further quantitative study. This set of runs were conducted at the highest temperature, 1400 °C and the highest pellet porosity, using uncompacted powder mixtures that would give the highest SiO generation rates. The curve of SiO generation at this temperature is shown in Figure 4.14. According to Figures 4.8 and 4.14, the rates of SiO generation are roughly constant in the proposed time periods: 1 hour at 1400 °C, 2 hours at 1350 °C, and 4 hours at 1300 °C.

To identify possible mechanisms involved in the Si/SiO_2 reaction, scanning electron microscopy (SEM) was used for analyzing the structural change of pellets. The compacting pressure of pellets was fixed at 526.6 MPa, and the temperature was changed from 1300 to 1400 °C. A pellet was heated for 10 minutes with Ar flow at each temperature. After the pellet was cooled down to room temperature, SEM pictures were taken for analyzing the changes in pellet surface between before and after the reaction. The SEM pictures are shown in Figure 4.15, where the picture of an unheated pellet is also included.

According to Figure 4.15, the vacancy appearing among particles becomes larger though the reaction proceeds for only 10 minutes. These phenomena are more pronounced at 1350 and 1400 °C. If the process is described by a pure solid-solid

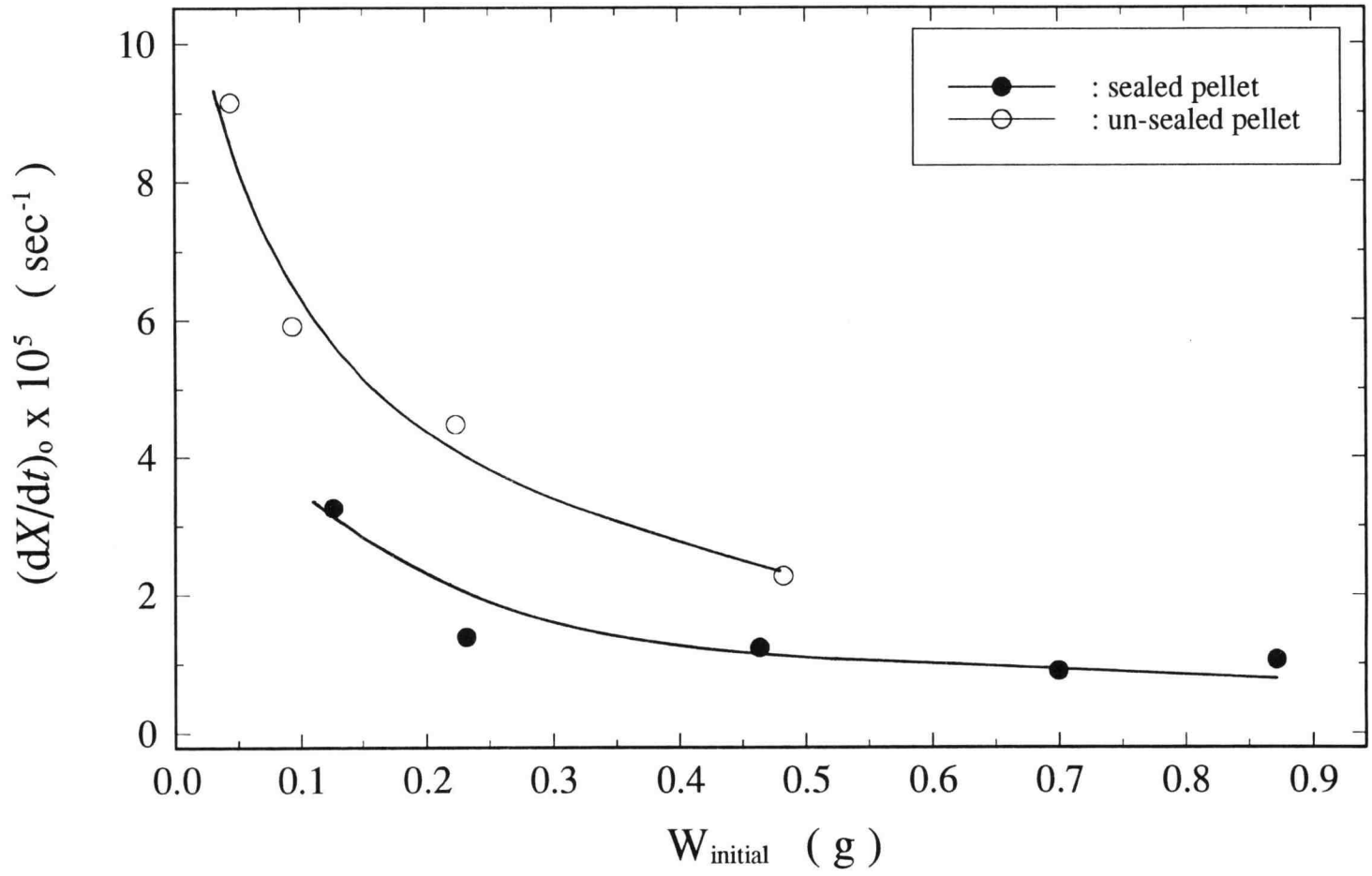

Figure 4.11 $(dX/dt)_o$ decreasing with $W_{initial}$ at 1294 °C

Table 4.5 Porosity effect on SiO generation at temperatures between 1294 and 1400 °C

Compacting pressure (MPa)		70.2	175.6	351.1	526.6	702.3
Porosity ε		0.48	0.43	0.38	0.34	0.32
$(dX/dt)_o \times 10^5$ (1/sec)	1294 °C†	3.37	–	–	2.27	2.13
	1300 °C‡	1.16	0.727	0.981	1.12	0.853
	1360 °C‡	2.92	3.01	2.90	2.834	–
	1400 °C‡	7.51	7.19	5.88	6.16	–

† : un-sealed pellets used

‡ : sealed pellets used

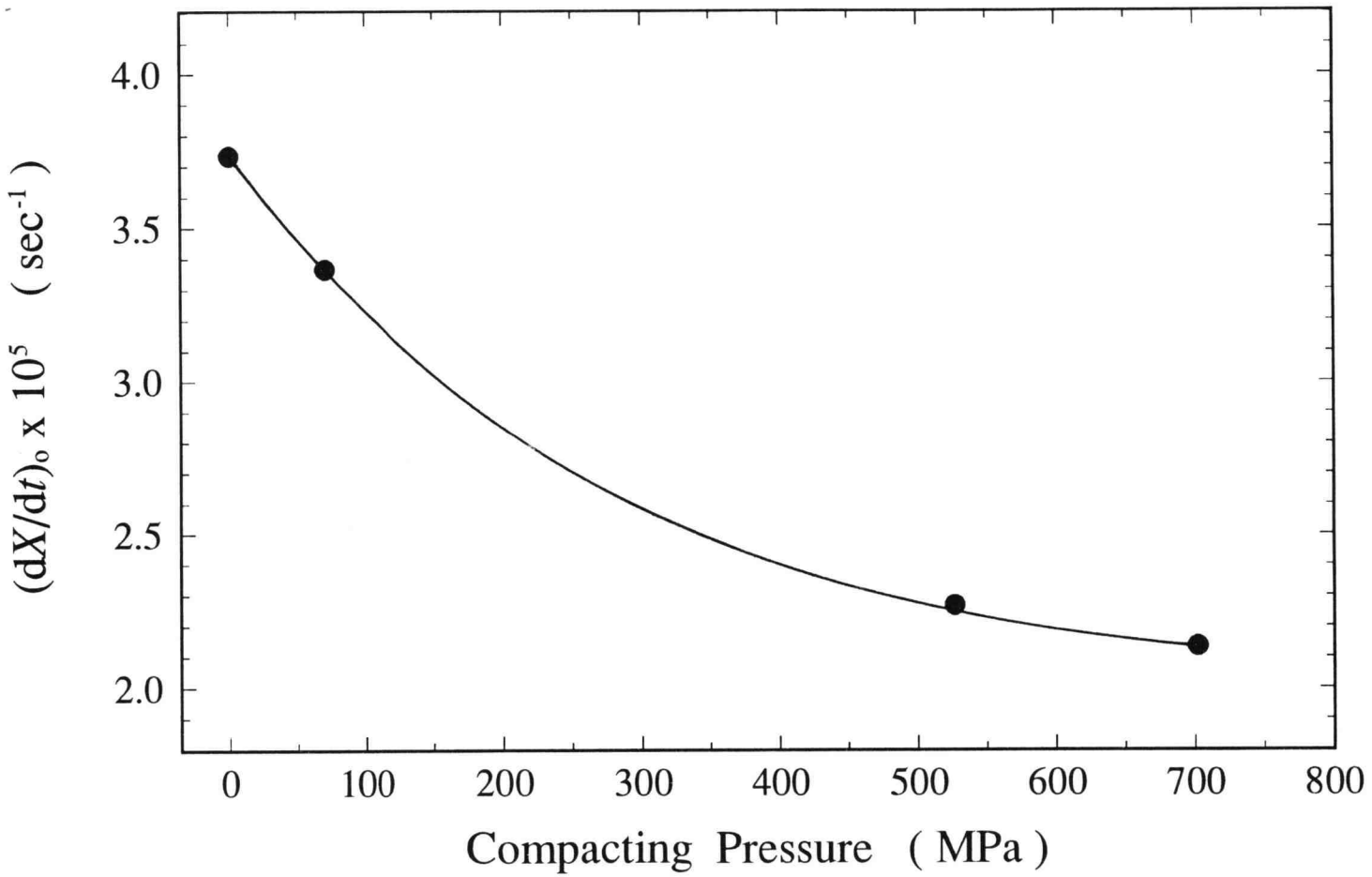

Figure 4.12 Effect of compacting pressure on initial SiO generation rate at 1294 °C, using unsealed pellets

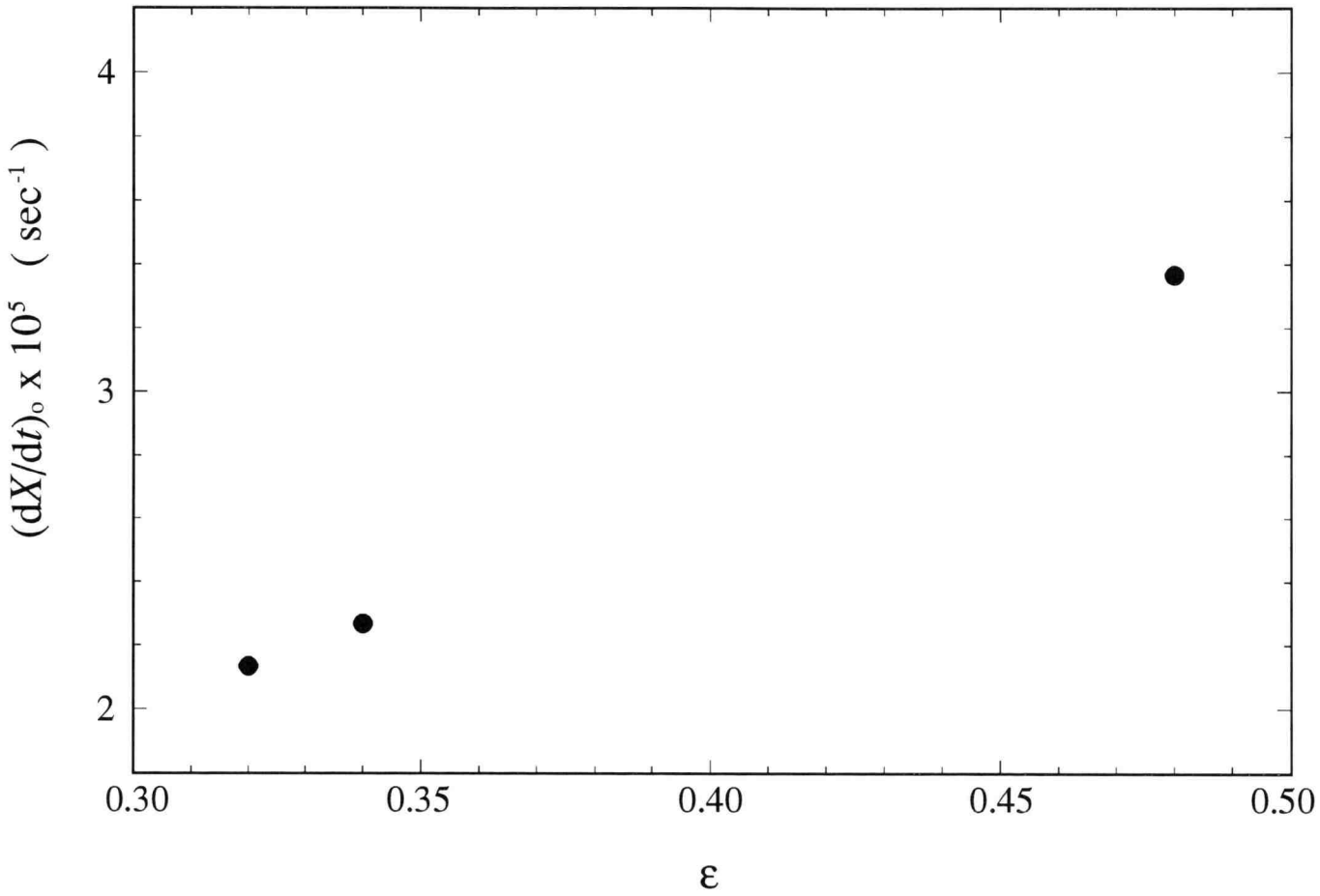

Figure 4.13 Effect of pellet porosity on initial SiO generation rate at 1294 °C, using unsealed pellets

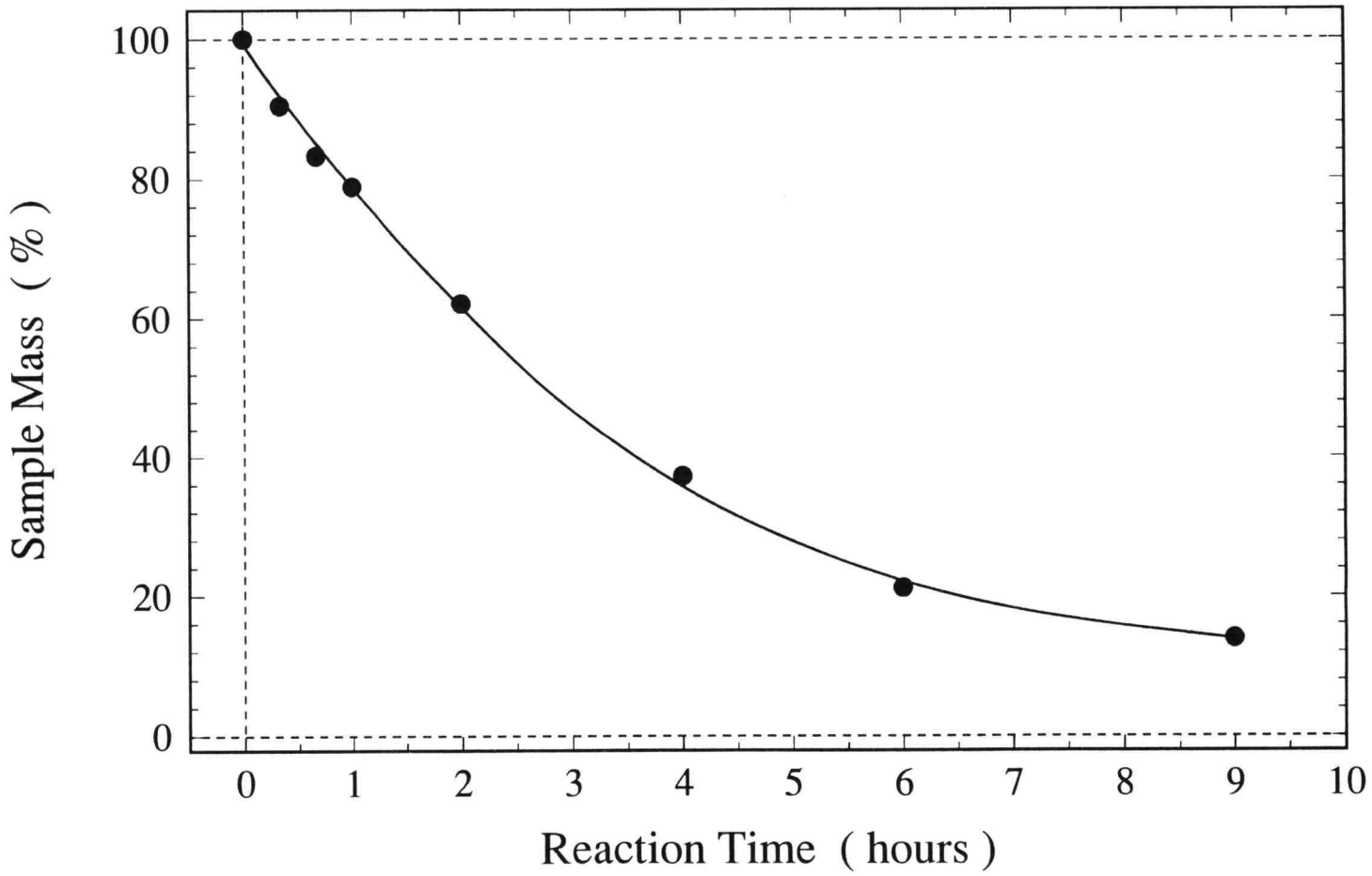

Figure 4.14 SiO generation curve in SiO generator at 1398 °C

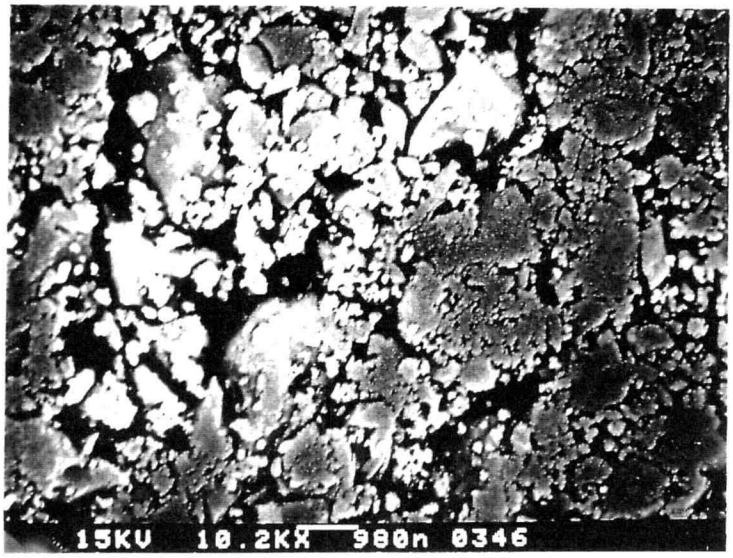

(a) unreacted pellet

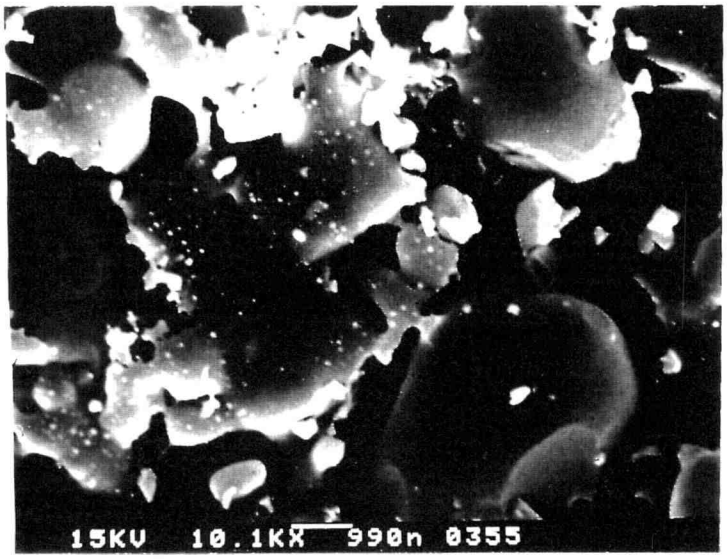

(b) reaction time: 10 minutes at 1300 °C

Figure 4.15 SEM images of reacted pellets, compacted at 526.6 MPa

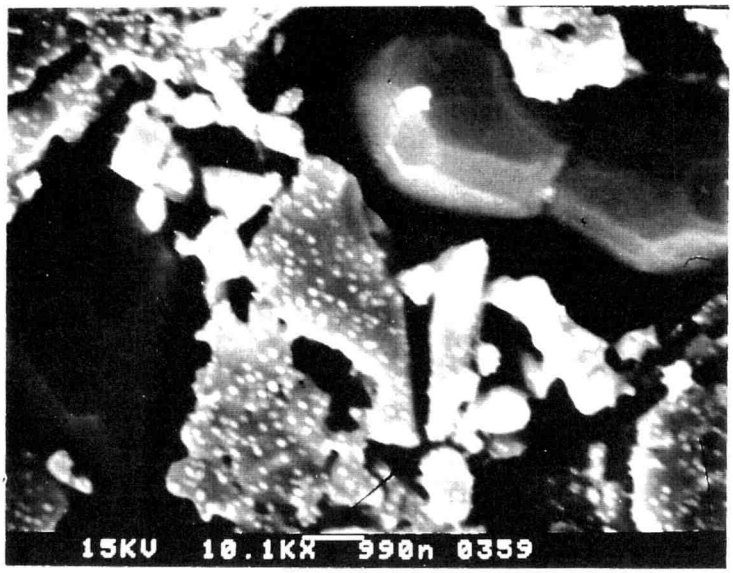

(c) reaction time: 10 minutes at 1350 °C

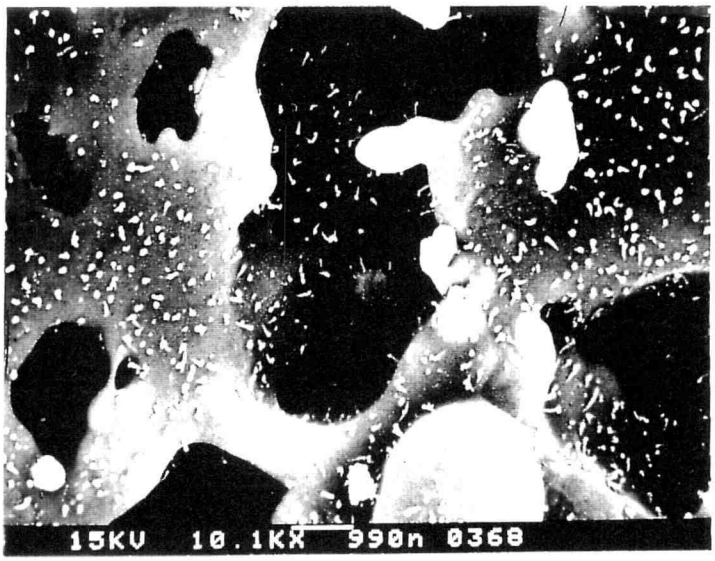

(b) reaction time: 10 minutes at 1400 °C

Figure 4.15 SEM images of reacted pellets, compacted at 526.6 MPa (continued)

reaction, physical contact should dominate the process because the reaction only occurs at the contacting interface of particles. No further reaction will proceed after a certain period of time due to negligible contact between Si and SiO_2 particles in the pellet. However, this assumption is not consistent with the experimental observations. The SiO generations were continuous at given temperatures though the rates decreased with reaction time. Thus, the reaction should not be a pure solid-solid reaction. Gas phase intermediates may be involved for the Si-SiO_2 reaction to proceed.

4.3 Ammonia Dissociation

Being a reactant gas, NH_3 plays an important role in producing Si_3N_4 according to Reaction (2.14). However, the amount of NH_3 entering the reacting zone is unclear due to its dissociation at high temperatures. Thus, a differential flow reactor was designed for determining the kinetics of NH_3 dissociation, as shown in Figure 3.3.

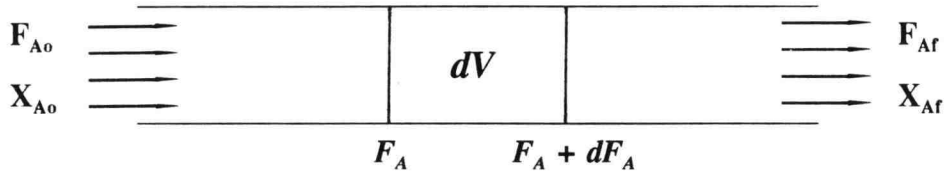

Figure 4.16 Notations for differential flow analysis

4.3.1 Derivation of Ammonia Dissociation Rate

Referring to Figure 4.16, a mass balance about the control volume *dV* can be expressed as

$$\textit{input} = \textit{output} + \textit{dissociation} + \textit{accumulation} \qquad (4.1)$$

where : input of NH_3 (moles/time) = F_A

output of NH_3 (moles/time) = $F_A + dF_A$

dissociation of NH_3 by reaction (moles/time) = $(-r_A)\, dV$

accumulation = 0 for steady state operations

For a gas phase reaction, the dissociation rate may be represented as

$$- r_A = k\, C_A^n \tag{4.2}$$

in which k is the reaction rate constant. Substituting all these terms into Equation (4.1), a differential equation is obtained as

$$F_A = (F_A + dF_A) + (-r_A)\, dV \tag{4.3}$$

or with $F_A = F_{Ao}(1 - X_A)$,

$$- dF_A = - d[F_{Ao} (1-X_A)] = F_{Ao}\, dX_A = (-r_A)\, dV \tag{4.4}$$

where X_A represents the extent of conversion of NH_3 dissociation. Considering the final conversion X_{Af} in the reactor, one can rearrange Equation (4.4) into an integral form.

$$\int_0^V \frac{dV}{F_{A_o}} = \int_0^{X_{A_f}} \frac{dX_A}{-r_A} \tag{4.5}$$

In Equation (4.5), the dissociation rate $(-r_A)$ is a function of concentration, such as Equation (4.2), that can be related to X_A. If the amount of NH_3 dissociation is small, NH_3 concentration can be assumed to be roughly constant in the reactor. Equation (4.5) can then be integrated into a simple form

$$\frac{V}{F_{A_o}} = \frac{X_{A_f}}{- r_{A,ave}} \tag{4.6}$$

or

$$-r_{A,ave} = \frac{F_{A_o} X_{A_f}}{V} \tag{4.7}$$

where $-r_{A,ave}$ is the average reaction rate and is assumed constant under the condition of low conversion of NH_3 in the reactor (practically ≤ 10%).

A series of $-r_{A,ave}$ values can be obtained from Equation (4.7) with different NH_3 inlets (F_{Ao}) at a fixed temperature. The inlet concentration of NH_3 (C_{Ao}) can be changed by adding inert gas into the feeding stream. Also, the outlet concentration of NH_3 (C_{Af}) can be directly measured from the outlet stream by the direct titration method. An average of C_{Ao} and C_{Af} is used to represent the constant concentration ($C_{A,ave}$) in the reactor. Substituting $-r_{A,ave}$ and $C_{A,ave}$ values into Equation (4.2) can determine the reaction order (n) as

$$\ln (-r_{A,ave}) = \ln k + n \ln (C_{A,ave}) \tag{4.8}$$

Thus, the order of NH_3 dissociation (n) is determined based on the slope of $ln(-r_{A,ave})$ versus $ln(C_{A,ave})$ plot.

However, the differential analysis is only suitable when conversions are low. In case of high conversions, the analysis is no longer accurate because it is not appropriate to make the assumption of constant concentration in the reactor. Due to the low conversion constraint, the reaction order should be determined at a low temperature whenever NH_3 dissociation is small in amount. After the reaction order has been determined, rate constant k can be calculated at high temperatures by the direct integral method [Levenspiel, 1972] from Equation (4.5), assuming that the reaction order is independent of temperature.

Due to the volume expansion in NH_3 dissociation, the fractional change (ε_A) in volume has to be considered in the reaction rate. One mole of NH_3 will decompose into 0.5 mole N_2 and 1.5 moles of H_2. Therefore, ε_A is equal to one for pure NH_3 inlets. In an inert-NH_3 mixture, ε_A is calculated on the basis of the following equation:

$$\epsilon_A = \frac{[f_{inert} + 2] - [f_{inert} + 1]}{f_{inert} + 1} = \frac{1}{f_{inert} + 1} \qquad \textbf{(4.9)}$$

where f_{inert} represents the volume ratio of inert gas to NH_3 in the inlet stream. Equation (4.2) can also be expressed in terms of conversion X_A

$$-r_A = k C_A^n = k C_{A_o}^n \left(\frac{1 - X_A}{1 + \epsilon_A X_A} \right)^n \qquad \textbf{(4.10)}$$

Substituting Equation (4.10) into Equation (4.5) gives

$$C_{A_o}^n \, k \, \frac{V}{F_{A_o}} = \int_0^{X_{A_f}} \left(\frac{1 + \epsilon_A X_A}{1 - X_A} \right)^n dX_A \qquad \textbf{(4.11)}$$

At high temperatures, pure NH_3 should be fed into the reactor and the outlet concentration (C_{Af}) and final conversion (X_{Af}) of NH_3 are determined by the titration method.

All variables in Equation (4.11) are known except for the rate constant (k). It should be noted that Equation (4.11) can not be integrated analytically due to the complexity except for special cases. Thus, the rate constant (k) at each temperature shall be calculated from Equation (4.11) with the aid of numerical integration. An Arrhenius-type relationship, $k = k_o \, e^{-E/RT}$, should hold between k and temperature if NH_3 dissociation rate follows Equation (4.2).

In other words, $ln(k)$ is linear with $1/T$, where the slope and intercept are equal to $-E/R$ and k_o, respectively. Thus, further tests on this relationship should be made.

4.3.2 Experimental Results

The kinetics of NH_3 dissociation was determined at temperatures in the range of 1185-1382 °C. Using the differential flow analysis, two series of runs (Table 4.6) were designed to determine the reaction order at 1185 and 1235 °C. The concentration dependency of NH_3 dissociation is shown in Figure 4.17, in which good linearity is observed at 1235 °C as well as at 1185 °C. The regressions indicate that the reaction order is 0.29 at 1185 °C and 0.33 at 1235 °C.

A low reaction order (0.29) implies that the dissociation rate has a low concentration dependency. The non-integer and small values as the order of reaction somewhat indicate that the dissociation process in the Al_2O_3 tube is complex. In this study, however, 1/3 was used to represent the reaction order rather than using 0.29. In using the reaction order of 1/3 instead of 0.29, further tests on the relationship between rate constant k and temperature become important. Therefore, the rate equation for pure NH_3 dissociation ($\varepsilon_A = 1$) can be represented by

$$-r_A = k\, C_A^{1/3} = k\, C_{A_o}^{1/3} \left(\frac{1 - X_A}{1 + X_A} \right)^{1/3} \qquad \textbf{(4.12)}$$

As mentioned earlier, the NH_3 dissociation is complex and may not be a homogeneous gas phase reaction. It is suspected that Al_2O_3 may be involved as a catalyst in the reaction. Under this concern, the catalytic effect of Al_2O_3 on the NH_3 dissociation was also studied. Before each run was initiated, the Al_2O_3 tube was heated at 1400 °C for one hour. After the system was cooled down to an operating temperature, NH_3 was continuously fed into the reactor at a fixed rate. The amount of NH_3 dissociation was also recorded continuously. The changes in NH_3 dissociation with reaction time are shown in Figure 4.18, in which maximum rates are observed around 1 hour after the beginning of NH_3 feeding at all the temperatures. The increase in NH_3 dissociation is significant at temperatures of 1332 and 1382 °C. It is suspected that some intermediates acting as catalysts could be formed on the Al_2O_3 tube surface during the reaction, especially at high temperatures.

Table 4.6 Differential flow analysis of NH_3 dissociation

Temp. (°C)	$(NH_3)_o$ (cm^3/min)★	Ar (cm^3/min)★	$(NH_3)_f$ (cm^3/min)★	X_A	P (atm)	$-r_{A,ave}$ (mole/m^3-sec)	$C_{A,ave}$ (mole/m^3)
1185	2009.6	0	1918.2	0.0455	1.238	10.267	9.90
	1472.5	512.4	1392.5	0.0543	1.238	8.983	7.33
	939.7	1039.6	867.7	0.0767	1.238	8.100	4.64
	660.6	1199.9	592.5	0.1031	1.238	7.650	3.42
	333.1	1357.6	278.5	0.1639	1.238	6.133	1.85
1235	2006.1	0	1798.1	0.1037	1.238	23.350	9.07
	1446.0	512.4	1264.4	0.1256	1.238	20.383	6.65
	875.2	1039.6	714.9	0.1831	1.238	17.983	4.01
	576.6	1199.9	438.5	0.2395	1.238	15.50	2.77

★ : referred to room temperature

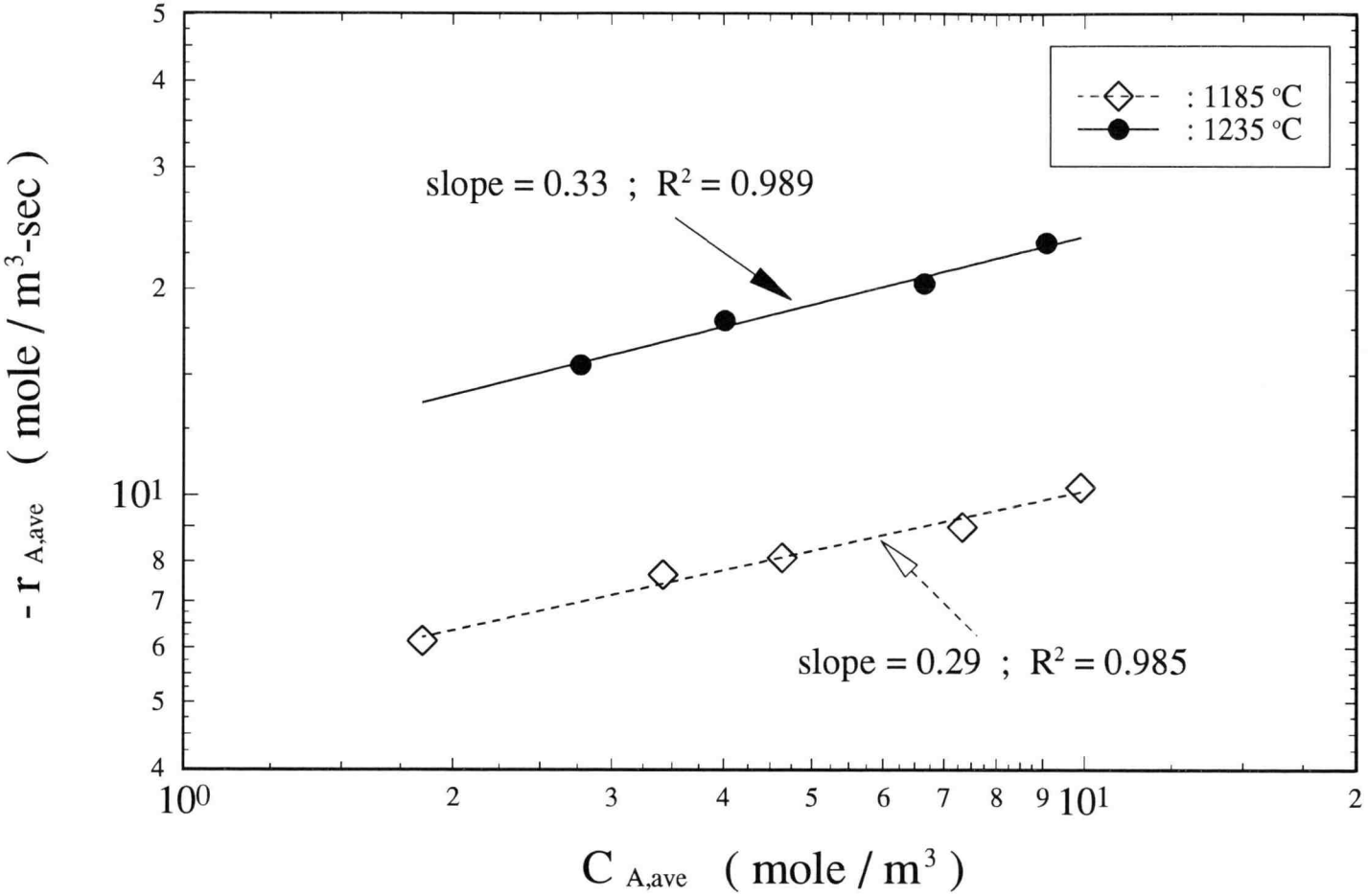

Figure 4.17 Differential flow analysis for determining reaction order of NH_3 dissociation

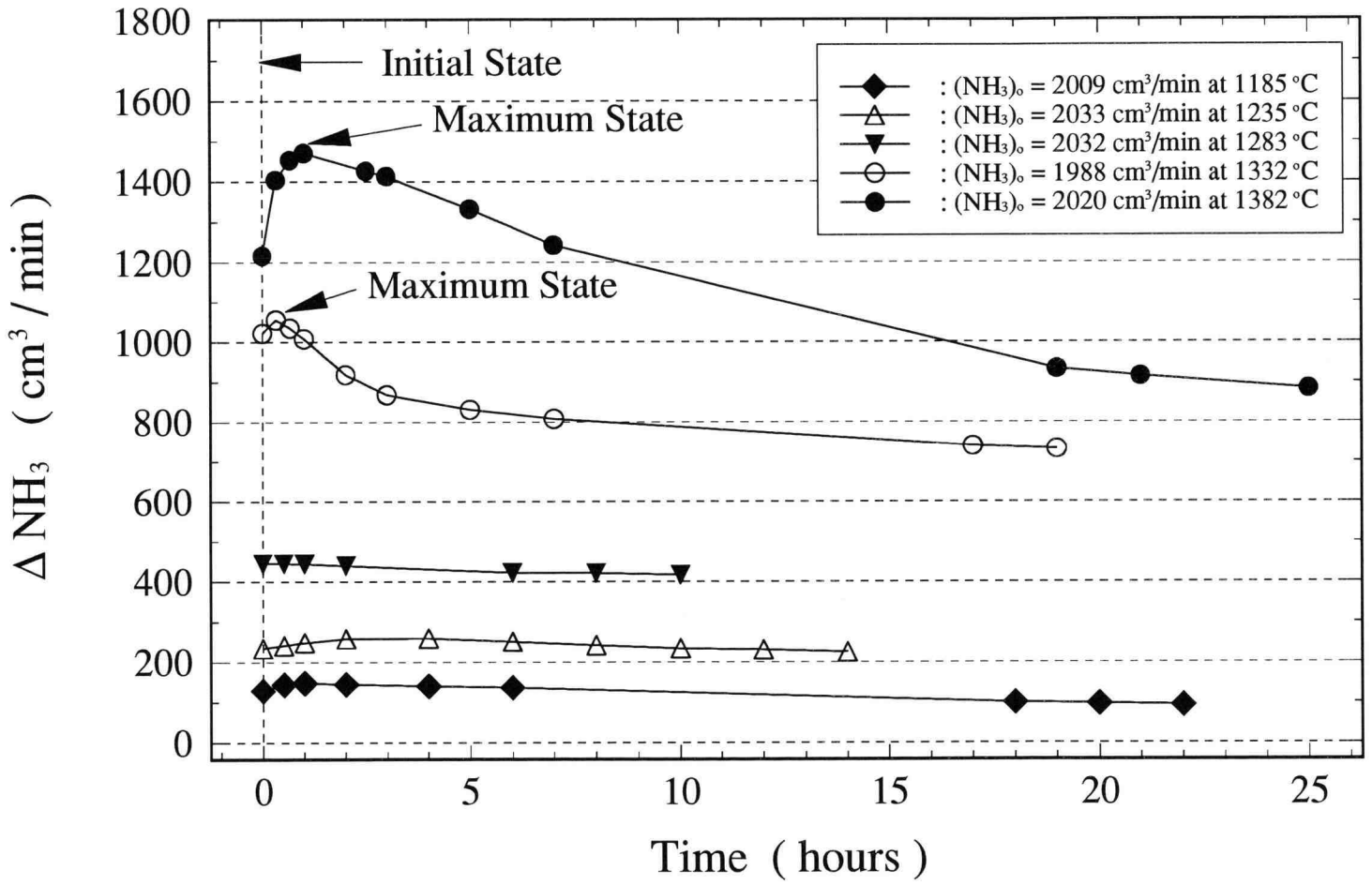

Figure 4.18 Time dependence of NH_3 dissociation rate in Al_2O_3 tube

When the NH_3 dissociation is initiated, some intermediates are supposed to be formed on the Al_2O_3 tube surface immediately. Due to the catalytic activities, the NH_3 dissociation is enhanced during the initial stage. When the surface is saturated with the intermediates, a maximum dissociation rate is reached; after this point, the rate decreases with reaction time because of the activity decay of intermediates.

The Al_2O_3 tube might be changed after the first run owing to the possible formation of intermediates on the surface. Under this concern, the reproducibility was tested using the same tube. After the tube was cooled down to room temperature, the two runs shown in Table 4.6, with pure NH_3 inlet at 1185 and 1235 °C, were repeated. The results showed that the dissociation of NH_3 did not change significantly: only about 1.5 % difference on the basis of the NH_3 inlet. Thus, it is believed that the surface intermediates become unstable whenever temperature is reduced to room temperature, and the Al_2O_3 tube recovers its original conditions.

With Equation (4.11), two levels of dissociation were used as the basis of the integral analysis: the initial extent of dissociation and the maximum extent of dissociation. These values were selected to determine the rate constant k because the SiO-NH_3 reaction was always terminated in 1-4 hours to maintain SiO generation rates roughly constant and the maximum dissociation of NH_3 was observed within the same time periods from the beginning of NH_3 supply. The calculated results are presented in Table 4.7. Figure 4.19 shows the rate constant k plotted against $1/T$, covering the temperature from 1185 to 1382 °C.

The regressions show a good linearity at both the initial and maximum states. The rate constants evaluated from two different levels of dissociation have a roughly identical apparent activation energy of 278 kJ/mole. Hence, the following rate equation based on the average value was used with Equation (4.11) to estimate the amount of NH_3 at the outlet of Al_2O_3 feeder.

$$-r_{NH_3} = 5.236\times10^{10} \times e^{-278/RT} \times C_{NH_3}^{1/3} \quad \left(\frac{mole}{m^3 \times \sec}\right) \qquad (4.13)$$

Table 4.7 Calculated k values on the basis of pure NH_3 inlets ($\varepsilon_A = 1$)

Status	Temperature (°C)	$(NH_3)_o$ (cm^3/min)†	X_{Af}	$Area^{\ddagger} = \int_0^{X_{Af}} \left(\frac{1 + X_A}{1 - X_A}\right)^{1/3} dX_A$	k ($mole^{2/3}/m^2$-sec)
At Initial State	1185	2009.0	0.0641	0.06549	6.7776
	1235	2032.7	0.1151	0.11577	12.2593
	1283	2031.7	0.2192	0.23618	25.2601
	1332	1987.7	0.5146	0.61988	65.5366
	1382	2020.0	0.6023	0.75368	81.8087
At Maximum State	1185	2009	0.0738	0.07568	7.8287
	1235	2032.7	0.1275	0.13309	14.0937
	1283	2031.7	0.2192	0.23618	25.2601
	1332	1987.7	0.5312	0.64435	68.1231
	1382	2020.0	0.7286	0.97052	105.3464

† : referred to room temperature

‡ : calculated numerically by a computer program (given in Appendix B)

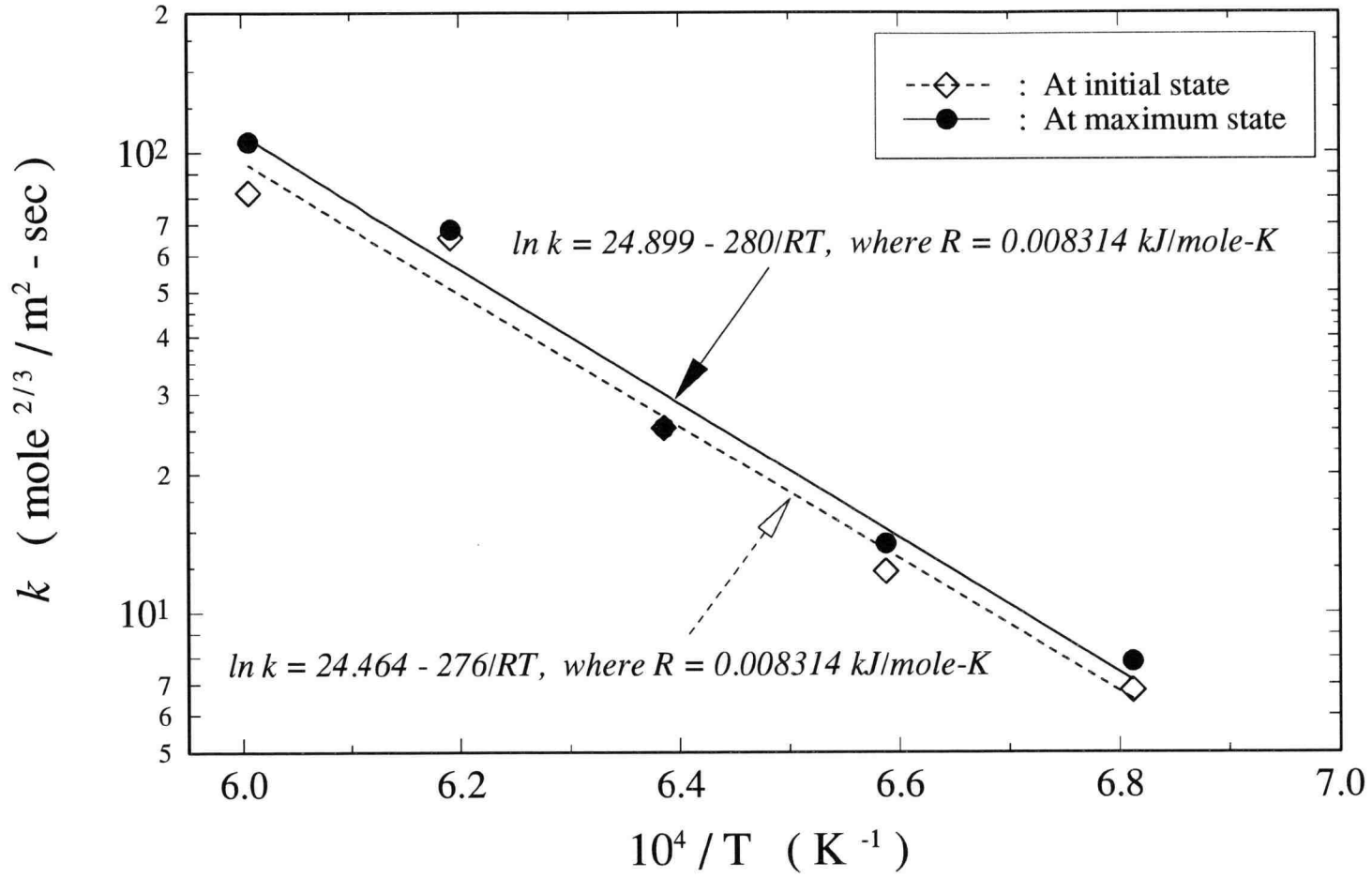

Figure 4.19 Arrhenius-type relationship between rate constant k and temperature

where R is 8.314×10^{-3} kJ/mole-K and T is in K. The apparent activation energy (E) and k_o are 278 kJ/mole and 5.236×10^{10} mole$^{2/3}$/m^2-sec, respectively.

4.4 Silicon Nitride Formation via SiO-NH_3 Reaction

Both the preliminary experiments or thermodynamic studies show that Si_3N_4 is produced from the reaction of NH_3 and SiO. After quantitative studies on the SiO generation and NH_3 dissociation, further kinetic study of the Si_3N_4 formation via Reaction (2.14) was accomplished using a tubular reactor at temperatures in the range of 1300-1400 °C. To supply sufficient NH_3, an Al_2O_3 tube having a small inside diameter was used in the system. It should be mentioned that both bent (30° tilted angle) and straight NH_3 feeders were used in the experiments.

As mentioned in Chapter 4.2, the generation rate of SiO decreases with time but is roughly constant during the initial stage of the reaction. The reaction time in each run was set to be short enough to use the constant rate range. Being critical due to the low rate of SiO generation, the reaction time for each run was set in the range of 1-4 hours depending on the reaction temperature: 1 hour at 1400 °C, 2 hours at 1350 °C, and 4 hours at 1300 °C.

4.4.1 Qualitative Experiments in Tubular Reactor

Several experiments (Table 4.8) using a bent NH_3 feeder were repeated at 1400 °C before the systematic studies were made. The main purpose of these runs was to find possible differences between the reactor (Figure 3.1) used in the preliminary experiments and the one designed for further kinetic studies (Figure 3.4).

These runs were carried out for a long enough time, 1-2 hours, to produce sufficient amounts of product for further analysis. The deposition of product was rather discrete and three different types of product were obtained at different longitudinal locations in the reactor: whiskers at the NH_3 outlet, location 1; crystals right downstream the whiskers, location 2; and very fine powder toward the outlet of

Table 4.8 Qualitative experiments with new tubular reactor at 1400 °C

Run No.†	**Q1400-01**	**Q1400-02**	**Q1400-03**
Compacting Pressure of Sample (MPa)	175.6	0	0
SiO Generation Temperature (°C)	1394	1394	1394
Reaction Temperature (°C)	1398	1398	1398
Reaction Time (hours)	2	1	1
$(dM_{SiO}/dt)_{Ave} \times 10^5$ (mole/min)	4.35	9.23	9.52
Reactant Ratio $(NH_3/SiO)^{\ddagger}$	339	160	155

† : Q in the run number is noted as a qualitative experiment

‡ : estimated by Equation (4.13)

the reactor, location 3 and the filter. The distributions of product, correlated to temperature profiles, are shown in Figure 4.20. It should be mentioned that the formation locations of whiskers and crystals imply that the SiO-NH_3 reaction is fast and may be instantaneous.

Location 1 is in the uniform temperature zone and location 2 extends slightly outside the uniform temperature zone to the place where the temperature decreases by about 50 °C. Location 3 is outside the reactor heating zone where temperature is below 300 °C. The new findings of crystals and fine powder formation in the SiO-NH_3 reaction result from the improved method for collecting the products, *i.e.*, using a set of short sampling tubes and a paper-filter.

A comparison between Figure 4.2 and Figure 4.21 indicates that the whiskers obtained in the reaction are also Si_3N_4, represented by the broad peak at wavenumbers between 850 and 1000 cm^{-1}. However, one hump is also seen at a wavenumber about 1050 cm^{-1} in Figure 4.21(a), which may be attributed to the Si-O bonding [Baraton *et al.*, 1982; Schalch *et al.*, 1985 and 1987; Sekine and Katayama, 1987]. Similar results are seen in the IR spectrum of filter-collected fine powder. As shown in Figure 4.21(c), both the Si-N and Si-O bonding are found at the same locations as those seen in the curve (a). It is believed that the whiskers obtained in these three runs have higher oxygen contents than those formed in the preliminary experiments due to the presence of Si-O bonding. However, crystalline Si-N bonding has been seen in Figure 4.21(b). The crystals are believed to be α-Si_3N_4 with low content of oxygen because of the absence of both the Si-O bonding and the characteristic peak of β-form in the plot.

According to the IR analysis, the whiskers and fine powder produced in the new reactor also contain Si_3N_4 product. Referring to Figure 4.2, one may find that the whiskers obtained in the preliminary experiments are α-Si_3N_4 crystals because of the presence of sharp peaks in the IR spectrum [Luongo, 1983]. Since no crystalline peak appears in Figures 4.21(a) and (c), these two products are believed to be amorphous.

In the preliminary experiments, the reaction time of each experiment was set for about 15 hours at 1350 °C. The amorphous whiskers may have had a chance of

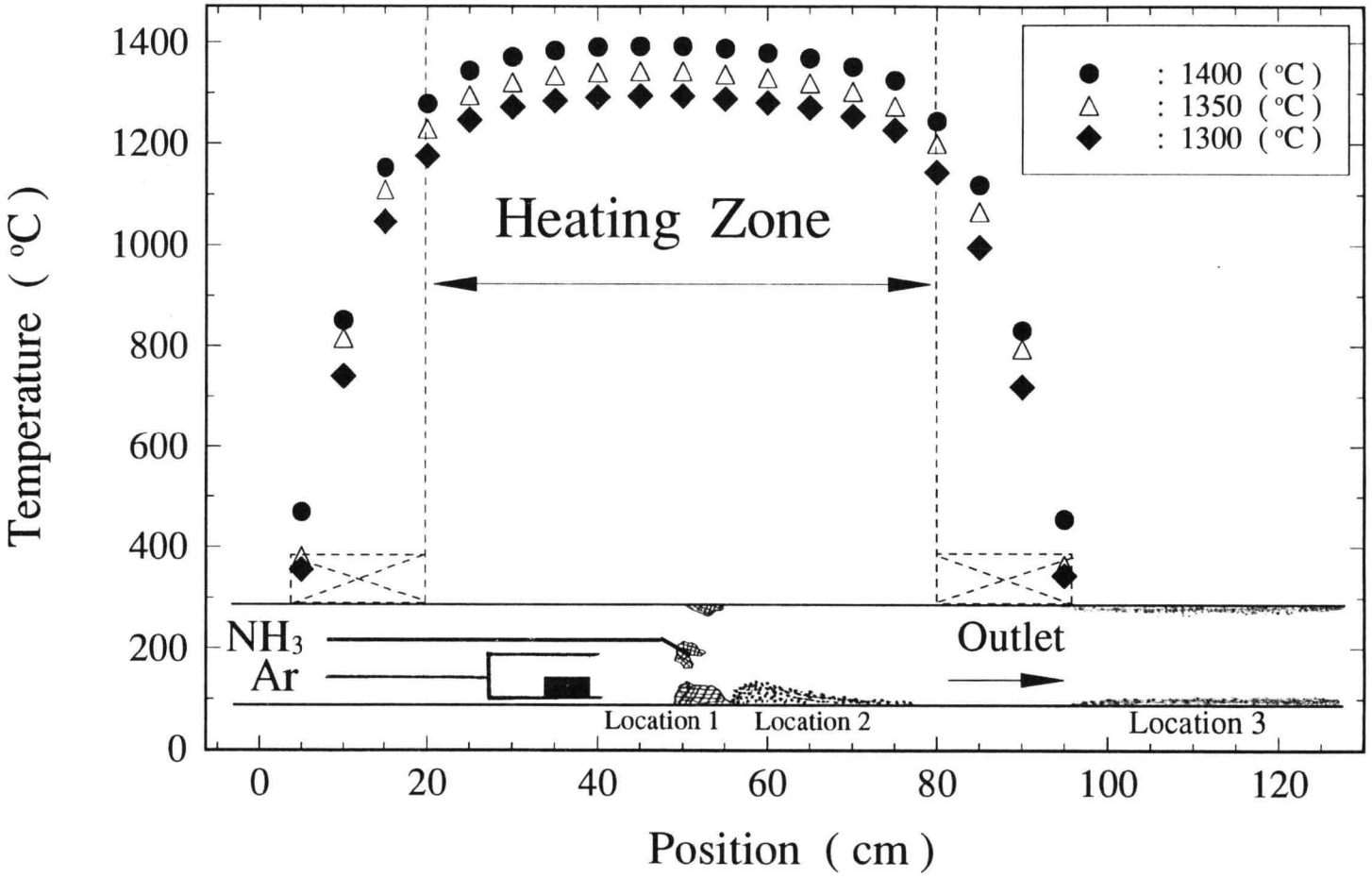

Figure 4.20 Product distributions via SiO-NH_3 reaction in tubular reactor

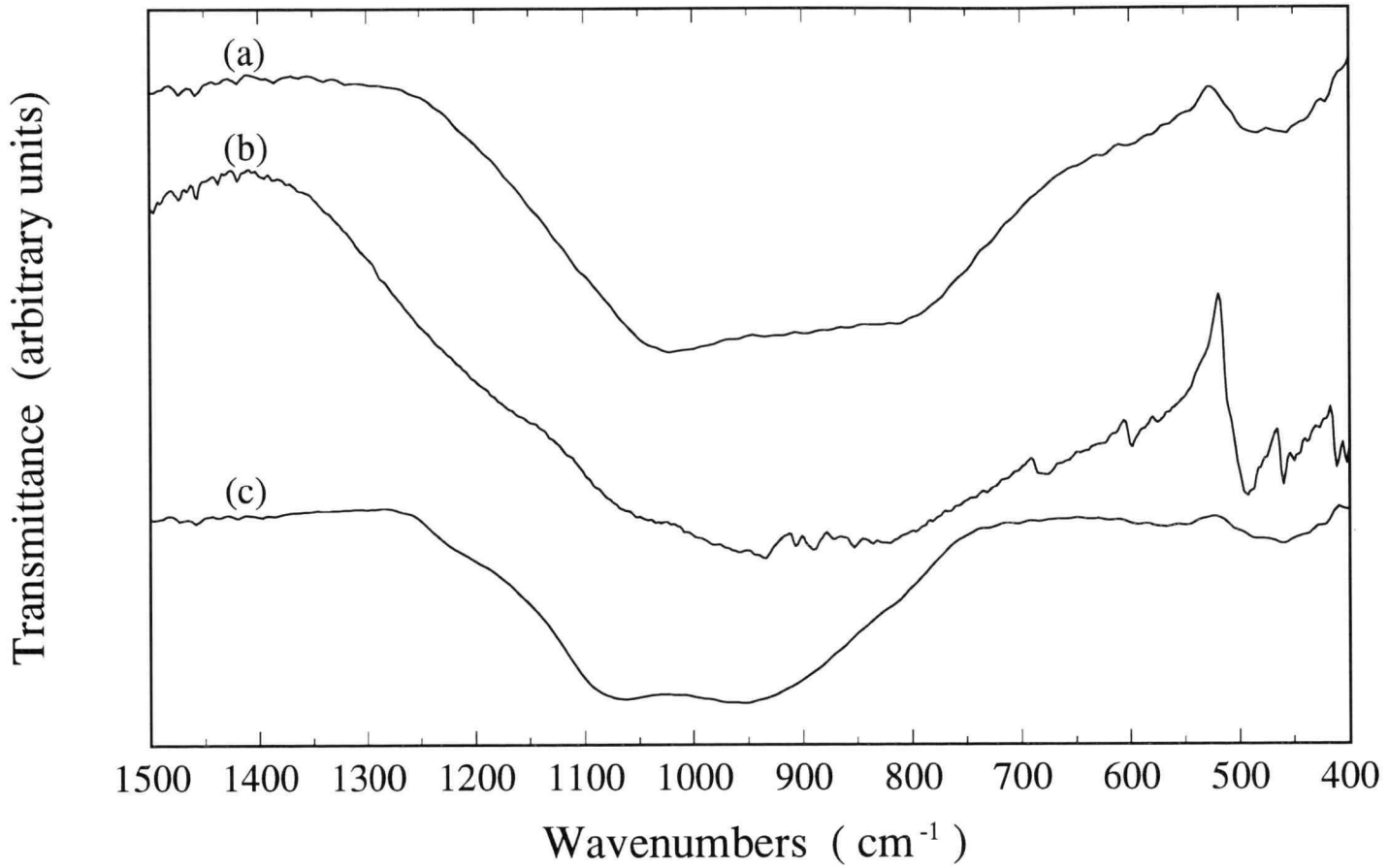

Figure 4.21 IR spectra of products formed in qualitative experiments at 1400 °C: (a) whiskers, (b) crystals, (c) filter-collected powder

being exposed to the dissociated NH_3 stream for a long time after the synthesis, leading to the progress of crystallization.

4.4.2 Quantitative Studies of SiO-NH_3 Reaction

Table 4.9 summarizes the distributions of product varying with reaction conditions. It should be mentioned that the molar NH_3/SiO feeding ratio in each run, estimated based on the kinetics of NH_3 dissociation obtained in Chapter 4.3, is in large excess of stoichiometric ratio. As seen in Table 4.9, the most favored product in the system is in the form of crystals, followed by either fine powder or whiskers.

The IR spectra of products are shown in Figures 4.22(a)-(c), which are similar to those observed in the qualitative study. According to the IR analysis, the whiskers and fine powder obtained at each temperature are amorphous. Not only the Si-N bonding (850-1000 cm^{-1}) but the Si-O bonding (about 1050 cm^{-1}) are clearly seen in the IR spectra. However, it is noteworthy that the Si-O bonding is not significant in the IR spectra of crystals formed in all the runs with using a bent NH_3 feeder. Also, the characteristic peak of β-form at 1040 cm^{-1} is not seen in the plot, implying that the crystals may be close to pure α-Si_3N_4.

4.4.2.1 Mass Distribution of Product in Reactor

Figure 4.20 shows the product distributions in the tubular reactor qualitatively. More precisely, the percentage of product mass precipitated in each sampling tube is shown in Figures 4.23(a)-(e). It is noteworthy that product collected by each sampling tube has roughly the same percentage though $(dM_{SiO}/dt)_{Ave}$ is increased in each series of runs. The results imply that the amount of product collected by each sampling tube is roughly proportional to $(dM_{SiO}/dt)_{Ave}$.

In all the runs, more than 50 wt% of the total products was collected by the sampling tube #1, the place of NH_3 outlet. A comparison of Figures 4.23(c) and

Table 4.9 Si_3N_4 synthesis and its distribution via SiO-NH_3 reaction in tubular reactor

Run No.*	CP† (MPa)	T_{SiO} (°C)	$T_{Reaction}$ (°C)	$(dM_{SiO}/dt)_{Ave} \times 10^4$ (g/min)	Molar Ratio $(NH_3/SiO)^{\#}$	Whiskers (wt%)	Crystal (wt%)	Fine Powder (wt%)	$(dM_{prd}/dt)_{Ave} \times 10^4$ (g/min)
B1400-01	526.7	1390	1394	16.83	594	10.2	65.8	24	17.25
B1400-02	175.6	1392	1395	21.27	470	15.8	65.3	18.9	21.46
B1400-03	0	1391	1394	31.86	314	18.7	68.7	12.6	33.59
S1400-01	526.7	1395	1400	15.69	582	20.0	66.7	13.3	16.53
S1400-02	175.6	1395	1400	16.04	569	16.4	66.5	17.1	15.52
S1400-03	0	1395	1400	30.33	301	23.4	61.8	14.8	28.93
B1350-01	175.6	1342	1345	9.21	1734	14.7	66.3	19	9.34
B1350-02	175.6	1343	1345	10.82‡	1476	9.4	68	22.6	11.45
B1350-03	0	1342	1344	11.32	1411	13.7	67.2	19.1	11.88
S1350-01	175.6	1351	1352	6.19	2440	≈ 0	64.3	35.7	6.24
S1350-02	0	1351	1353	10.92	1383	2.5	54.5	43	10.96
S1350-03	175.6	1351	1352	12.65‡	1194	5.9	52.5	41.6	13.20

Table 4.9 Si_3N_4 synthesis and its distribution via SiO-NH_3 reaction in tubular reactor (continued)

Run No.★	CP† (MPa)	T_{SiO} (°C)	$T_{Reaction}$ (°C)	$(dM_{SiO}/dt)_{Ave} \times 10^4$ (g/min)	Molar Ratio (NH_3/SiO)♯	Whiskers (wt%)	Crystal (wt%)	Fine Powder (wt%)	$(dM_{prd}/dt)_{Ave} \times 10^4$ (g/min)
S1300-01	526.7	1301	1305	3.13	6247	1.3	86.1	12.6	2.95
S1300-02	175.6	1301	1305	3.55	5508	6.3	78.2	15.5	3.63
S1300-03	0	1301	1305	5.27	3710	3.7	77.1	19.2	5.35

★ : B ≡ tilted nozzle, S ≡ straight nozzle

† : CP ≡ pellet compacting pressure

‡ : two compacted pellets used

♯ : molar ratios of NH_3 and SiO are calculated by the computer program shown in Appendix C

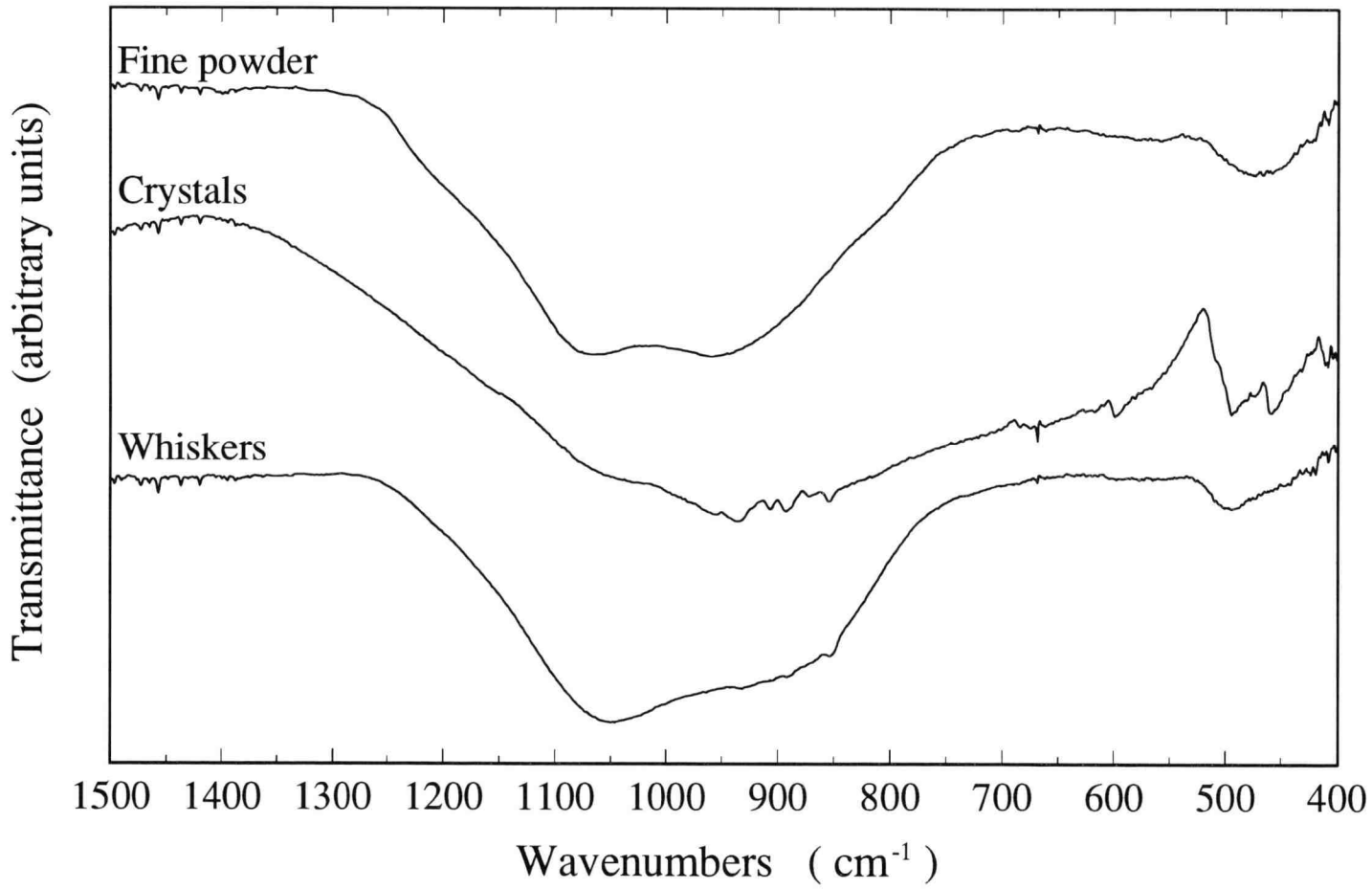

Figure 4.22(a) IR spectra of products formed at 1400 °C: (a) whiskers, (b) crystals, (c) fine powder

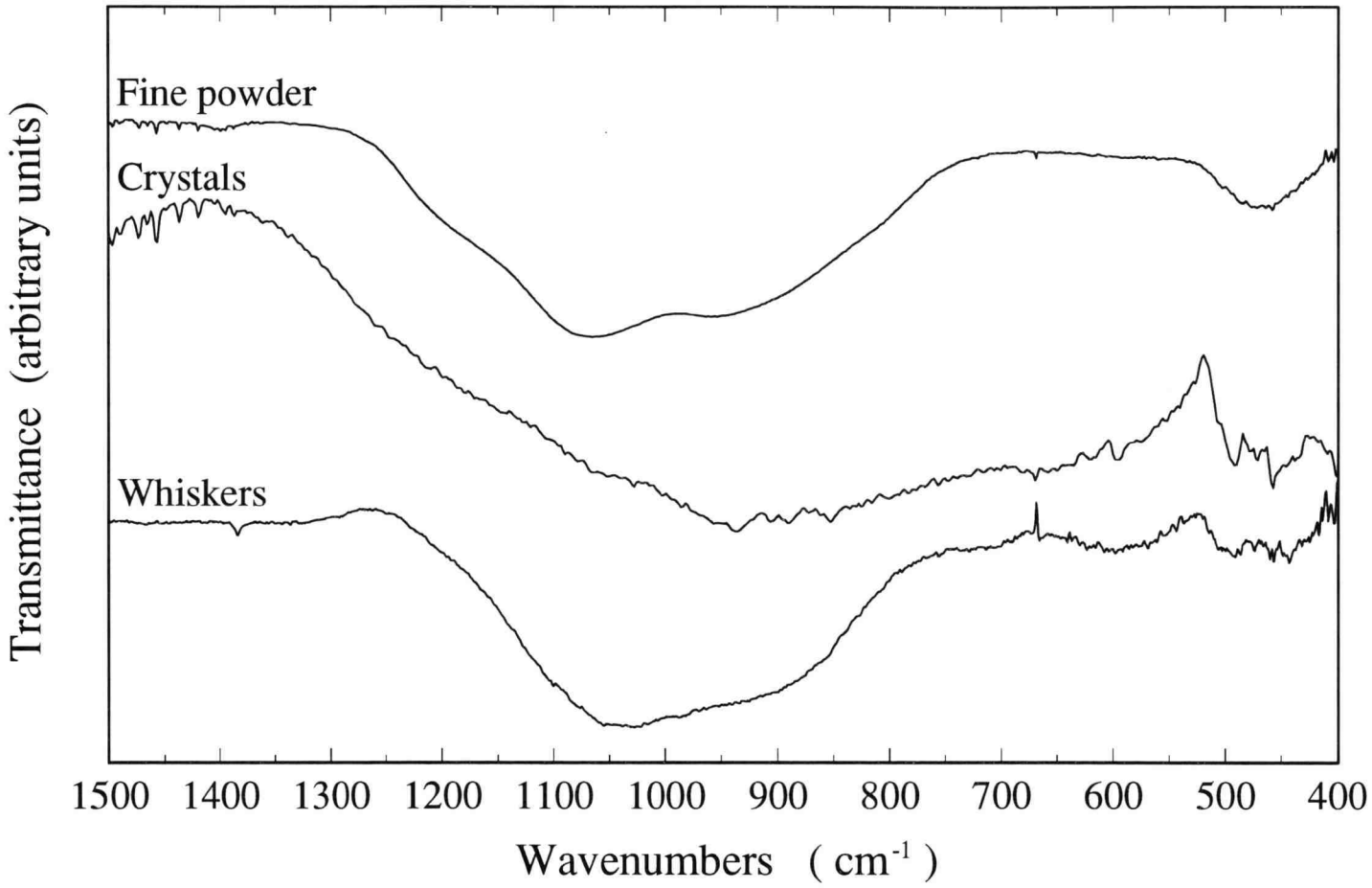

Figure 4.22(b) IR spectra of products formed at 1350 °C: (a) whiskers, (b) crystals, (c) fine powder

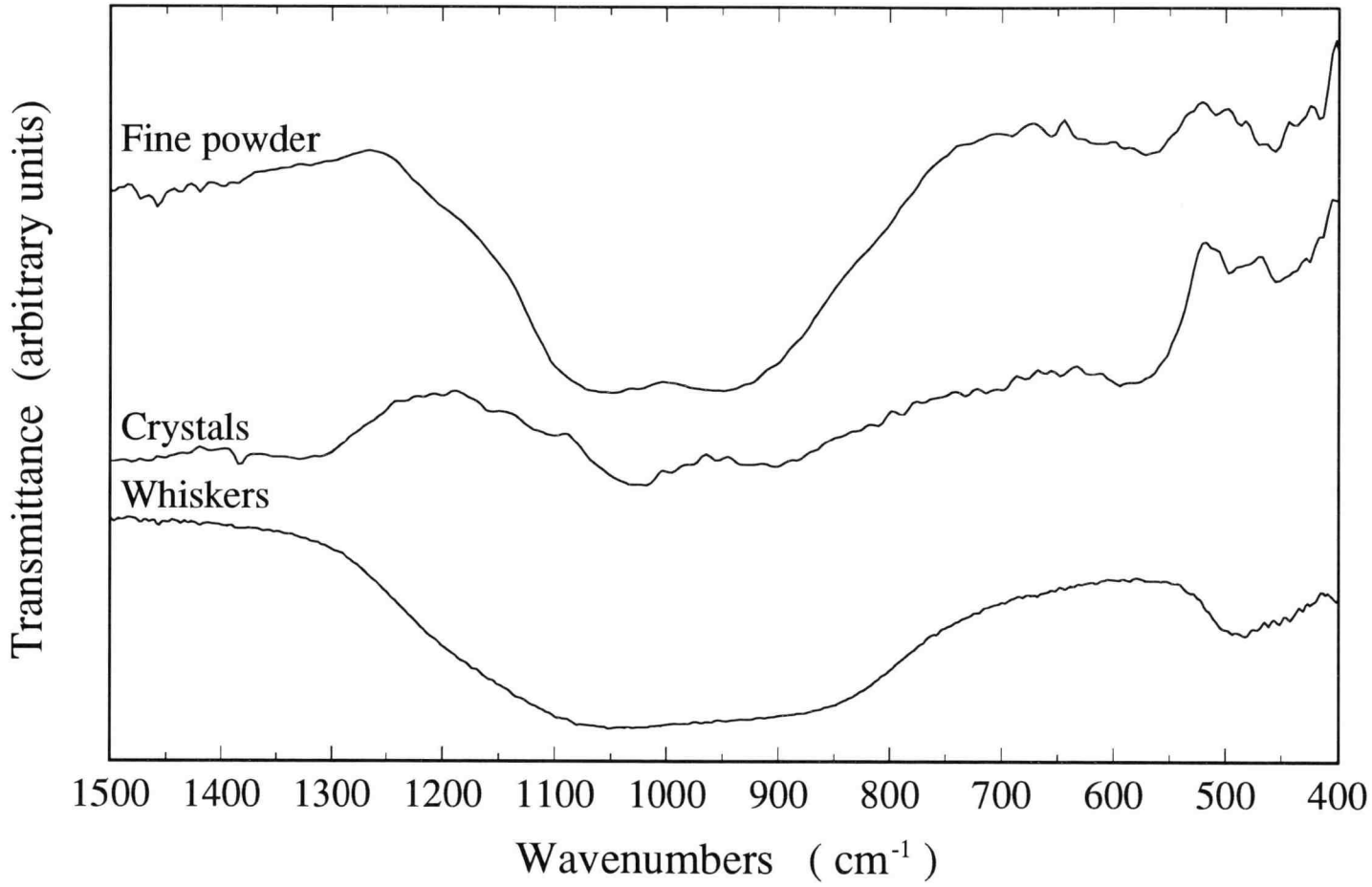

Figure 4.22(c) IR spectra of products formed at 1300 °C: (a) whiskers, (b) crystals, (c) fine powder

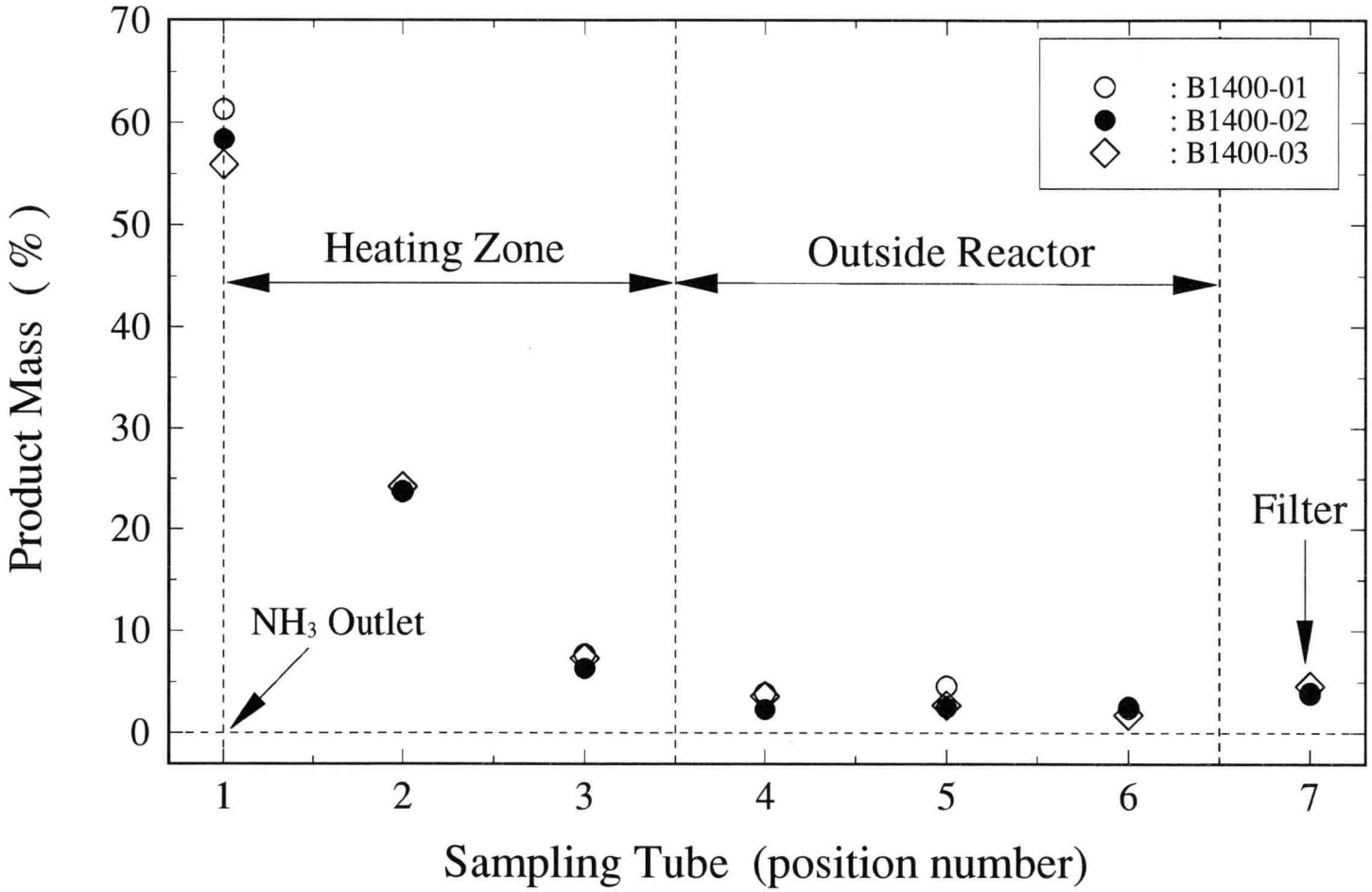

Figure 4.23(a) Mass distribution of products in tubular reactor at 1400 °C, using a bent NH_3 feeder

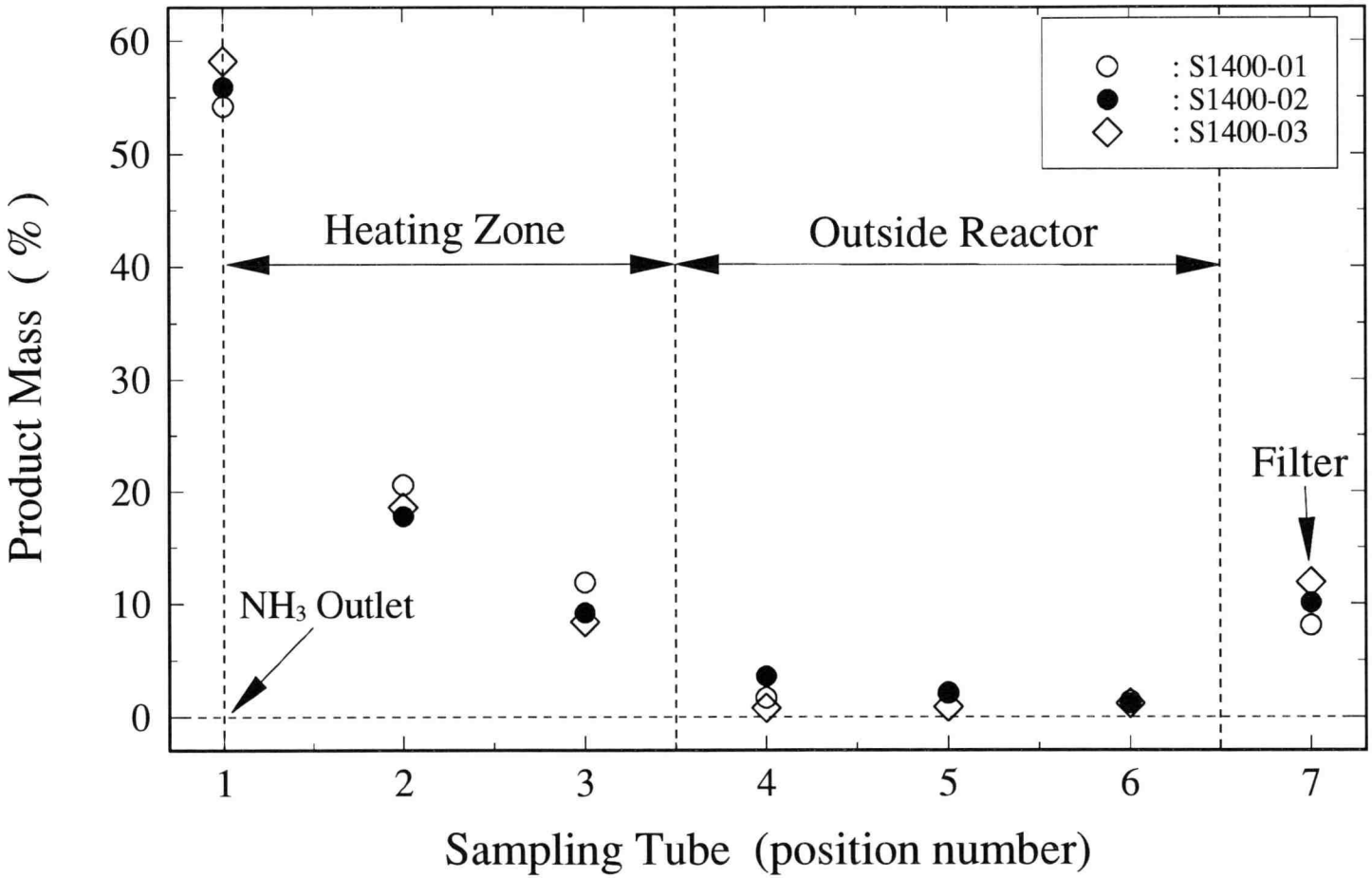

Figure 4.23(b) Mass distribution of products in tubular reactor at 1400 °C, using a straight NH_3 feeder

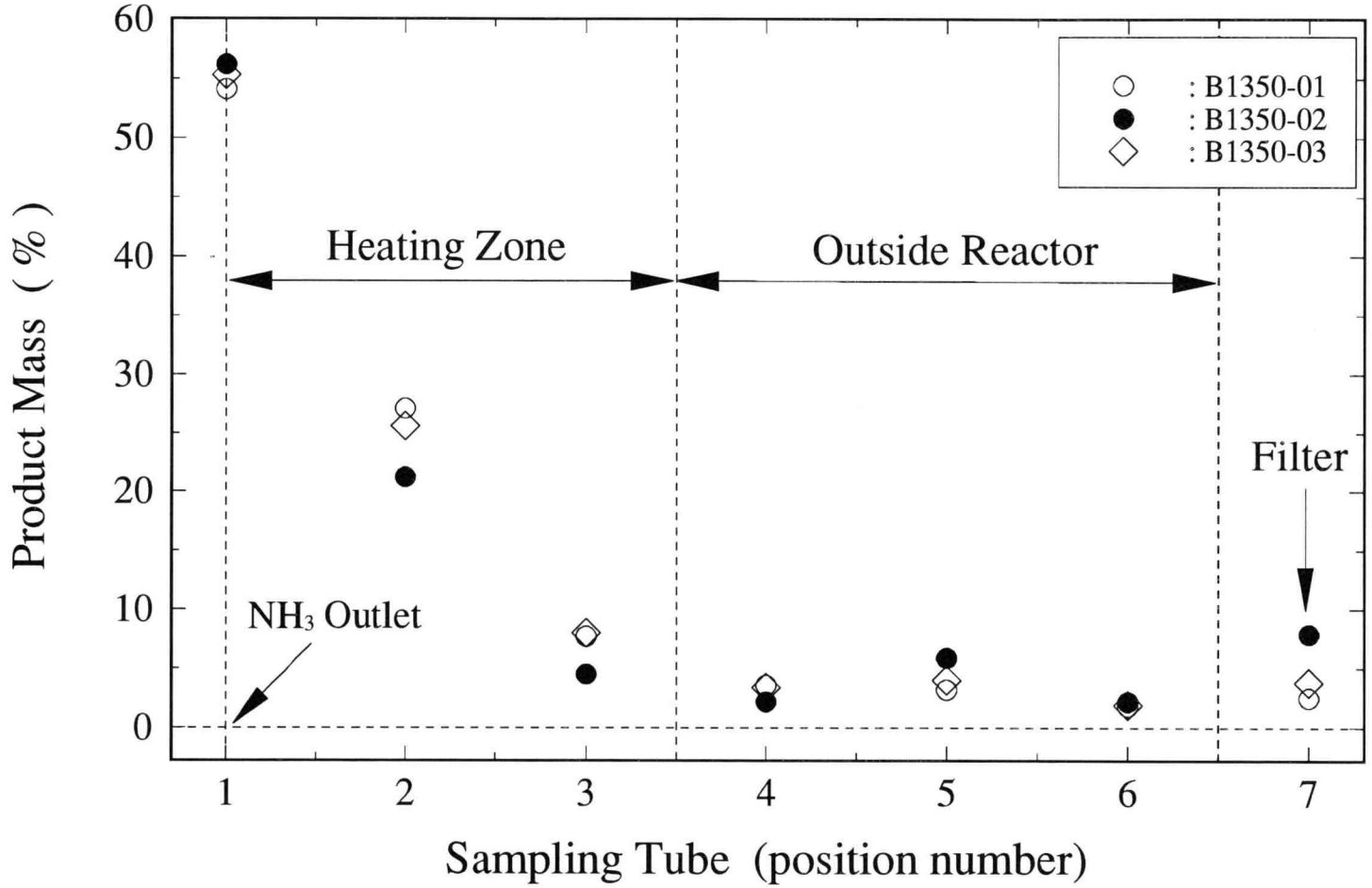

Figure 4.23(c) Mass distribution of products in tubular reactor at 1350 °C, using a bent NH_3 feeder

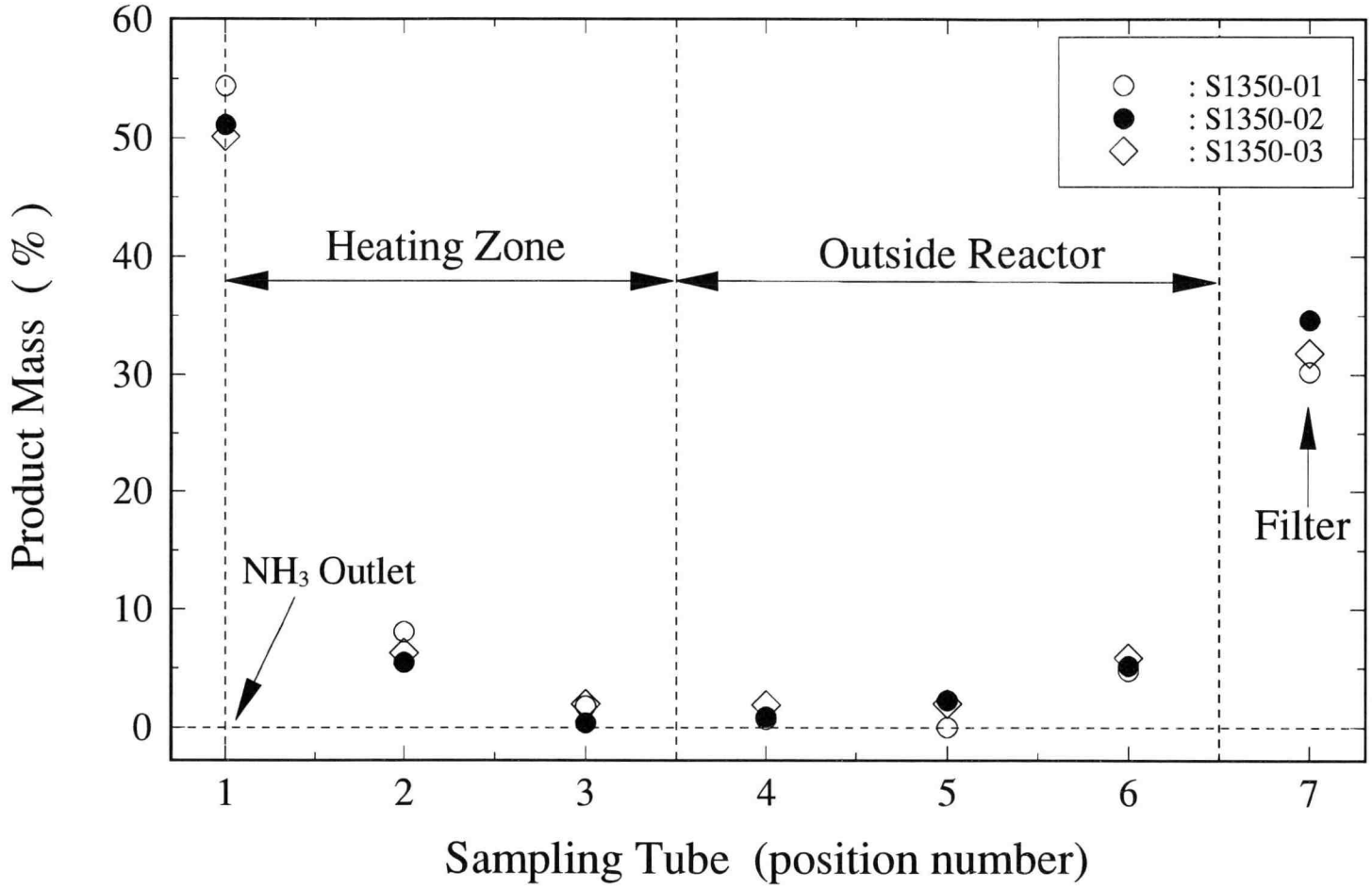

Figure 4.23(d) Mass distribution of products in tubular reactor at 1350 °C, using a straight NH_3 feeder

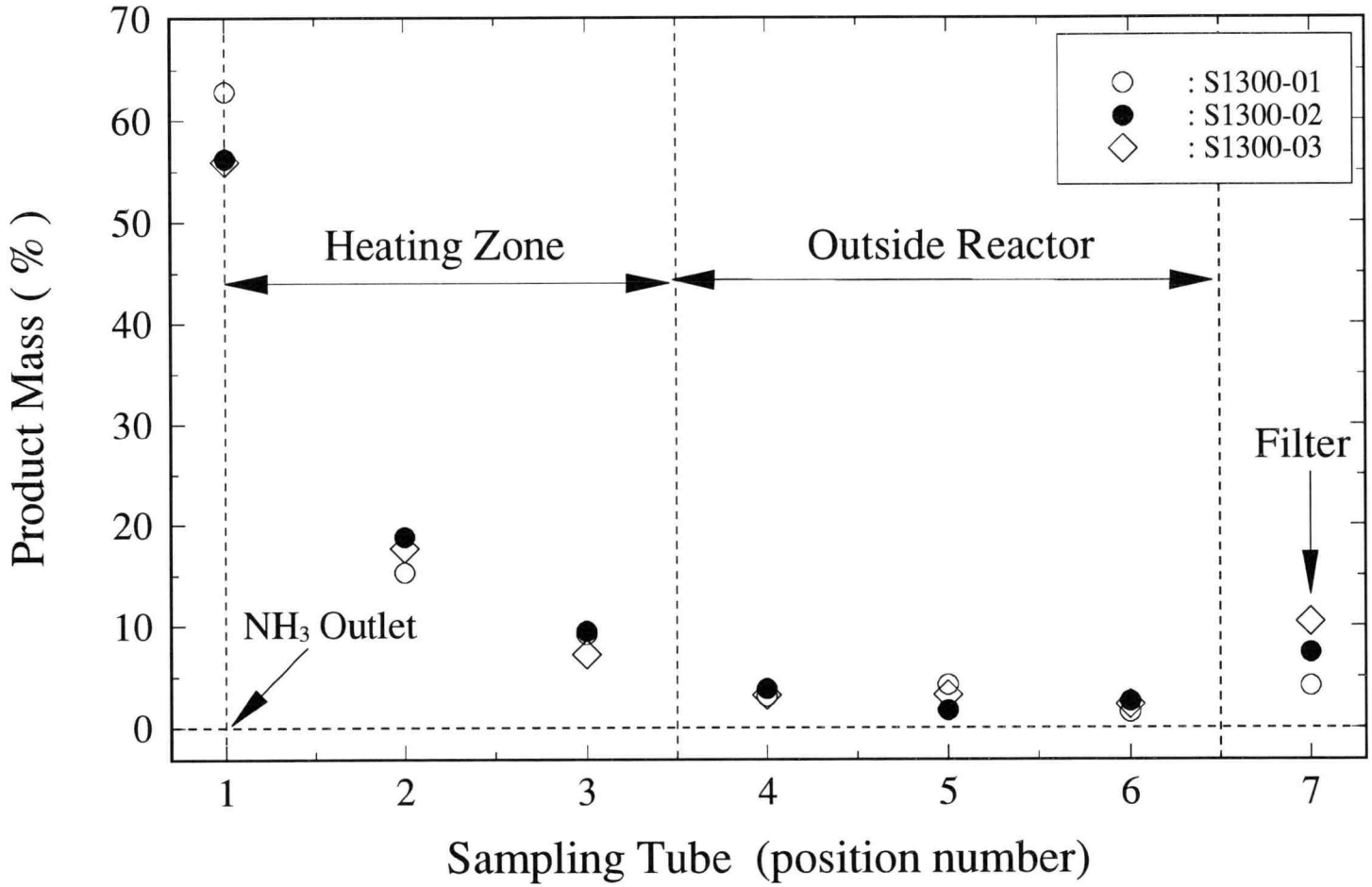

Figure 4.23(e) Mass distribution of products in tubular reactor at 1300 °C, using a straight NH_3 feeder

4.23(d) shows a dramatic increase in the filter-collected powder when a straight NH_3 feeder is used at 1350 °C. However, the change of product distribution is not significant though the straight feeder is used at 1400 °C.

4.4.2.2 Product Morphology

Scanning electron microscopy (SEM) and transmission electron microscopy (TEM) were used to identify the morphology of products. Not only the product shape but also its size are of interest in the analysis.

Figure 4.24(a) shows the SEM images of unheated whiskers with variety of shapes and diameters, ranging from about 0.5 to about 4 μm. These whiskers are amorphous as indicated by XRD charts shown in Figure 4.25(a), which is consistent with their IR spectra. Figure 4.24(b) shows the SEM images of crystals, that precipitated on the reactor wall at location 2. The product is an assembly of ploycrystals of pure α-Si_3N_4, as shown in Figure 4.25(b). The TEM images of unheated powder collected by the filter are shown in Figure 4.24(c), suggesting that the powder is composed of about 20 nm average-sized grains. This nanophase powder is also amorphous, as shown in Figure 4.25(c).

Without exposing to air, the whiskers and nanophase powder were crystallized in a N_2 stream at 1560 °C for 2 hours. The SEM images of crystallized whiskers and nanophase powder are shown in Figure 4.24(d) and (e), respectively. It is seen that whiskers keep roughly their original shapes even after the crystallization. However, nanophase powder is no longer spherical after being crystallized. The powder has turned into aggregates, probably due to sintering during the crystallization. A lower temperature or shorter residence time may be needed to inhibit the morphology change of such fine powder in the crystallization.

An attempt was made to reduce the aggregation of nanophase powder for its crystallization. The powder was crystallized at lower temperature of 1300 °C in a dissociated NH_3 stream for 5 hours. The SEM images of heated powder are shown in Figure 4.24(f), composed of about 100 nm clusters. A comparison between Figures

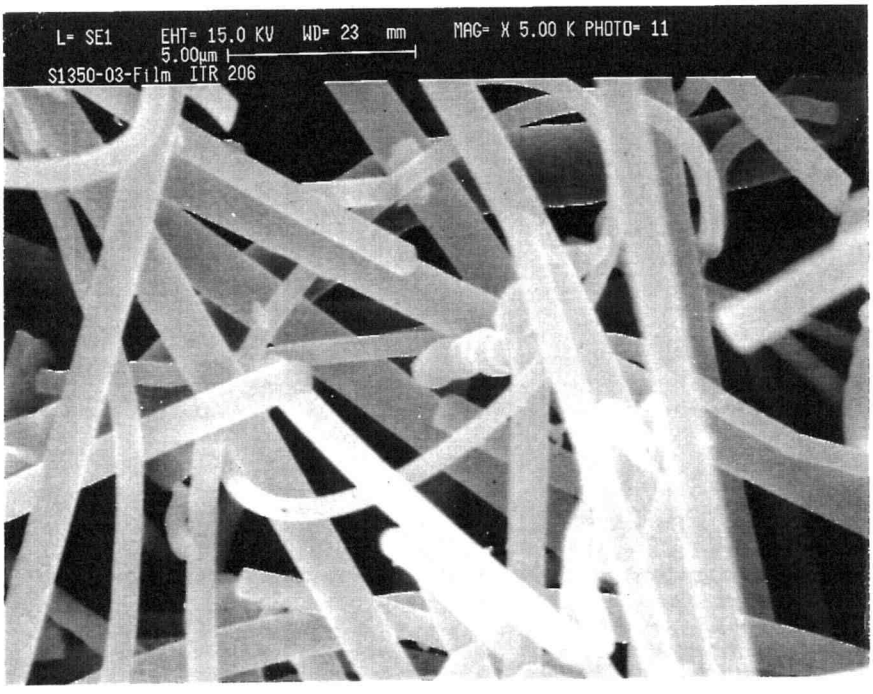

Figure 4.24(a) SEM images of whiskers

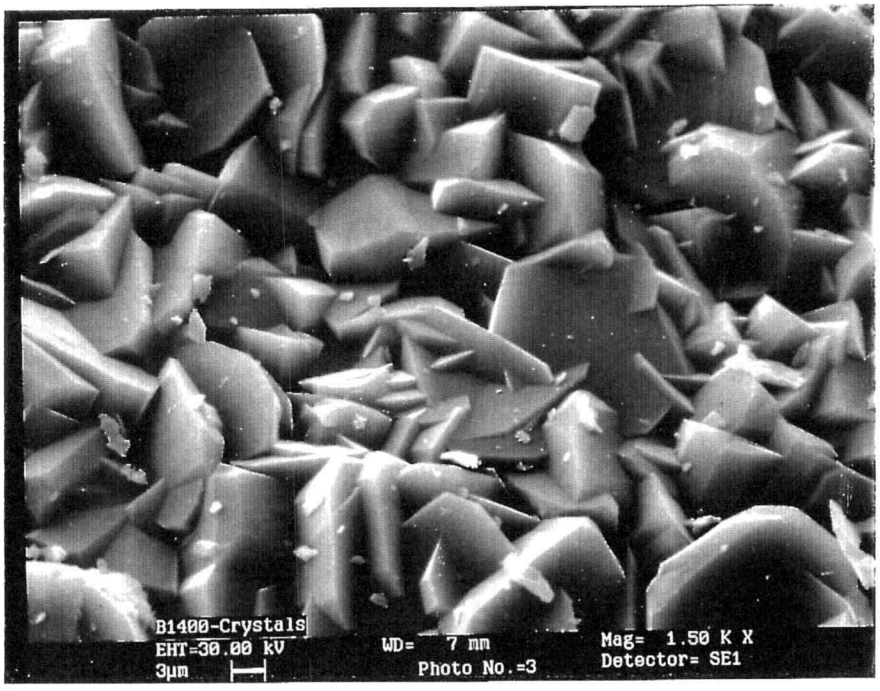

Figure 4.24(b) SEM images of crystals

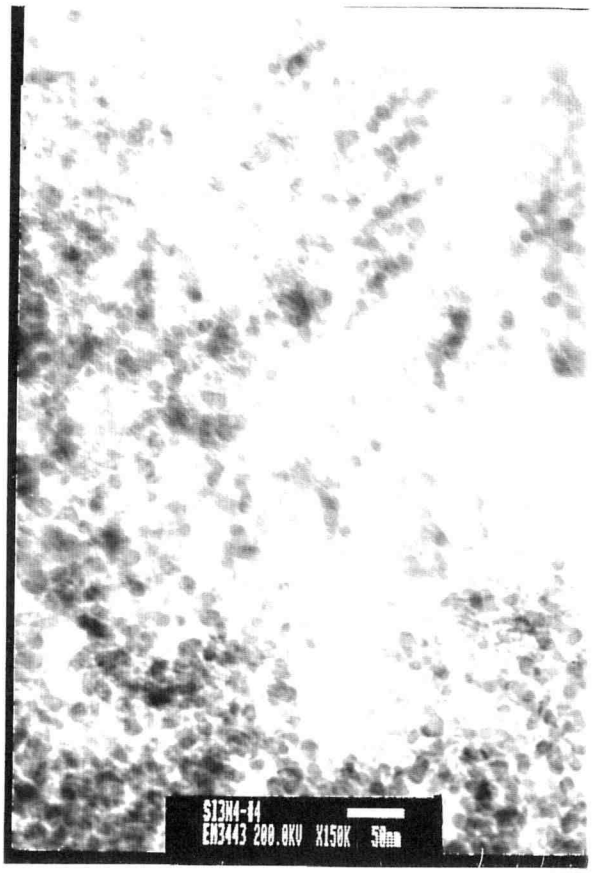

Figure 4.24(c) TEM images of filter-collected powder

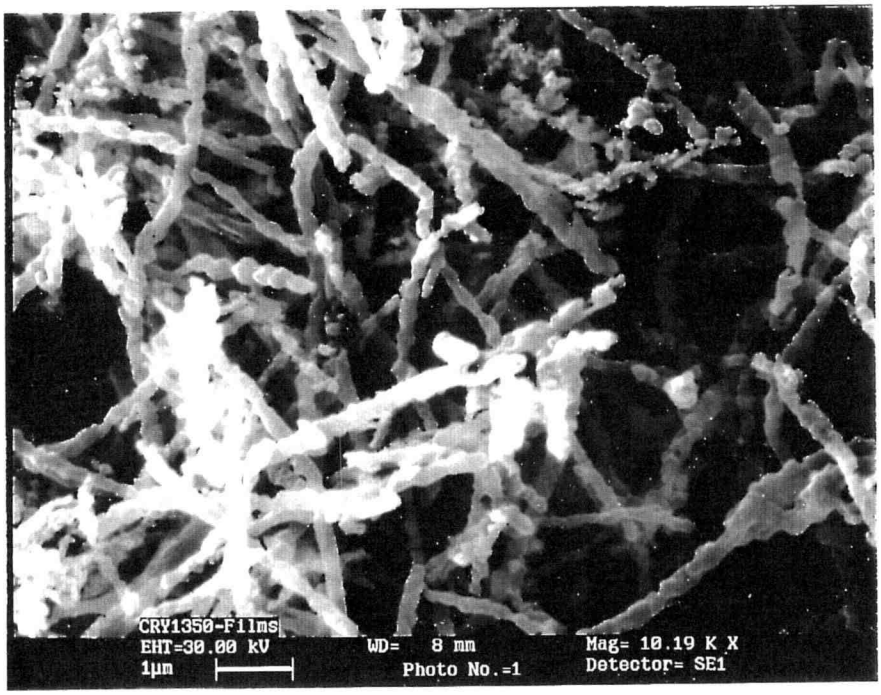

Figure 4.24(d) SEM images of crystallized whiskers

Figure 4.24(e) SEM images of crystallized nanophase powder

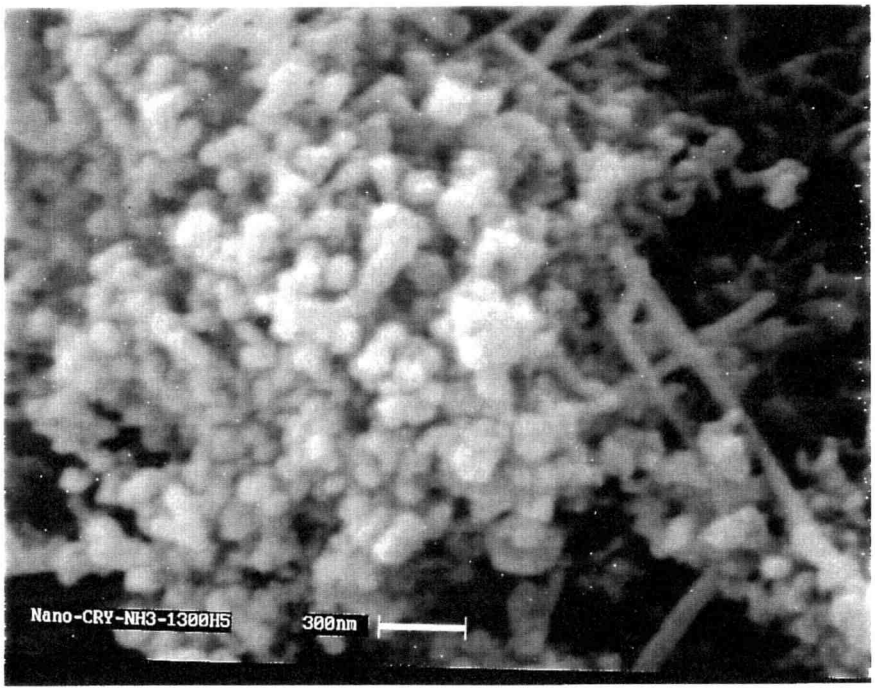

Figure 4.24(f) SEM images of crystallized nanophase powder

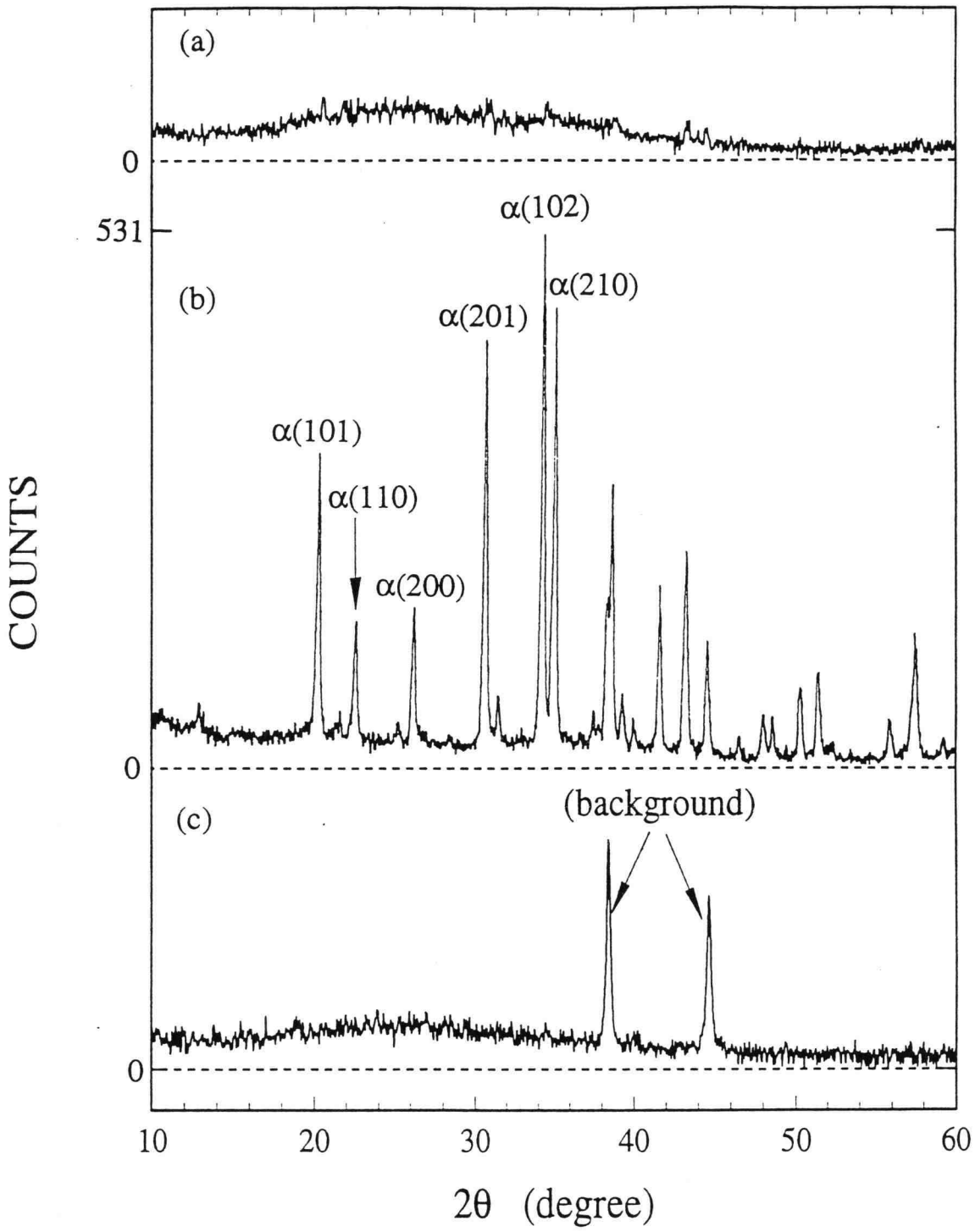

Figure 4.25 XRD charts of unheated products formed at 1400 °C: (a) whiskers, (b) crystals, (c) nanophase powder

4.24(e) and (f) indicates that the aggregation of powder was significantly reduced under the operating conditions.

4.4.2.3 Product Composition

X-ray diffraction has shown that the whiskers and nanophase powder are both amorphous silicon nitride. IR and element analyses were hence used to characterize the products in these two forms. Figure 4.22 has shown Si-N bonding in the region between 850 and 1000 cm^{-1}. However, Si-O bonding is also seen at a wavenumber of about 1050 cm^{-1} in the IR spectra of whiskers and nanophase powder at any given temperatures. It should be noted that this Si-O bonding is not found in Figure 4.2, where the whiskers were crystallized due to a long exposure time under dissociated NH_3 at 1350 °C after the synthesis.

It has been reported that amorphous Si_3N_4 is easily oxidized by the ambient oxygen/moisture in air [Yamada, 1993; van Weeren *et al.*, 1993]. Thus, an attempt was made to clarify this oxidation effect. After being synthesized, amorphus whiskers and nanophase powder were crystallized in the reactor without exposing to air before the crystallization. The IR analysis of the crystallized products is shown in Figure 4.26. No Si-O bonding is found in the IR spectra of products, which is similar to the result shown in Figure 4.2.

The oxygen contents of amorphous products also showed an increase with time, i.e., 8.8 wt% in three weeks and up to 17 wt% in three months after the synthesis. As given in Table 4.1, the oxygen content of crystallized whiskers, without exposing to air before the crystallization, is only 1.6 wt% in mass. Therefore, the Si-O bonding observed in unheated amorphous products is considered to have formed because of the oxygen/moisture in air.

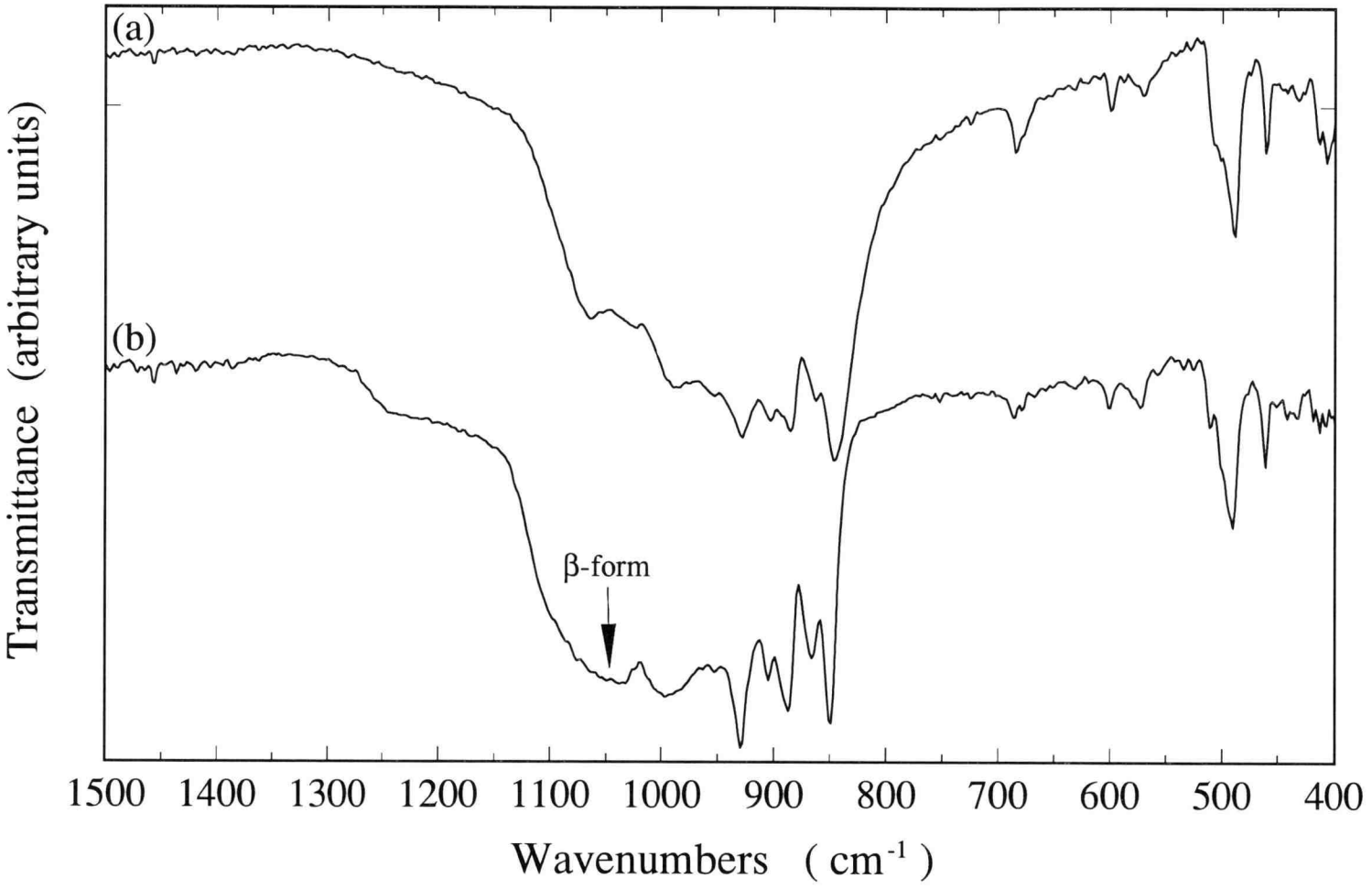

Figure 4.26 IR spectra of crystallized products, not exposed to air before the crystallization: (a) whiskers, (b) nanophase powder

4.4.2.4 Rate of SiO-NH_3 Reaction

According to the stoichiometry of SiO-NH_3 reaction given in Reaction (2.14), one gram of SiO will yield 1.06 grams of Si_3N_4. The production rates, $(dM_{prd}/dt)_{Ave}$, are plotted against the SiO generation rates, $(dM_{SiO}/dt)_{Ave}$, in Figure 4.27, using the data obtained at temperatures between 1300 and 1400 °C. A good proportional relationship has been obtained in the plot, and the coefficient of 1.01 indicates that the reaction is almost instantaneous at temperatures in the range studied, yielding 95% of the theoretical product.

4.4.2.5 Effect of $(dM_{SiO}/dt)_{Ave}$ on Product Distribution

Runs B1400-01 through -03 presented in Table 4.9 show that the yield of whiskers increases when $(dM_{SiO}/dt)_{Ave}$ increases at 1400 °C, but the sum of the whiskers and nanophase powder remains roughly constant ($\approx$ 35%). In contrast to the whiskers, the crystals are not affected by the SiO generation rate. About 65% of the total products is in the form of crystals in all the runs at this temperature. Similar results were obtained at 1350 °C. In runs B1350-01 through -03, the yield of each type of product is roughly constant: whiskers $\approx$ 12 wt%, crystals $\approx$ 67 wt%, and fine powder $\approx$ 21 wt%. The effect of $(dM_{SiO}/dt)_{Ave}$ on the crystal formation is negligibly small when a bent NH_3 feeder is used at this temperature.

Different results were obtained using a straight NH_3 feeder at 1300 and 1350 °C. When $(dM_{SiO}/dt)_{Ave}$ increases, the yield of crystals decreases, leading to an increase in the yields of whiskers and nanophase powder. However, the effect of $(dM_{SiO}/dt)_{Ave}$ is not significant at 1400 °C. The yield of each type of product is roughly constant though $(dM_{SiO}/dt)_{Ave}$ is changed in runs S1400-01 through -03.

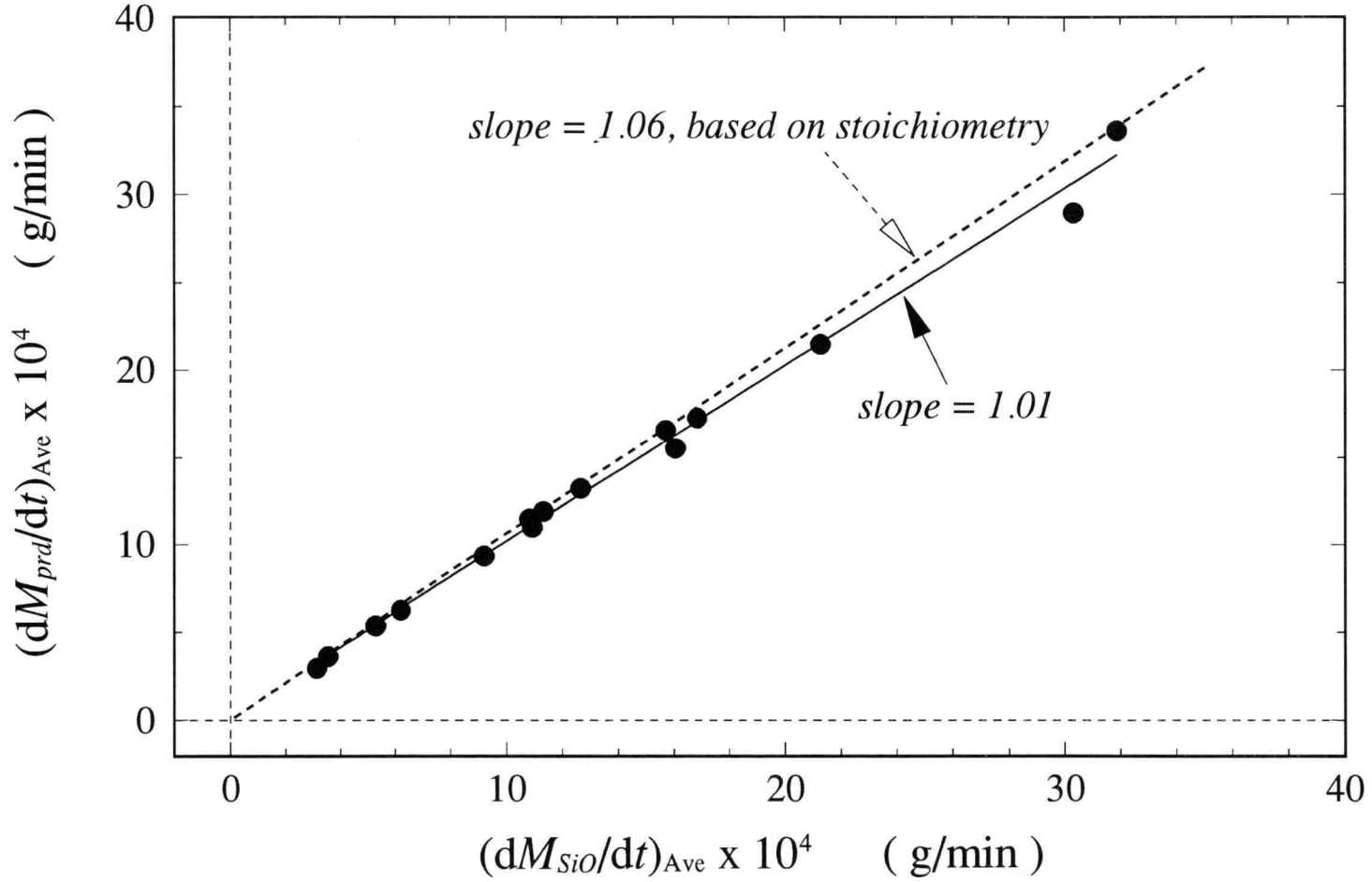

Figure 4.27 Comparison between SiO generation rate and product formation rate

4.4.2.6 Effect of NH_3 Inlet Pattern

According to Table 4.9, the formation of whiskers and nanophase powder is affected by the way of NH_3 feeding at 1350 °C. The yields of whiskers and crystals increased when a bent NH_3 feeder was used. In other words, more nanophase powder formed when feeding NH_3 with a straight Al_2O_3 tube.

Determining the flow behaviors in the NH_3 feeder and reactor tube is essential to find out the effect of NH_3 feeding. The Reynolds numbers of gas flow in the NH_3 feeder and tubular reactor are given in Table 4.10. SiO is ignored in the calculations due to its small amount compared to other species (Ar, NH_3, N_2, and H_2). The results indicate that the gas flow in the NH_3 feeder and reactor tube were laminar under the operating conditions.

Although the gas flow was laminar in both the reactor tube and NH_3 feeder, the 30° tilted nozzle would have caused impinging gas flow against the tube wall, which enhanced the formation of whiskers at location 1. With a straight NH_3 feeder, more product was carried out of the reactor because of the reduction of the impingement effect.

In addition, the X-ray diffraction, Figures 4.28(a)-(d), shows that the product formed at location 2 becomes partly amorphous in the runs using a straight NH_3 feeder. A comparison of Figures 4.28(a) and (b) indicates that the crystals are well developed when a bent Al_2O_3 feeder is used at 1400 °C. Similar results are shown in the plots (c) and (d), in which the crystals are obtained at 1350 °C. The reason of this crystal change remains unclear in this study. However, it has been found that the crystals formed in the SiO-NH_3 reaction are pure α-form without any β-content.

4.5 Crystallization of Amorphous Products

It has been reported that amorphous Si_3N_4 can be crystallized in N_2 or Ar gas at a temperature of 1500 °C or higher [Wada *et al.*, 1981; Allaire and Langlois, 1992]. However, Figure 4.2 implies that the whiskers may be crystallized under a stream of

Table 4.10 Physical properties of gas flow in reactor system

Position of gas flow	**Temp.** (°C)	**Flow Rate** (cm^3/min)‡	**Viscosity μ** $\times 10^5$ (kg/m-sec)†	**Density ρ** (kg/m^3)†	**Reynolds Number** ($\rho d\upsilon_o/\mu$)
Tubular Reactor	1300	Ar = 14622	7.081	0.231	43.2
		NH_3 = 5420			
		N_2 = 938			
		H_2 = 2812			
	1350	Ar = 15086	7.199	0.210	42.4
		NH_3 = 4057			
		N_2 = 1735			
		H_2 = 5205			
	1400	Ar = 15551	7.279	0.187	42.5
		NH_3 = 1746			
		N_2 = 3006			
		H_2 = 9016			

Table 4.10 Physical properties of gas flow in reactor system (continued)

Position of gas flow	**Temp.** (°C)	**Flow Rate** (cm^3/min)‡	**Viscosity μ** $\times 10^5$ (kg/m-sec)†	**Density ρ** (kg/m^3)†	**Reynolds Number** ($\rho d\upsilon_o/\mu$)
Ammonia Feeder	1350	NH_3 = 4435	54.248	0.0895	95.1
		N_2 = 1662			
		H_2 = 4985			
	1400	NH_3 = 2344	52.865	0.073	97.5
		N_2 = 2706			
		H_2 = 8124			

† : cited from the ChemCad [1993]

‡ : referred to reaction temperature

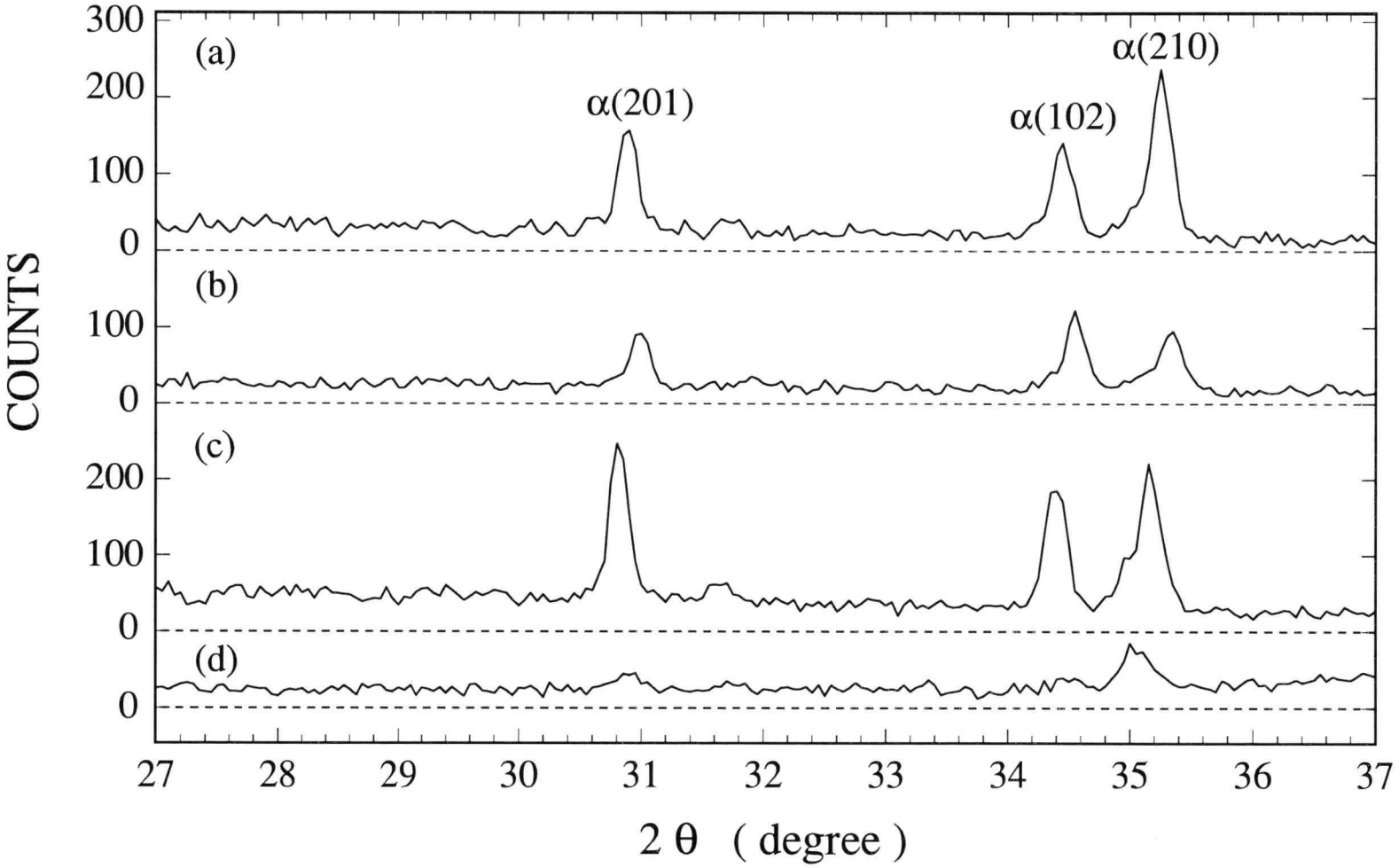

Figure 4.28 XRD charts of crystals formed at location 2, using: (a) bent NH_3 feeder at 1400 °C, (b) stright NH_3 feeder at 1400 °C, (c) bent NH_3 feeder at 1350 °C, (d) straight NH_3 feeder at 1350 °C

dissociated NH_3 at 1350 °C, as indicated by the crystalline peaks appearing in the IR spectrum.

In this study, amorphous whiskers and nanophase powder collected from a few runs were heated in the reactor tube for the crystallization in an NH_3, N_2, or N_2/H_2 mixture-gas stream at temperatures in the range from 1300 to 1560 °C. It should be mentioned that conditions were selected so that NH_3 fully dissociated before entering the reactor at these temperatures. The progress of crystallization with an increase in the heating time was investigated by both the X-ray diffraction and IR analysis.

4.5.1 Crystallization of Nanophase Powder

The crystallization of nanophase powder, unexposed to air, was investigated at 1300 °C in dissociated NH_3. The IR analysis of the product transformation is shown in Figure 4.29 where the crystallization of powder begins in 2 hours. It is found that α-crystalline peaks are well developed in the IR spectrum of powder after heating for 5 hours. The X-ray diffraction (Figure 4.30) further supports the results obtained from the IR analysis. As shown in Figure 4.30, crystalline peaks have developed after 2-hour heating, and nearly pure α-Si_3N_4 crystals are found well developed in 5 hours.

In N_2, nanophase powder was not crystallized at all at 1300 °C even after heating for 5 hours, as shown in Figure 4.31(b). However, Figure 4.31(a) indicates that the powder could be crystallized in 2 hours at 1560 °C, yielding Si_3N_4 crystals containing 62% α-form and 38% β-form. Further IR analysis is shown in Figure 4.32, in which no crystalline peak is found in nanophase powder heated in N_2 for 5 hours at 1300 °C. It should be mentioned that a characteristic β-form absorption is clearly seen at a wavenumber about 1040 cm^{-1}, showing a good agreement with the high β-content indicated by the XRD results in Figure 4.31(a).

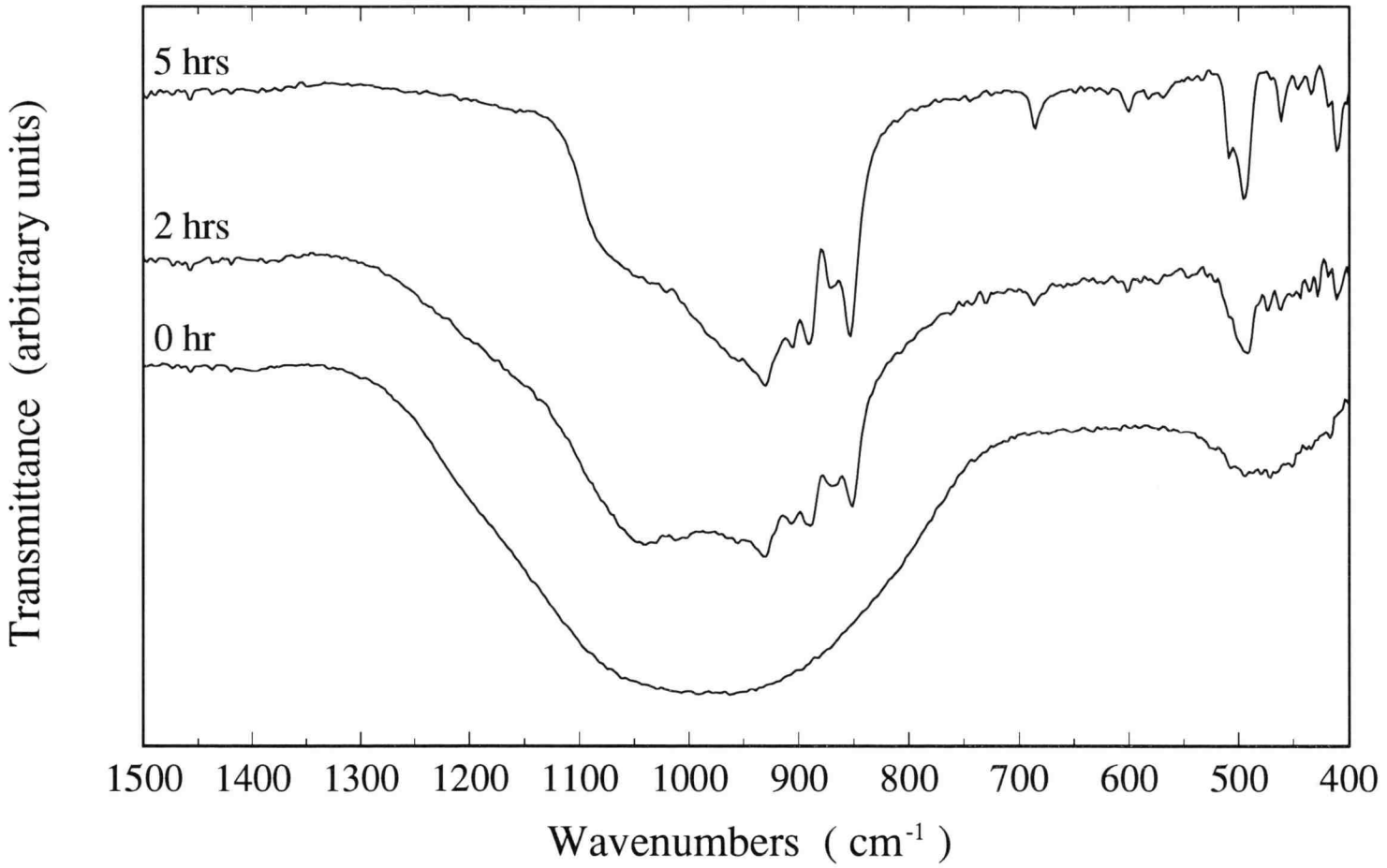

Figure 4.29 IR spectra of nanophase powder, heated for different lengths of time at 1300 °C in dissociated NH_3

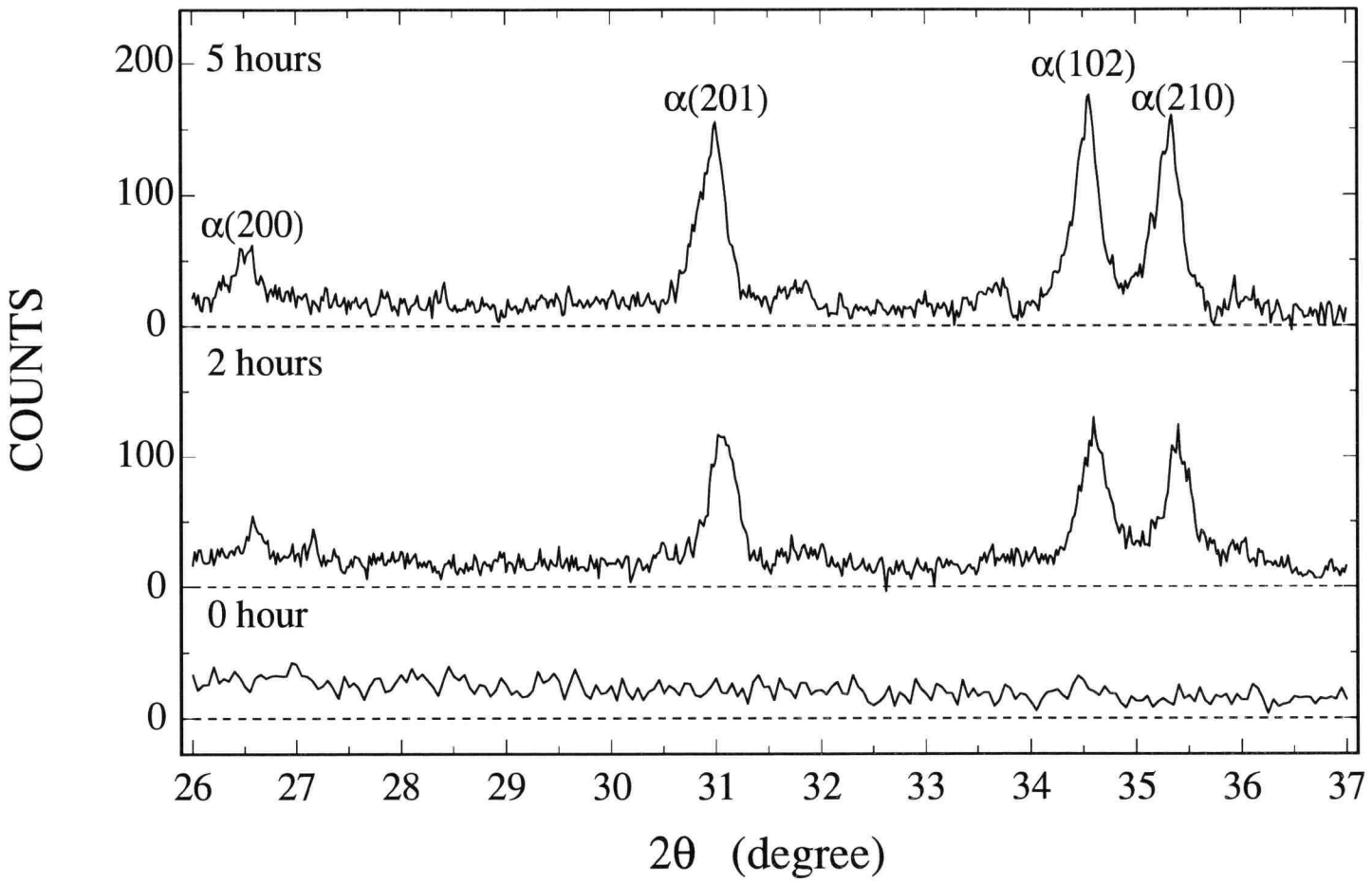

Figure 4.30 XRD charts of nanophase powder, heated for different lengths of time at 1300 °C in dissociated NH_3

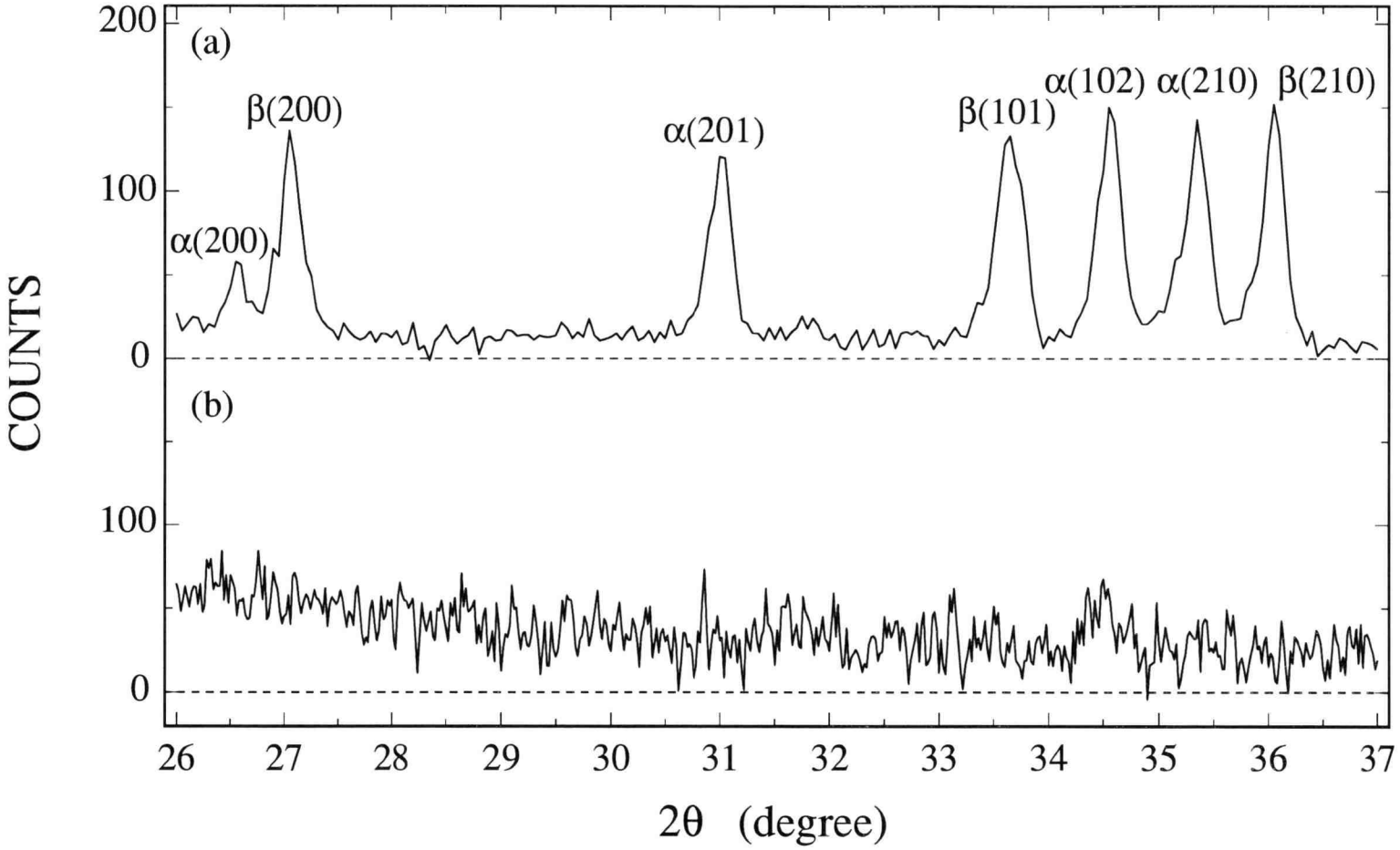

Figure 4.31 XRD charts of nanophase powder, heated in N_2: (a) at 1560 °C for 2 hours, (b) at 1300 °C for 5 hours

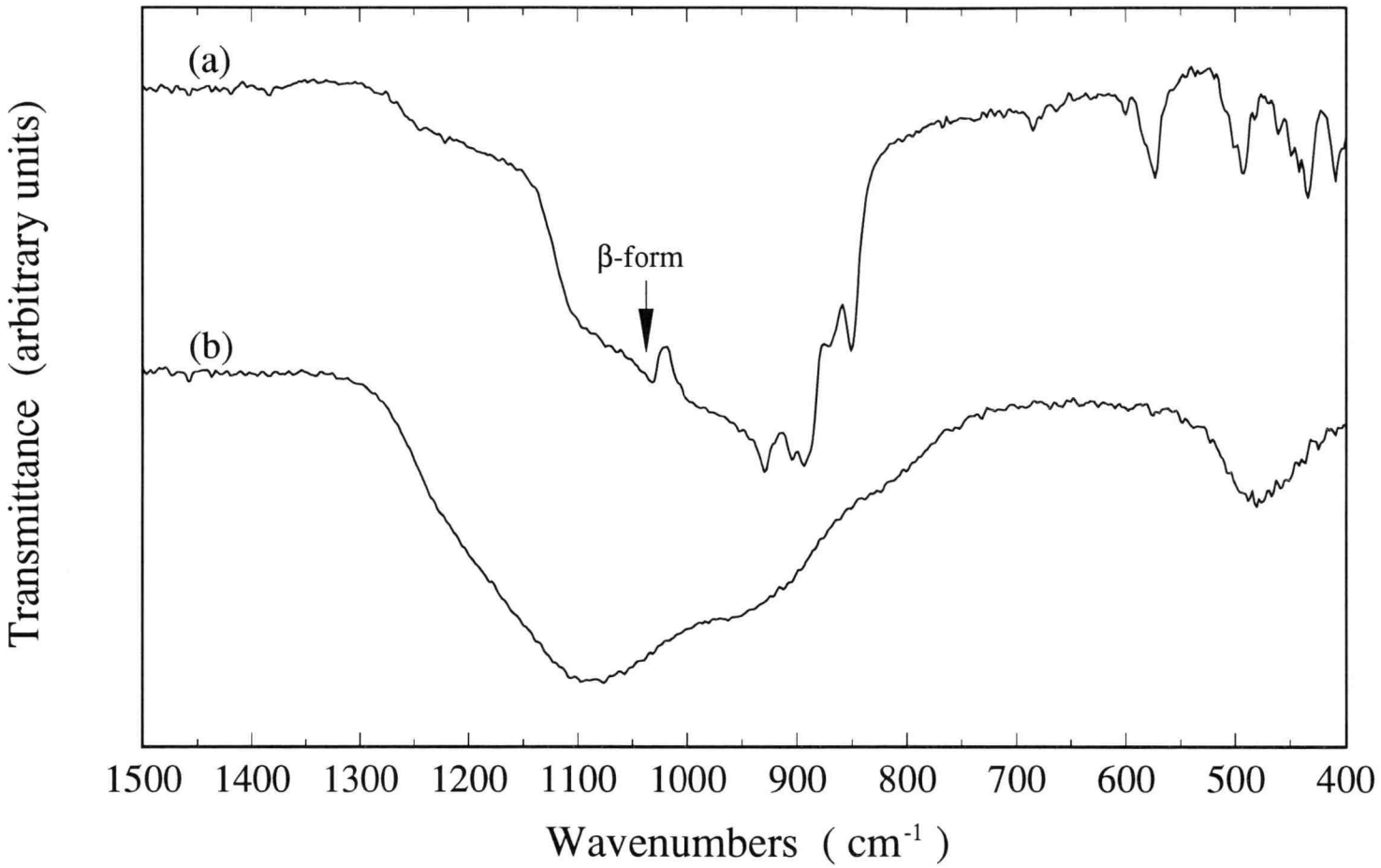

Figure 4.32 IR spectra of nanophase powder, heated in N_2: (a) at 1560 °C for 2 hours, (b) at 1300 °C for 5 hours

4.5.2 Crystallization of Whiskers

Systematic experiments were made to study the crystallization of amorphous whiskers in dissociated NH_3 at temperatures between 1300 and 1400 °C. Figures 4.33(a)-(b) show the IR spectra of whiskers heated for different lengths of time at the prescribed temperatures. In Figure 4.33(a), crystalline peaks are seen after heating whiskers for 5 hours but Si_3N_4 crystals are not well developed as indicated by the X-ray diffraction shown in Figures 4.34(a). To crystallize the product, the product needed to be heated for at least 5 hours at 1350 °C, as shown in Figures 4.33(b) and 4.34(b). About 9% β-form develops in Si_3N_4 crystals after the 8-hour heating of whiskers. Figures 4.33(c) and 4.34(c) show that the crystallization of whiskers is initiated in 2 hours and nearly pure Si_3N_4 crystals are well developed after the 5-hour heating at 1400 °C.

Figure 4.35(a) suggests that heating the amorphous whiskers at 1560 °C for 2 hours in N_2 yields Si_3N_4 crystals containing roughly the same fraction of β-form as obtained in dissociated NH_3 at 1350 °C for 8 hours, Figure 4.34(b). However, the amorphous whiskers are not crystallized at all in N_2 even after the 8-hour heating at 1350 °C, as shown in Figure 4.35(b).

4.5.3 Effect of Gaseous Environment

The effect of gaseous atmosphere for crystallization was investigated at 1350 °C using amorphous whiskers. Without exposing to air after the synthesis, whiskers were heated in: (a) a dissociated NH_3 stream, (b) N_2/H_2 mixed gas, or (c) a N_2 stream at 1350 °C for 8 hours. The IR spectra of the heated products are shown in Figure 4.36, in which the crystalline peaks in (b) and (c) are not significant compared to those shown in (a). Further XRD shown in Figure 4.37 is consistent with the IR analysis. It is obvious that N_2 does not enhance crystallization at all. Although N_2/H_2 may promote the crystallization, the progress of crystallization is not as well developed as in the dissociated NH_3 stream.

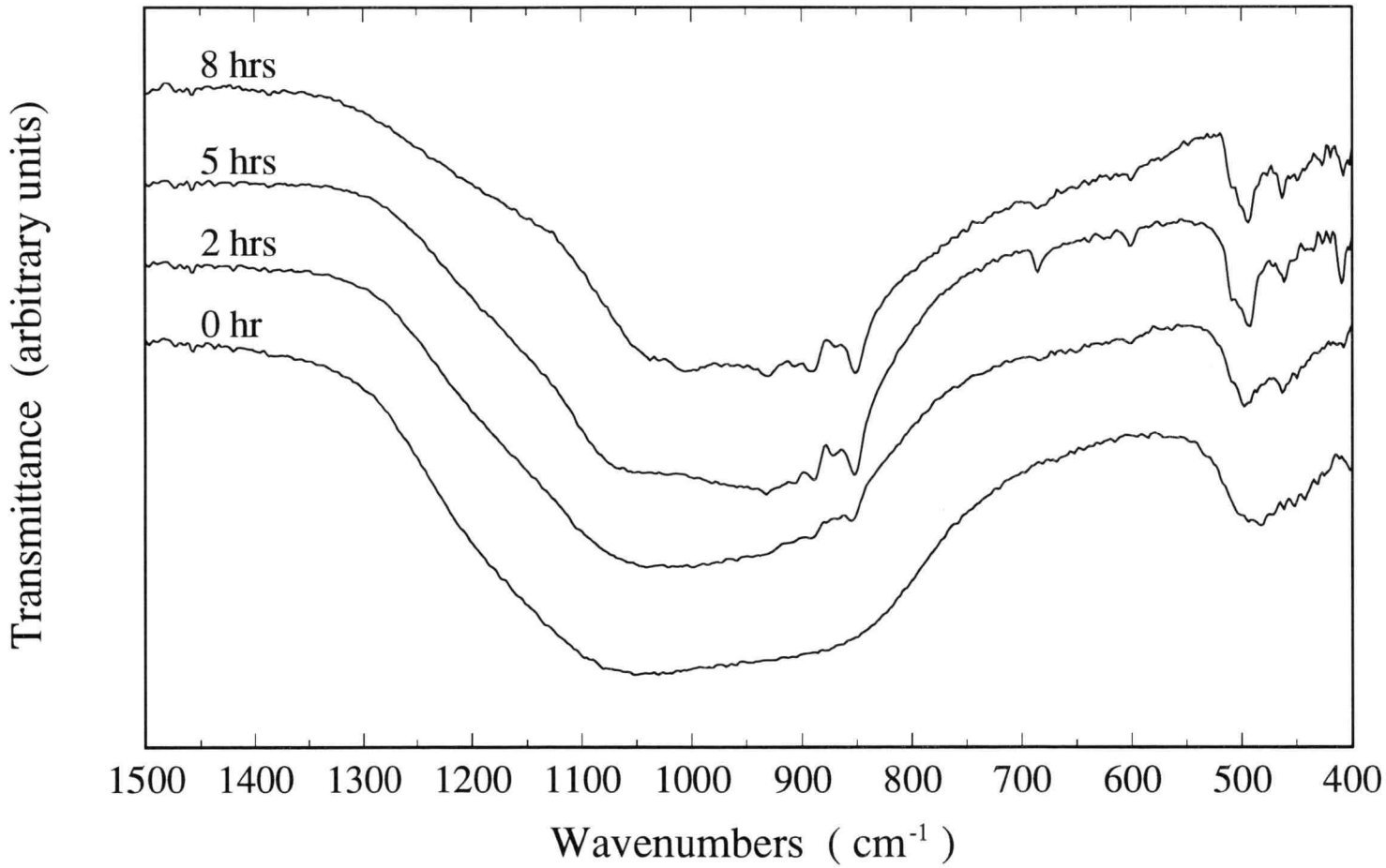

Figure 4.33(a) IR spectra of whiskers, heated for different lengths of time at 1300 °C in dissociated NH_3

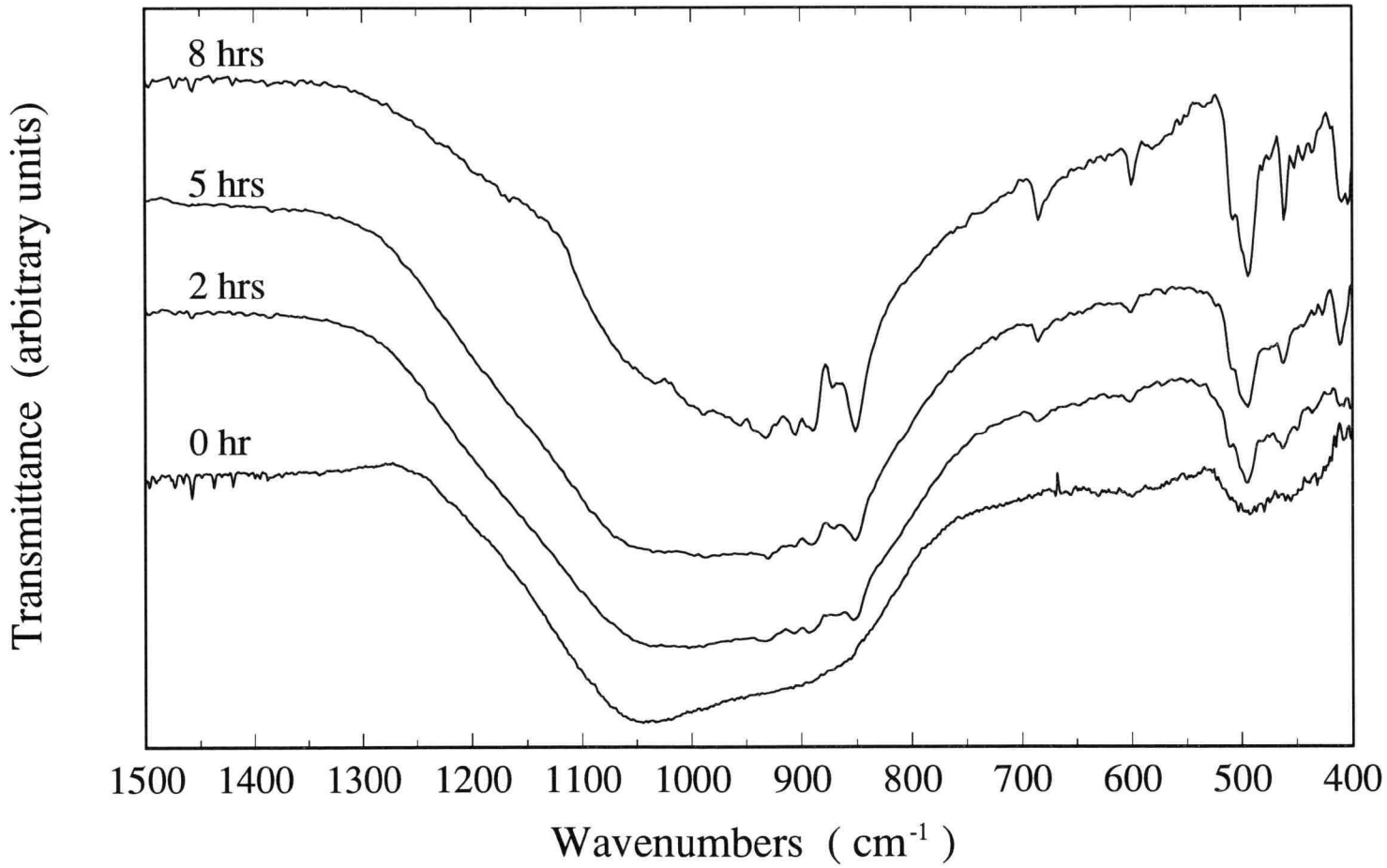

Figure 4.33(b) IR spectra of whiskers, heated for different lengths of time at 1350 °C in dissociated NH_3

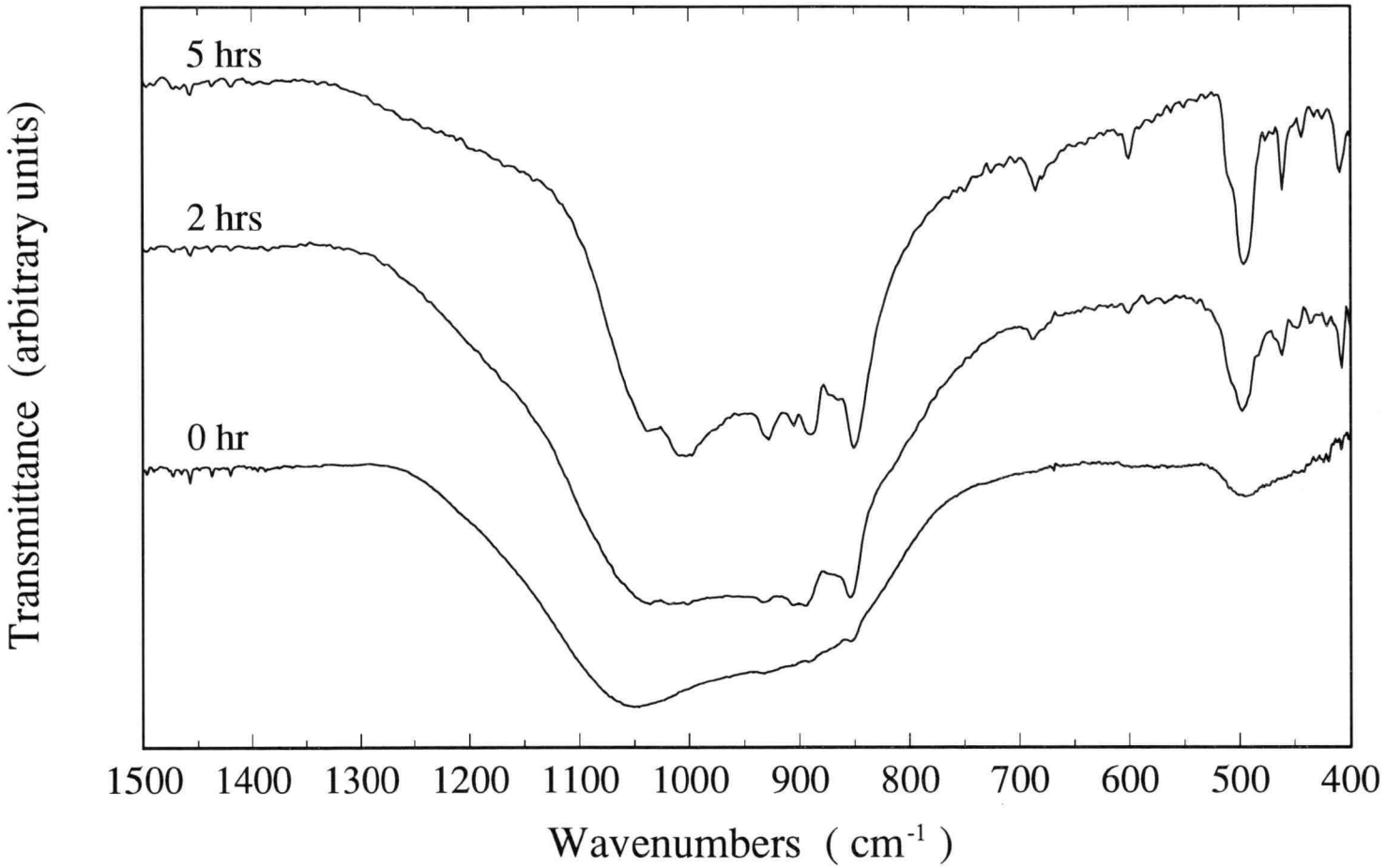

Figure 4.33(c) IR spectra of whiskers, heated for different lengths of time at 1400 °C in dissociated NH_3

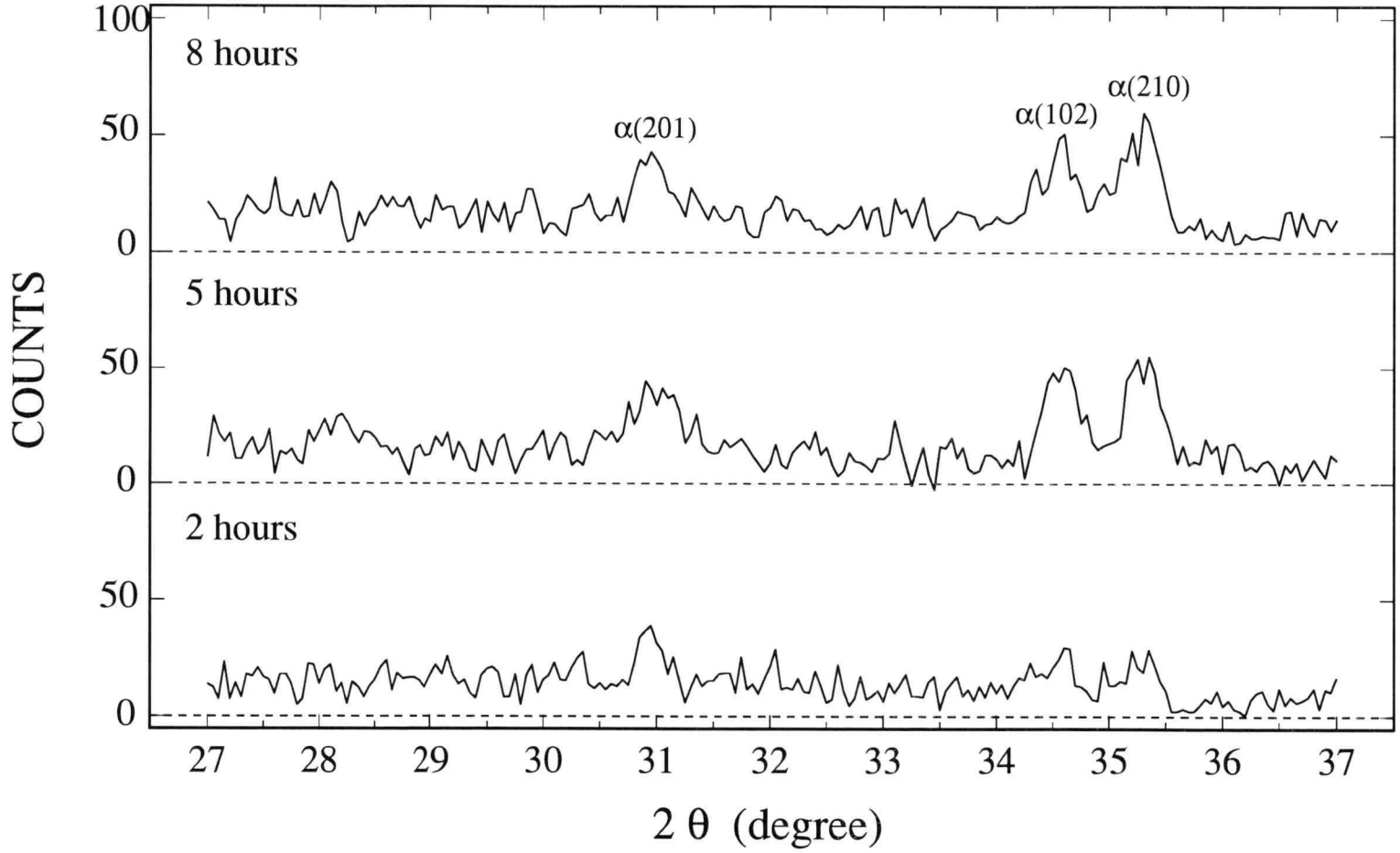

Figure 4.34(a) XRD charts of whiskers, heated for different lengths of time at 1300 °C in dissociated NH_3

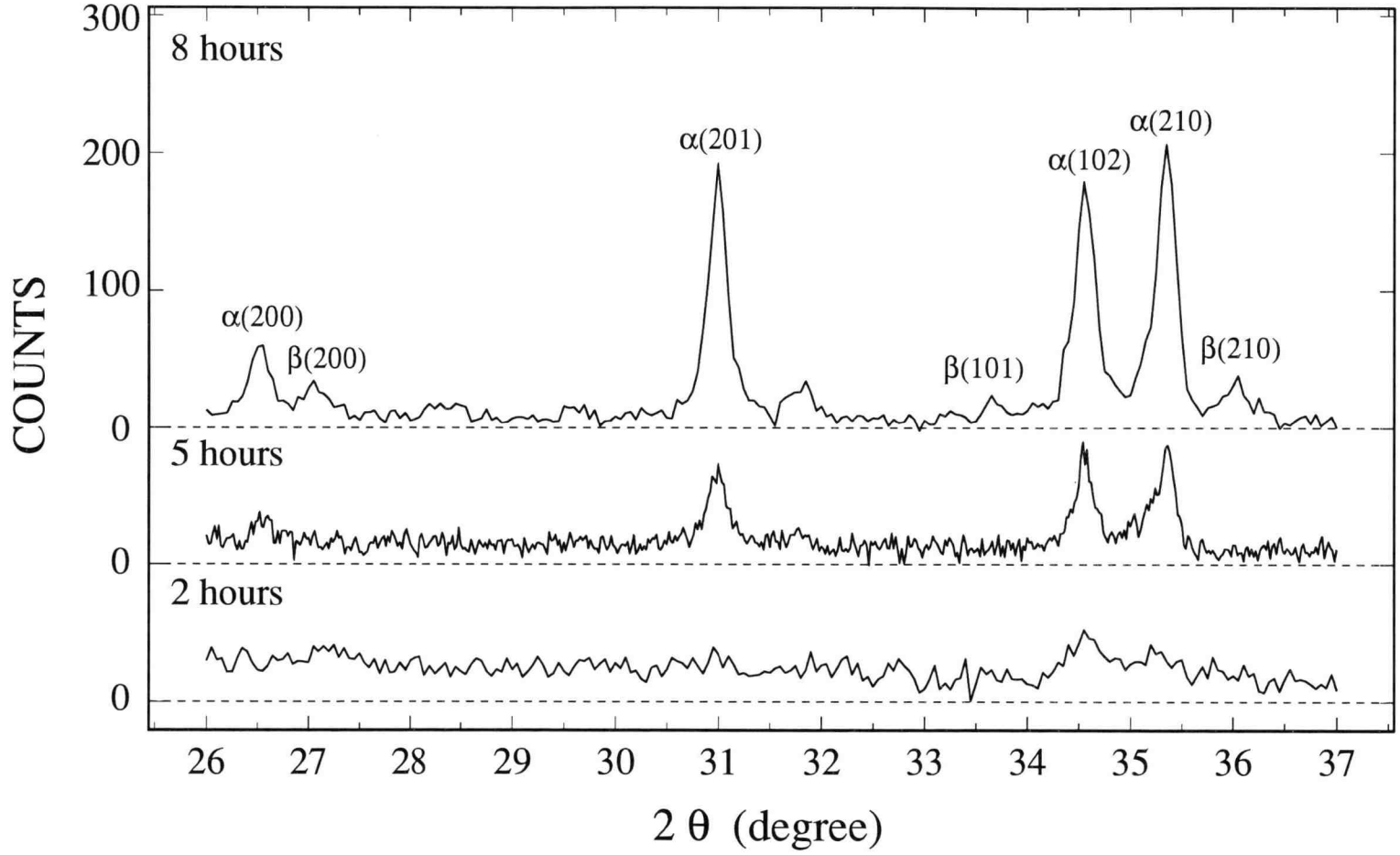

Figure 4.34(b) XRD charts of whiskers, heated for different lengths of time at 1350 °C in dissociated NH_3

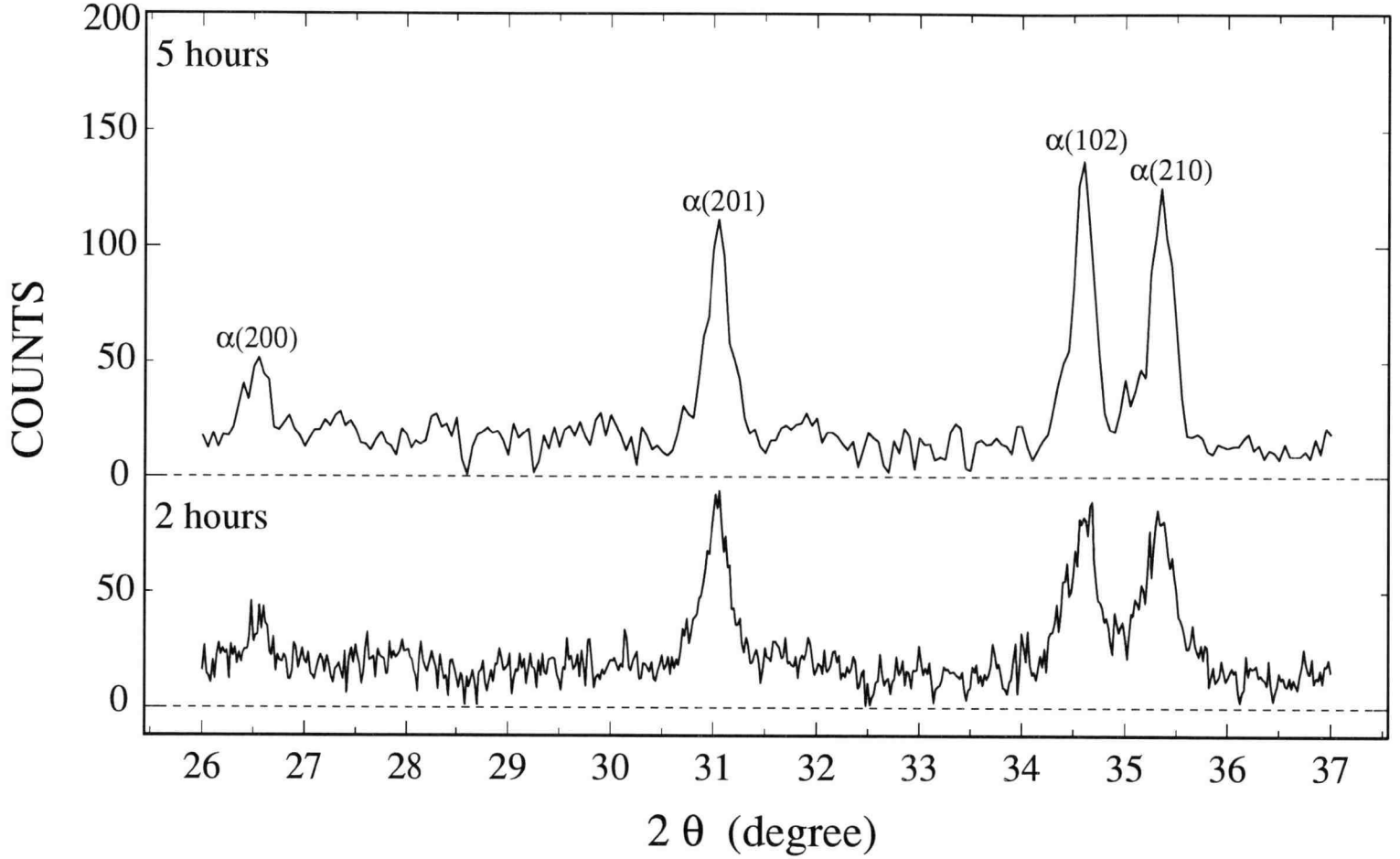

Figure 4.34(c) XRD charts of whiskers, heated for different lengths of time at 1400 °C in dissociated NH_3

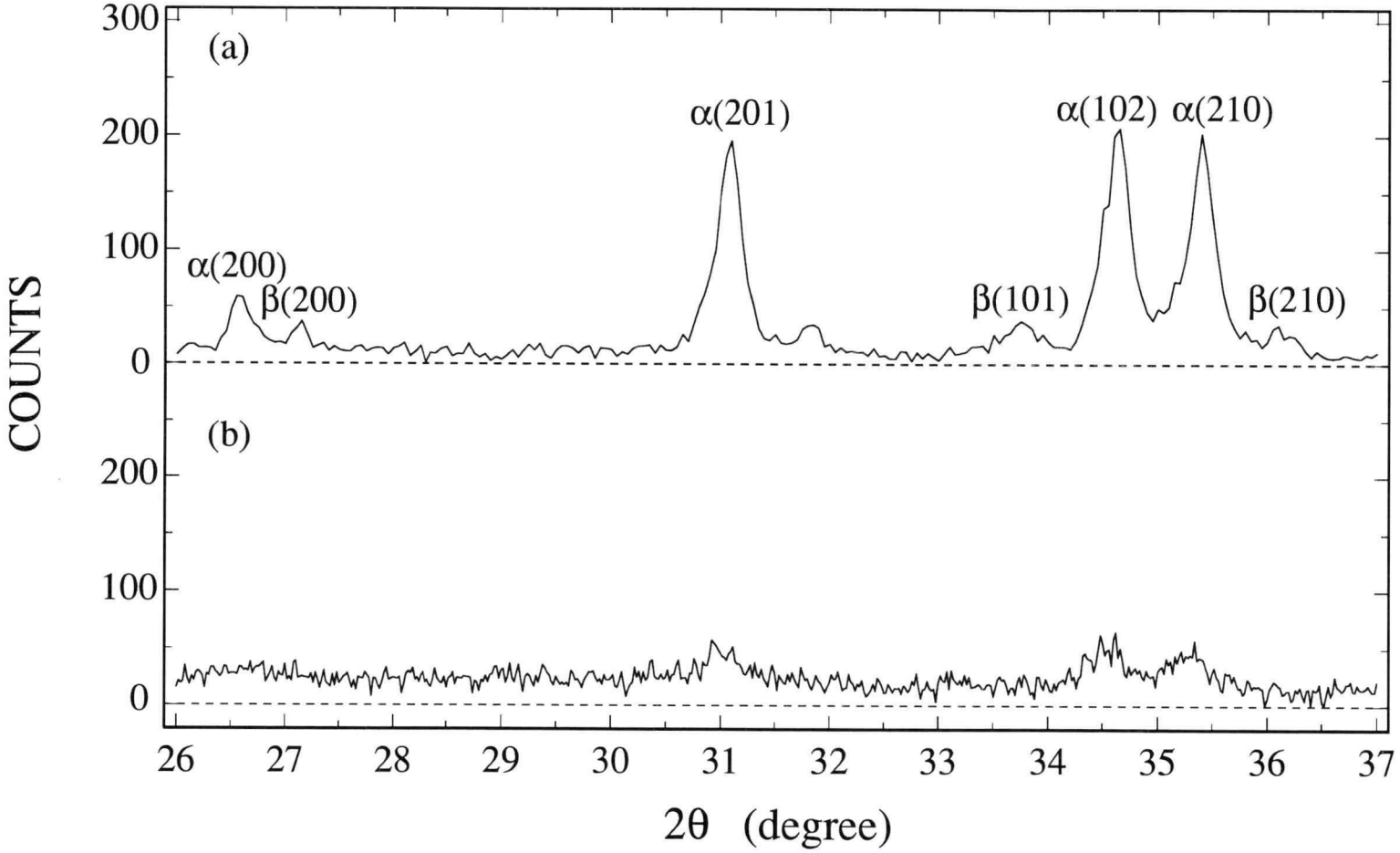

Figure 4.35 XRD charts of whiskers, heated in N_2: (a) at 1560 °C for 2 hours, (b) at 1350 °C for 8 hours

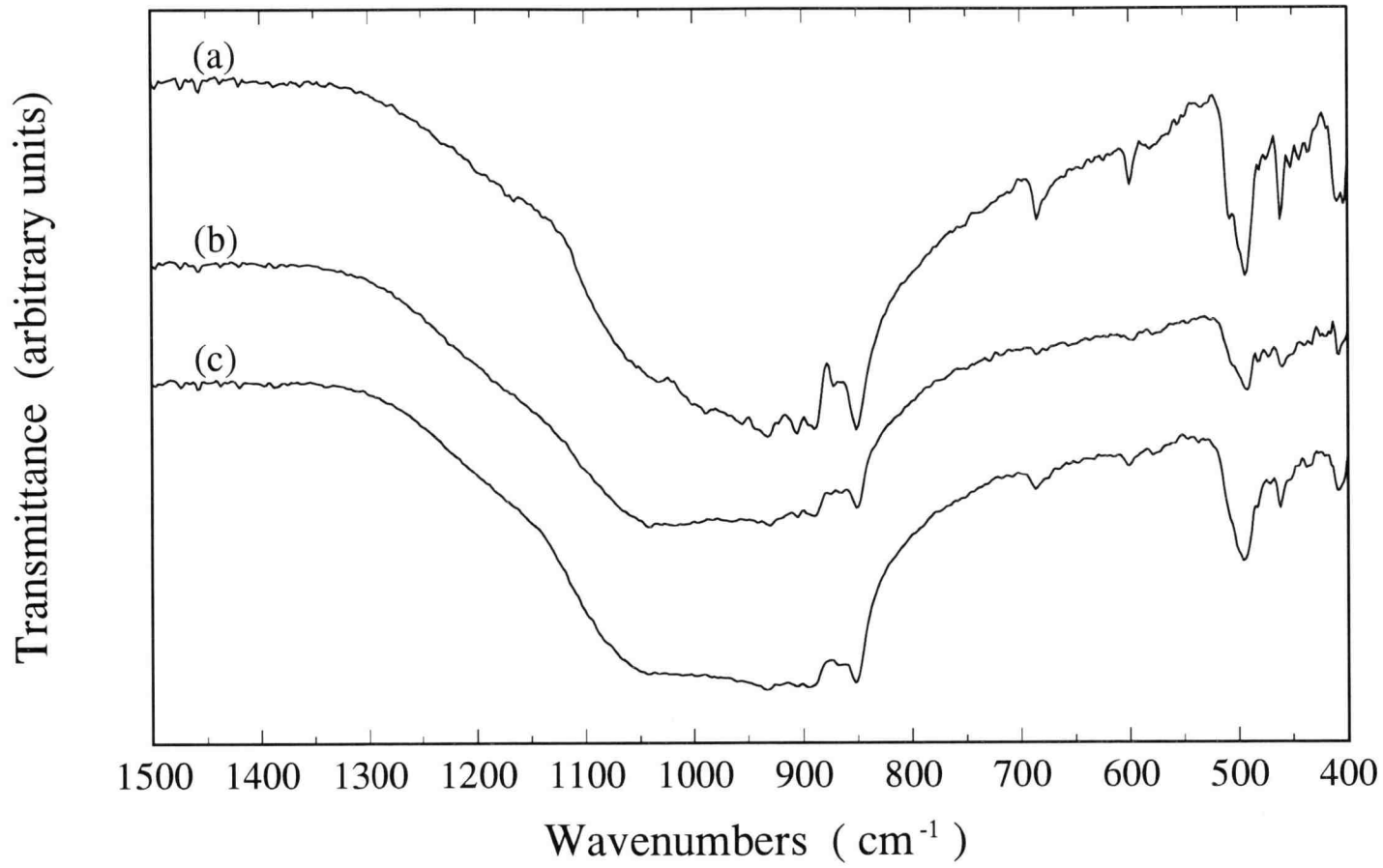

Figure 4.36 IR spectra of whishers, heated at 1350 °C for 8 hours: (a) in dissociated NH_3, (b) in N_2 (40 vol%) and H_2 (60 vol%), (c) in pure N_2

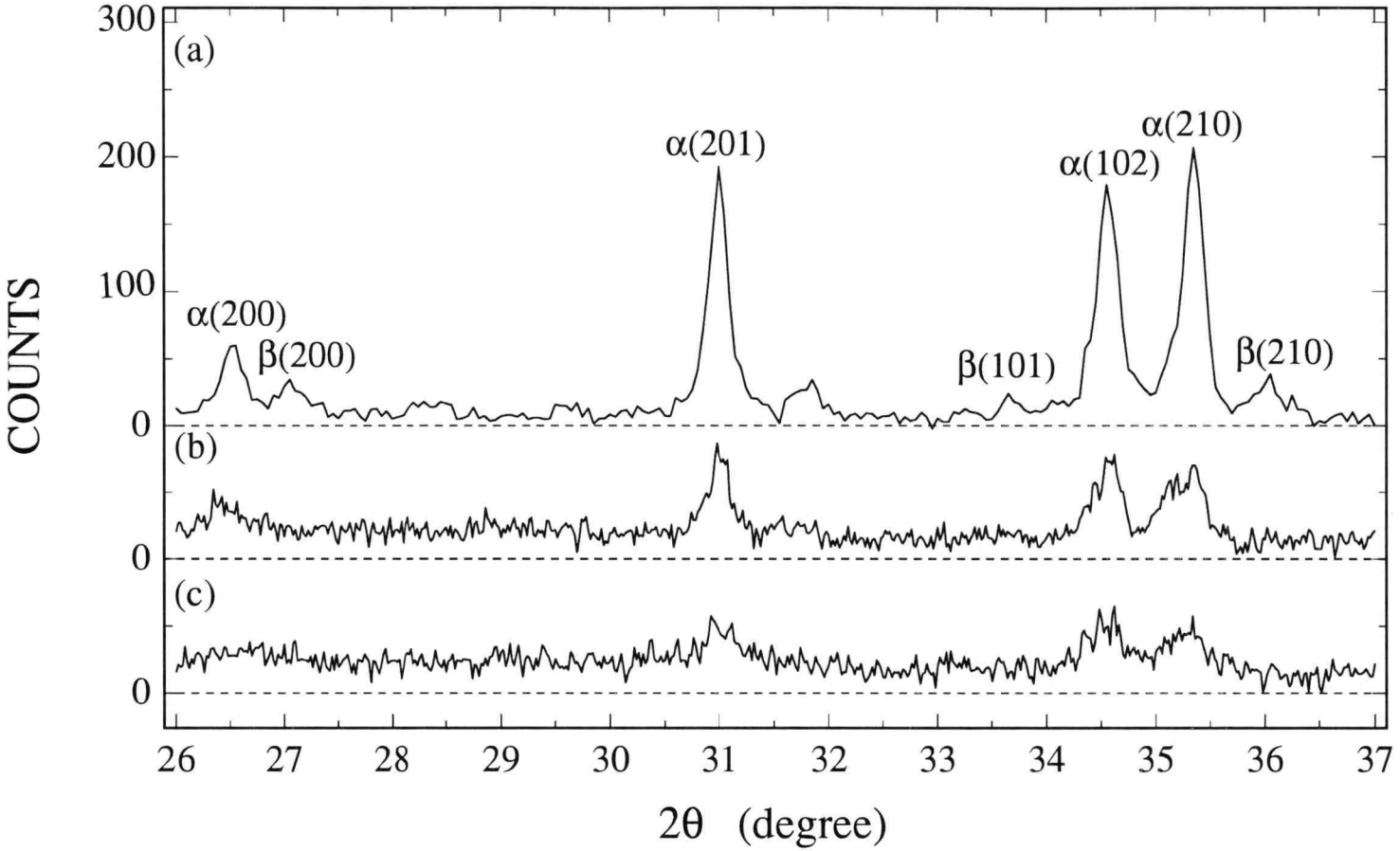

Figure 4.37 XRD charts of whiskers, heated at 1350 °C for 8 hours: (a) in dissociated NH_3, (b) in N_2 (40 vol%) and H_2 (60 vol%), (c) in pure N_2

Similar results were obtained in the crystallization of nanophase powder at 1300 °C. No crystalline peaks are found in Figure 4.38(b), in which the powder is heated in pure N_2 for 5 hours. Well-developed crystalline peaks are found in the IR spectrum of powder that was crystallized in dissociated NH_3 at the same conditions. In addition, Figure 4.38(a) also suggests that the crystallized powder is close to pure α-Si_3N_4 because no significant β-form peak is seen in the spectrum. A comparison of the XRD charts of the products is presented in Figure 4.39, showing a good agreement with the IR analysis. The nanophase powder was not crystallized at all though it was heated in N_2 at 1300 °C for 5 hours. In contrast to N_2 atmosphere, almost pure α-Si_3N_4 crystals are found well developed under dissociated NH_3 at 1300 °C in 5 hours.

At the same conditions, dissociated NH_3 showed a more enhanced effect on the crystallization than N_2/H_2 mixture-gas. Active intermediates, such as NH and NH_2 formed in the dissociation of NH_3 [Hulthen and Nakamura, 1927; Gaviola and Wood, 1928; Lavin and Bates, 1930; Duncan and Wilson, 1932], may be involved in the crystallization process. However, no further study on this effect was performed.

The experiments have shown that both the gaseous environment and operating temperature dominate the crystallization of amorphous Si_3N_4. According to Figures 4.33 and 4.34, optimal conditions regarding the temperature and heating time may exist in the crystallization process in dissociated NH_3, which have not been found in this research.

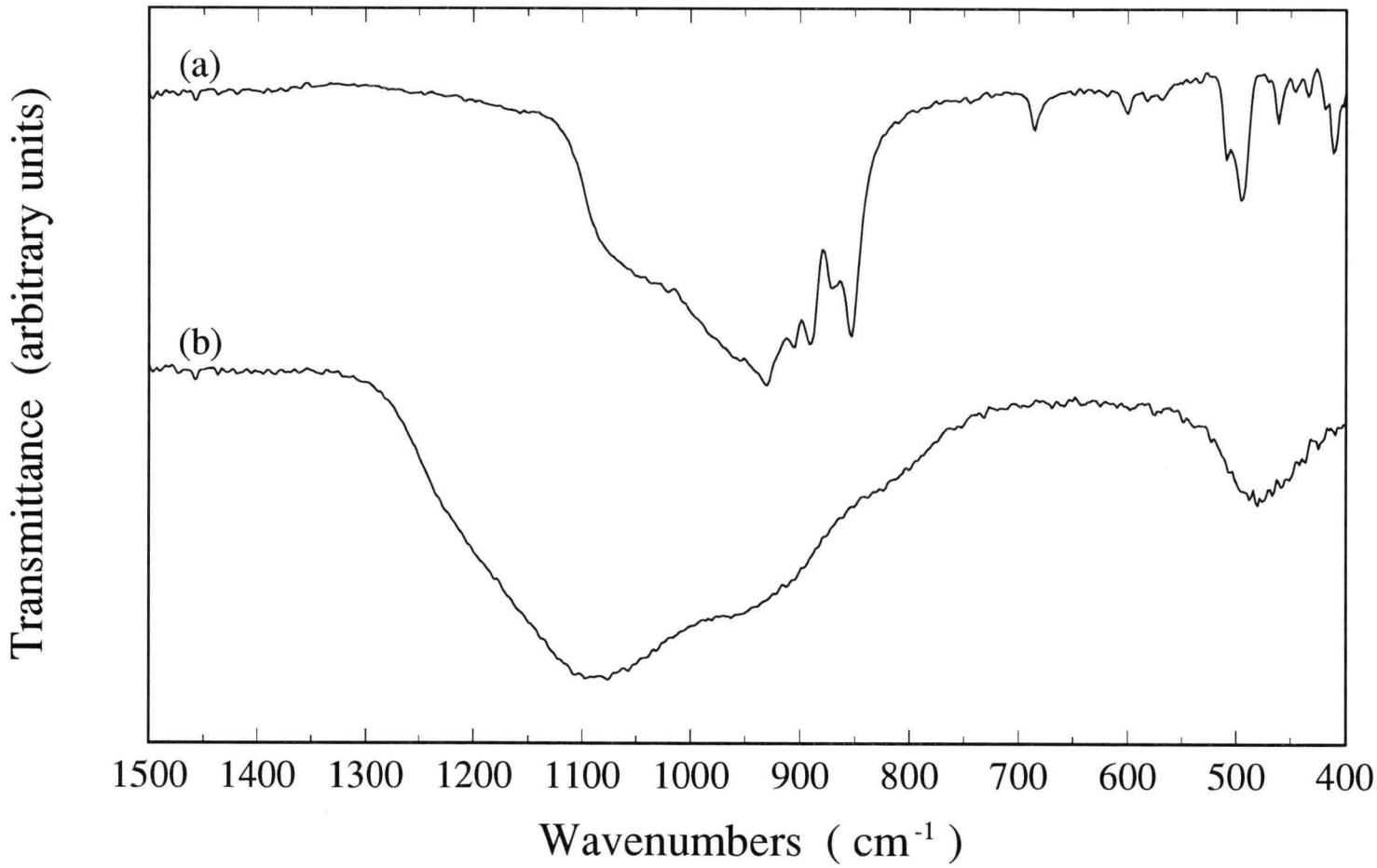

Figure 4.38 IR spectra of nanophase powder, heated at 1300 °C for 5 hours: (a) in dissociated NH_3, (b) in pure N_2 hours

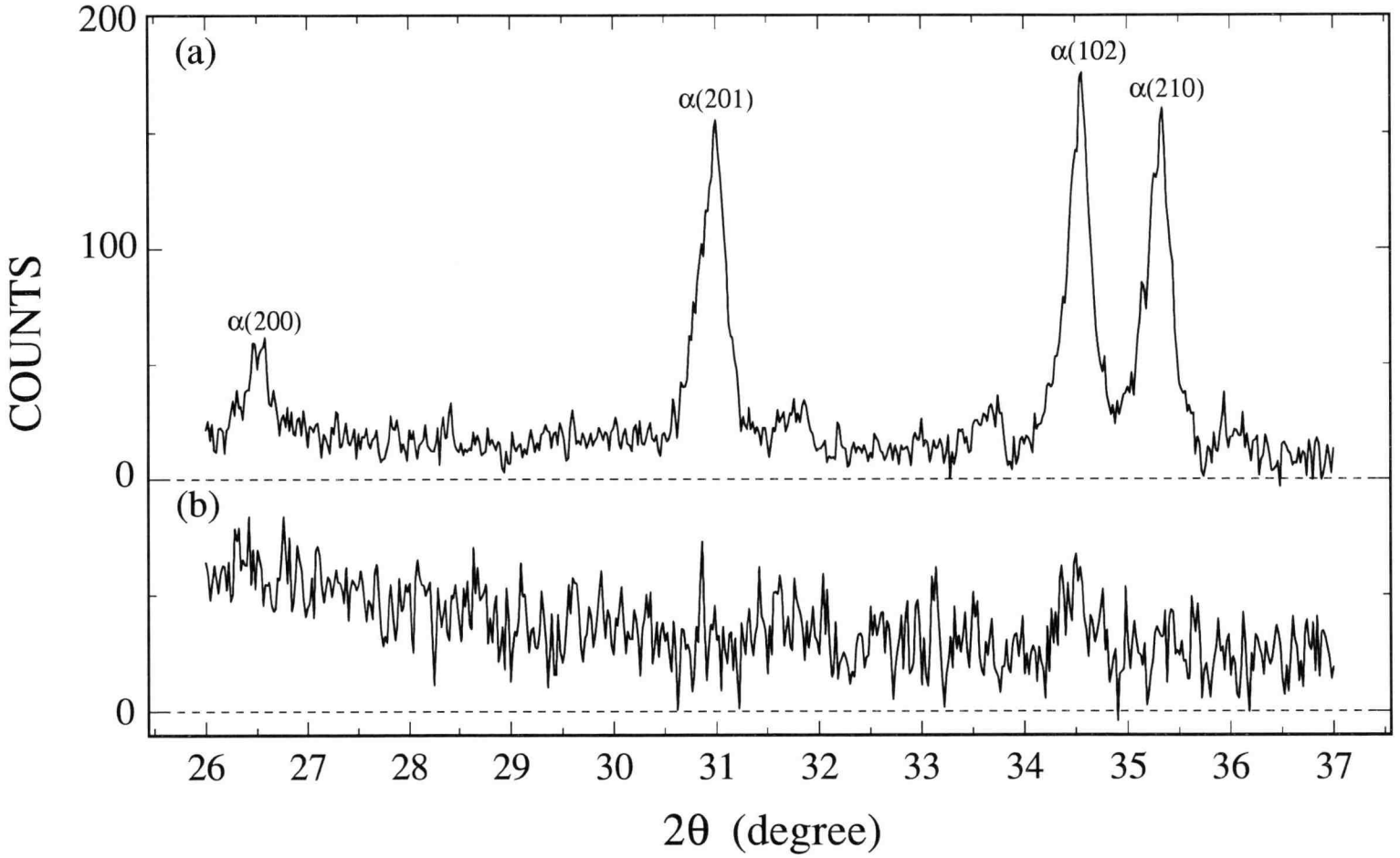

Figure 4.39 XRD charts of nanophase powder, heated at 1300 °C for 5 hours: (a) in dissociated NH_3, (b) in pure N_2 hours

CHAPTER 5

MATHEMATICAL MODELING OF SiO GENERATION: SOLID-SOLID REACTION

As discussed in Chapter 4.2, the SiO generation is considered to be limited by the pore diffusion step. Although the microscopic mechanism of Si-SiO_2 reaction remains unclear, the overall process may be characterized by the SiO vapor diffusing through the porous pellets into the bulk stream. The reaction system is schematically shown in Figure 5.1 with notations helpful for modeling the process.

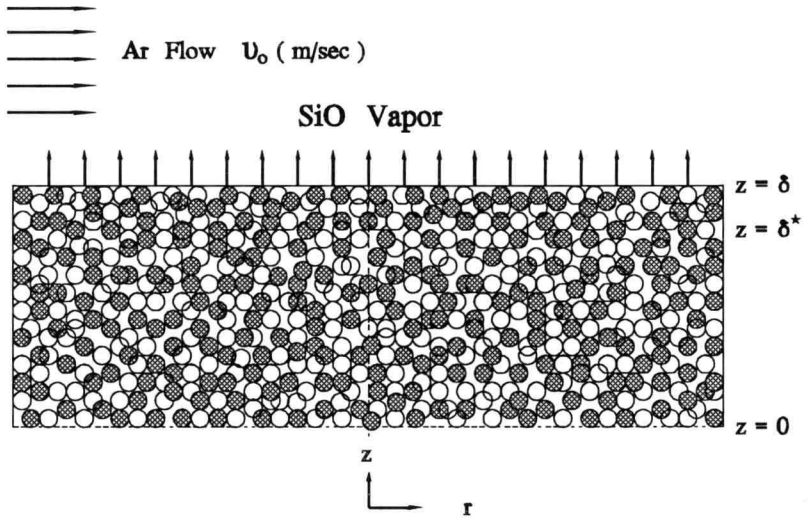

Figure 5.1 Notations for SiO generation process

Essentially, the SiO generation process can be separated into two parts: diffusion and convection. SiO vapor diffuses through pores in a pellet to the surface; then, it is carried downstream by the Ar flow. Understanding the transport mechanisms occurring in porous solid is an essential step for modeling the process.

The transport of gases through porous media may be described by four independent diffusion processes:

(1) Continuum diffusion: transport caused by concentration gradients, temperature gradients and external forces.

(2) Knudsen diffusion: transport dominated by gas molecule-pore wall collisions.

(3) Surface diffusion: transport due to surface concentration gradients.

(4) Viscous flow: transport driven by external pressure gradients.

Since small pellets (diameter: 12.7 mm; thickness ≈ 3.18 mm) are used in this study, temperature and pressure are assumed to be uniform in the pellet. Also, no external forces or external pressure gradients are applied to the pellets. Surface diffusion is neglected owing to high temperature and Ar flow. Because of the symmetrical geometry of pellets, diffusion in the θ direction in the pellet may be neglected. In addition, radial diffusion can be ignored when the radial side of pellet is sealed by ceramic glue, or the pellet thickness is much less than the pellet diameter. On the basis of these assumptions, the process may be characterized by the continuum diffusion and Knudsen diffusion in the axial direction, i.e., in the z direction.

5.1 Model Derivations

In a binary mixture of SiO and Ar, the molecule diffusion flux caused by the molecular density gradient is given by

$$J_{SiO} = - D_{SiO\text{-}Ar} \frac{dn_{SiO}}{dz} \qquad \left(\frac{molecules}{m^2 \text{ sec}} \right) \tag{5.1}$$

In terms of molecular fluxes of SiO and Ar, the diffusion flux of SiO is given as

$$J_{SiO} = N_{SiO} - \frac{n_{SiO}}{n} (N_{SiO} + N_{Ar}) = N_{SiO} - y_{SiO} N \quad with\ N = N_{SiO} + N_{Ar} \tag{5.2}$$

in which y_{SiO} represents the molar fraction of SiO vapor in the binary mixture: $y_{SiO} = n_{SiO}/n = P_{SiO}/P$. If SiO is dilute in the system, the convective term ($y_{SiO}\, N$) in Equation

(5.5) can be ignored. According to Equation (2.12), the vapor pressure of SiO is equal to 184 Pa at 1300 °C and 878 Pa at 1400 °C. Since the system pressure is roughly constant (101.3 kPa) in the reactor, y_{SiO} should be less than 0.00867 at temperatures below 1400 °C.

Combining Equations (5.1) and (5.2) gives the SiO molecular flux induced by the continuum diffusion as

$$N_{SiO} = - D_{SiO-Ar} \frac{dn_{SiO}}{dz} \qquad \left(\frac{molecules}{m^2 \text{ sec}} \right) \tag{5.3}$$

For the SiO flux caused by Knudsen diffusion, indicated subscript K, it is customary to express in a differential form [Knudsen, 1950].

$$J_{SiO,K} = - D_{SiO,K} \frac{dn_{SiO}}{dz} \qquad \left(\frac{molecules}{m^2 \text{ sec}} \right) \tag{5.4}$$

These two diffusions caused by the molecular density gradient are in series and interrelated as [Mason and Evans III, 1969]

$$- \frac{dn_{SiO}}{dz} = \left(\frac{1}{D_{SiO-Ar}} + \frac{1}{D_{SiO,K}} \right) N_{SiO} \tag{5.5}$$

Rearranging Equation (5.5) gives

$$N_{SiO} = - \frac{\overline{D}_{SiO-Ar} \, \overline{D}_{SiO,K}}{\overline{D}_{SiO-Ar} + \overline{D}_{SiO,K}} \frac{dn_{SiO}}{dz} = - \overline{D}_{SiO} \frac{dn_{SiO}}{dz} \tag{5.6}$$

or

$$N^{\star}_{SiO} = \frac{N_{SiO}}{N_o} = - \frac{n \, \overline{D}_{SiO}}{N_o} \frac{dy_{SiO}}{dz} = - \frac{P \, \overline{D}_{SiO}}{RT} \frac{dy_{SiO}}{dz} \qquad \left(\frac{mole}{m^2 \text{ sec}} \right) \tag{5.7}$$

where N_o is the Avogadro constant and hence $N^{\star}_{SiO}$ is the molar flux of SiO. It should be noted that an effective diffusion coefficient has been applied to Equations (5.6) and (5.7), which depends on the pore structure of medium and is given by

$$\frac{1}{\overline{D}_{SiO}} = \frac{1}{\overline{D}_{SiO-Ar}} + \frac{1}{\overline{D}_{SiO,K}} \tag{5.8}$$

where

$$\overline{D}_{SiO-Ar} = \frac{\epsilon}{\tau} D_{SiO-Ar} \quad ; \quad \overline{D}_{SiO,K} = \frac{\epsilon}{\tau} D_{SiO,K} \tag{5.9}$$

In Equation (5.8), ε is the void fraction and τ is the tortuosity in the porous medium. The tortuosity (τ) can be related to ε and is often represented as $1/\varepsilon^n$, where n can be any arbitrary value but n = 1 is most common.

5.2 Pseudo Steady State Approach

Since the diffusion fluxes in the r and θ directions are neglected, the equation of continuity reduces to

$$\epsilon \frac{\partial C_{SiO}}{\partial t} + \frac{\partial N^{\star}_{SiO}}{\partial z} = 0 \tag{5.10}$$

Pseudo steady state may be assumed to describe the process due to a low rate of SiO generation through the pellet. Compared to the diffusion of SiO, the change in solid structure due to the depletion of solid reactants is negligibly slow at any given time period. Thus, a simple form is obtained from Equation (5.10) as

$$\frac{dN^{\star}_{SiO}}{dz} = 0 \quad ; \quad N^{\star}_{SiO} = constant \tag{5.11}$$

The equilibrium pressure of SiO vapor ($P_{SiO,eq}$) may be achieved at a certain depth below the pellet surface, denoted as $z = \delta^\star$, because Si and SiO_2 are well-mixed in the pellet. In other words, $y_o = P_{SiO,eq}/P_{system}$ at the locations of $0 \le z \le \delta^\star$. If $N^\star_{SiO}$ is constant, Equation (5.7) can be integrated as

$$\frac{R\ T\ N^\star_{SiO}}{P\ \overline{D}_{SiO}} \int_{\delta^\star}^{\delta} dz = -\int_{y_o}^{y_s} dy_{SiO} \tag{5.12}$$

or

$$N^\star_{SiO} = \frac{P\ D_{SiO}}{R\ T} \frac{(y_o - y_s)}{\delta - \delta^\star} = \frac{C\ D_{SiO}}{\delta - \delta^\star}(y_o - y_s) \tag{5.13}$$

where y_o and y_S are the molar fractions of SiO vapor at $z = \delta^\star$ and $z = \delta$.

y_S is unknown, but can be related to the convection term. At the pellet surface, molar flux ($N^\star_{SiO}$) should be equal to the mass transfer rate of SiO, which is carried out by Ar flow.

$$N^\star_{SiO} = k_m\ C\ (y_S - y_B) = k_m\ C\ y_S \tag{5.14}$$

where k_m is the mass transfer coefficient. In Equation (5.14), it is also assumed that no SiO vapor exists in the bulk stream of Ar, i.e., $y_B = 0$, because SiO vapor is swept away by the Ar stream. Substituting Equation (5.14) into Equation (5.13) gives $N^\star_{SiO}$ as

$$N^\star_{SiO} = \frac{C\ k_m\ \overline{D}_{SiO}\ y_o}{(\delta - \delta^\star)\ k_m + \overline{D}_{SiO}} = K_{SiO}\frac{P_{SiO,eq}}{R\ T} \tag{5.15}$$

where $C\ y_o = P_{SiO,eq}/RT$ and

$$\frac{1}{K_{SiO}} = \frac{\delta - \delta^\star}{\overline{D}_{SiO}} + \frac{1}{k_m} \tag{5.16}$$

Equation (5.16) implies that two limited steps are involved in the process: pore diffusion and film mass transfer. As mentioned in Chapter 4, the process is limited by the pore diffusion step. In other words, the resistance of external mass transfer is much less than that of the pore diffusion in Equation (5.16). Thus, Equations (5.15) and (5.16) is simplified as

$$\frac{1}{K_{SiO}} \rightleftharpoons \frac{\delta - \delta^{\star}}{\overline{D}_{SiO}} \tag{5.17}$$

and

$$N_{SiO}^{\star} \rightleftharpoons \frac{\overline{D}_{SiO}}{\delta - \delta^{\star}} \frac{P_{SiO,eq}}{R\,T} \tag{5.18}$$

On the basis of the mass conservation, the generation rate of SiO vapor can be derived for the process.

$$N_{SiO}^{\star} \times (\textit{surface area}) \times (\textit{diffsuing time}) = \frac{\textit{pellet weight loss}}{\textit{SiO molar mass}} \tag{5.19}$$

or

$$N_{SiO}^{\star} \times (\frac{\pi\, d_{pellet}^2}{4}) \times dt = \frac{W_t - W_{t+dt}}{M_{SiO}} = \frac{W_{initial} \times dX}{M_{SiO}} \tag{5.20}$$

$W_{initial}$ and M_{SiO} represent the initial mass of pellet and molar mass of SiO. During the initial stage when the solid depletion is not significant, (dX/dt) is obtained according to Equations (5.18) and (5.20).

$$(\frac{dX}{dt}) = \frac{M_{SiO}\pi d_{pellet}^2}{4\,W_{initial}} \frac{\overline{D}_{SiO}}{\delta - \delta^{\star}} \frac{P_{SiO,eq}}{R\,T} = \frac{M_{SiO}}{\rho\,\delta_{initial}} \frac{\overline{D}_{SiO}}{\delta - \delta^{\star}} \frac{P_{SiO,eq}}{RT} \tag{5.21}$$

where ρ is the pellet apparent density.

5.3 Model Inspection

The effects of pellet porosity, that affects $\bar{D}_{SiO}$ in Equation (5.21), and thickness were used to test the proposed model. In the study of porosity effect, the initial mass of each pellet, thus the initial pellet thickness, was controlled to be roughly the same while the pellet porosity was changed from 0.48 to 0.32. To support the proportional relationship between (dX/dt) and $1/W_{initial}$ (or $1/\delta_{initial}$), two series of runs were made at 1294 and 1400 °C where the pellet porosity was fixed at 0.34 and 0.48, respectively.

5.3.1 Effect of Pellet Porosity (ε)

As discussed in Chapter 4, (dX/dt) increases with an increase in the pellet porosity. In terms of ε and τ, Equation (5.21) can be rewritten in a simple form.

$$\left(\frac{dX}{dt}\right) = \frac{\Phi}{\delta - \delta^*} \frac{\epsilon}{\tau} \tag{5.22}$$

where

$$\Phi = \frac{M_{SiO}\ \pi\ d_{pellet}^2}{4\ W_{initial}} \frac{D_{SiO-Ar}\ D_{SiO,K}}{D_{SiO-Ar} + D_{SiO,K}} \frac{P_{SiO,eq}}{RT} \tag{5.23}$$

Although $W_{initial}$ was controlled to be roughly the same in each run, an average mass of the pellets was used to represent $W_{initial}$ in each series of experiments. At fixed $W_{initial}$ and T, (dX/dt) should be proportional to $\varepsilon/\tau(\delta - \delta^*)$ as shown in Equation (5.22). As mentioned earlier, the tortuosity (τ) of pellets can be assumed to be $1/\varepsilon$ in many cases. Thus, Equation (5.22) becomes

$$\left(\frac{dX}{dt}\right) = \Phi \frac{\epsilon^2}{\delta - \delta^*} \tag{5.24}$$

It is also expected that $\delta - \delta^*$ increases with an increase in ε. Assuming that $\delta - \delta^* = \alpha \times \varepsilon^m$ gives

$$\left(\frac{dX}{dt}\right) = \frac{\Phi}{\alpha} \epsilon^{2-m} \qquad (5.25)$$

The data presented in Table 4.5 are used to test Equation (5.25) at given temperatures. Plotting (dX/dt) against ε in log-log scale is shown in Figure 5.2. The regressions indicate that the slope at each temperature is roughly the same, yielding that $2 - m = 0.64$, or $m = 1.36$.

It is necessary to determine $D_{SiO\text{-}Ar}$ and $D_{SiO,K}$ prior to finding the parameter α in Equation (5.25). Due to the lack of information of $D_{SiO\text{-}Ar}$ in the literature, $D_{CO2\text{-}Ar}$ has been used because SiO and CO_2 have the same molar mass. According to Cussler [1987], $D_{CO2\text{-}Ar}$ is 1.326×10^{-5} m^2/sec at 276.2 K. Since diffusion coefficient is roughly proportional to $T^{3/2}$, $D_{CO2\text{-}Ar}$ should be about 1.802×10^{-4} at 1300 °C. It should be mentioned that $D_{SiO\text{-}Ar}$ is estimated on the basis of this value at other temperatures. In addition, $D_{SiO,K}$ is calculated on the basis of the following equation for a dilute gas [Evans *et al.*, 1961].

$$D_{SiO,K} = 4850\, d_{pore} \sqrt{\frac{T}{M_{SiO}}} \qquad (\ cm^2/\text{sec}\ ) \qquad (5.26)$$

where d_{pore} is in cm and T is in K. Since $D_{SiO,K}$ varies with d_{pore}, an average pore diameter of pellets is used to calculate $D_{SiO,K}$ at each temperature.

According to Figure 5.2 and Equation (5.25), the calculations for determining the parameter α are summarized in Table 5.1. As shown in the table, α is roughly constant though the temperature is increased from 1300 to 1400 °C. On the basis of this finding, an average value (3.196×10^{-4}) was taken to represent α. Thus, $\delta - \delta^* = 3.196\times10^{-4} \times \varepsilon^{1.36}$ m. The small α value, that is, a small value of $\delta - \delta^*$ in the range of 67.9-117.8 μm suggests that $P_{SiO,eq}$ can be achieved near the pellet surface though the pellet porosity increases. Substituting all the constants into Equation (5.25) gives

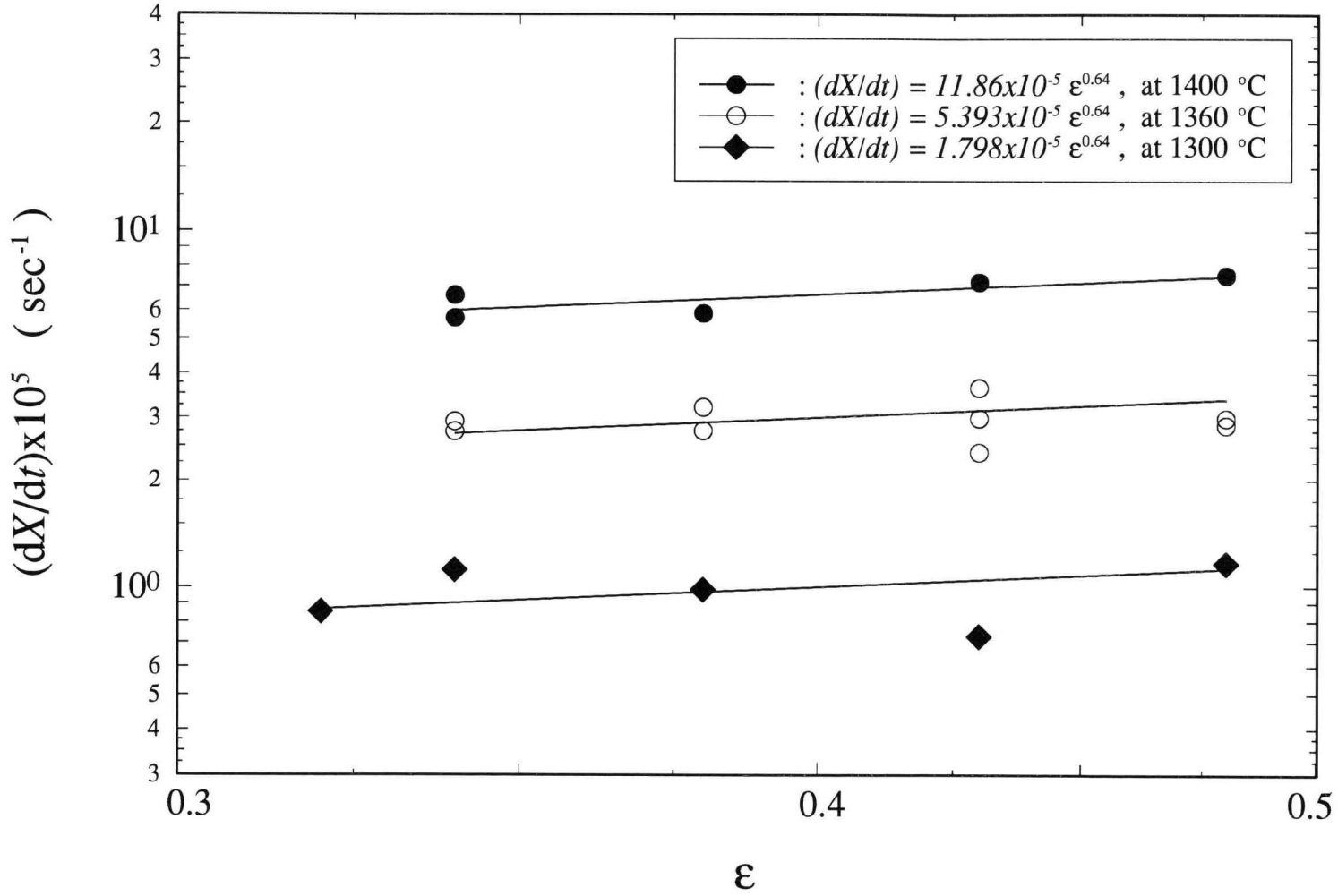

Figure 5.2 Porosity effect of pellet on SiO generation rate

Table 5.1 Calculations for determining parameter α in Equation (5.25)

T (°C)	$\Phi/\alpha \times 10^5$ (1/sec)*	$(W_{initial})_{Ave}$ (g)	$\bar{d}_{pore}$ (Å)	$P_{SiO,eq}$ (Pa)†	$D_{SiO\text{-}Ar} \times 10^4$ (m^2/sec)	$D_{SiO,K} \times 10^5$ (m^2/sec)‡	$\Phi^\# \times 10^8$	$\alpha \times 10^4$ (m)
1400	11.86	0.44281	1734	878	1.977	5.186	3.264	2.753
1360	5.393	0.44102	1734	481	1.906	5.123	1.808	3.352
1300	1.798	0.45321	1562	184	1.802	4.530	0.6264	3.484

$\star$: cited from Figure 5.2

$\dagger$: calculated on the basis of Equation (2.12)

$\ddagger$: calculated on the basis of Equation (5.26)

$\#$: calculated on the basis of Equation (5.23)

$$\left(\frac{dX}{dt}\right) = 1.3006\times10^{4} \times d_{pellet}^{2} \times \frac{D_{SiO\text{-}Ar}\, D_{SiO,K}}{D_{SiO\text{-}Ar} + D_{SiO,K}} \frac{P_{SiO,eq}}{T} \frac{\epsilon^{0.64}}{W_{initial}} \qquad (5.27)$$

5.3.2 Effect of Pellet Thickness ($\delta_{initial}$ or $W_{initial}$)

Equation (5.27) indicates that (dX/dt) should be proportional to $1/W_{initial}$ at fixed ε and T. Therefore, Figures 4.10 and 4.11 have been modified to test the relationship between (dX/dt) and $W_{initial}$ obtained at 1294 and 1400 °C. As seen in Figure 5.3, good linearity exists between (dX/dt) and $1/W_{initial}$ in both the series of experiments.

Equation (5.27) also suggests that (dX/dt) should go to zero when $1/W_{initial}$ approaches zero. The regressions show that (dX/dt) is equal to 4.529×10^{-6} sec^{-1} at 1294 °C or 2.516×10^{-5} sec^{-1} at 1400 °C as $1/W_{initial}$ is extrapolated to zero. These results imply that other process may be involved in the generation process, where (dX/dt) can be represented by the following equation:

$$\left(\frac{dX}{dt}\right)_{measured} = \left(\frac{dX}{dt}\right)_{impurity} + \left(\frac{dX}{dt}\right)_{SiO} = intercept + slope \times \frac{1}{W_{initial}} \qquad (5.28)$$

The reaction times in these two series of experiments were set for one hour at 1294 °C, and 20 minutes at 1400 °C. The intercepts, shown in Figure 5.3, imply that about 1.65 wt% of sample will be lost without producing SiO vapor at 1294 °C and the loss of sample mass will increase to 3.02 wt% at 1400 °C.

As indicated by Kondo *et al.* [1976], the mass loss of silica-gel (SiO_2) in the heat-treatment resulted from two sources: absorbed water and surface hydroxyl groups. The absorbed water will escape at 150 °C, and about 6 wt% of its surface hydroxyl groups will be removed when temperature reaches 700 °C. In this case, a sample loss of 3 wt% could be due to the removal of the hydroxyl groups because of the equal-

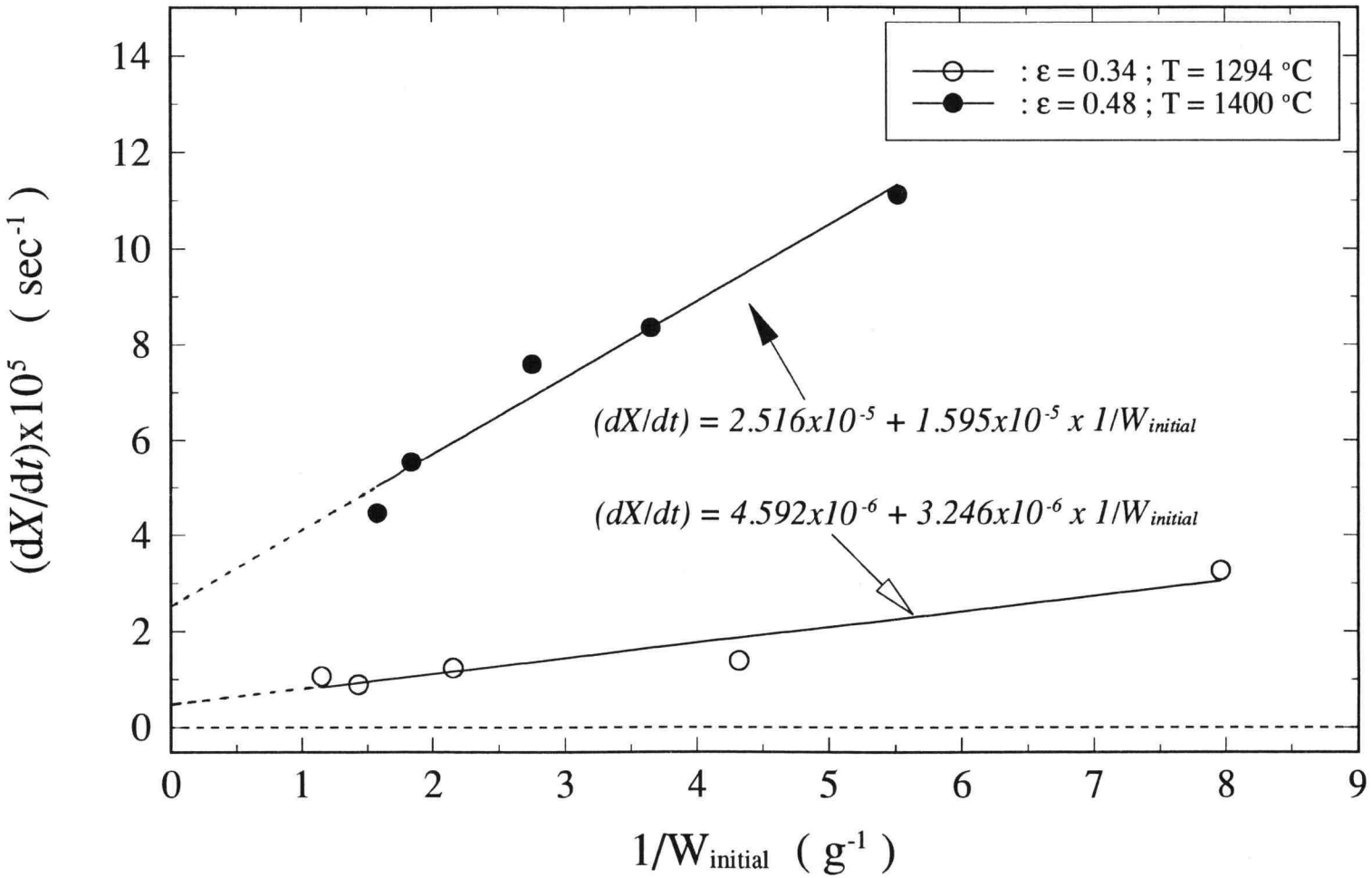

Figure 5.3 Thickness effect of pellet on SiO generation

molar-ratio of Si and SiO_2 in the compacted pellet. This value is close to those obtained from the intercepts in Figure 5.3. However, no further study on this effect was performed in this research.

The slopes shown in Figure 5.3 are also used to test Equation (5.27), shown in Table 5.2. As seen in the table, the experimental data support the model well at 1294 °C. The difference between the experimental data and the predicted value becomes more significant at 1400 °C. It should be mentioned that Equation (2.12) for estimating $P_{SiO,eq}$ is obtained at temperatures between 997 and 1327 °C. Thus, the departure of predicted value from the experimental data at 1400 °C may be due to the inappropriate estimation of $P_{SiO,eq}$ using this equation. However, the proportional relationship between (dX/dt) and $1/W_{initial}$ shown in Equation (5.27) is well supported by the experiments at these two temperatures.

Equation (5.27) indicates that (dX/dt) only depends on $P_{SiO,eq}$ if $W_{initial}$, T and ε are kept constant. Also, it should be noted that the structure of pellet is supposed to change with reaction time. Therefore, Equation (5.27) can be simplified as

$$\textit{Initial Conversion Rate} = \left(\frac{dX}{dt}\right)_o = \kappa P_{SiO,eq} \qquad (5.29)$$

where κ is constant, *i.e.*, depending on diffusion coefficients and other physical properties of solid.

Modifying Equation (2.12), one may find that the Gibbs free energy change of the SiO generation reaction is 341.7 kJ/mole, which is given as

$$P_{SiO,eq} = 4.102 \times 10^{13} \times e^{\frac{-341.7}{R\,T}} \quad (Pa) \qquad (5.30)$$

where R is 0.008314 kJ/mole-K. Since $(dX/dt)_o$ is only proportional to $P_{SiO,eq}$, the energies appearing in Figure 4.9 are essentially from the Gibbs free energy change of the SiO generation reaction modified by the activation energy of diffusion coefficients.

According to Equations (5.29), (30), and Figure 4.9, κ can be obtained for each process. From the experiments conducted in the SiO generator, κ can be expressed as

Table 5.2 Calculated results of SiO generation rate using Equation (5.24)

T (°C)	ε	d_{pore} (Å)	$P_{SiO,eq}$ (Pa)	$D_{SiO\text{-}Ar} \times 10^4$ (m^2/sec)	$D_{SiO,K} \times 10^5$ (m^2/sec)	*slope* × 10^6 (g/sec)†	*slope* × 10^6 (g/sec)‡
1294	0.34	991	166.7	1.792	2.868	2.766	3.246
1400	0.48	2575	878	1.977	7.701	38.14	15.95

† : calculated from Equation (5.27)

‡ : cited from Figure 5.3

$$\kappa = \kappa_o \times e^{-\frac{E_a}{RT}} = 1.317 \times 10^{-8} \times e^{-\frac{-31.7}{RT}} \quad \left(\frac{1}{Pa \times \sec} \right) \tag{5.31}$$

Also, the TGA analysis suggests that

$$\kappa = \kappa_o \times e^{-\frac{E_a}{RT}} = 5.539 \times 10^{-7} \times e^{-\frac{5.3}{RT}} \quad \left(\frac{1}{Pa \times \sec} \right) \tag{5.32}$$

where R is 8.314×10^{-3} kJ/mole and T is in K.

The energies shown in Equations (5.31) and (5.32) are the apparent activation energies resulting from the diffusion coefficients ($D_{SiO\text{-}Ar}$ and $D_{SiO,K}$), in which the values should be on the order of a few kilo-joules per mole. However, the energy shown in Equation (5.31) is not acceptable because of its negative sign.

It should be noted that this value is evaluated based on the experiments conducted in the SiO generator. In the SiO generator, $(dX/dt)_o$ was calculated on the basis of the loss of sample mass divided by the reaction time that was fixed at 1 hour at all temperatures except at 1400 °C (0.5 hour). Under this situation, $(dX/dt)_o$ was under-estimated due to the long reaction time. The errors are more pronounced at higher temperatures of 1350 and 1400 °C, leading to a decrease in the slope as seen in Figure 4.9. Therefore, the apparent activation energy obtained in the SiO generator has become negative, as given in Equation (5.31).

The TGA analysis shows a good agreement with Equation (5.27) because of the accuracy of determining $(dX/dt)_o$. As seen in Equation (5.32), the apparent activation energy of diffusion coefficients is 5.3 kJ/mole, that is on the same order as the predicted. From a viewpoint of activation energy, the experiments also support the proposed model well.

CHAPTER 6

FORMATION MECHANISM OF SILICON NITRIDE

It has been shown that the SiO-NH_3 reaction is instantaneous at temperatures in the range of 1300-1400 °C. Since NH_3 highly decomposes into N_2 and H_2 at such high temperatures, the mechanism of SiO-NH_3 reaction remains unclear owing to the co-existence of N_2 and H_2 with NH_3 in the reactor. Under this situation, systematic experiments were made to clarify the formation mechanism of Si_3N_4 in the reaction.

6.1 Reactant Effect

In Chapter 4.1, the preliminary study indicated that no whiskers were obtained when N_2 was mixed with H_2 as a reactant gas at 1350 °C. However, the runs made in the preliminary study were repeated at temperatures between 1300 and 1400 °C, using the longer tubular reactor as shown in Figure 3.4.

Three reactions were taken into consideration to identify possible reactants involved in the Si_3N_4 formation.

$$\mathbf{3\ SiO(g) + 2\ N_2(g) \rightarrow Si_3N_4(s) + 1.5\ O_2(g)} \quad \textbf{(2.3)}$$

$$\mathbf{3\ SiO(g) + 2\ N_2(g) + 3\ H_2(g) \rightarrow Si_3N_4(s) + 3\ H_2O} \quad \textbf{(2.13)}$$

$$\mathbf{3\ SiO(g) + 4\ NH_3(g) \rightarrow Si_3N_4(s) + 3\ H_2O(g) + 3\ H_2(g)} \quad \textbf{(2.14)}$$

The Gibbs free energy changes of these three reactions have been shown in Figure 2.1, in which Reaction (2.14) is thermodynamically favored because of the large negative values of ΔG^o at temperatures in the range studied. The operating conditions and experimental results are summarized in Table 6.1. It should be noted that runs B1400-03, B1350-03, and S1300-03 are cited from Table 4.9.

Table 6.1 Experimental conditions of runs for studying reactant effect on Si_3N_4 formation

Run No.†	N_2 (cm^3/min)‡	H_2 (cm^3/min)‡	NH_3 (cm^3/min)‡	T_{SiO} (°C)	$T_{Reaction}$ (°C)	$(dM_{SiO}/dt)_{Ave} \times 10^5$ (mole/min)	Deposits formed outside the heating zone (wt%)
N2-1400	891	0	0	1387	1391	7.112	92.5
MIX-1400	186	571	0	1388	1391	6.60	90.7
B1400-03	0	0	1382	1391	1394	7.228	12.6
MIX-1350	1068	353	0	1352	1353	3.222	94.5
B1350-03	0	0	1382	1342	1344	2.568	13.0
MIX-1300	186	571	0	1299	1302	1.510	86.1
S1300-03	0	0	1382	1301	1305	1.195	17.8

† : using uncompacted sample (C.P. = 0 MPa)

‡ : referred to room temperature

6.1.1 Product Distributions

When NH_3 was replaced by pure N_2 at 1400 °C, no whiskers were found at location 1, neither were crystals at location 2. Similar results were obtained using a mixture of N_2 (25 %) and H_2 (75 %) instead of NH_3 at any temperatures in the range studied. These phenomena were similar to those observed in the preliminary study though the reacting zone was increased. The mass distributions of product in the reactor are shown in Figures 6.1(a)-(c).

Whenever excess NH_3 was fed by a bent Al_2O_3 feeder, only about 15 wt% of the total product was carried by the gas flow out of the heating zone. However, the product distributions inside the reactor tube were changed dramatically when pure N_2 or N_2/H_2 mixture was used as a reactant gas. It was found that the majority of product ($\approx$ 50 wt%) was deposited right at the exit of furnace, the location that reaction temperature dropped to about 400 °C. Besides, the color of product changed from opaque-white (feeding excess NH_3) to dark-yellow-brown (using N_2 or N_2/H_2 mixture) toward the filter.

6.1.2 Transformation of Product Based on IR Analysis

IR analysis indicates that products formed at all the locations have similar spectra. Thus, the powder collected by the filter was used to clarify qualitatively the product transformation via the IR analysis. A comparison among the IR spectra of products on the reactant effect is shown in Figures 6.2(a)-(c). The IR spectra of powder formed in the runs using N_2 or N_2/H_2 mixture gas were not well-made because of the difficulty making transparent films for IR analysis due to the dark-yellow-brown color of product.

As shown in Figures 6.2(a)-(c), Si-N bonding assigned in the region between 850 and 1000 cm^{-1} is not significant for products obtained using N_2 or N_2/H_2 mixture gas compared to those obtained in the runs feeding excess NH_3. A characteristic peak

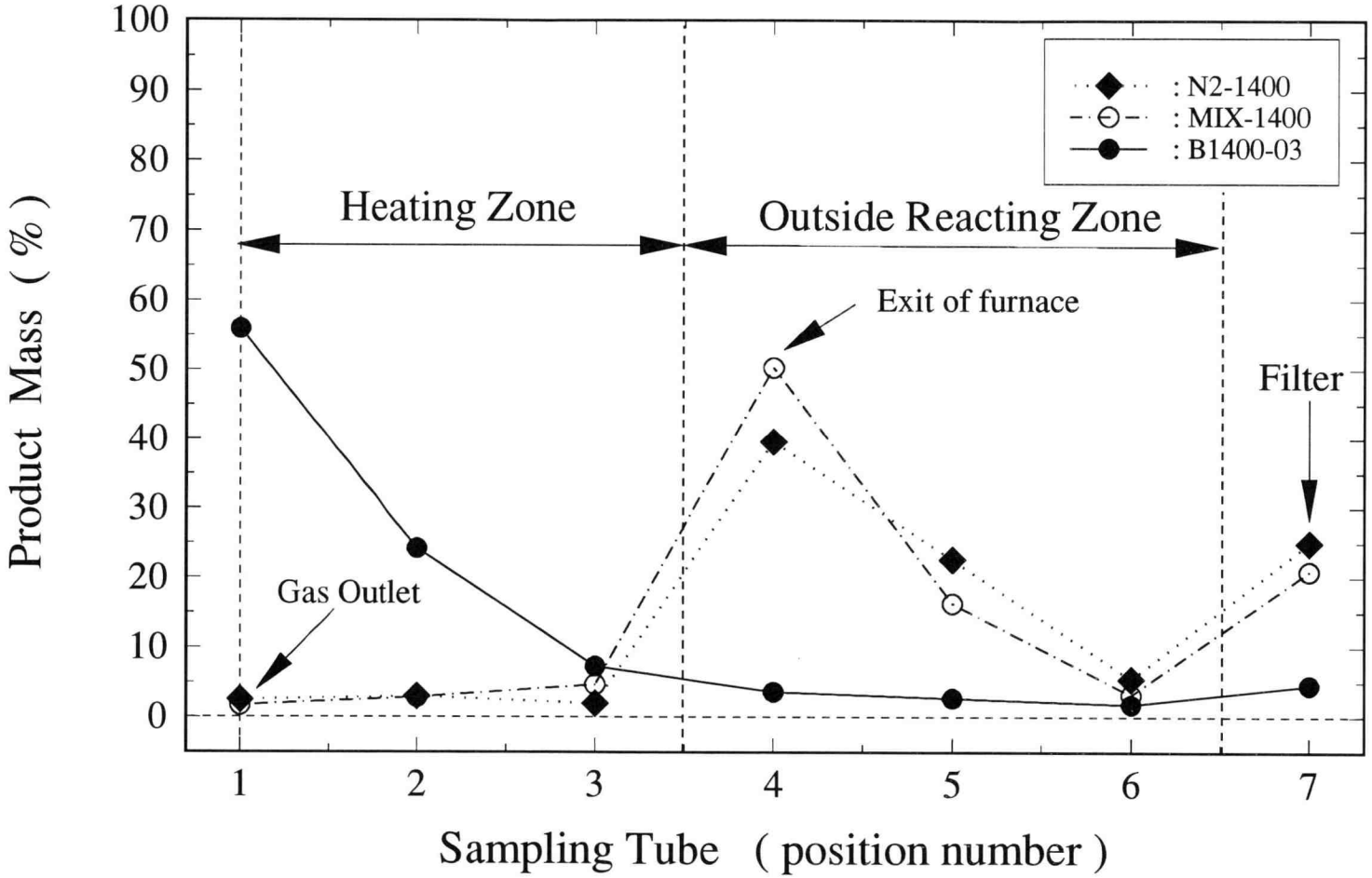

Figure 6.1(a) Reactant effect on product distribution at 1400 °C

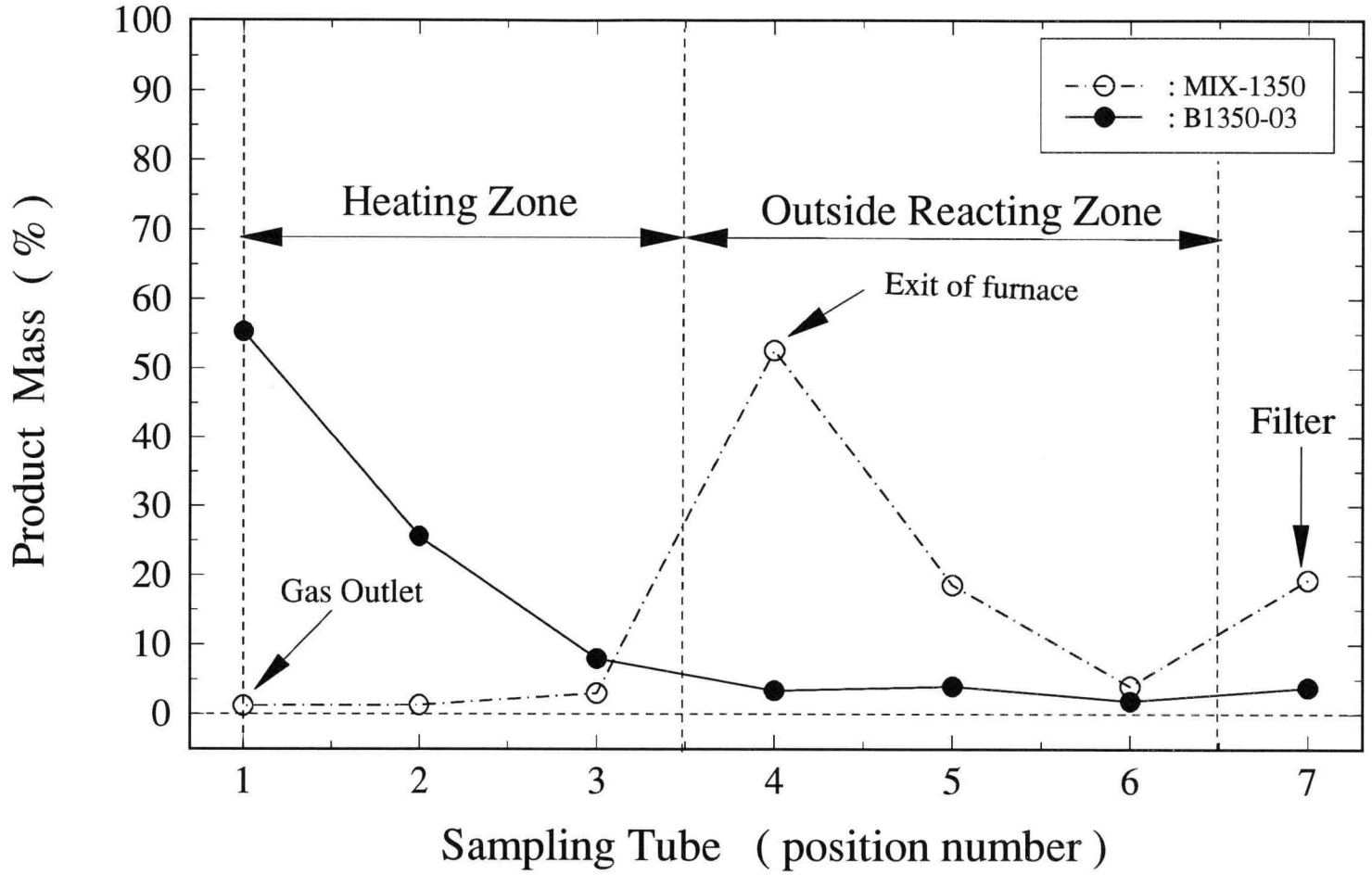

Figure 6.1(b) Reactant effect on product distribution at 1350 °C

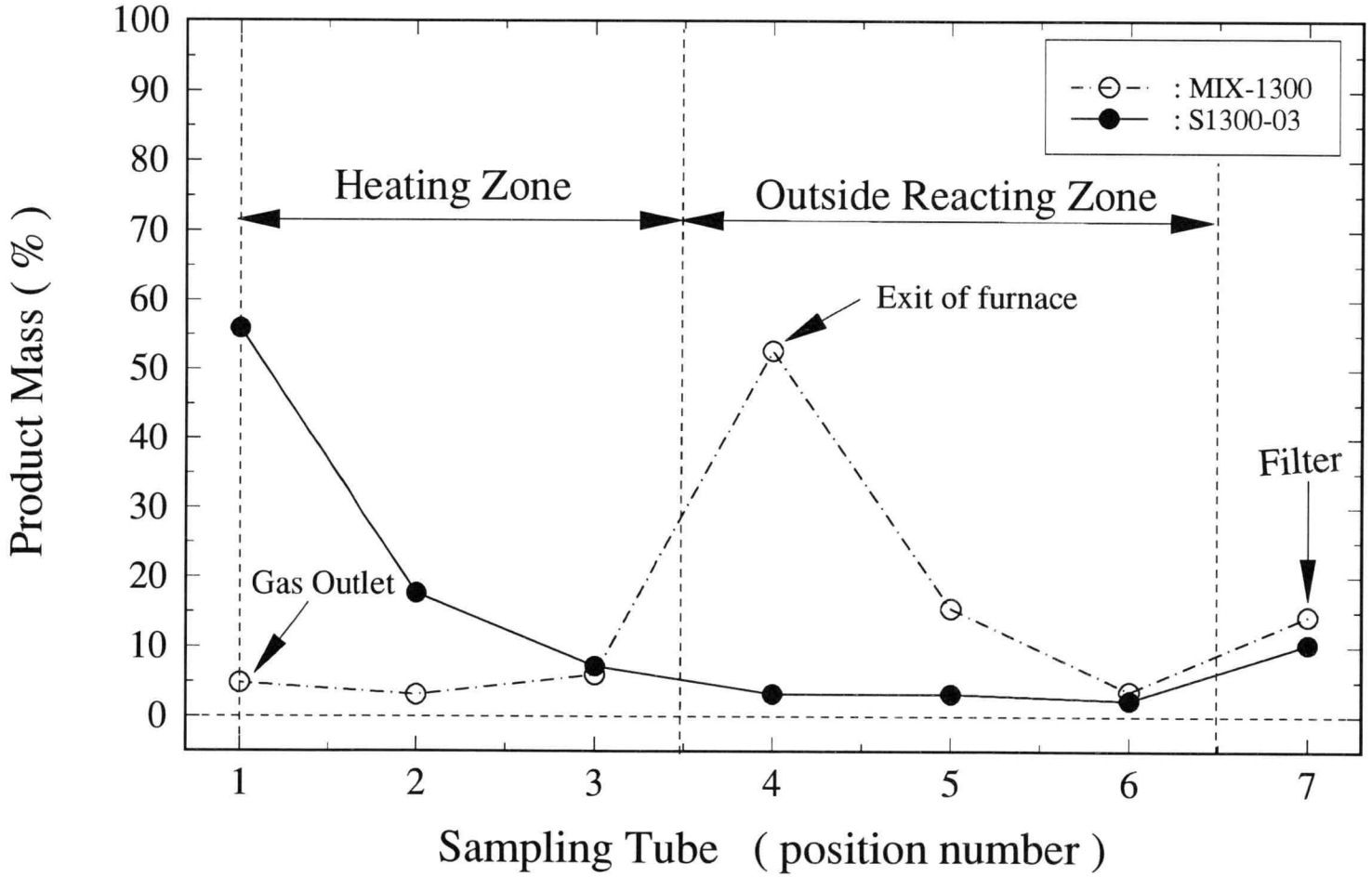

Figure 6.1(c) Reactant effect on product distribution at 1300 °C

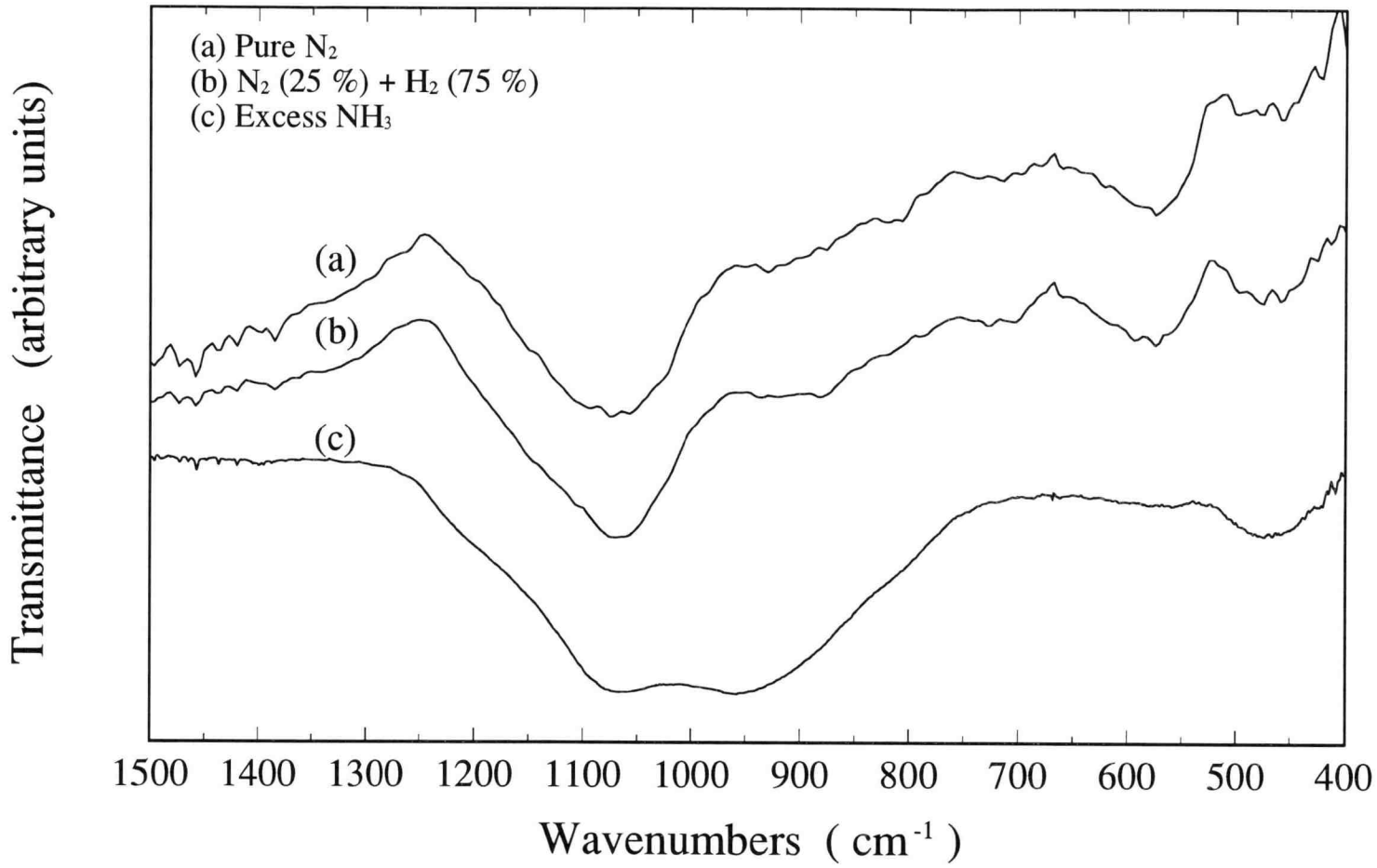

Figure 6.2(a) IR spectra of filter-collected powder formed at 1400 °C in different gaseous environments

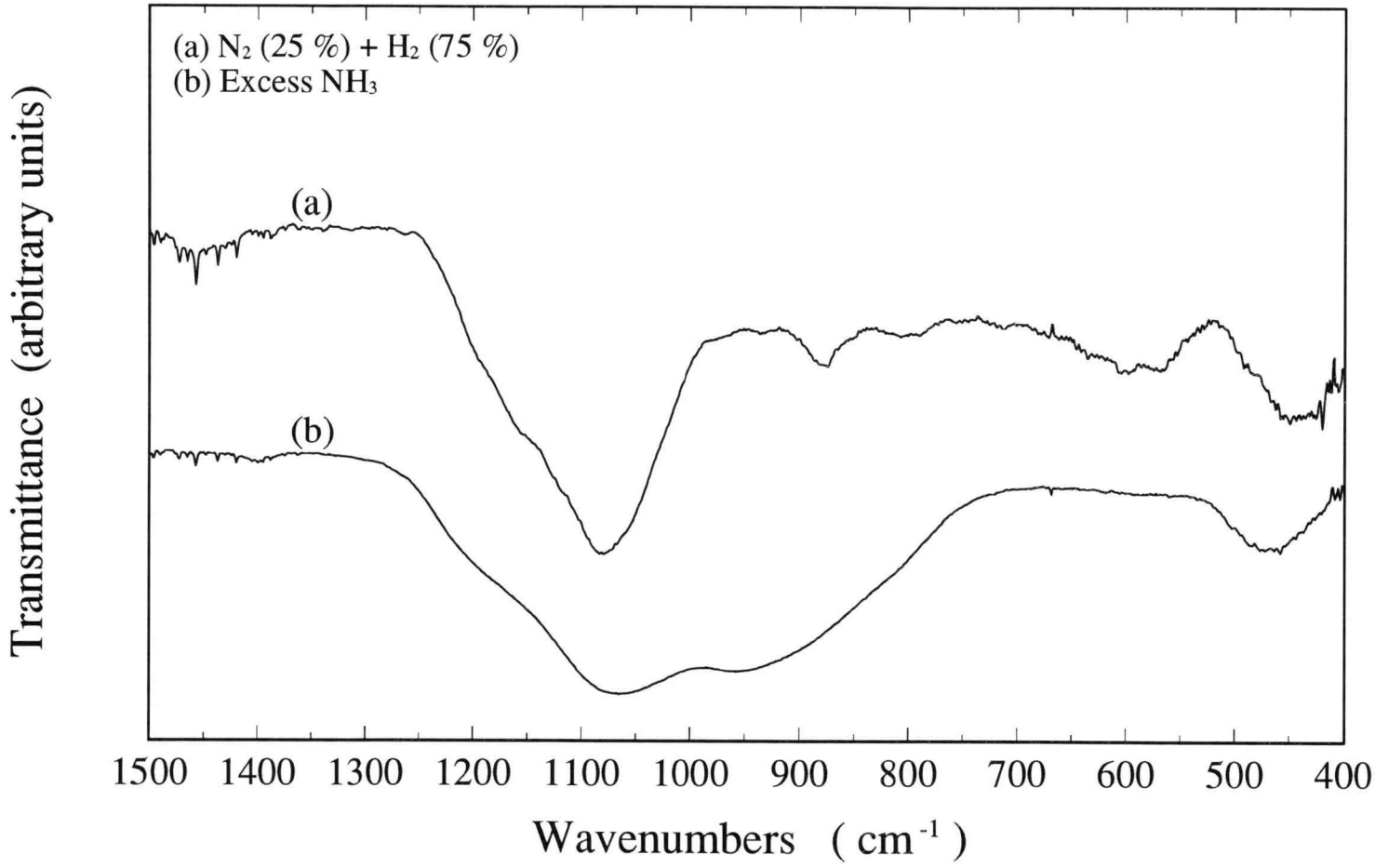

Figure 6.2(b) IR spectra of filter-collected powder formed at 1350 °C in different gaseous environments

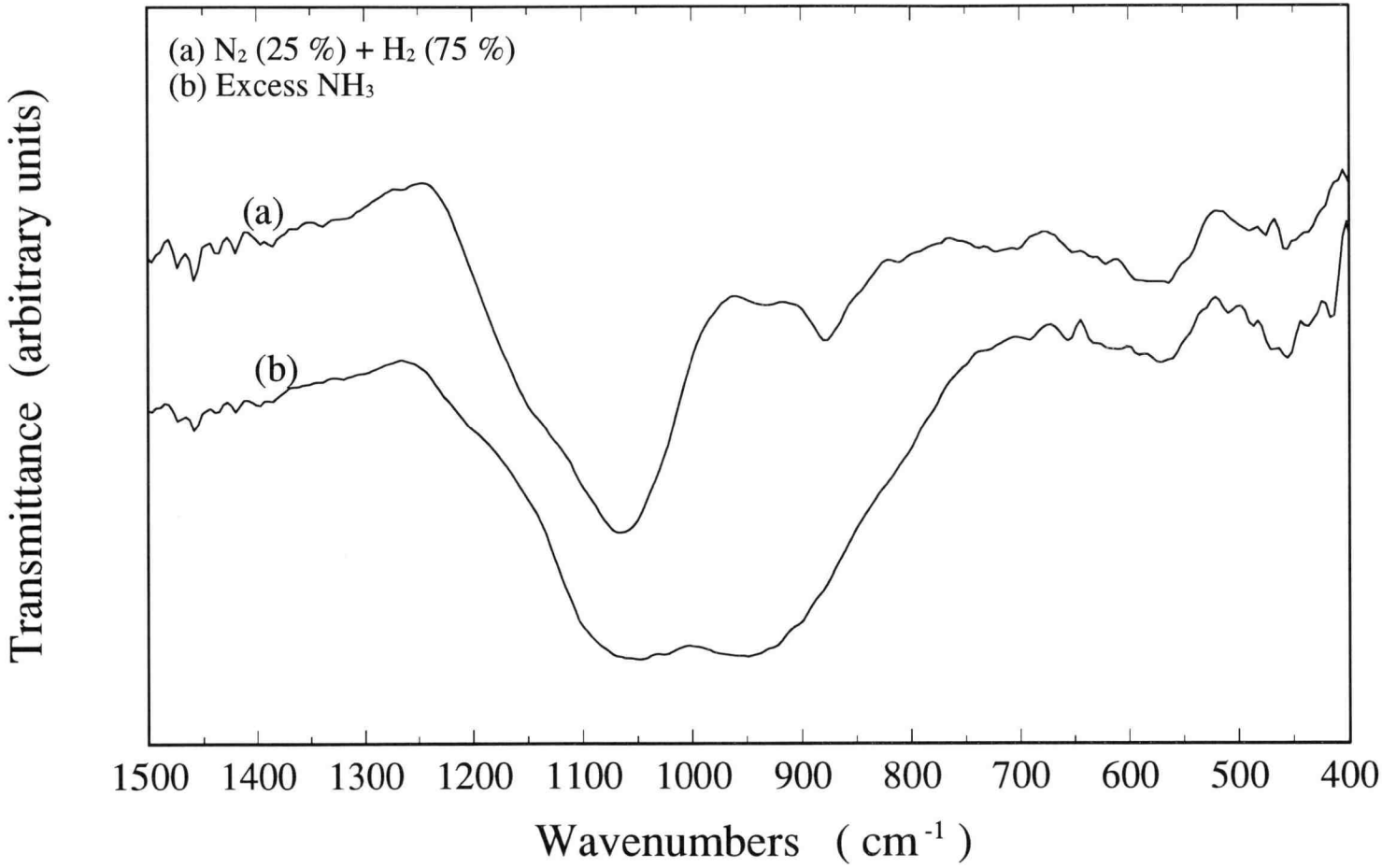

Figure 6.2(c) IR spectra of filter-collected powder formed at 1300 °C in different gaseous environments

appearing at wavenumber about 1100 cm^{-1} is attributed to Si-O bonding which may result from the presence of SiO_2.

According to thermodynamic calculations, the SiO-N_2 and SiO-N_2-H_2 reactions are not favored at temperatures in the range studied. Thus, un-reacted SiO vapor may condense back to an amorphous mixture of Si and SiO_2 due to the temperature drop toward the reactor exit, which is consistent with the experimental observation. This may be the reason why most product was deposited right at the exit of furnace, as shown in Figures 6.1(a)-(c).

It is concluded that NH_3 is the essential reactant dominating the formation of Si_3N_4 in the SiO-NH_3 reaction. Excess NH_3 is required for converting SiO vapor into Si_3N_4 in this process. According to the IR analysis and thermodynamic calculations, it is also believed that products obtained in the SiO-N_2 and SiO-N_2-H_2 reactions are an amorphous mixture of Si and SiO_2.

6.2 NH and NH_2 Effect on Si_3N_4 Formation

Reactions (2.3) and (2.13) are not feasible at temperatures between 1300 and 1400 °C. However, other intermediates such as NH or NH_2 may be formed in the NH_3 dissociation at such high temperatures as mentioned in Chapter 4.5. In this case, reactants involved in the SiO-NH_3 reaction are also unclear. The residual amount of NH_3 at the outlet of Al_2O_3 feeder can be predicted from Equation (4.13). Thus, several runs were made to force NH_3 to be fully decomposed into N_2 and H_2 before reacting with SiO vapor.

In addition, radicals (NH and NH_2) may no longer be active due to a longer residence time or temperature drop in the system. Thus, other experimental runs were made where NH_3 was once fully decomposed in a long Al_2O_3 tube, inserted through the furnace outside the reactor, cooled down to room temperature to make up a mixture of N_2/H_2, and then recycled back into the reactor to identify the possibility for radicals to react with SiO for the formation of Si_3N_4. The modified set-up of NH_3 feeding is shown in Figure 6.3.

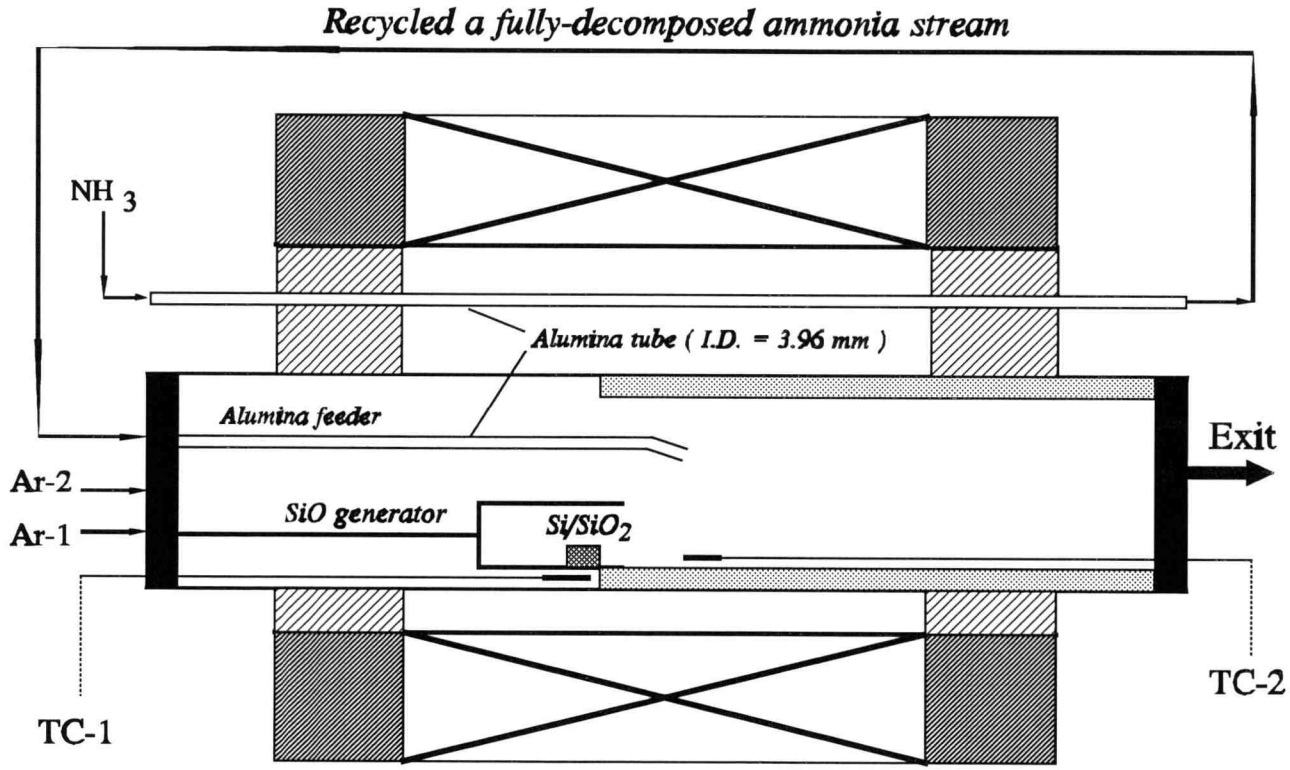

Figure 6.3 Modified experimental set-up of NH_3 feeding system

To clarify the effect of active radicals on the Si_3N_4 formation, the following three reactions are considered:

$$NH_3(g) \rightarrow I^*(g) \quad (6.1)$$

$$I^*(g) \rightarrow N_2(g) + H_2(g) \quad (6.2)$$

$$SiO(g) + I^*(g) \rightarrow Si_3N_4(s) + H_2O(g) \quad (6.3)$$

No stoichiometric coefficients are given in these three reactions because intermediates (I^*) formed in the NH_3 dissociation remain unclear.

Five runs were conducted in the tubular reactor. The experimental conditions and results are summarized in Table 6.2. It should be mentioned that the amount of NH_3 at the outlet of Al_2O_3 feeder is calculated based on Equation (4.13). Further IR analysis was used to identify possible change in the product.

6.2.1 Product Distribution

Three different types of products were still obtained in the experiments. As shown in Figures 6.4(a)-(c), the product distributions in the reactor are slightly different from those runs using excess NH_3 as reactant gas. It was found that product formed at the exit of furnace increased, especially at higher temperatures of 1350 and 1400 °C. However, the changes are not significant as they are compared to those shown in Figures 6.1(a)-(c).

The formation locations of whiskers and crystals were the same as those shown in Figure 4.20, except for run RCY-1400. Whenever excess NH_3 was used, whiskers only deposited in the sampling tube #1 (right at the outlet of Al_2O_3 feeder) in all the runs. In the run of recycling the fully-decomposed NH_3 stream (RCY-1400), whiskers were found in the sampling tubes #1 through #3 which were the same location for crystal deposition. However, it should be mentioned that this location change of whisker formation was found only in run RCY-1400 that was operated at 1400 °C.

Table 6.2 Experimental conditions of runs for studying radical effect on Si_3N_4 formation

Run No.†	**NH_3 Feeding** (cm^3/min)‡	**NH_3 Outlet** (cm^3/min)‡	**T_{SiO}** (°C)	**$T_{Reaction}$** (°C)	***(dSiO/dt)$_{Ave}$*** $\times 10^5$ (mole/min)	**Deposits formed outside the heating zone** (wt%)
FUL-1400	368	0	1391	1394	7.428	26.3
RCY-1400	368	0	1391	1393	7.053	18.1
B1400-03	1382	543	1391	1394	7.228	12.6
FUL-1350	368	0	1352	1353	2.633	11.9
RCY-1350	368	0	1351	1352	3.322	17.9
B1350-03	1382	868	1342	1344	2.568	13.0
RCY-1300	368	0	1302	1304	1.515	6.1
S1300-03	1382	1063	1301	1305	1.195	17.8

† : using uncompacted sample (C.P. = 0 Mpa)
FUL ≡ NH_3 fully decomposed at the outlet of Al_2O_3 feeder ;
RCY ≡ recycling a fully decomposed NH_3 stream into the reactor as shown in Figure 6.3

‡ : referred to room temperature and calculated by the program given in Appendix C

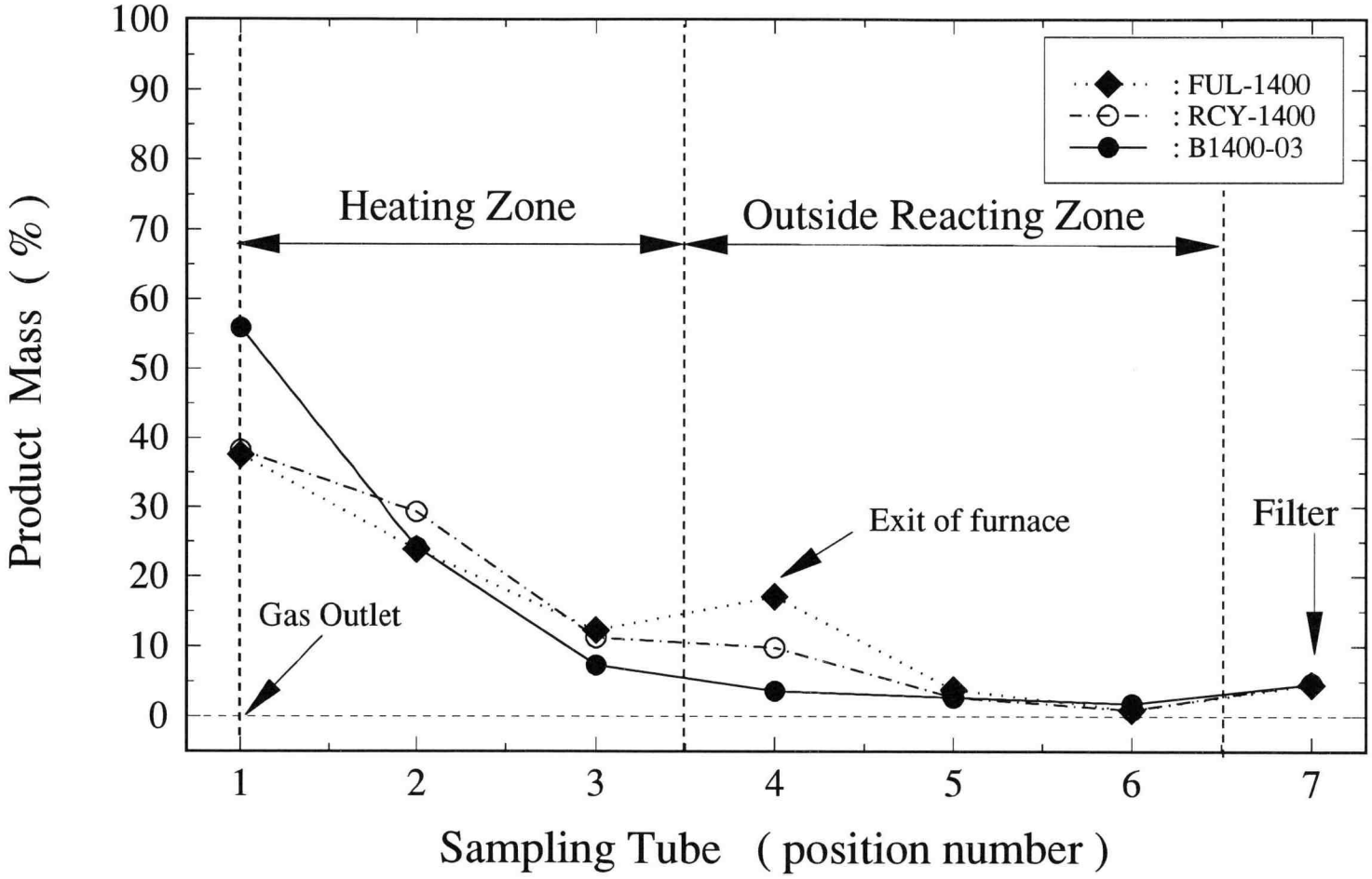

Figure 6.4(a) Radical Effect on product distribution at 1400 °C

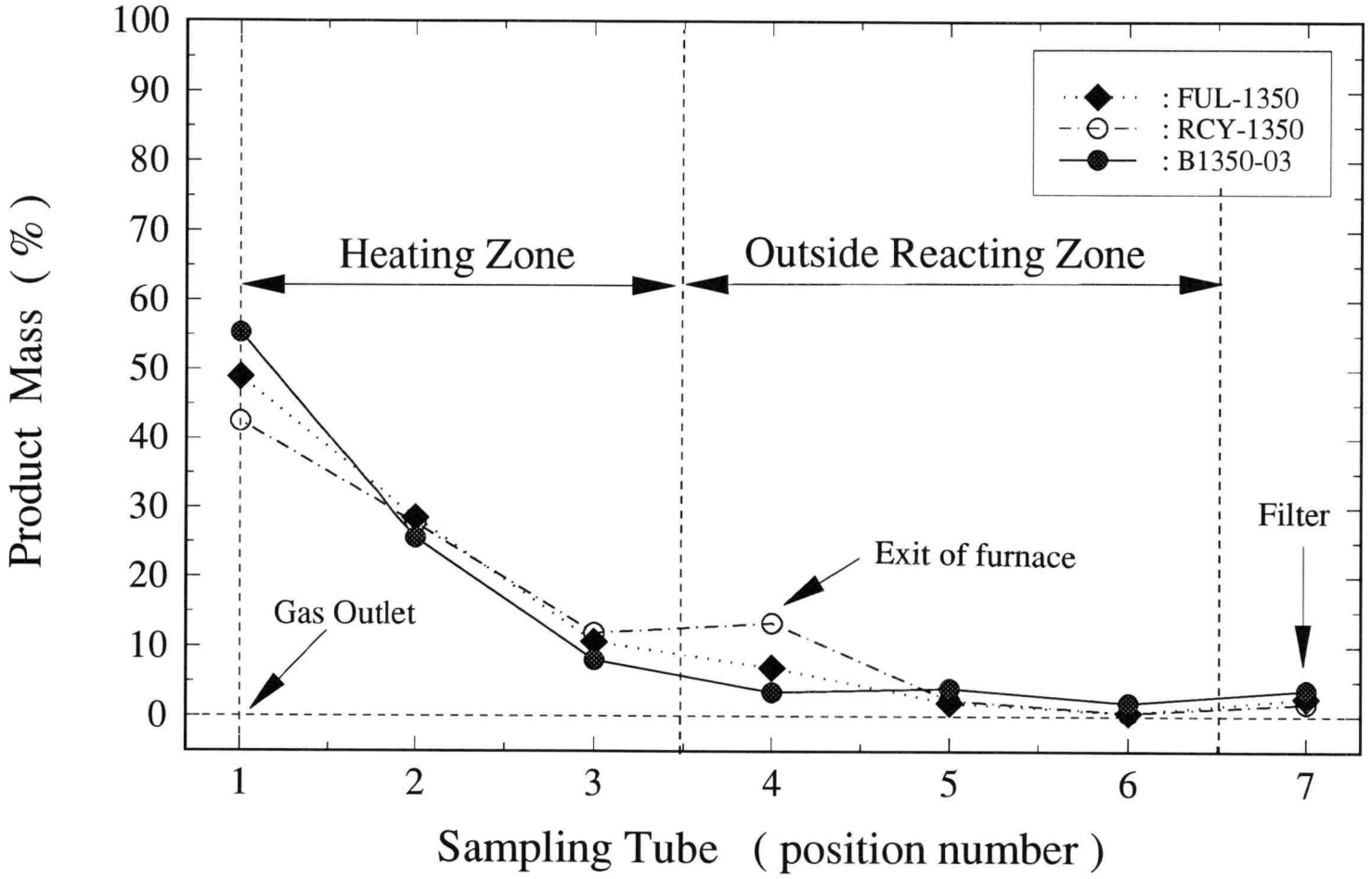

Figure 6.4(b) Radical Effect on product distribution at 1350 °C

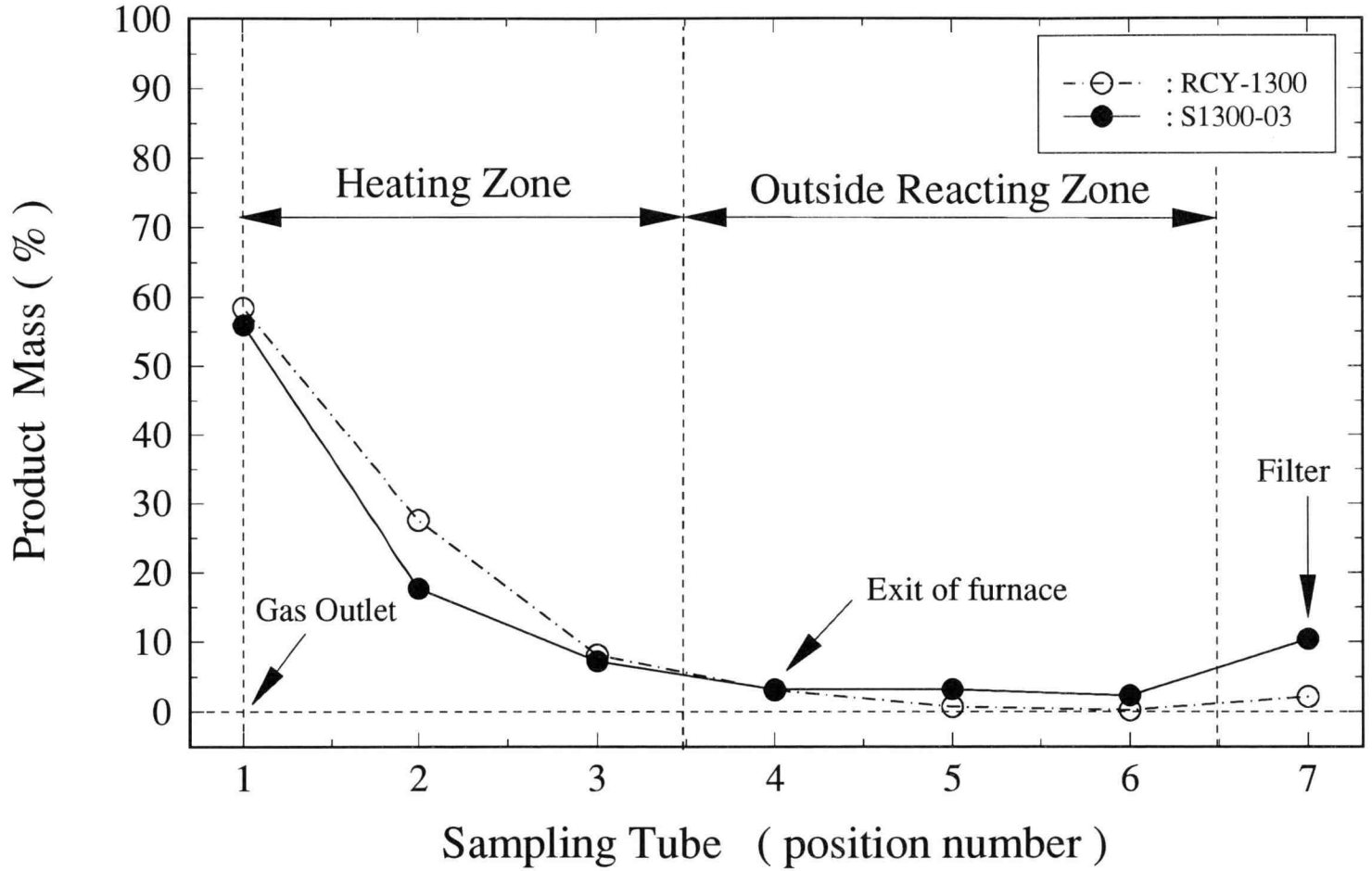

Figure 6.4(c) Radical Effect on product distribution at 1300 °C

6.2.2 Transformation of Product Based on IR Analysis

The IR spectra of whiskers and crystals obtained in the FUL and RCY runs are shown in Figures 6.5(a)-(c) and 6.6(a)-(c), respectively. Products formed at locations 1 and 2 have similar IR spectra to those obtained in the runs with feeding excess NH_3. However, the Si-O bonding appearing at 1100 cm^{-1} in the products becomes significant, especially in the run of recycling dissociated NH_3 at 1400 °C. According to the IR analysis, it is believed that Si_3N_4 whiskers and crystals were formed in the FUL and RCY runs, but a certain amount of SiO_2 is also contained. It is noteworthy that whiskers formed in the fully dissociated NH_3 contain Si_3N_4 crystals while those obtained in excess NH_3 are amorphous. As shown in Figures 6.5(a) and (b), the sharp peaks of crystalline Si_3N_4 are clearly seen at wavenumbers between 850-950 cm^{-1}. This finding also supports the enhanced effect of dissociated NH_3 on the crystallization of amorphous Si_3N_4, that has been discussed in Chapter 4.5.

However, the IR spectrum of filter-collected powder has a dramatic change on as seen in Figures 6.7(a) and (b). In Figure 6.7(a), the Si-N bonding has completely disappeared and the Si-O bonding is clearly seen in the spectra. Thus, the filter-collected powder from FUL-1400 and RCY-1400 runs is close to a mixture of Si and SiO_2. A little hump at 950 cm^{-1} seen in Figure 6.7(b) indicates that Si_3N_4 may be contained in the powder, but its amount should be negligible compared to SiO_2.

It should be mentioned that filter-collected powder produced in run RCY-1300 is too little for further IR analysis. Thus, the IR spectrum of the powder is not included in Figure 6.7.

6.2.3 Residual NH_3 in Feeding Stream

The formation of Si_3N_4 whiskers and crystals in the runs of recycling fully-decomposed NH_3 was far beyond the expectation. Thus, residual NH_3 remaining in the dissociated stream was taken into consideration. Using the GIBBS program

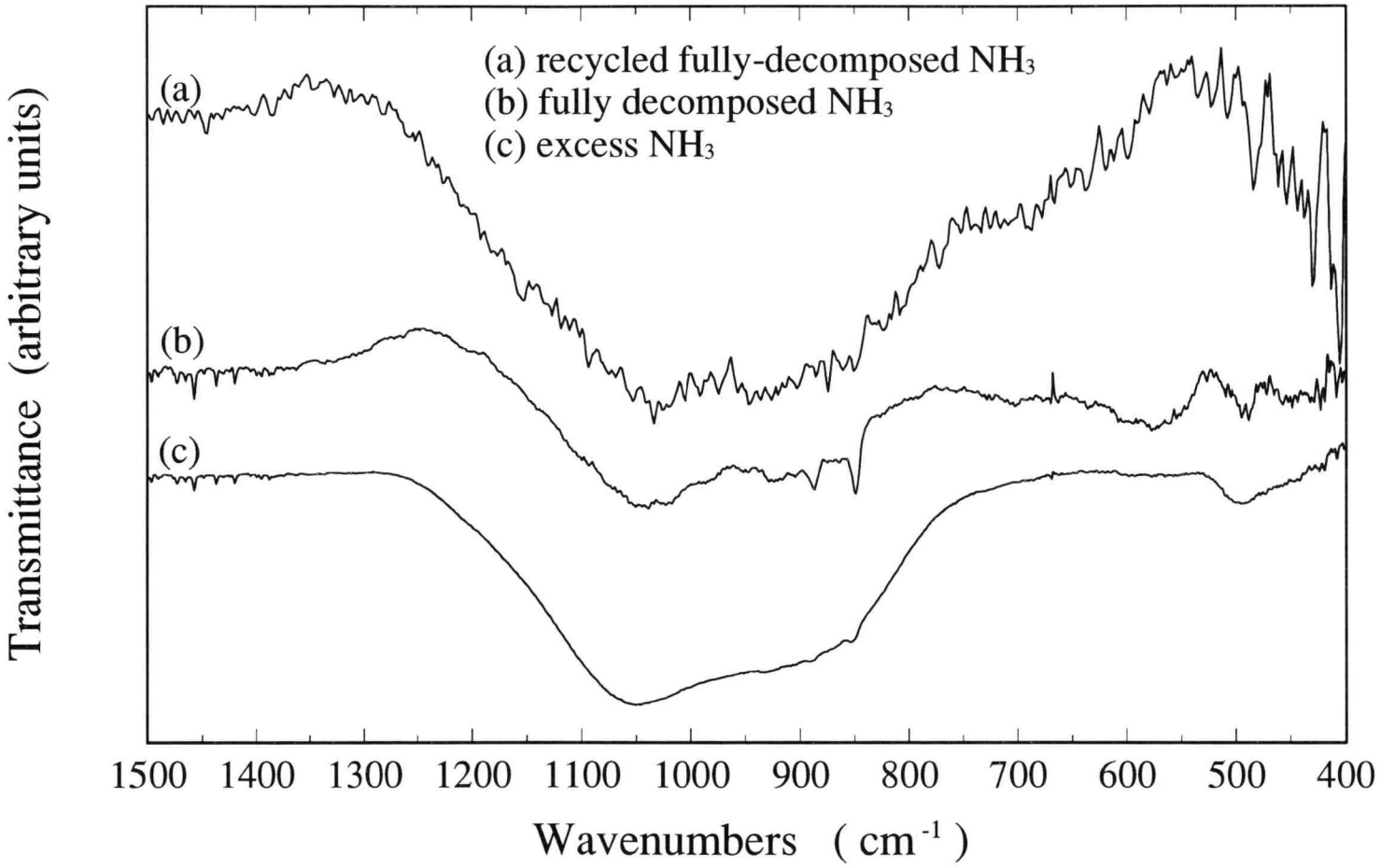

Figure 6.5(a) IR spectra of unheated whiskers formed at 1400 °C under different conditions of NH_3 dissociation

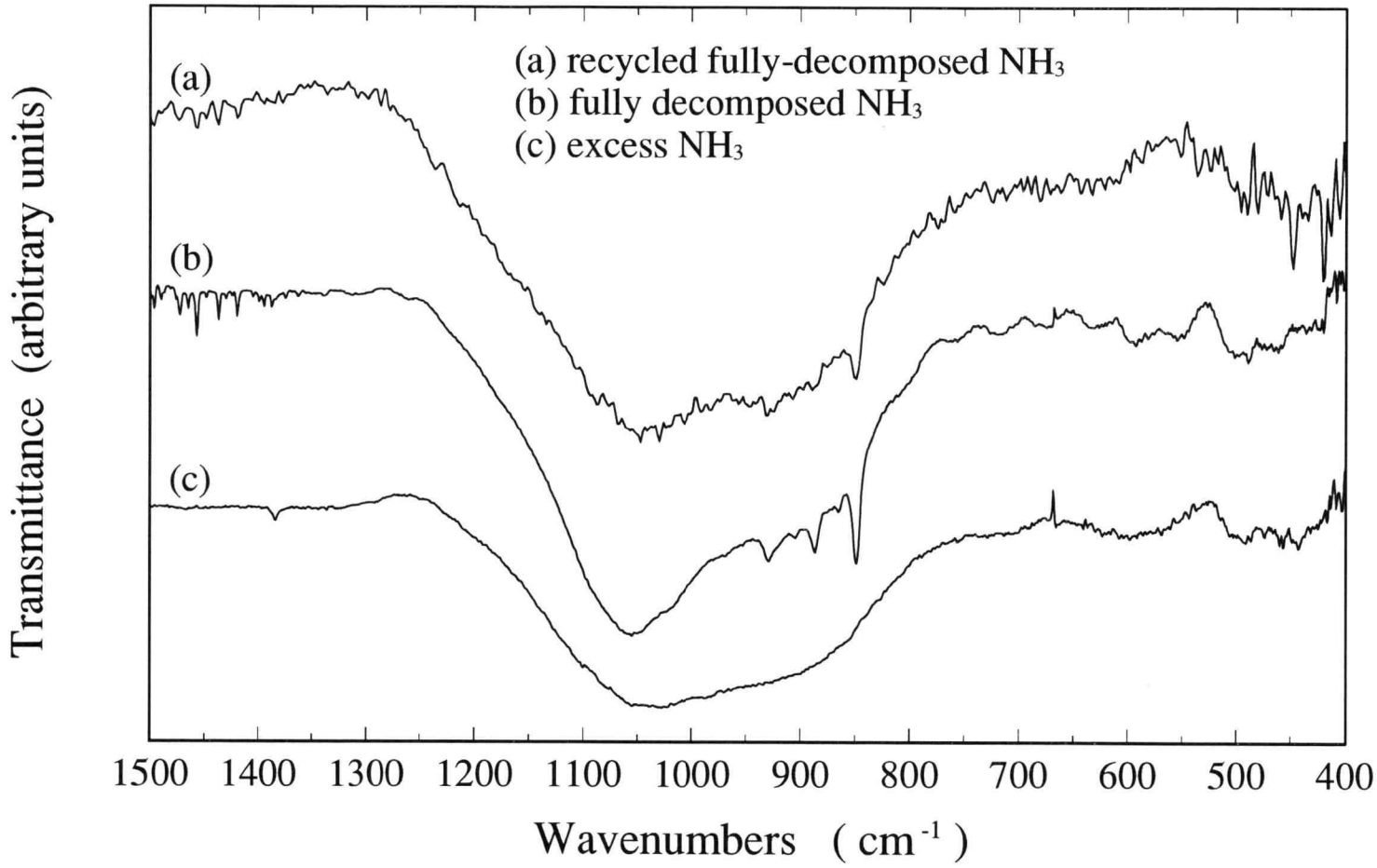

Figure 6.5(b) IR spectra of unheated whiskers formed at 1350 °C under different conditions of NH_3 dissociation

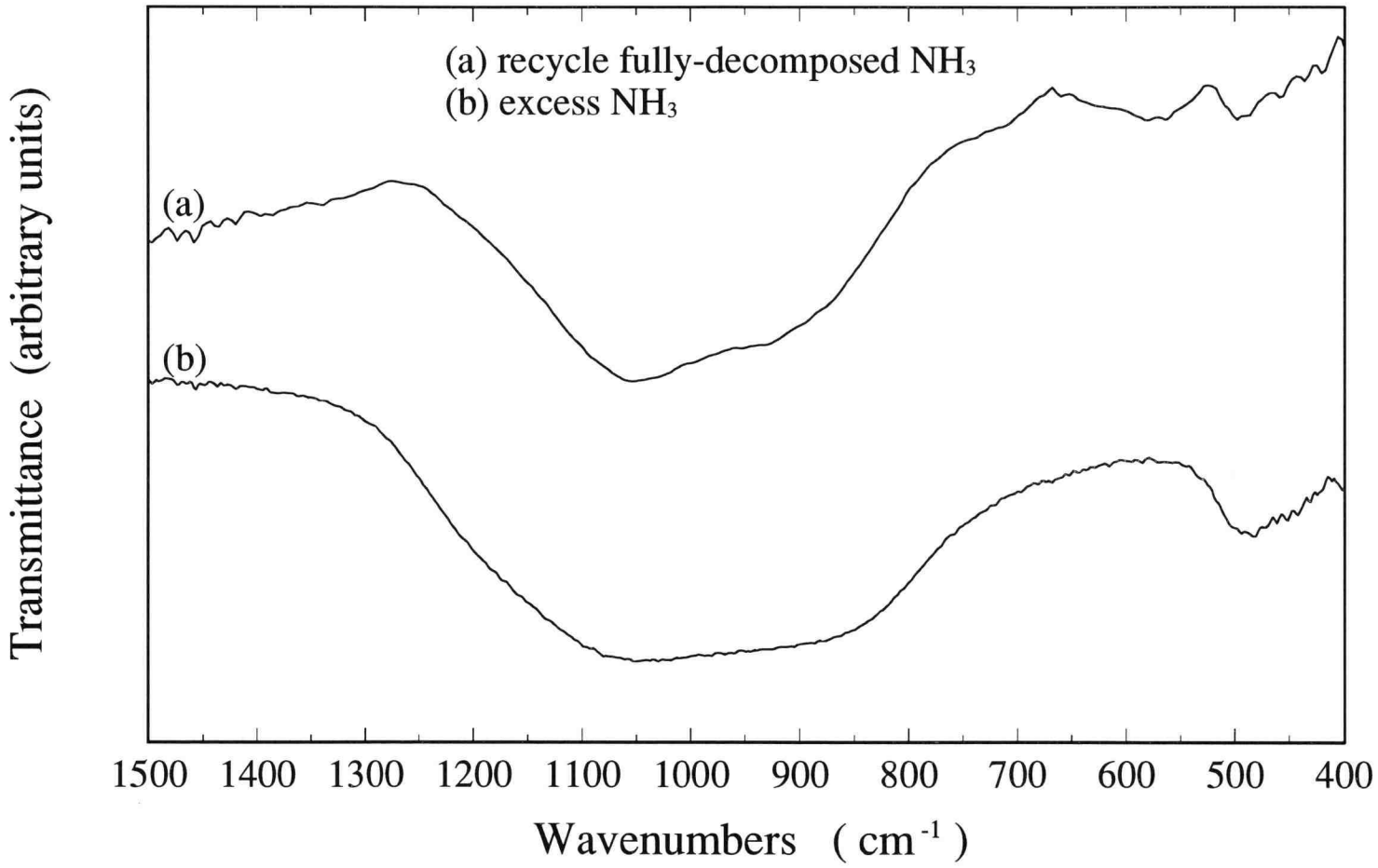

Figure 6.5(c) IR spectra of unheated whiskers formed at 1300 °C under different conditions of NH_3 dissociation

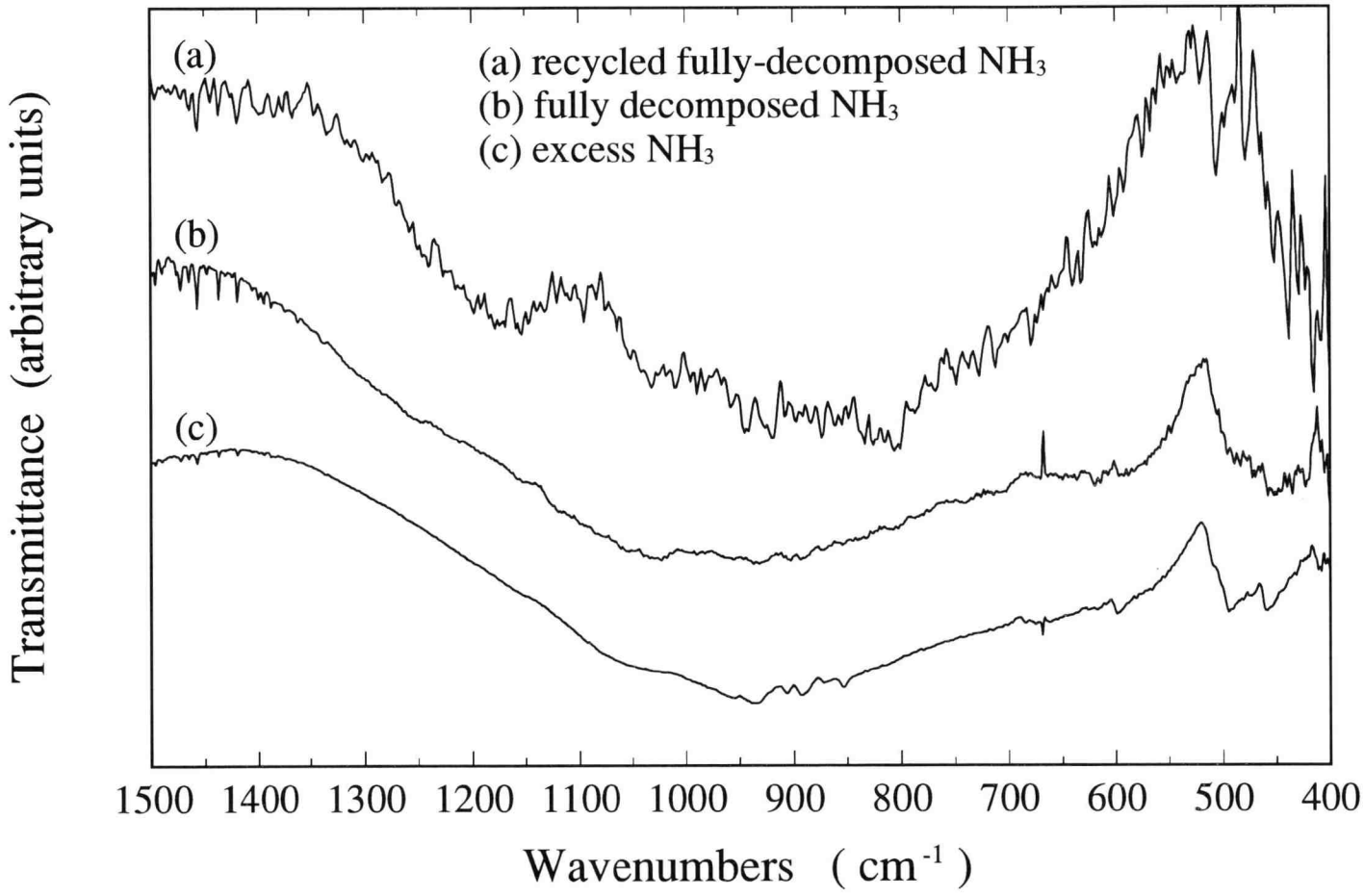

Figure 6.6(a) IR spectra of unheated crystals formed at 1400 °C under different conditions of NH_3 dissociation

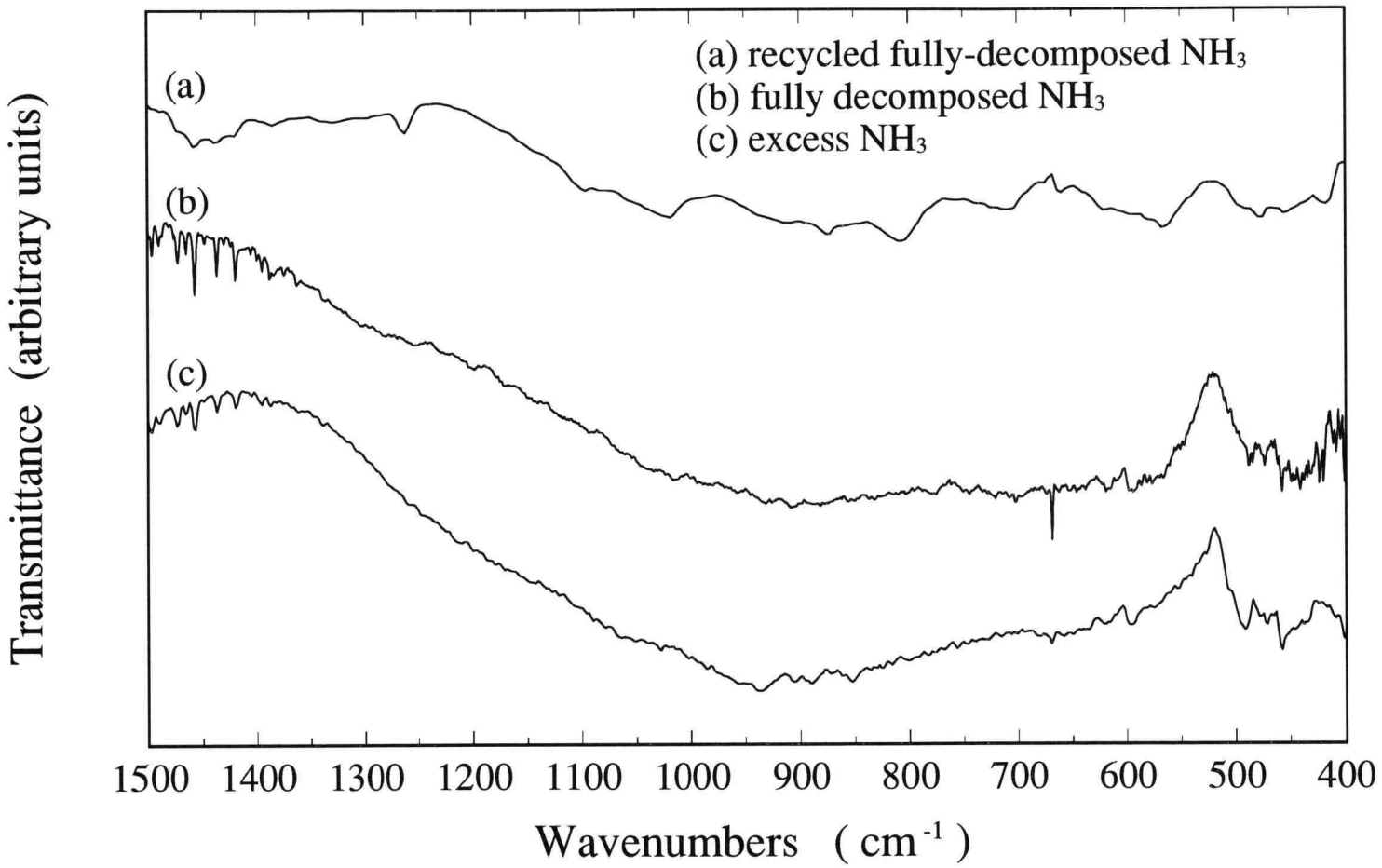

Figure 6.6(b) IR spectra of unheated crystals formed at 1350 °C under different conditions of NH_3 dissociation

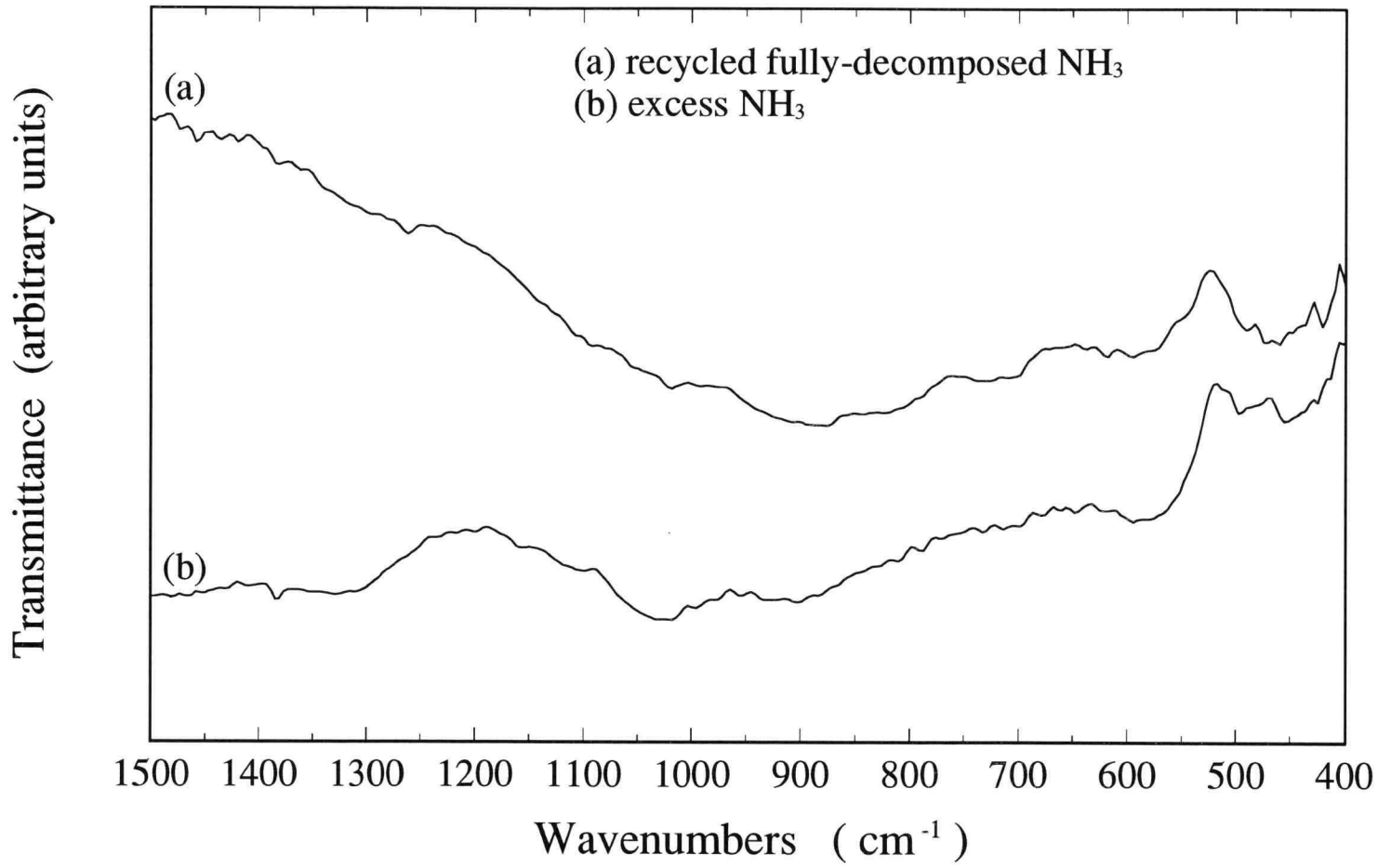

Figure 6.6(c) IR spectra of unheated crystals formed at 1300 °C under different conditions of NH_3 dissociation

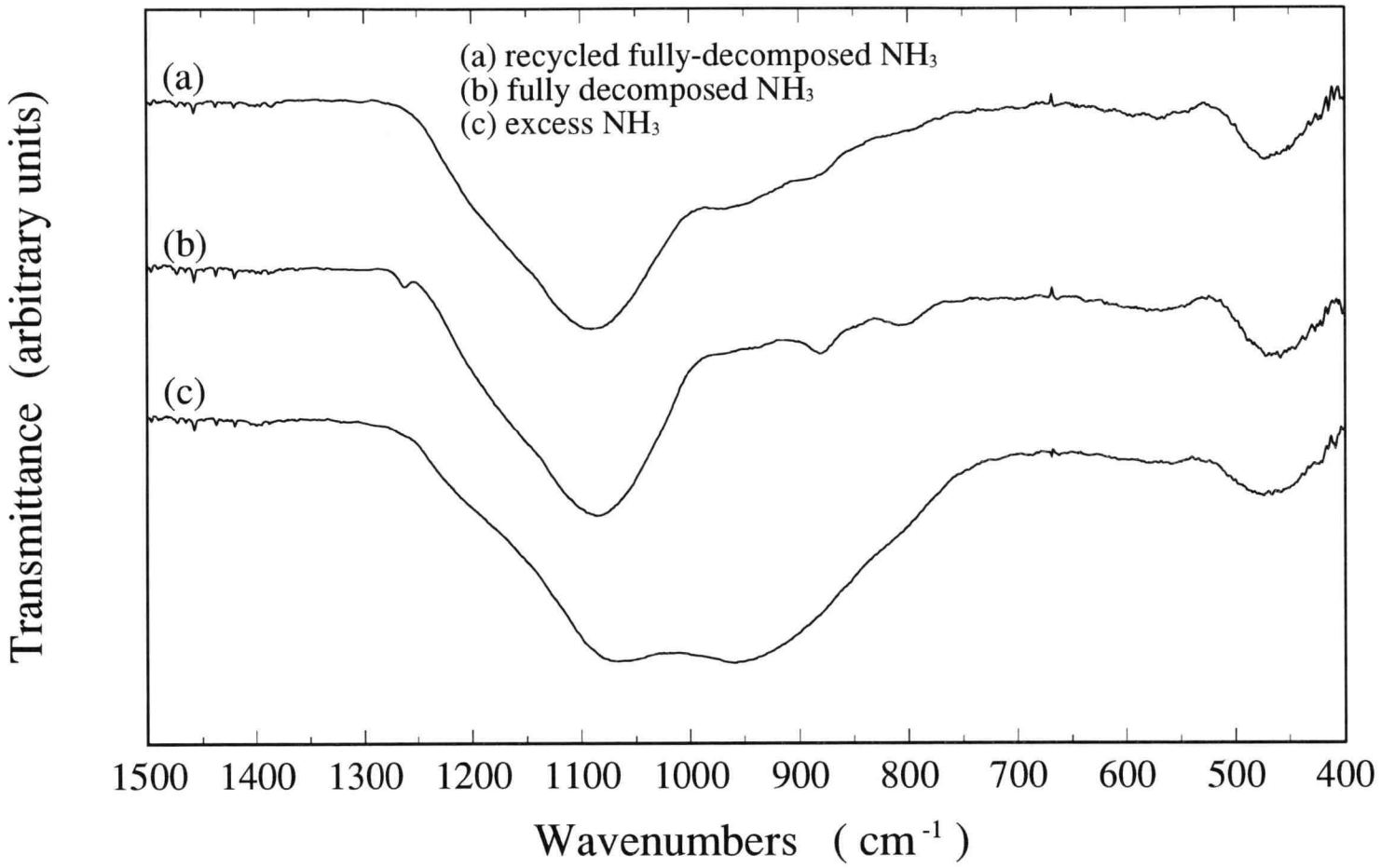

Figure 6.7(a) IR spectra of unheated powder formed at 1400 °C under different conditions of NH_3 dissociation

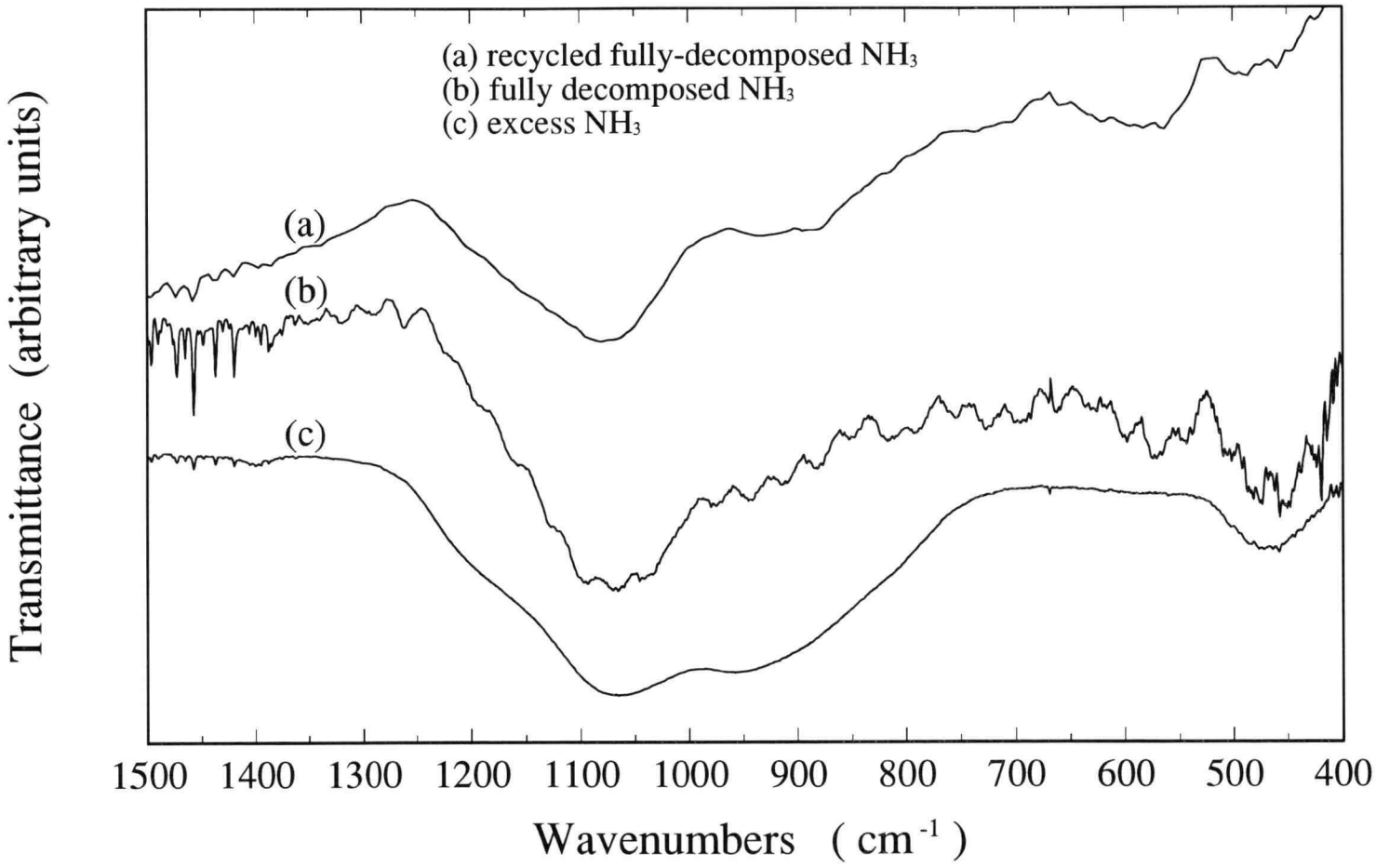

Figure 6.7(b) IR spectra of unheated powder formed at 1350 °C under different conditions of NH_3 dissociation

(Appendix A), the equilibrium compositions of NH_3 dissociation are calculated and shown in Table 6.3.

As shown in Table 6.3, intermediates NH and NH_2 are negligible compared to the other species in the system. Thus, the effect of NH and NH_2 radicals on the formation of Si_3N_4 may be negligible. On the other hand, about 0.0024 % of NH_3 remains undissociated toward equilibrium at 1427 °C. This fraction is equivalent to the amount of NH_3 of 0.0332 cm^3/min (or 1.36×10^{-6} mole/min) reaching the reacting zone at temperatures in the range studied. This is about one order magnitude less than $(dM_{SiO}/dt)_{Ave}$ in the reaction. However, the NH_3 stream may not reach the equilibrium because of the short residence time in a small diameter of the Al_2O_3 feeder. In this case, the amount of residual NH_3 entering the reacting zone may be higher than the equilibrium value mentioned above.

Thus, remaining NH_3 in the feeding stream may convert a portion of SiO into Si_3N_4 because the SiO-NH_3 reaction is instantaneous, which may be the reason why Si_3N_4 whiskers and crystals were formed in the FUL and RCY runs. No Si-N bonding was found in the filter-collected powder probably because of the full consumption of the remaining NH_3.

Since NH_3 feeding was fixed in all the runs, remaining NH_3 in the RCY runs should be less than in the FUL runs owing to a longer residence time needed to reach the reacting zone. As mentioned earlier, the whiskers formed in run RCY-1400 were rather scattered in the sampling tubes #1 through #3. Since NH_3 was highly dilute in this run, the location change of whisker formation may be caused by the dilution of NH_3 in the reaction.

Residual NH_3 effect on the Si_3N_4 formation in the FUL and RCY runs is also supported by the IR analysis. As shown in Figure 6.6(a), Si-O bonding at about 1100 cm^{-1} is clearly seen in the IR spectrum of crystals produced in run RCY-1400. This Si-O bonding is not significant in the crystals formed in run FUL-1400. Besides, Si-N bonding in the filter-collected powder becomes more significant in Figure 6.7(b) because more NH_3 is remaining at a lower temperature of 1350 °C, leading to forming a certain amount of nanophase Si_3N_4 powder.

Table 6.3 Equilibrium calculations of NH_3 dissociation

$NH_3(g) \rightleftharpoons N_2(g) + H_2(g) + NH(g) + NH_2(g)$ *initial mole of NH_3 = 1 mole*		
Compound	1327 °C	1427 °C
	composition (mole)	composition (mole)
NH_3	3.074×10^{-5}	2.403×10^{-5}
N_2	0.4999846	0.4999880
H_2	1.499954	1.4999640
NH	0	0
NH_2	9×10^{-9}	1.0×10^{-8}
	dimensionless G/RT = -42.419	dimensionless G/RT = -42.788

It is suggested from these experimental results that NH_3 is the essential reactant for converting SiO into Si_3N_4. SiO hardly reacts with N_2 even in the presence of H_2 in the temperature range investigated. Whenever NH_3 has fully decomposed into N_2 and H_2, no nanophase Si_3N_4 powder is produced. Active radicals such as NH and NH_2 may be involved in the reaction, but the effect is not significant compared to NH_3.

CHAPTER 7

CONCLUSIONS AND RECOMMENDATIONS OF FUTURE WORK FOR Si_3N_4 SYNTHESIS VIA SiO-NH_3 REACTION

7.1 Conclusions

The synthesis of Si_3N_4 via the SiO-NH_3 reaction was studied in a tubular flow reactor at temperatures between 1300 and 1400 °C. SiO vapor was generated from Si/SiO_2 compacts, and then carried by Ar gas into the reacting zone where the reaction with NH_3 proceeded. The dissociation of NH_3 was also investigated before studying the SiO-NH_3 reaction. Amorphous Si_3N_4 obtained as one of forms of product was crystallized into α and β crystals at temperatures in the range of 1300-1560 °C.

This study can be divided into four independent parts: generation of SiO vapor, NH_3 dissociation, Si_3N_4 formation, and crystallization of amorphous Si_3N_4. Thus, the conclusions of the SiO-NH_3 reaction will focus on individual parts, which are given in the following sections.

7.1.1 Generation of SiO Vapor

According to the SEM images, it is suspected that the Si-SiO_2 reaction is not a pure solid-solid reaction. Although the intrinsic reaction mechanism still remains unclear, the following conclusions can be made from the overall reaction:

(1) The SiO generation from Si/SiO_2 compacts is roughly constant during the initial stage. After a certain period of time, the generation rate decreases with reaction time. The decrease in the generation rate may result from the structural change of individual grains in the pellet, leading to poor physical contact between Si and SiO_2 grains due to the consumption of these two.

(2) An Arrhenius type relationship holds between the initial rate and reaction temperature in the range studied. The apparent activation energies obtained using the TGA and SiO generator are 347 and 310 kJ/mole, respectively.

(3) In a stagnant Ar, the SiO generation is controlled by the mass transfer through the film on the pellet surface. With sufficient flow of Ar through the SiO generator, the film resistance vanishes and the process is limited by the internal pore diffusion step. The rate of SiO generation is inversely proportional to the initial thickness (or initial mass) of the pellet, which has been explained by a simple diffusion model developed in this study.

(4) The higher the pellet porosity (ε) the higher the SiO generation rate. Based on the model, $(dX/dt)_o$ is correlated to be proportional to $\varepsilon^{0.64}$ at any temperature in the range investigated. The equilibrium pressure of SiO vapor may be achieved at location $3.196\times10^{-4} \times \varepsilon^{1.36}$ m deep from the pellet surface when there is Ar flow in the SiO generator.

7.1.2 Ammonia Dissociation

The differential flow analysis was used to determine the dissociation rate of NH_3 in an Al_2O_3 tube. According to the experimental findings, the conclusions of this part are given below:

(1) The dissociation rate varies with time, once increasing to a peak and then decreasing to an ultimate stable value. The variation is more pronounced at higher temperatures of 1350 and 1400 °C. It is suspected that complex activation and deactivation of Al_2O_3 surface are involved in the dissociation process.

(2) At temperatures in the range of 1185-1382 °C, an 1/3 order rate equation can describe the NH_3 dissociation in the Al_2O_3 tube. The rate constant k can be expressed as: $k = 5.236\times10^{10} \exp(-278/RT)$, where R is 8.314×10^{-3} kJ/mole-K and T is in K.

(3) The Al_2O_3 tube recovers its original conditions whenever it is once cooled down to room temperature and reheated to the preceding temperature.

7.1.3 Formation of Silicon Nitride

Si_3N_4 was successfully produced in both amorphous and crystalline forms from the SiO-NH_3 reaction at temperatures in the range studied. Based on the experimental results, the following conclusions are made:

(1) The Si_3N_4 formation via the SiO-NH_3 reaction is instantaneous when NH_3 is in large excess, yielding three different types of product: amorphous whiskers (0.5-4 μm in diameter), α-polycrystals, and amorphous nanophase powder (20 nm in diameter). The most favored product in the system is in the form of α-crystals, followed by either nanophase powder or whiskers.

(2) NH_3 is essential for converting SiO into Si_3N_4, and SiO does not react with N_2 even in the presence of H_2.

(3) When NH_3 is fully decomposed before contacting with SiO, small amounts of nitride whiskers and crystals form. However, no nanophase Si_3N_4 powder is obtained in the reaction.

(4) The method of NH_3 feeding affects the formation of whiskers and nanophase powder. The impingement of gas flow against the tube wall is an important factor for the formation of whiskers.

(5) Amorphous whiskers and nanophase powder are oxidized by ambient oxygen and moisture after the synthesis, leading to an increase in oxygen content with time.

7.1.4 Crystallization of Amorphous Product

Amorphous products were crystallized at temperatures in the range of 1300-1560 °C, depending on product types and gaseous environment.

(1) When dissociated NH_3 is used, nanophase powder can be crystallized at 1300 °C in 5 hours while whiskers are crystallized at 1350 °C in 8 hours.

(2) The crystallization of whiskers as well as nanophase powder progresses in N_2 when they are heated at 1560 °C for 2 hours.

(3) Dissociated NH_3 has a more enhanced effect on the crystallization than N_2/H_2 mixture-gas, suggesting that intermediates from NH_3 dissociation are involved in the crystallization process.

Since the SiO-NH_3 reaction is instantaneous at temperatures in the range studied, it is difficult to identify the reaction mechanism. Although systematic studies have been made, the mechanism of producing both the crystalline and amorphous Si_3N_4 has not been clarified.

According to the literature, the strength and toughness of sintered parts can be increased significantly with an addition of amorphous whisker into α-Si_3N_4 crystals [Chu and Singh, 1990; Homeny and Neergard, 1990]. Whiskers obtained in the reaction may be applied to improve the toughness and strength of sintered parts.

Nanophase powder obtained in the process can be crystallized to be raw Si_3N_4 powder. Further grinding of such fine powder is unnecessary for molding and sintering parts that follow. Also, nanophase silicon nitride, in particular, has several advantages over regular sub-micron sized powder, including sinterability at lower temperatures, better plasticity, and processability of sintered products [Karch *et al.*, 1987; Gleiter, 1989]. The SiO-NH_3 process may provide nanophase Si_3N_4 powder at reduced cost.

It has been found that α-Si_3N_4 without any β-form is produced in this process. It should be mentioned that about 65 wt% of the total product is in the form of pure

α-Si_3N_4 at 1400 °C. Further study of the SiO-NH_3 reaction will make it possible to produce pure α-form crystals without any amorphous products. The best would be the continuous production of very fine α-form powder, not in the form of crystal aggregates, which is not included in this study.

7.2 Recommendations for Future Work

In order to make this study more complete, some recommendations for future work are listed as follows:

(1) The intrinsic mechanism of the SiO generation remains unclear. According to the SEM images, it is suspected that gaseous intermediates may be involved in the reaction process, which should be characterized as a gas-solid reaction. Thus, changing the particle size of either Si or SiO_2 powder may provide some information to identify the reaction mechanism.

(2) It is believed that three types of product are affected by the impingement of NH_3 flow against the tube wall. Thus, changing the reactor from the current horizontal set-up to a vertical one may inhibit the formation of whiskers and crystals, leading to an increase in nanophase amorphous powder. When sufficient heating is followed, the nanophase powder may be crystallized into α-Si_3N_4 nanophase powder.

(3) As shown in Table 4.10, a dramatic increase in the amount of nanophase powder is obtained using a straight NH_3 feeder at 1350 °C. However, no significant effect is observed at 1400 °C. It is suggested from this table that there may be an optimal temperature to produce favored nanophase powder, which needs to be studied further.

(4) Increasing the SiO generation rate and reducing the NH_3 dissociation are two key factors for producing Si_3N_4 in this process. However, they are contradictory to each other in the current experimental set-up. To increase the production efficiency, these two parts should be separated in a reactor in the future study. SiO vapor may be

generated at a temperature higher than the melting point of Si (1412 °C) to simply increase the amount of SiO. Once SiO is generated, it can be diluted and carried by Ar to a lower temperature to react with NH_3, avoiding appreciable dissociation of NH_3.

(5) The enhancement effect of dissociated NH_3 on the crystallization of amorphous Si_3N_4 is unclear. Further study on this effect may be needed.

CHAPTER 8

SiC SYNTHESIS VIA SiO-CH_4 REACTION

8.1 Introduction

Silicon carbide (SiC) is another promising ceramic material used in a variety of engineering and electrical fields, due to its superior properties at high temperature. The great majority of SiC has been produced by the carbothermic reduction of silica according to

$$\mathbf{3\ C(s) + SiO_2(s) \rightarrow SiC(s) + 2\ CO(g)} \qquad \textbf{(8.1)}$$

It is believed that the above overall reaction consists of two steps: the generation of SiO and the formation of SiC from the SiO. Or,

$$\mathbf{SiO_2(s) + C(s) \rightarrow SiO(g) + CO(g)} \qquad \textbf{(8.2)}$$

and

$$\mathbf{SiO(g) + 2\ C(s) \rightarrow SiC(s) + CO(g)} \qquad \textbf{(8.3)}$$

The carbothermic reaction needs to be carried out at high temperatures, usually between 1700 and 2300 K [Ono and Kurachi, 1991; Krstic, 1992; Weimer *et al.*, 1993; Urretavizcaya and López, 1994]. According to Weimer *et al.* [1993], Reaction (8.3) is the rate limiting step of the process and high temperature operation is needed for this gas-solid reaction to proceed at a reasonable rate.

An attempt has been made in this study to apply the technology for generating SiO to other processes, one of which is the SiC synthesis with methane (CH_4), used as a substitute for C, because of the availability of high-grade and inexpensive raw material. It is also suspected that the SiO-CH_4 reaction is similar to the SiO-NH_3 reaction that has been discussed in Chapters 2-7. The product is expected to be in various forms including whiskers, crystals, and fine particles.

8.2 Thermodynamic Considerations

Figure 8.1 shows that the following reaction has large negative values of the Gibbs free energy change at temperatures in the range of 1200-1800 K.

$$\mathbf{SiO(g) + CH_4(g) \rightarrow \beta\text{-}SiC(s) + H_2O(g) + H_2(g)} \qquad \mathbf{(8.4)}$$

However, CH_4 decomposes at such high temperatures under consideration:

$$\mathbf{CH_4(g) \rightarrow C(s) + 2\ H_2(g)} \qquad \mathbf{(8.5)}$$

It is hence important to suppress the CH_4 decomposition to keep a high efficiency of the use of CH_4. The effect of adding H_2 on the reduction of the equilibrium fractional decomposition of CH_4 has been calculated by the GIBBS program (given in Appendix A) and shown in Figure 8.2. The calculations indicate that H_2 needs to be present in great excess to inhibit the decomposition of CH_4 at temperatures above 1400 K.

With considering other possible products such as C and SiO_2 formed in the system, the equilibrium compositions of Reaction (8.4) are calculated by the GIBBS program. The effect of adding H_2 into the system is also evaluated in terms of the conversion of SiO into product SiC at different mixing ratios of H_2/SiO and CH_4/SiO, as shown in Figure 8.3.

The calculated results show that excess CH_4 is needed for converting all SiO vapor into SiC at 1600 K. Without adding any H_2, a maximum yield of SiC ($\approx$ 100 %) will be obtained at CH_4/SiO = 5. An increase of H_2 also increases the product yield of SiC in the system. As shown in the plot, the SiC yield has been increased to about 100 % at a lower ratio of CH_4/SiO = 2 when H_2/SiO is increased from 0 to 10. However, this enhancement effect is negligible when the H_2/SiO ratio is greater than 10, as shown in Figure 8.3.

The thermodynamic calculations have shown a potential route to synthesize SiC from Reaction (8.4). The results of the feasibility test for producing SiC from the

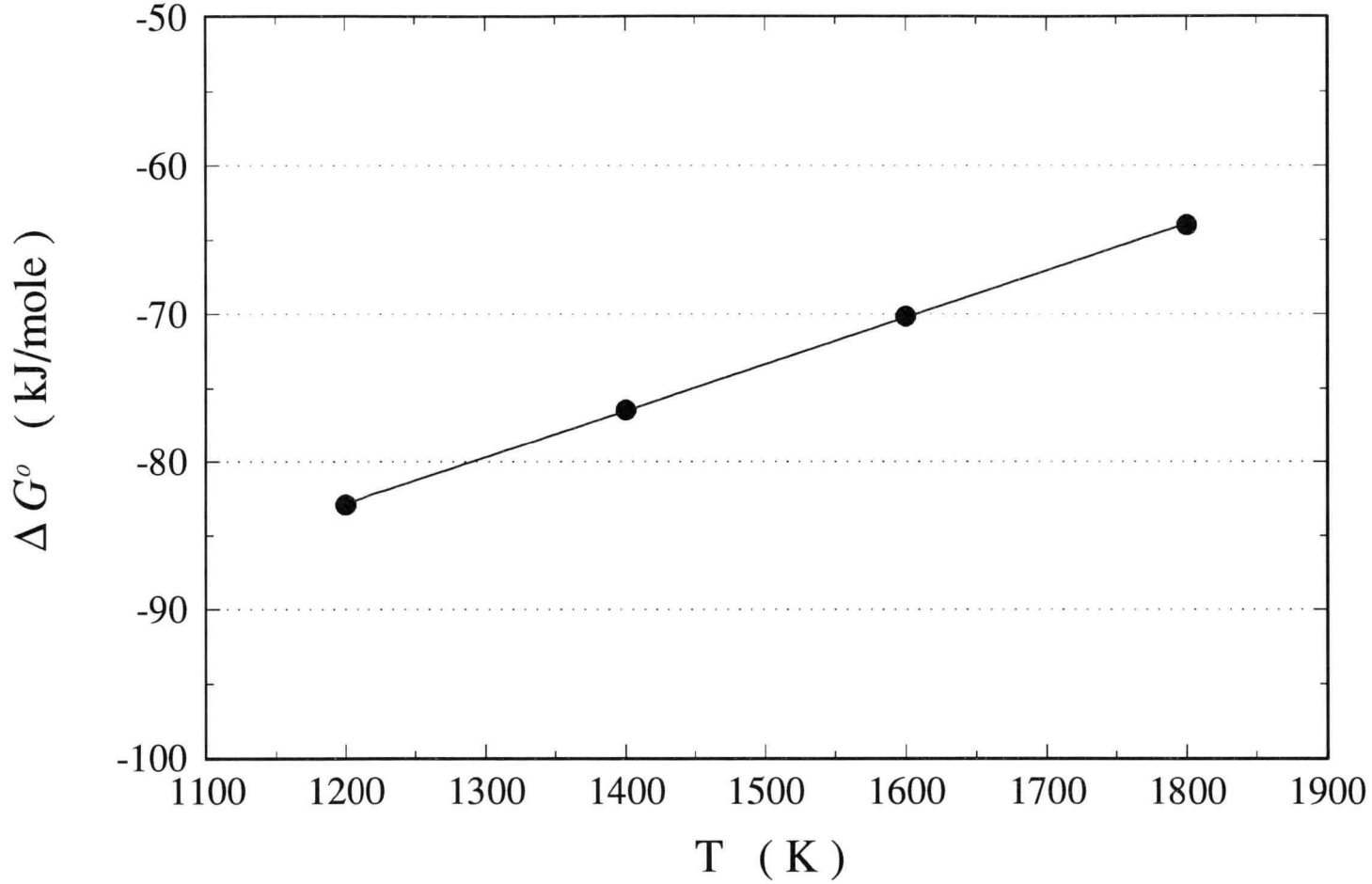

Figure 8.1 Gibbs free energy changes of Reaction (8.4) [JANAF, 1985]

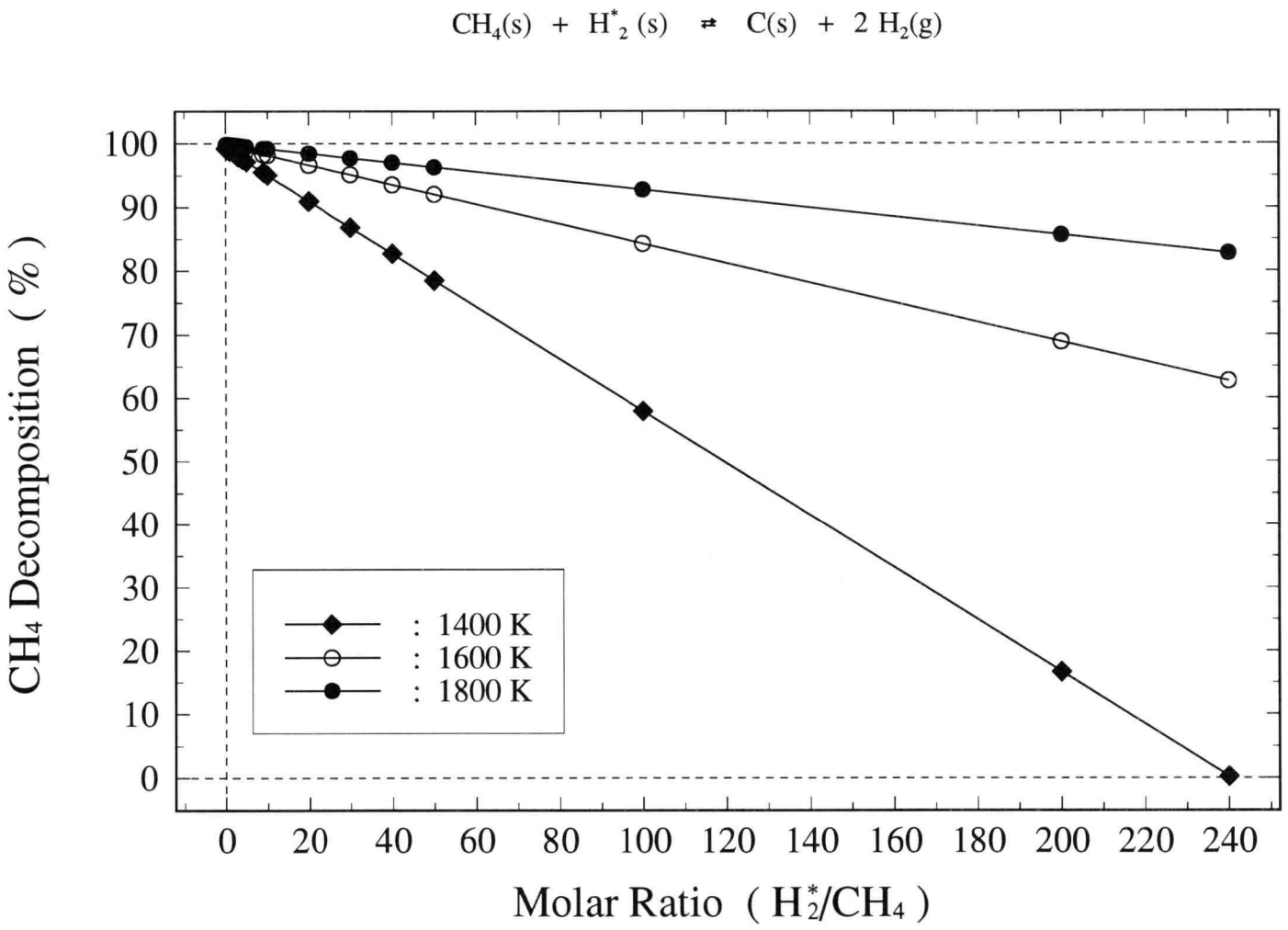

Figure 8.2 Effect of adding H_2 on CH_4 decomposition

$$SiO(g) + CH_4(g) + H^*_2(g) \rightleftharpoons SiC(s) + C(s) + SiO_2(s) + CO(g) + CO_2(g) + H_2(g) + O_2(g) + H_2O(g)$$

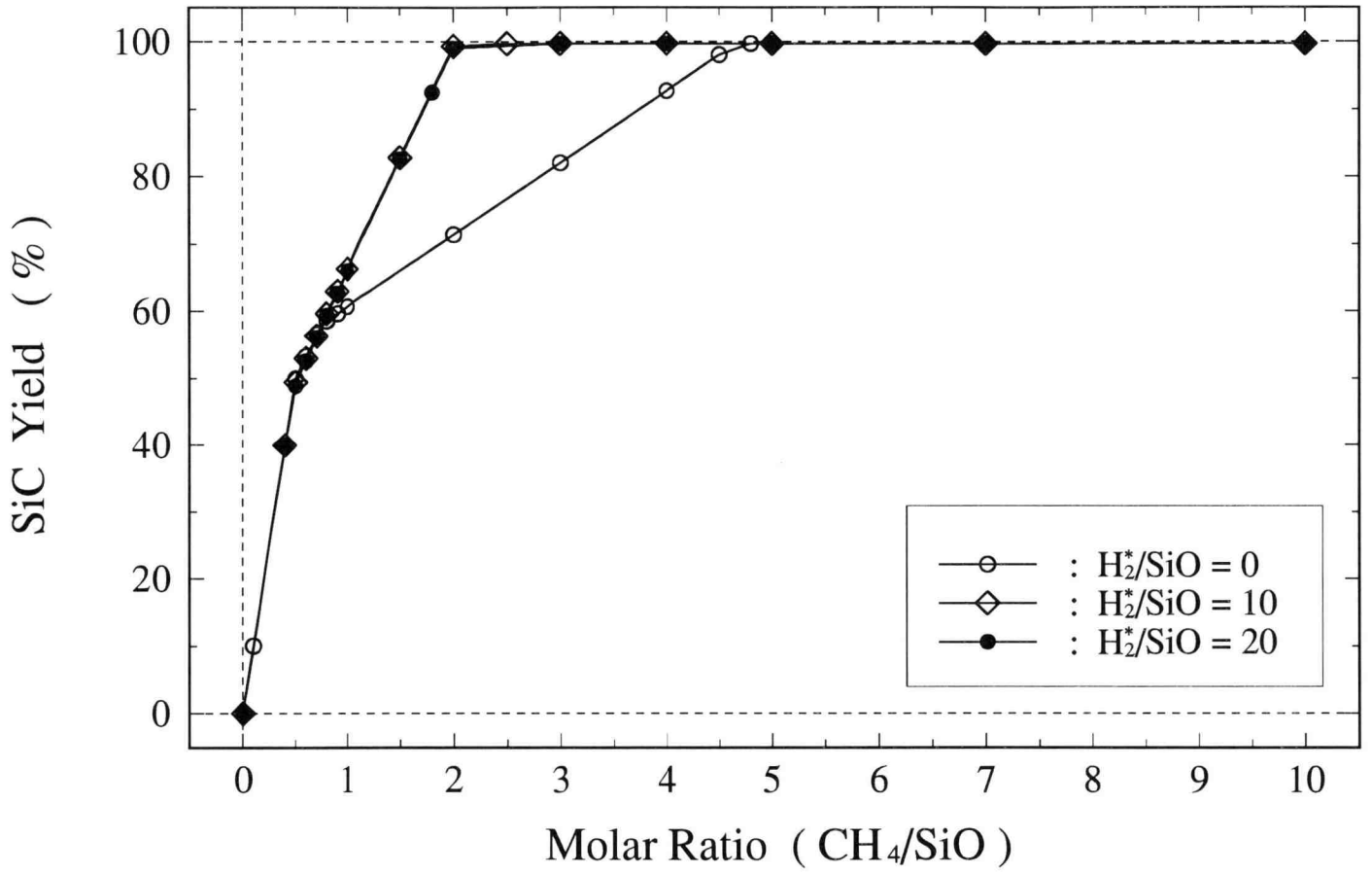

Figure 8.3 Equilibrium conversion of SiO into SiC via SiO-CH_4 reaction at 1600 K

$SiO\text{-}CH_4$ reaction, carried out at temperatures of 1300 and 1400 °C using the current experimental set-up, are described in this chapter.

8.3 Experiments

The experimental apparatus used to investigate the synthesis of SiC from the $SiO\text{-}CH_4$ reaction is shown in Figure 8.4, that is a modification of the set-up shown in Figure 3.4. A flask was used instead of a paper-filter owing to a significant amount of fine C carry-over toward the reactor exit. Four runs using a bent CH_4 feeder were made to test the feasibility of SiC synthesis via Reaction (8.4) at 1300 and 1400 °C. The operating conditions of these four runs are summarized in Table 8.1.

Product scraped from the inner wall of each sampling tube was heated in either an air stream, or a stream of air (33 %) and Ar (67 %) mixture-gas at temperatures between 600 and 1100 °C to eliminate carbonaceous by-product. Further IR, XRD, SEM, and energy dispersive X-ray (EDX) analysis were used for the characterization of product. The reference IR spectra for Si-C [Sasaki *et al.*, 1989; Chen *et al.*, 1990; DiGregorio and Furtak, 1993] and Si-O [Falk and Karunanithy, 1989] was used for identifying SiC and SiO_2 in the product in the reaction. Also, powder XRD data [Li et al., 1994; Narayan et al., 1994; Biernachi and Watzak, 1989] were used for identifying SiC crystals and graphite, respectively.

8.4 Results and Discussion

Visual observation indicated that the decomposition of CH_4 was significantly reduced by adding H_2 into the CH_4 stream. However, no quantitative analysis regarding the reduction effect of H_2 was made and the mixing ratio of H_2/CH_4 was fixed at about 8.

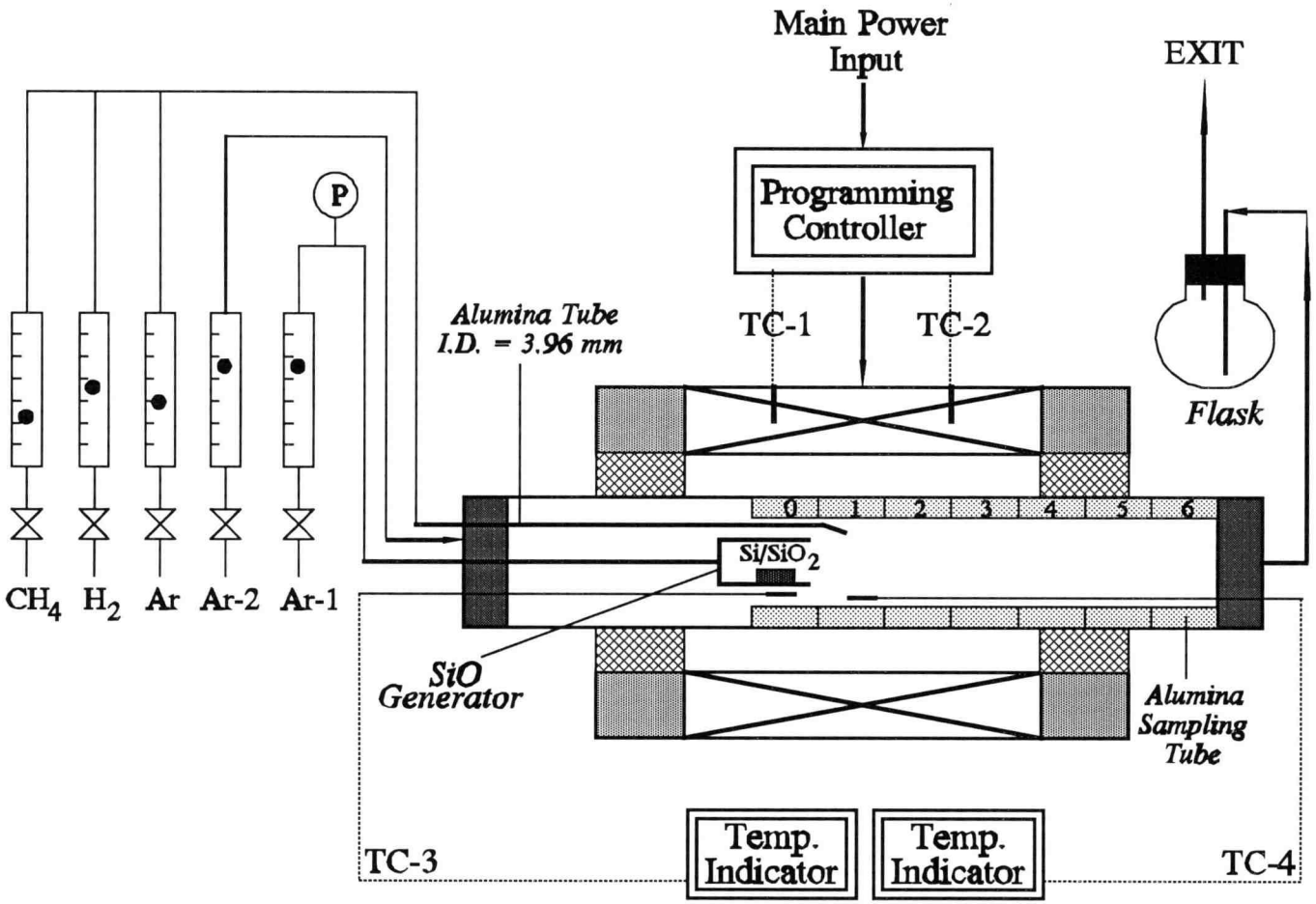

Figure 8.4 Experimental apparatus for SiO-CH_4 reaction

Table 8.1 Experimental conditions of SiO-CH_4 reaction in tubular reactor

Conditions	SIC1300-01	SIC1400-01	SIC1400-02	SIC1400-03
Ar-1 flow rate* (cm^3/min)	1387	1387	1387	1357
Ar-2 flow rate* (cm^3/min)	947	947	947	947
Ar flow rate* (cm^3/min)	0	0	0	3349
H_2/Ar flow rate* (cm^3/min)	2156	3609	2513	623
CH_4 feeding rate* (cm^3/min)	317	465	317	80
SiO generation temperature (°C)	1299	1396	1396	1396
SiO-CH_4 reaction temperature (°C)	1304	1402	1402	1402
Reaction time (hours)	7	3	3	3

★ : referred to room temperature

8.4.1 Product Distribution

Similar to those observed in the SiO-NH_3 reaction, different types of product were obtained on the sampling-tube wall at different locations along the reactor axis: whiskers, crystals, and carbonaceous by-product. Fibrous whiskers were obtained on the inner wall of #1 sampling tube, the place right at the outlet of the CH_4 feeder. In addition, greenish crystals (noted as crystal-1) were also found at the locations right downstream the whiskers inside the sampling tube #1. It should be mentioned that greenish crystals (indicated as crystal-2) were deposited on the external sampling-tube wall along the clearance between sampling tubes (#1 through #4) at 1400 °C.

Hard-shiny carbonaceous product was deposited on the inner wall of sampling tubes #1-3 and partly #4 (the exit of furnace). A certain amount of fine-black powder was also found on the external sampling-tube wall, which is the same location as crystal-2,. Visual observation suggests that these two carbonaceous products may have different morphologies. The reason of forming the hard-shiny carbonaceous product inside the heating zone remains unclear in this study. The majority of fine-black powder was deposited at the place toward the downstream of reacting zone (sampling tubes #4-6) and partly collected by the flask mounted at the exit of reactor tube.

8.4.2 Product Characterization

Figure 8.5 shows the XRD charts of unheated product formed at 1300 °C. As shown in the curve (a), several peaks indicating SiC are identified as well as a peak for carbon in the crystal-1. However, no significant SiC peaks are found in the product collected by the sampling tubes (b) #2 and (c) #5. The significant peak intensity for carbon appearing at 2θ around 26° suggests that the majority of product found downstream the CH_4 outlet is graphite.

Similar XRD charts are obtained in the product formed at 1400 °C. Figure 8.6 shows that unheated crystal-1 and whiskers are crystalline SiC with a small amount of carbon. According to the curves (c) and (d), carbonaceous product formed down-

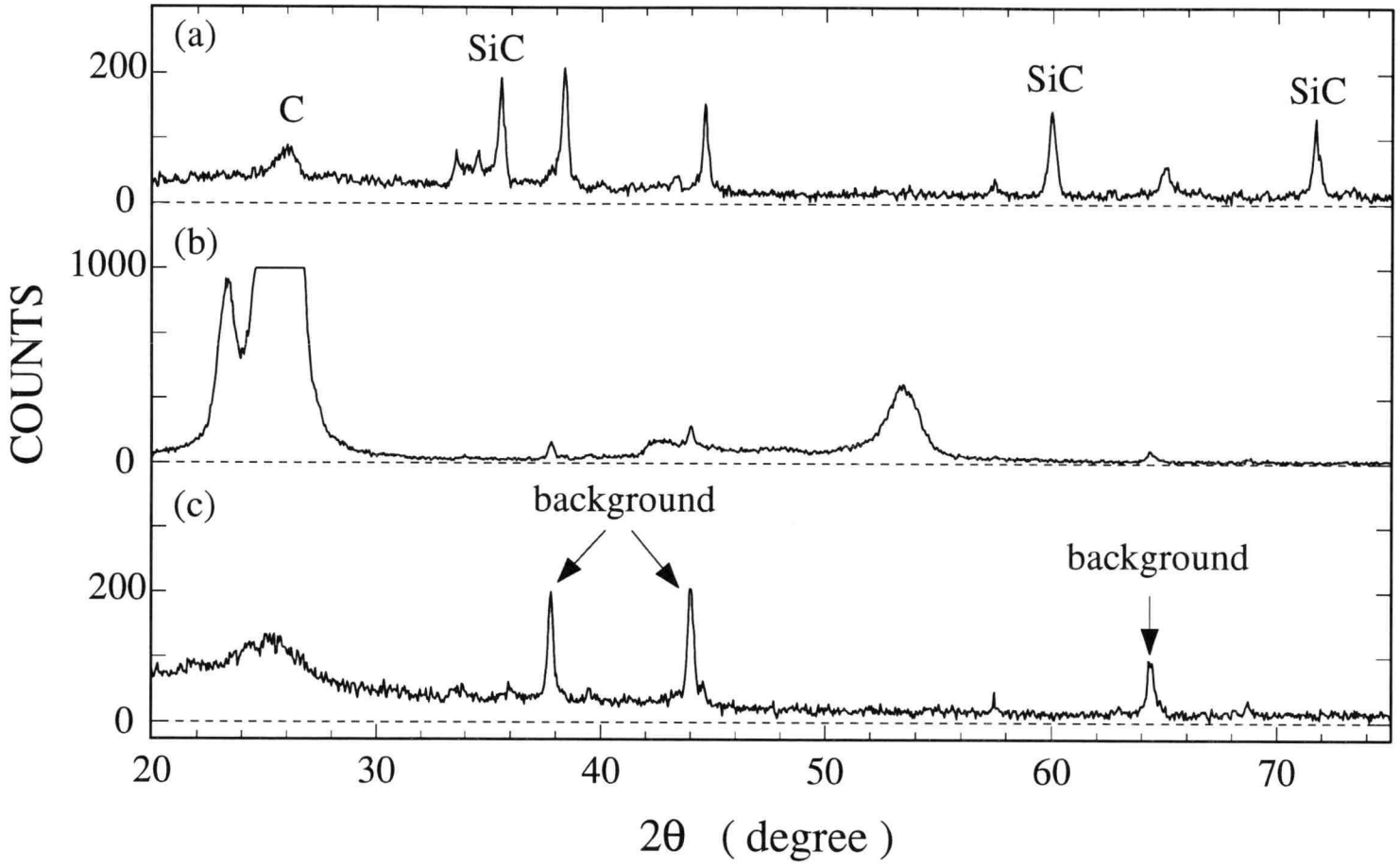

Figure 8.5 XRD charts of unheated products formed at 1300 °C: (a) crystals in sampling tube #1, (b) deposits in sampling tube #2, (c) deposits in sampling tube #5

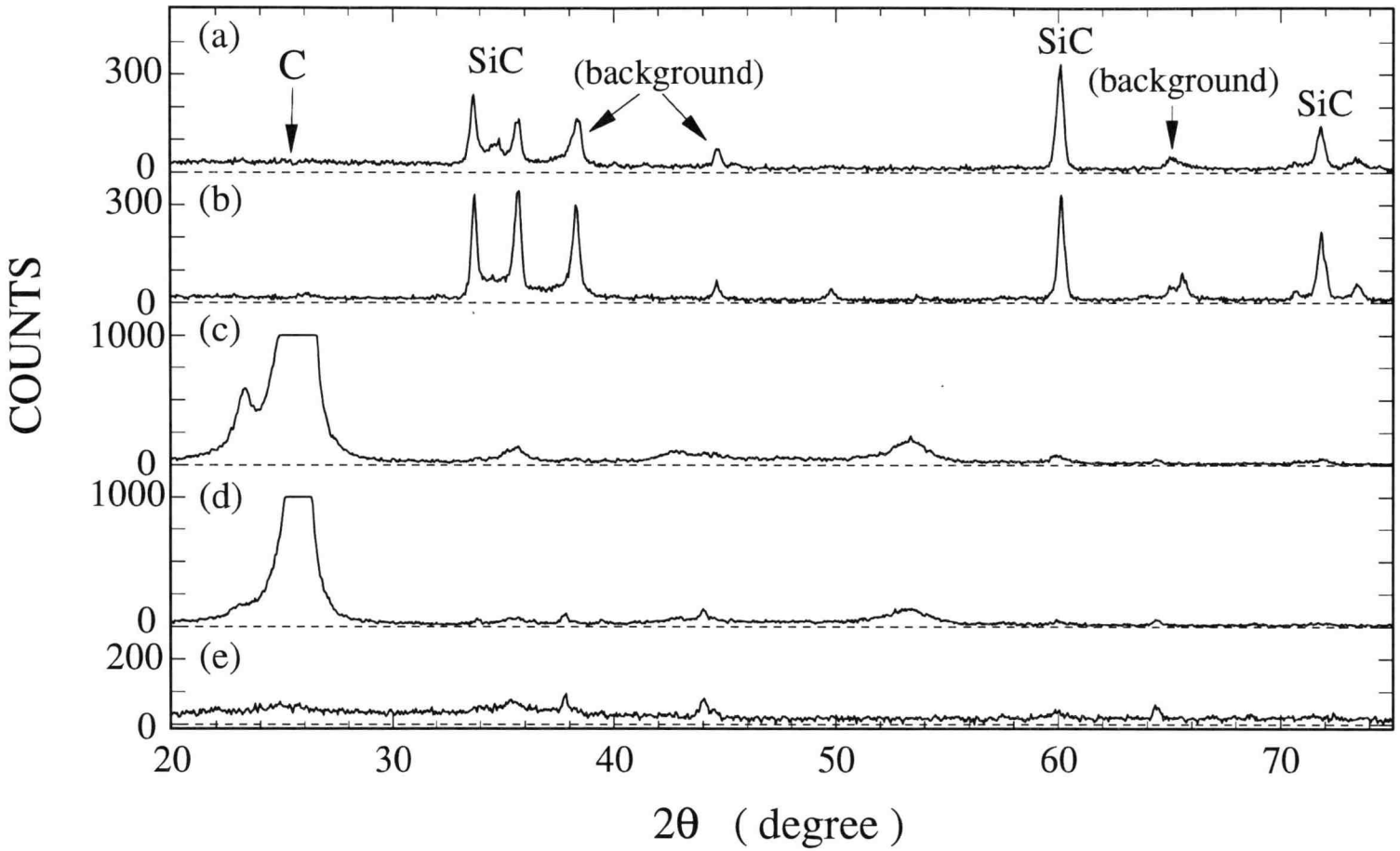

Figure 8.6 XRD charts of unheated products formed at different locations at 1400 °C: (a) crystals in sampling tube #1, (b) whiskers in sampling tube #1, (c) sampling tube #2, (d) sampling tube #4, (e) sampling tube #6

stream the CH_4 feeder is mainly graphite. It is noteworthy that no significant carbon peak appears in the fine-black powder, (e), collected by the sampling tube #6. It is suspected that carbonaceous product collected by each sampling tube may also have different composition.

IR analysis was hence used to identify the possible change of product formed at different locations in the reactor. The IR spectra of unheated products formed at 1400 °C are shown in Figure 8.7, where the Si-C bonding is clearly seen in both the (a) crystal-1 and (b) whiskers. No bonding is found in the hard-shiny carbonaceous product, (c) and (d), collected by the sampling tubes #2 and #4. Thus, these products may be close to pure carbon, which is consistent with the XRD analysis mentioned earlier.

Also, energy dispersive X-ray (EDX) analysis indicates that the shiny carbonaceous product collected in the sampling tube #2 contains 99 atom% C and 1 atom% Si. Since oxygen content in the product is negligible, 1 atom% Si should be attributed to the tiny amount of SiC existing in the product.

However, fine-black powder collected by the sampling tube #6 has different IR spectrum. As shown in Figure 8.7(e), one characteristic Si-O bonding has been clearly seen at a wavenumber of about 1050 cm^{-1}. Unreacted SiO vapor may be carried by the gas flow out of the reacting zone, and has condensed back to Si and SiO_2 owing to the temperature drop toward the reactor exit. Therefore, product deposited outside the reacting zone (sampling tubes #5 and #6) mainly contains fine amorphous carbon powder and the mixture of Si and SiO_2.

8.4.3 Heat Treatment of Carbon Elimination

The deposition of SiC product can be distinguished from carbonaceous product in the reactor. However, a certain amount of carbon is contained in the SiC product, as shown in Figure 8.5. Thus, the SiC product was heated in an air stream at 1100 °C to eliminate the carbon. A comparison between Figures 8.8(a) and (b) suggests that this heating operation is useful for eliminating carbonaceous product. Similar results

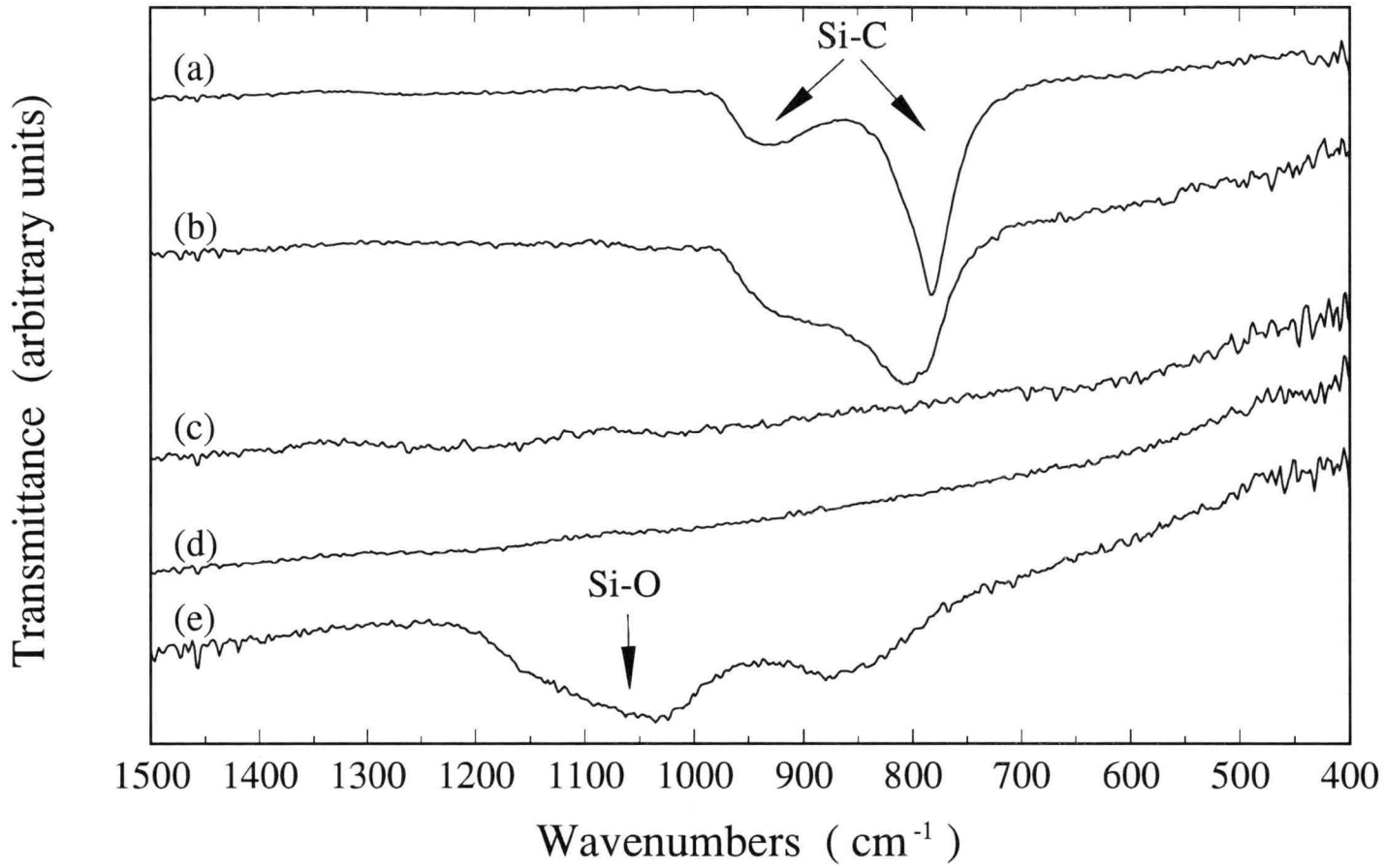

Figure 8.7 IR spectra of unheated products formed at different locations at 1400 °C: (a) crystals in sampling tube #1, (b) whiskers in sampling tube #1, (c) sampling tube #2, (d) sampling tube #4, (e) sampling tube #6

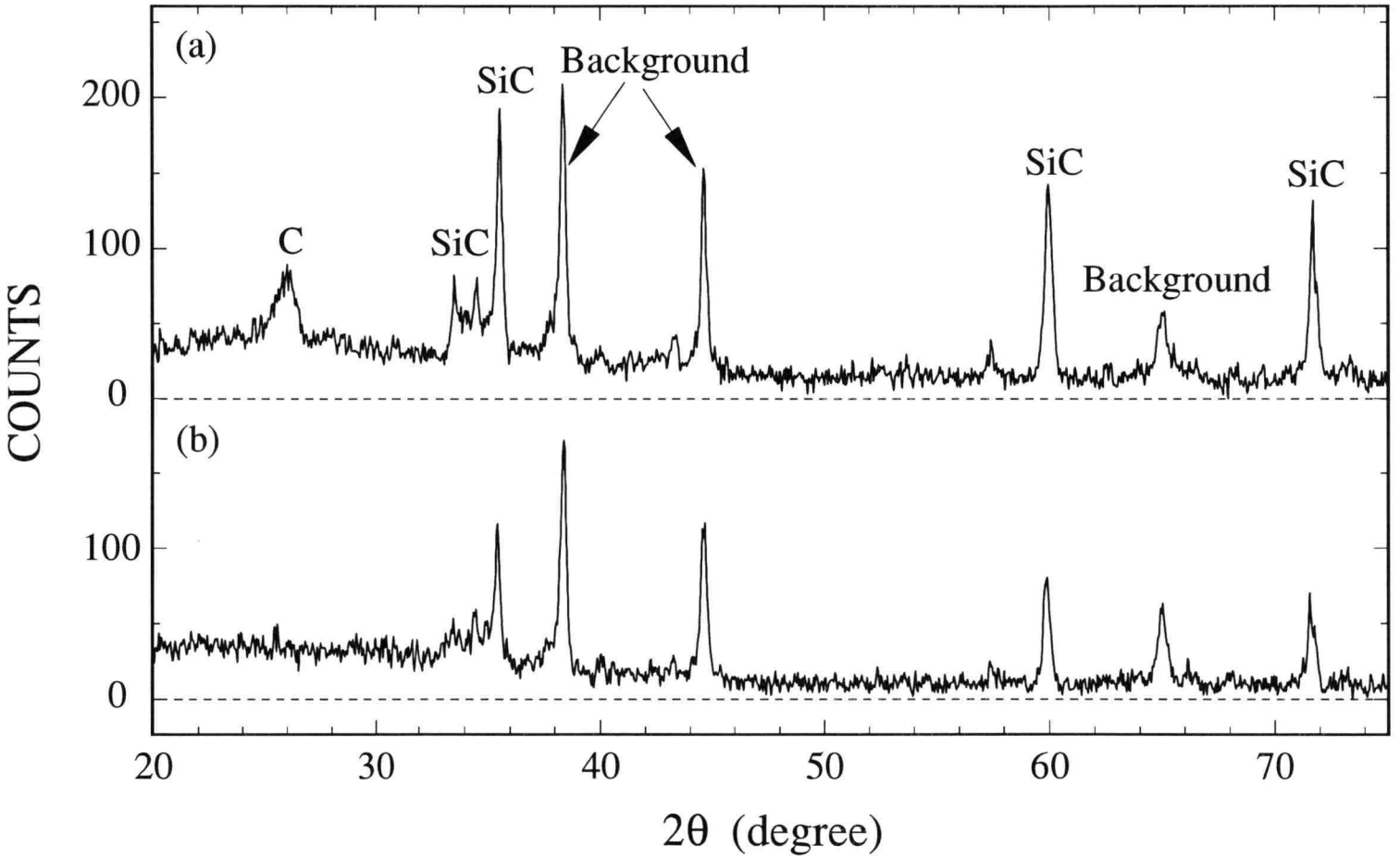

Figure 8.8 XRD charts of crystals produced at 1300 °C: (a) unheated, (b) heated in air at 1100 °C

are shown in Figure 8.9, where no carbon peak is seen in all the XRD charts of SiC product after the heat treatment.

To find possible transformation of SiC product, IR analysis was made before and after the elimination of carbon. Figure 8.10 shows the IR spectra of crystals, in which Si-O bonding attributed to SiO_2 is clearly seen in the product, (b), heated in air at 1100 °C. Similar results are obtained on purifying the products formed at 1400 °C. As shown in Figure 8.11, all the products contain SiO_2 once they are heated in an air stream at 1100 °C.

It is suspected that further oxidation of the SiC product have occurred during the heat treatment, leading to the formation of SiO_2. However, the results are inconsistent with the finding that no further oxidation of SiC occurs in the heating in air at 1000 °C [Falk and Karunanithy, 1989]. In order to clarify the oxidation of SiC crystals, a series of runs were made.

Crystal-1 formed at 1400 °C was heated for one hour at different temperatures in a mixed-gas stream of air (33 %) and Ar (67 %). The IR spectra of heated products are shown in Figure 8.12. The progress of SiC oxidation with temperature is clearly shown by the appearance of an Si-O absorption peak at a wavenumber of about 1100 cm^{-1}. SiC product seems to be slightly oxidized at 700 °C, and the oxidation of product becomes more pronounced at 900 °C. After being heated at 1100 °C, Si-O bonding is well developed in the product. According to Figure 8.12, heating temperature needs to be as low as 700 °C under the prescribed gas environment in the future study.

8.4.4 Product Morphology

Products were carefully scraped out of the reactor for SEM analysis. Figure 8.13(a) shows the SEM images of unheated crystal-1, collected from the inner wall of sampling tube #1. Crystals have turned into aggregates and the shapes and sizes cannot be identified from the images. The SEM images of unheated whiskers are shown in Figure 8.13(b), in which the whisker radii are about 0.2 μm.

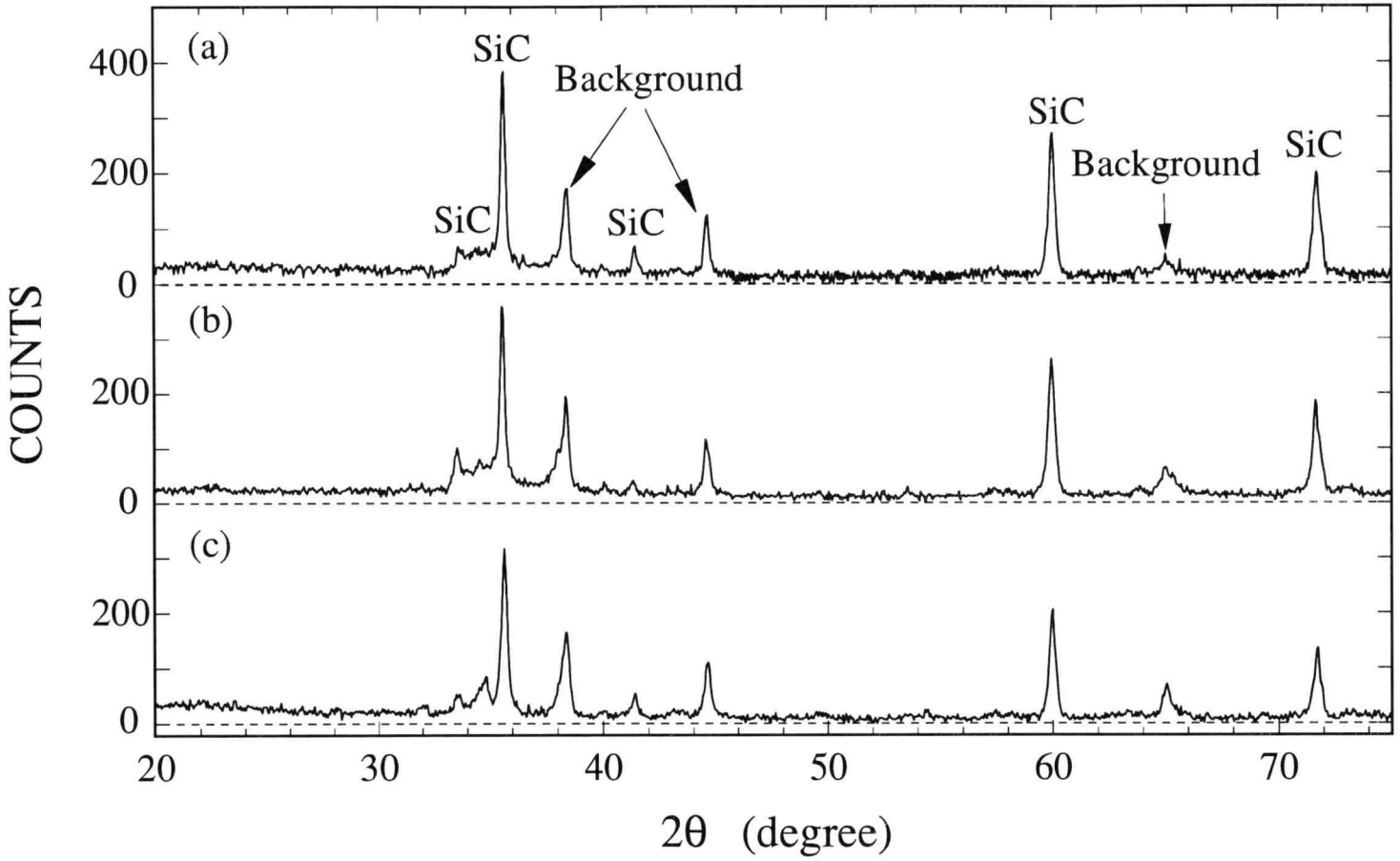

Figure 8.9 XRD charts of heated products formed at 1400 °C: (a) whiskers, (b) crystals deposited in sampling tube #1, (c) crystals deposited on the external wall around the clearance between sampling tubes (#1 through #4)

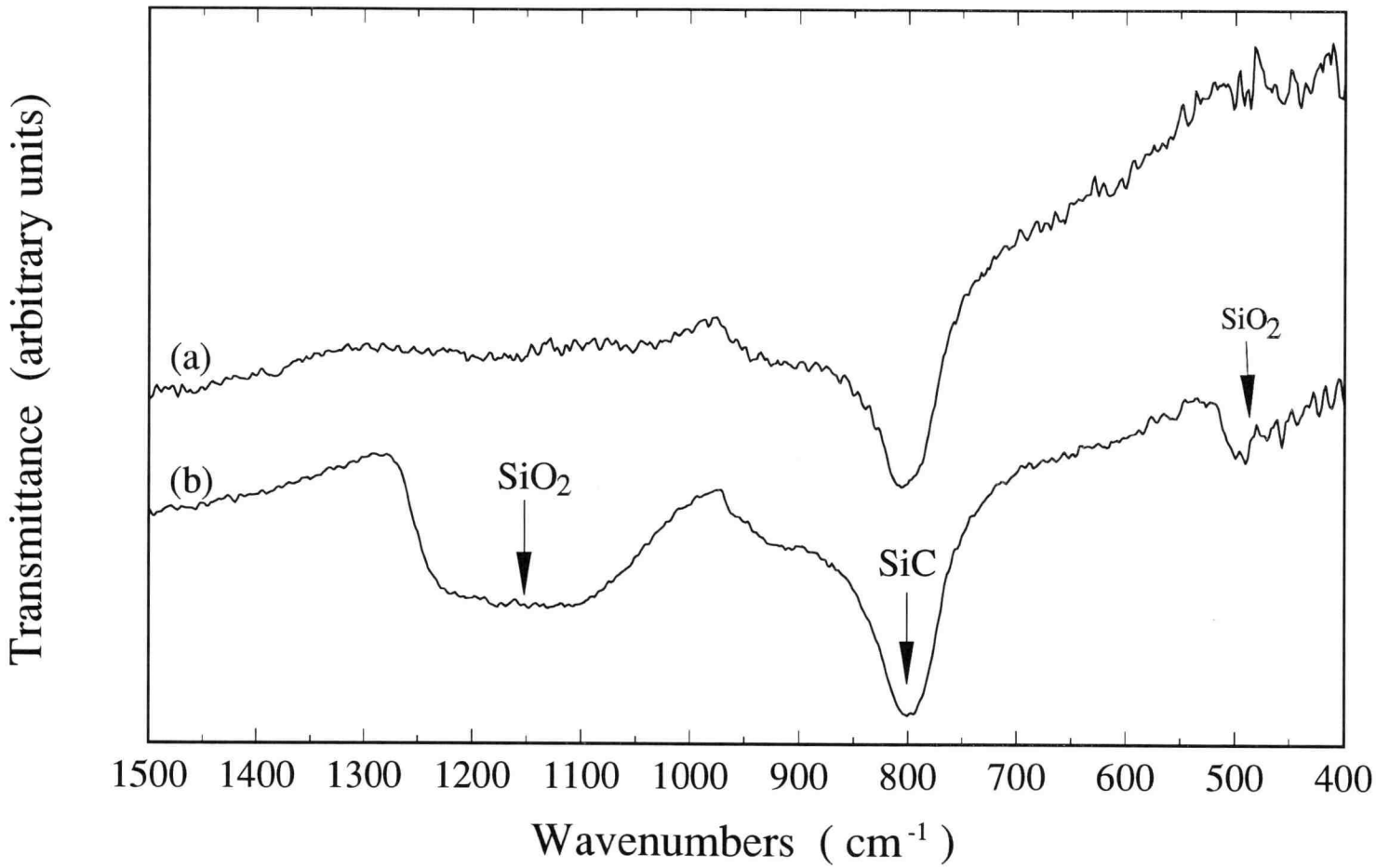

Figure 8.10 IR spectra of crystals formed at 1300 °C: (a) unheated, (b) heated in an air stream at 1100 °C

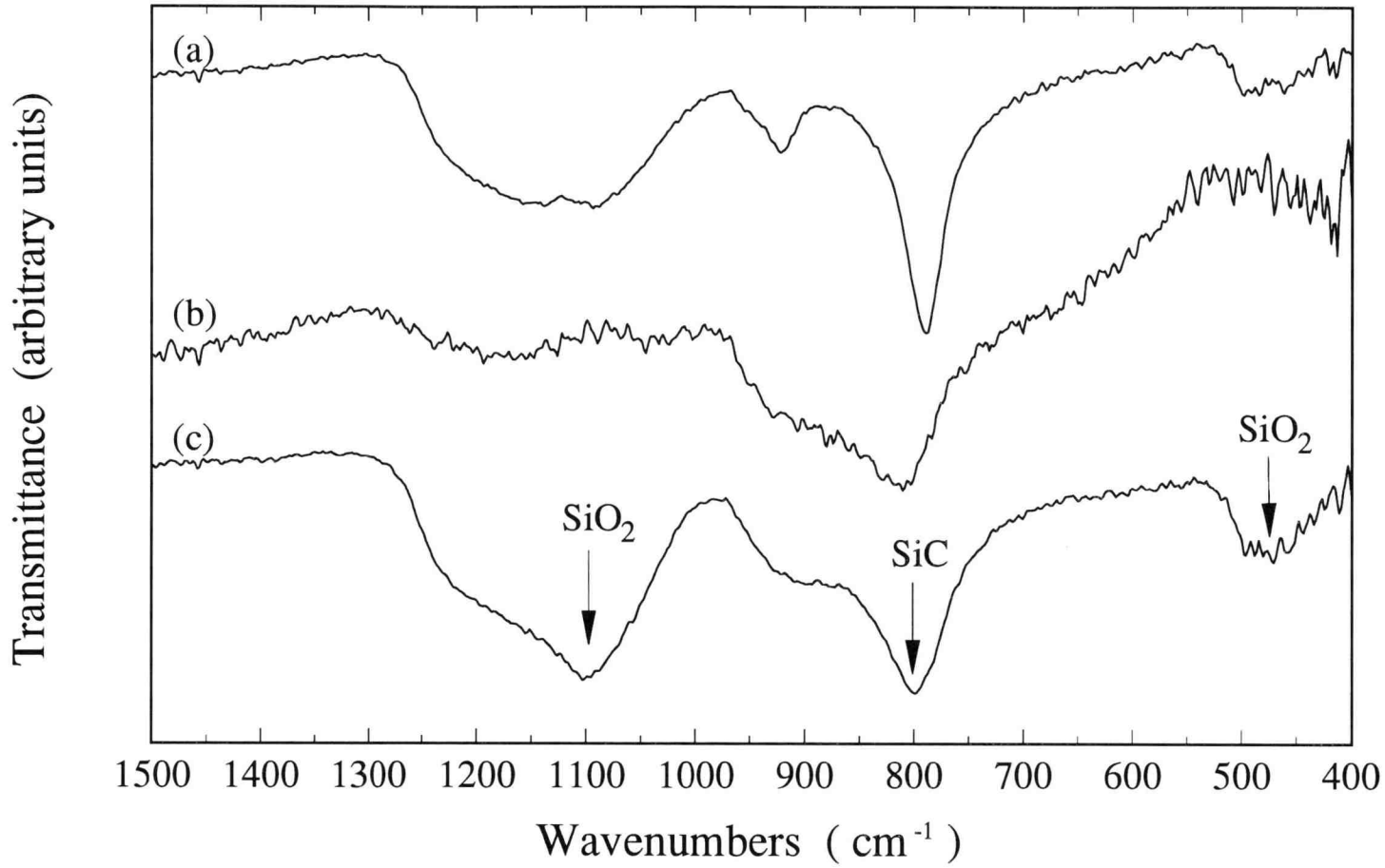

Figure 8.11 IR spectra of heated products formed at 1400 °C: (a) whiskers, (b) crystals deposited in sampling tube #1, (c) crystals deposited on the external sampling-tube wall around the clearance between sampling tubes (#1 through #4)

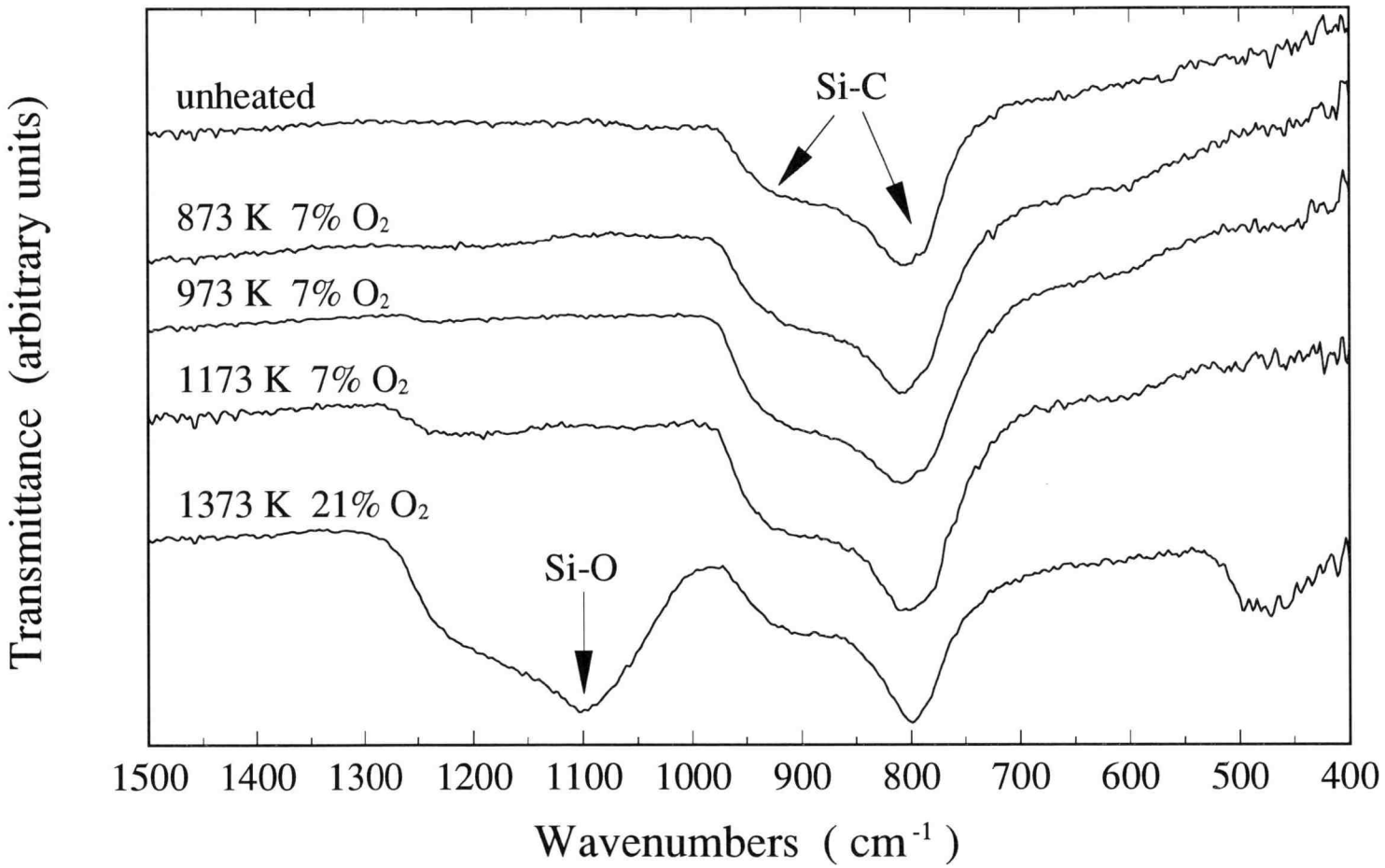

Figure 8.12 IR spectra of crystals, heated at different temperatures for one hour

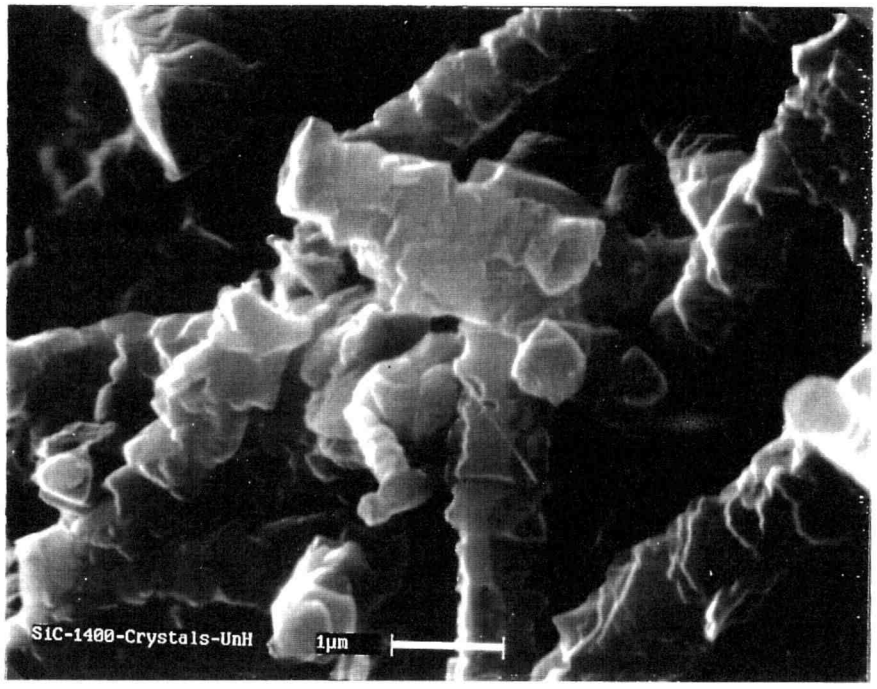

Figure 8.13(a) SEM images of unheated crystals, formed at 1400 °C

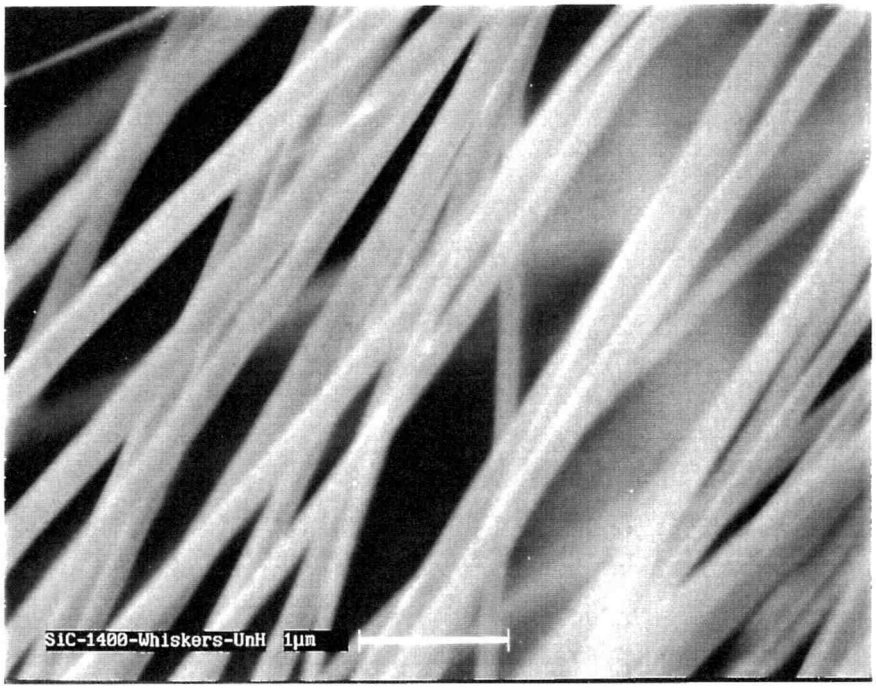

Figure 8.13(b) SEM images of unheated whiskers, formed at 1400 °C

SEM analysis was used to find possible changes of product morphology in the heat treatment. Figures 8.13(c) shows the morphology of crystals, heated in the stream of gas mixture of air (33 %) and Ar (67 %) at 700 °C. Any significant change from unheated crystals is not observed. This finding also supports the IR analysis shown in Figure 8.12, which indicates that the oxidation of crystals is negligible at 700 °C.

However, different results were obtained when product was heated in an air stream at 1100 °C. Figure 8.13(d) shows the SEM images of heated crystals, in which very fine grains with radii on the order of 10 nm are found on the surface of crystals. Similar phenomenon was seen in the SEM images of heated whiskers, shown in Figure 8.13(e). The surface of individual whiskers is no longer smooth, and the shape seems somewhat deformed. According to the SEM images shown in Figures 8.13(a)-(e), it is concluded that oxidation of SiC crystals and whiskers occurred during the heat treatment at 1100 °C in an air stream.

Fine-black powder collected by sampling tubes placed toward downstream the reacting zone was also heated in air at 1100 °C. The color of powder changed from black to nearly opaque-white after the heat treatment. Figure 8.13(f) shows that the heated powder has a particle size of about 100 nm. The IR analysis (Figure 8.14) indicates that the fine powder may be close to pure SiO_2. However, the presence of SiO_2 may result from the oxidation of SiC in the heat treatment, or the condensation of unreacted SiO vapor due to the temperature drop toward the reactor exit.

8.4.5 Product Yields

Table 8.2 summarizes the results of these four runs in terms of the distributions of product as well as the total yield of SiC obtained from SiO generated. Due to the co-existence of SiC and C in each sampling tube, the amount of SiC was evaluated based on the mass of product collected by scraping after the C elimination. It should be noted that SiO_2 contained in the product is not taken into consideration because of the limited information obtained in this preliminary study.

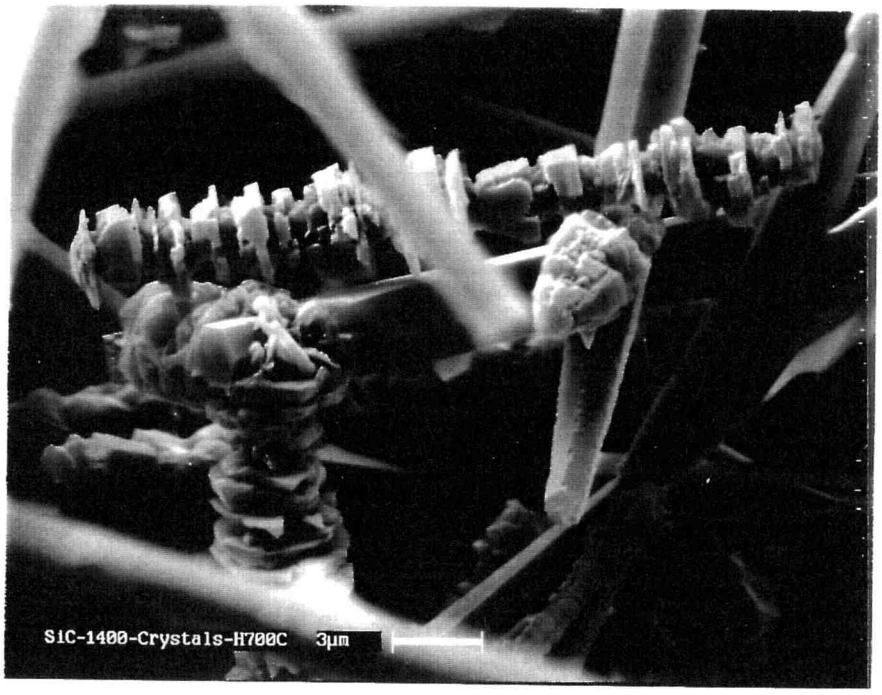

Figure 8.13(c) SEM images of crystals, heated at 700 °C in air/Ar mixture gas

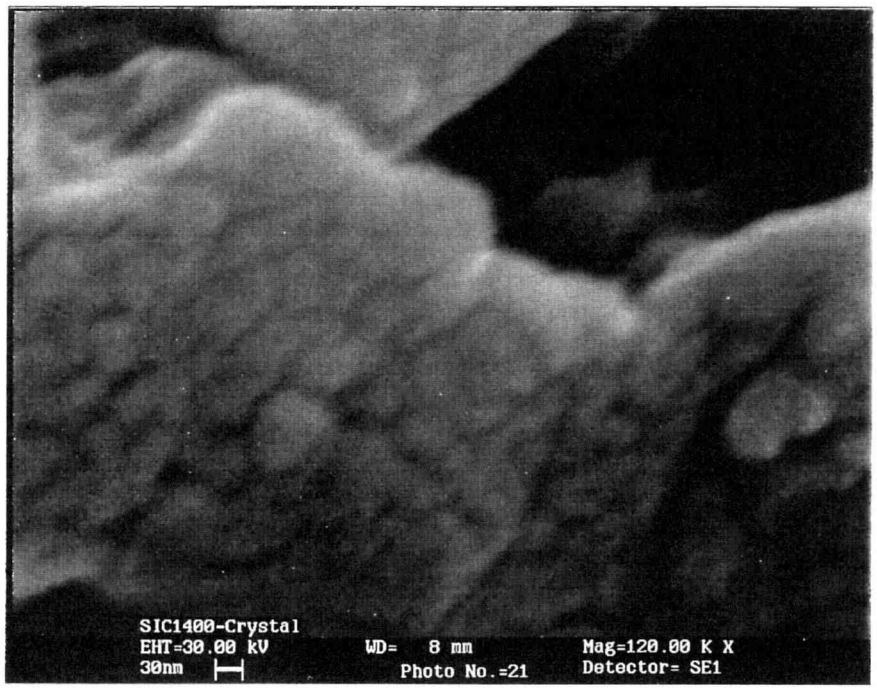

Figure 8.13(d) SEM images of crystals, heated at 1100 °C in air

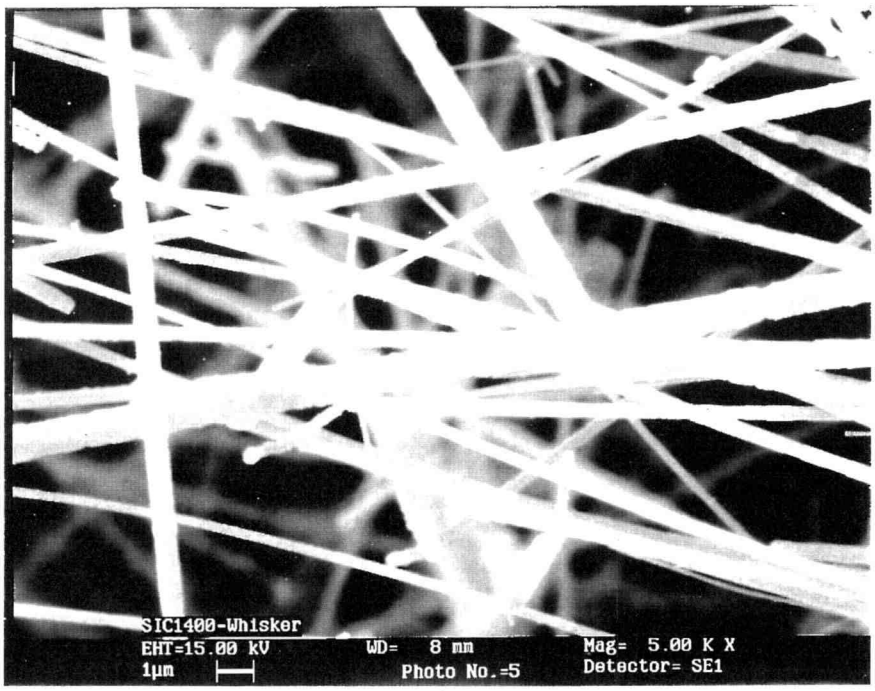

Figure 8.13(e) SEM images of whiskers, heated at 1100 °C in air

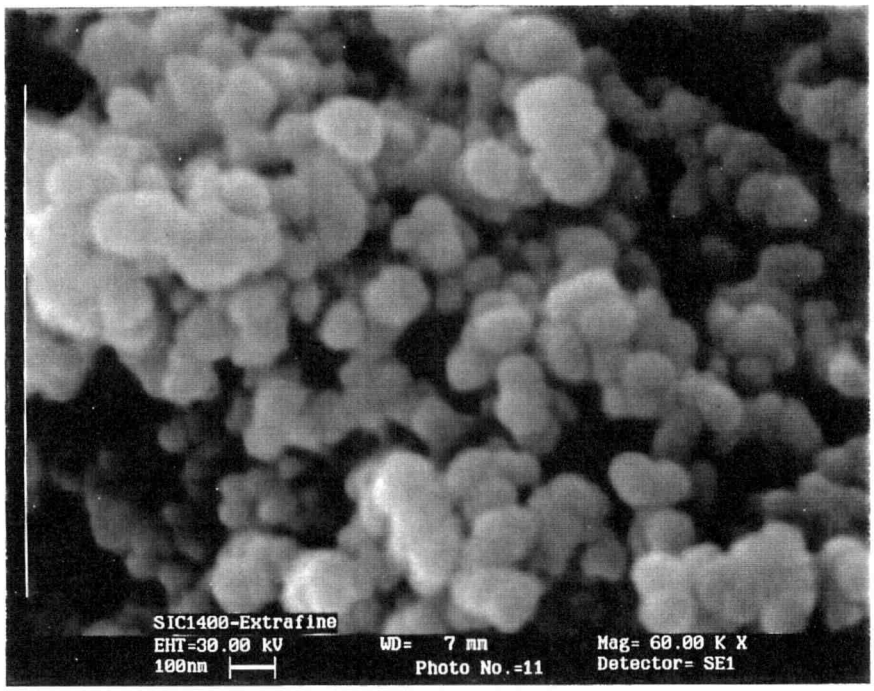

Figure 8.13(f) SEM images of fine-black powder, heated at 1100 °C in air

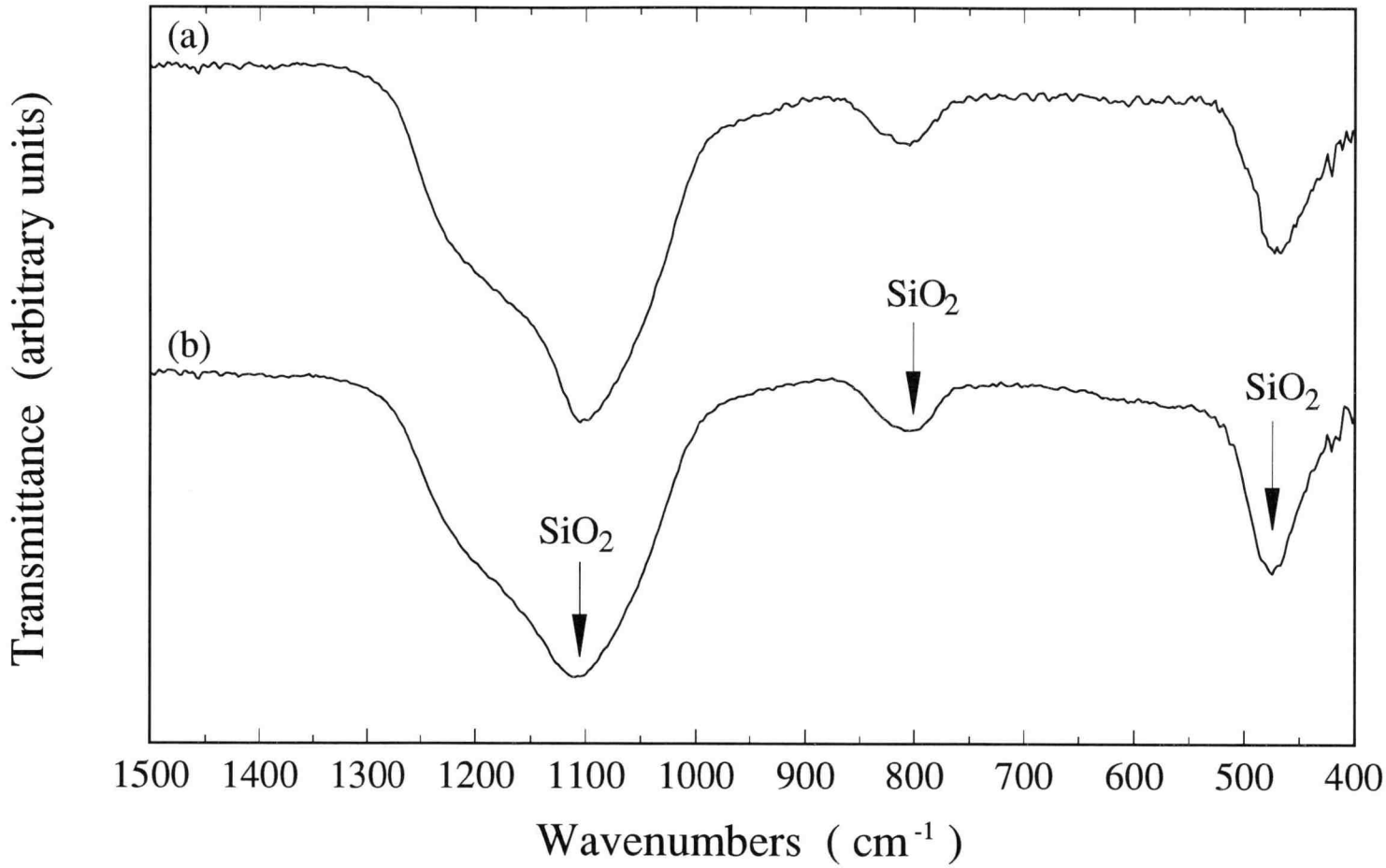

Figure 8.14 IR spectra of heated fine powder, deposited in: (a) sampling tube #4, (b) sampling tube #6

Table 8.2 SiC formation and its distribution within tubular reactor

Run No.	T_{RXN} (°C)	$(dM_{SiO}/dt)_{Ave} \times 10^4$ (g/min)	CH_4	H_2 (cm^3/min)	Ar	SiC Yield (%)#	Whiskers (wt%)★	Crystal-1 (wt%)†	Crystal-2 (wt%)‡
SIC1300-01	1300	5.142	317	2156	0*	4.5	≈ 0	≈ 4.5	≈ 0
SIC1400-01	1400	21.733	465	3609	0	30.1	12.8	11.8	5.5
SIC1400-02	1400	26.219	317	2513	0	22.0	3.2	11.1	7.7
SIC1400-03	1400	29.311	80	623	3349	3.3	≈ 0	0.7	2.6

: 1 gram of SiO will produce 0.9091 gram of SiC according to Reaction (8.4)

★ : right at the outlet of CH_4 feeder (inside the sampling tube #1)

† : on the inner wall of sampling tube #1

‡ : on the outer wall among the clearance between the sampling tubes

* : Ar mixed with CH_4/H_2

The total yield of SiC is about 5 % at 1300 °C, which is mainly from the crystals. Table 8.2 indicates that the SiC yield strongly depends on the amount of CH_4 feeding at 1400 °C, ranging from 3.3 % to about 30 %. It has been found that greenish crystals are the favored product followed by whiskers in these four runs.

The SiC yield is roughly linear with the feeding ratio of CH_4 to SiO at 1400 °C, as shown in Figure 8.15. This linear relationship implies that the SiC production is affected by the feeding amount of CH_4. It is hence suspected that the amount of CH_4 entering the reacting zone may be insufficient for converting all SiO vapor into SiC product in these four runs. However, no further study was made because the kinetics of CH_4 decomposition remains unclear in this preliminary study.

8.5 Conclusions

These four preliminary experiments have shown a feasible way to synthesize SiC from Reaction (8.4) at temperatures of 1300 and 1400 °C. SiC was produced in two different forms: crystalline whiskers with radii about 0.2 μm, and poly-crystals with various shapes and sizes of aggregates. The yield of SiC based on SiO generated totaled to about 5 % at 1300 °C, and up to about 30 % at 1400 °C depending on the feeding amount of CH_4. It has been found that the optimal temperature for the C-elimination process is about 700 °C under a stream of air (33 %) and Ar (67 %) mixture-gas.

According to the literature, SiC whiskers are also an important reinforcement material in the fabrication of advanced ceramic composites. Thus, SiC whiskers produced from the SiO-CH_4 reaction can also be added to improve the strength and toughness of final β-Si_3N_4 composites during the sintering process [Lundberg *et al.*, 1987; Buljan *et al.*, 1987; Sigh *et al.*, 1988].

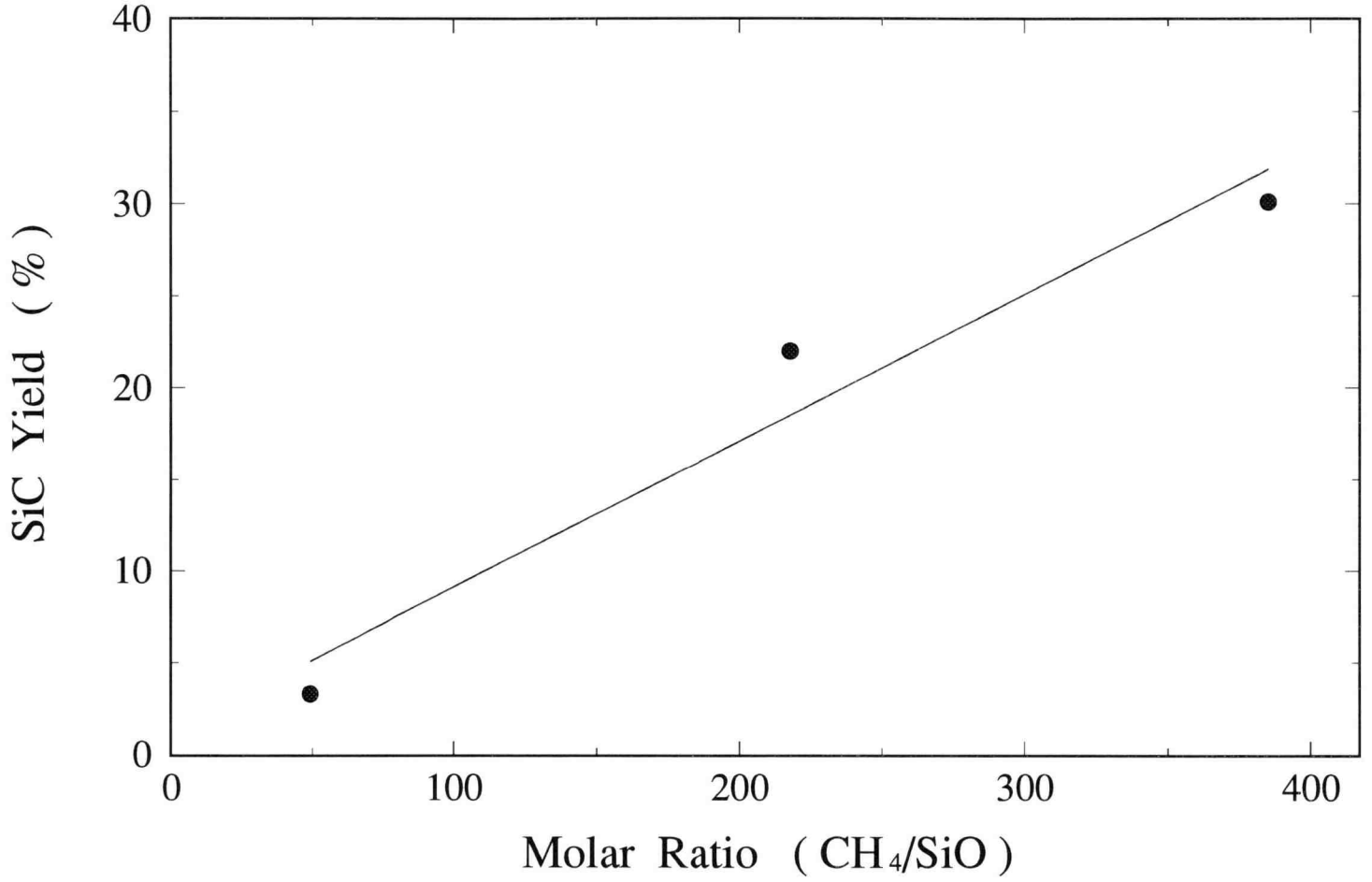

Figure 8.15 Linear relationship between SiC yield and molar feed ratio of CH_4/SiO at 1400 °C

8.6 Recommendations for Future Work

The SiO-CH_4 reaction still remains unclear though four preliminary runs were made. The following recommendations may be helpful for someone continuing the further study on this reaction.

(1) The decomposition of CH_4 needs to be determined prior to the investigation of the kinetics of this reaction.

(2) To increase the efficiency of CH_4 use at high temperature, more H_2 may be added into the CH_4 feeding stream to reduce the CH_4 decomposition in the future study. Thus, the reduction effect of H_2 on the CH_4 decomposition should be clarified.

(3) The concern of CH_4 decomposition may be neglected if the SiO-CH_4 reaction can be carried out at temperatures higher than 1400 °C. In this case, SiC can be produced simultaneously from the SiO-CH_4 and SiO-C reactions in the system, *i.e.*, Reactions (8.3) and (8.4).

(4) Changing the reactor from the current horizontal set-up to a vertical one may be necessary for producing fine SiC powder without forming aggregates.

CHAPTER 9
SUMMARY

The application of SiO vapor to the synthesis of Si-based ceramics has been shown in this study. After being generated from Si/SiO_2 mixtures at high temperature, SiO can be transferred to any place for desired reactions. In this study, SiO is carried by Ar gas into a reacting zone where the reaction with either NH_3 or CH_4 proceeds to form Si_3N_4 or SiC product at temperatures between 1300 and 1400 °C.

Most effort has been made to investigate the kinetics of SiO ammonization for Si_3N_4 synthesis at temperatures in the range studied. It has been found that the Si_3N_4 formation via the $SiO\text{-}NH_3$ reaction is instantaneous when NH_3 is in large excess. Since the reaction has instantaneous rates, the production cost of Si_3N_4 may have a chance of being reduced, especially for producing nano-sized powder.

Chapter 8 describes the experimental findings that the formation of SiC from the $SiO\text{-}CH_4$ reaction is feasible at temperatures of 1300 and 1400 °C. On the basis of SiO generated, the yield of SiC is only about 5 % at 1300 °C, and up to 30% at 1400 °C. All the preliminary runs were made for qualitative purposes. Therefore, further quantitative studies are necessary to clarify this reaction.

BIBLIOGRAPHY

Aboaf, J.A., "Some Properties of Vapor Deposited Silicon Nitride Films Obtained by the Reaction of $SiBr_4$ and NH_3," *J. Electrochem. Soc.: Solid State Science*, **116**[12], 1736-1740(1969).

Allaire, F. and Dallaire, S., "Synthesis and Characterization of Silicon Nitride Powders Produced in a D.C. Thermal Plasma Reactor," *J. Mater. Sci.*, **26**[24], 6736-6740 (1991).

Allaire, F. and Langlois, R., "Factors influencing the crystallization of ultrafine plasma-synthesized silicon nitride as a single powder and in composite SiC-Si_3N_4 powder," *J. Mater. Sci.*, **27**[5], 1265-1270(1992).

Baraton, M.I., Labbe, J.C. and Quintard, P., "Vibrational Assignments of A Covalent Ceramic Material: Si_2ON_2," *J. Molecular Structure*, **79**, 333-336(1982).

Barsoum, M., Kangutar, P. and Koczak, M.J., "Nitridation Mechanisms of Silicon Powder Compacts," *Ceram. Eng. Sci. Proc.*, **10**[7-8], 794-806(1989).

Barsoum, M., Kangutar, P. and Koczak, M.J., "Nitridation Kinetics and Thermodynamics of Silicon Powder Compacts," *J. Am. Ceram. Soc.*, **74**[6], 1248-1253(1991).

Biernacki, J.J. and Wotzak, G.P., "Stoichiometry of the C + SiO_2 Reaction," *J. Am. Ceram. Soc.*, **72**[1], 122-129(1989).

Brady, G.W., "A Study of Amorphous SiO," *J. Phys. Chem.*, **63**[7], 1119-1120(1959).

Buljan, S.T., Baldoni, J.G., and Huckabee, M.L., "Si_3N_4-SiC Composites," *Am. Ceram. Soc. Bull.*, **66**[2], 347-352(1987).

ChemCad **3.0**, Chemstations, Inc., Houston, Texas, 1993.

Chen, L., Goto, T., and Hirai, T., "Infrared absorption of β-SiC particles prepared by chemical vapour deposition," *J. Mater. Sci.*, **25**[10], 4273-4278(1990).

Chu, C.Y. and Singh, J.P., "Mechanical Properties and Microstructure of Si_3N_4-Whisker-Reinforced Si_3N_4 Matrix Composites," *Ceram. Eng. Sci. Proc.*, **11**[7-8], 709-720(1990).

Cunningham, A.L. and Davies, L.G., "Preparation and Characterization of a Novel Form of Si_3N_4 Fiber," *15th Nat. SAMPLE Symp. Exhib.*, 209-217(1969).

Cussler, E.L., Chap. 5, p.106, in Diffusion, Cambridge University Press, New York, 1987.

DiGregoria, J.F. and Furtak, T.E., "Characterization of SiC whiskers through infrared absorption spectroscopy," *J. Appl. Phys.*, **73**[12], 8506-8513(1993).

Duncan, A.B.F. and Wilson, D.A., "Intermediate Products in the Thermal Decomposition of Ammonia," *J. Am. Chem. Soci.*, **54**[1], 401-402(1932).

Durham, B.G., Murtha, M.J., and Burnet, G., "Si_3N_4 by the Carbothermal Ammonolysis of Silica," *Adv. Ceram. Mater.*, **3**[1], 45-48(1988).

Durham, S.J.P., Shanker, K., and Drew, R.A.L., "Carbothermal Synthesis of Silicon Nitride: Effect of Reaction Conditions," *J. Am. Ceram. Soc.*, **74**[1], 31-37(1991).

Eriksson, G., "Thermodynamic Studies of High Temperature Equilibria," *Acta Chem. Scand.*, **25**, 2651-2658(1971).

Evans, R.B., Watson, G.M. and Mason, E.A., " Gaseous Diffusion in Porous Media at Uniform Pressure," *J. Chem. Phys.*, **35**[6], 2076-2083(1961).

Falk, M. and Karunanithy, S., "Determination of SiO2 in SiC Whiskers by Infrared Absorption Spectroscopy," *Mater. Sci. Eng.*, **A114**, 209-212(1989).

Gaviola, E. and Wood, R.W., "Photosensitized Band Fluorescence of OH, HgH, NH, H_2O, and NH_3 Molecules," *Phil Mag. Ser. 7*, **6**[XL], 1191-1210(1928).

Gazzara, C.P. and Messier, D.R., "Determination of Phase Content of Si_3N_4 by X-Ray Diffraction Analysis," *Am. Ceram. Bull.*, **56**[9], 777-780(1977).

Gleiter, H., "Nanocrystalline Materials," *Prog. Mater. Sci.*, **33**[4], 223-315(1989).

Harrison, R.H. and Kobe, K.A., "Thermodynamics of Ammonia Synthesis and Oxidation," *Chem. Eng. Prog.*, **49**[7], 349-353(1953).

Homeny, J. and Neergaard, L.J., "Mechanical Properties of β-Si_3N_4-Whisker/Si_3N_4 Matrix Composites," *J. Am. Ceram. Soc.*, **73**[11], 3493-3496(1990).

Hulthen, E. and Nakamura, S., "The Spectra of NH Compounds," *Nature*, **119**[2989], 235-236(1927).

Itoh, T., "Preparation of Pure α-Silicon Nitride from Silicon Powder," *J. Mater. Sci.*, **9**, 19-20(1990).

JANAF Tables, J. Phys. Chem. Ref. Data **14**, Suppl. 1, 1985.

Jovanovic, Z.R., Kimura, S. and Levenspiel, O., "Effects of Hydrogen and Temperature on the kinetics of the Fluidized-Bed Nitridation of Silicon," *J. Am. Ceram. Soc.*, **77**[1], 186-192(1994).

Jovanovic, Z.R. and S. Kimura, "Use of Two-Phase Standards of Unknown Compositions to Determine Calibration Constants for Powder XRD by Linear Regression," *J. Am. Ceram. Soc.*, **77**[8], 2226-2228(1994).

Karch, J., Birringer, R., and Gleiter, H., "Ceramics ductile at low temperature," *Nature*, **330**[6148], 556-557(1987).

Knacke, O., Kubaschewski, O. and Hesselmann, K., Thermochemical Properties of Inorganic Substances, 2nd Ed., Springer-Verlag, New York, 1991.

Knudsen, M., The Kinetic Theory of Gases, 3rd Ed., Methuen, London, 1950.

Kondo, S., Fujiwara, F., and Muroya, M., "The Effect of Heat-Treatment of Silica Gel at High Temperature," *J. Colloid and Interface Sci.*, **55**[2], 421-430(1976).

Krstic, V.D., "Production of Fine, High-purity Beta Silicon Carbide Powders," *J. Am. Ceram. Soc.*, **75**[1], 170-174(1992).

Kubaschewski, O. and Chart, T.G., "Silicon Monoxide Pressures due to the Reaction between Solid Silicon and Silica," *J. Chem. Thermodynamics*, **6**[5], 467-476 (1974).

Larson, R.S., "Kinetics of Silicon Nitride Chemical Vapor Deposition from Silicon Tetrafluoride and Ammonia," *J. Am. Ceram. Soc.*, **76**[8], 1930-1936(1993).

Lavin, G.I. and Bates, J.R., "The Ammonia Discharge Tube," *Proc. Nat. Acad. Sci.*, **16**[12], 804-808(1930).

Lee, W.Y., Strife, J.R. and Veltri, R.D., "Low-Pressure Chemical Vapor Deposition of α-Si_3N_4 from SiF_4 and NH_3: Nucleation and Growth Characteristics," *J. Am. Ceram. Soc.*, **75**[10], 2803-2808(1992).

Levenspiel, O., Chap. 3, pp.108-111, in Chemical Reaction Engineering, 2nd Ed., John Wiely Inc., New York, 1972.

Li, Y.L., Liang, Y., Zheng, F., and Hu, Z.Q., "Carbon Dioxide Laser Synthesis of Ultrafine Silicon Carbide Powders from Diethoxydimethysilane," *J. Am. Ceram. Soc.*, **77**[6], 1662-1664(1994).

Lin, D., "Gibbs Free Energy Minimization Method for High Temperature Equilibrium studies," *Class Report: CHE 505 (Reading and Conference)*, submitted to Dr. Shoichi Kimura, Chemical Engineering Department, Oregon State University, 1993.

Lin, S.C.H. and Joshi, M., "Structure of Silicon Monoxide," *J. Electrochem. Soc.: Solid State Science*, **116**[12], 1740-1742(1969).

Lin, S.S., "Mass Spectrometric Studies of the Nitridation of Silicon," *J. Am. Ceram. Soc.*, **58**[7-8], 271-273(1975).

Lundberg, R., Nyberg, B., Williander, K., Persson, M., and Carlsson, R., "Processing of whiskers-reinforced ceramics," *Composites*, **April**, 125-127(1987).

Luongo, J.P., "Infrared Characterization of α- and β-Crystalline Silicon Nitride," *J. Electrochem. Soc.: Solid-State Science and Technology*, **130**[7], 1560-1562(1983).

Mason, E.A. and Evans, R.B.III, "Graham's Laws: Simple Demonstrations of Gases in Motion; Part I, Theory," *J. Chem. Ed.*, **46**[6], 358-364(1969).

Messier, D.L. and Croft, W.J., "Silicon Nitride," p.131-191, in Preparation and Properties of Solid State Materials, vol. **7**, edited by W.R. Wilcox, Marcel Dekker, Inc., New York, 1982.

Morgan, P.E.D., "Structuring Chemical Technology to Produce Cost-Effective Ceramic Products on the Large Scale," *Am. Ceram. Soc. Bull.*, **72**[7], 65-70(1993).

Narayan, J., Ranghunathan, R., Chowdhury, R., and Jagannadham, K., "Mechanism of combustion synthesis of silicon carbide," J. Appl. Phys., **75**[11], 7252-7257 (1994).

Ono, K. and Kurachi, Y., "Kinetic studies on β-SiC formation from homogeneous precursors," *J. Mater. Sci.*, **26**, 388-392(1991).

Sasaki, Y., Nishina, Y., Sato, M., and Okamura, K., "Optical-phonon states of SiC small particles studied by Raman scattering and infrared absorption," *Phy. Rev. B*, **40**[3], 1762-1772(1989).

Schalch, D., Scharmann, A. and Wolfrat, R., "The Role of Hydrogen in Silicon Nitride and Silicon Oxynitride Films," *Thin Solid Films*, **124**[3-4], 301-308(1985).

Schalch, D., Scharmann, A. and Wolfrat, R., "IR Transmittance Studies of Hydrogen Free and Hydrogenated Silicon Nitride and Silicon Oxynitride Films Deposited by Reactive Sputtering," *Thin Solid Films*, **155**[2], 301-308(1987).

Sekine, M. and Katayama, S., "Preparation of Silicon Oxynitride Glass Fibers by Ammonolysis of Silica Gels," *J. Non-Crystalline Solids*, **134**[3], 199-207(1991).

Sheppard, L.M., "Cost-Effective Manufacturing of Advanced Ceramics," *Am. Ceram. Soc. Bull.*, **70**[4], 692-701(1991).

Shon, H. Y. and Szekely, J., "Reactions between Solids through Gaseous Intermediates-I: Reactions Controlled by Chemical Kinetics," *Chem. Eng. Sci.*, **28**, 1789-1801(1973).

Singh, J.P., Goretta, K.C., Kupperman, D.S., Routbort, J.L., and Rhodes, J.R., "Fracture Toughness and Strength of SiC-Whiskers-Reinforced Si_3N_4 Composites," *Adv. Ceram. Mater.*, **3**[4], 357-360(1988).

Sjöberg, J., Rundgren, K., Pompe, R. and Larsson, B., "Preparation of Si_2N_2O Based Sintered Bodies from Powders made by Nitridation of Amorphous Silica in Ammonia", pp.535-543, in High Tech. Ceramics, Edited by P. Vincenzini, Elsevier Science Publishers B.V., Amsterdam, 1987.

Tamhankar, S.S. and Doraiswamy, L.K., "Analysis of Solid-Solid Reactions: A Review," *J. AIChE*, **25**[4], 561-581(1979).

Toropov, N.A. and Barzakovskii, V.P., Chap. VII, pp.115-140, in High-Temperature Chemistry of Silicates and Other Oxide Systems, Translated by C.N. Turton and T.I. Turton, Consultants Bureau, New York, 1966.

Urretavizcaya, G., and Porto López, J.M., "Growth of SiC whiskers by VLS process," *J. Mater. Res.*, **9**[11], 2981-2986(1994).

van Weeren, R., Carrasquillo, G., Leone, E., Curran, S., and Danforth, S.C., "Laser Synthesized Silicon Nitride Powder: Chemical and Physical Characteristics," *Proceedings of the Symposium on Silicon-Based Structural Ceramics*, PACRIM Meeting, Honolulu, HI, Nov. 7-10, 47-54(1993).

Wada, N., Solin, S.A., Wong, J. and Prochazka, S., "Raman and IR Absorption Spectroscopic Studies on α, β, and Amorphous Si_3N_4," *J. Non-Crystalline Solids*, **43**[1], 7-15(1981).

Weimer, A.W., Nilsen, K.J., Cochran, G.A., and Roach, R.P., "Kinetics of Carbothermal Reduction Synthesis of Beta Silicon Carbide," *J. AIChE*, **39**[3], 493-503(1993).

Wild, S., Grieveson, P., and Jack, K.H., p.385, in Special Ceramics, vol. **5**, British Ceramic Research Association, 1972.

Winslow, S.G., "Silicon Nitride Powder," *Am. Ceram. Soc. Bull.*, **72**[4], 99-103(1993).

Yamada, T., "Preparation and Evaluation of Sinterable Silicon Nitride Powder by Imide Decomposition Method," *Am. Ceram. Soc. Bull.*, **72**[5], 99-106(1993).

APPENDICES

APPENDIX A

The following program, GIBBS, is derived for the equilibrium calculations of any arbitrary multi-phase reaction system. The program is written in Fortran language, in which the concept and procedure follow the work by Eriksson [1971]. Detailed instructions of using this program have been given in the class report [Lin, 1993].

```
CCCCCCCCCCCCCCCCCCCCCCCCCCCCCCCCCCCCCCCCCCCCCCCCCCCCCCCCCCCCCCCCCCCC
CCCCCCCCCCCCCCCCCCCCCCCCCCCCCCCCCCCCCCCCCCCCCCCCCCCCCCCCCCCCCCCCCCCC
CCCC                                                              CCCC
CCCC                    PROGRAM  NAME : GIBBS                     CCCC
CCCC                                                              CCCC
CCCCCCCCCCCCCCCCCCCCCCCCCCCCCCCCCCCCCCCCCCCCCCCCCCCCCCCCCCCCCCCCCCCC
CCCCCCCCCCCCCCCCCCCCCCCCCCCCCCCCCCCCCCCCCCCCCCCCCCCCCCCCCCCCCCCCCCCC
C
C
      DOUBLE PRECISION A,B,F,W,X,Y,G,C,ERR,TRX,GIBBS,RATIO,FORM,EQ,
     &                 ELEM,REAC,COMP,TOLERR,ADD1,ADD2,CONT
      DIMENSION A(50,20),B(20),F(50),W(20),X(50),Y(50),G(50),C(50,2),
     &          TRX(50,50),ERR(50),FORM(50,2),EQ(2,12),ELEM(20),
     &          REAC(30,2),COMP(30),NELI(50)
      OPEN (UNIT=1,FILE='RESULT.01',STATUS='UNKNOWN')
      OPEN (UNIT=2,FILE='RESULT.02',STATUS='UNKNOWN')
      OPEN (UNIT=3,FILE='RESULT.03',STATUS='UNKNOWN')
      OPEN (UNIT=4,FILE='RESULT.04',STATUS='UNKNOWN')
      OPEN (UNIT=5,FILE='RESULT.05',STATUS='UNKNOWN')
      OPEN (UNIT=6,FILE='RESULT.06',STATUS='UNKNOWN')
      OPEN (UNIT=7,FILE='RESULT.07',STATUS='UNKNOWN')
      OPEN (UNIT=8,FILE='RESULT.08',STATUS='UNKNOWN')
      OPEN (UNIT=9,FILE='RESULT.09',STATUS='UNKNOWN')
      OPEN (UNIT=10,FILE='INPUT.DAT',STATUS='OLD')
      OPEN (UNIT=11,FILE='MATRIX.DAT',STATUS='UNKNOWN')
C
C
      NDATA=1
      WRITE(*,1)
 1    FORMAT(24(/))
      WRITE(*,*)'-------------------------------------------------',
     &'-------'
      WRITE(*,*)' '
```

```
      WRITE(*,*)'    This computer program is used for a (i) pure gas ',
     &'phase, '
      WRITE(*,*)'or (ii) gas + immiscible liquid + solid phases system.'
      WRITE(*,*)' '
      WRITE(*,*)'-------------------------------------------------',
     &'-------'
      WRITE(*,*)' '
      WRITE(*,*)'*****  Case (i) a pure gas phase ---->  Enter "1" '
      WRITE(*,*)'  *****  Case (ii) multiple phases ---->  Enter "2" '
      READ(*,*)NCASE
      WRITE(*,1)
      WRITE(*,*)' ----->  Please key in your reaction equation.'
      DO 2 I=1,2
2         READ(*,3)(EQ(I,J),J=1,12)
3     FORMAT(12A5)
      WRITE(*,1)
4     WRITE(*,*)'---> How many components are present in the system ?'
      READ(*,*)NT
      WRITE(*,1)
      WRITE(*,*)'---> How many elements are present in the system ?'
      READ(*,*)NE
      IF(NCASE.EQ.1)NP=NCASE
      IF(NCASE.EQ.1)N=NT
      IF(NCASE.EQ.1) GO TO 5
      WRITE(*,1)
      WRITE(*,*)'----> How many phases are present in the system ?'
      READ(*,*)NP
5     NGIBB=NT-NP
      IF(NGIBB.GE.0)GO TO 10
      WRITE(*,*)'----> Sorry!! Your system is against Gibbs phase rule.'
      WRITE(*,*)'  ****  F=C+2-Ph. ---->  Please check it !!!!  ****'
      GO TO 999
10    IF(NCASE.EQ.1)GO TO 11
      WRITE(*,1)
      WRITE(*,*)'---->  Is there a gas phase in the system ?'
      WRITE(*,*)' '
      WRITE(*,*)'       *****  Enter "1"  ---->  Yes '
      WRITE(*,*)'             *****  Enter "2"  ---->  No '
      READ(*,*)N1
      NG=0
      IF(N1.EQ.2)GO TO 12
      WRITE(*,1)
      WRITE(*,*)'----> How many components are in the gas phase ?'
      READ(*,*)N
      WRITE(*,1)
11      NG=1
```

```
12     NS=NP-NG
       WRITE(*,13)NG,NS
13     FORMAT('----> Totally, there are ',I1,' gas phase and ',I2,
      &' solid phase(s) in the system.'//7X,'**** Is this brief concl',
      &'usion correct?  Enter "1" = Yes',/13X,'****  Otherwise, enter',
      &' "2" = No  ')
       READ(*,*)N2
       IF(N2.EQ.1)GO TO 14
       WRITE(*,1)
       WRITE(*,*)'----> Do you want to start from the beginning?'
       WRITE(*,*)' '
       WRITE(*,*)'      *** "1" = Yes ----> Start from the beginning.'
       WRITE(*,*)'        *** "2" = No ----> Exit the current program.'
       READ(*,*)N21
       IF(N21.EQ.1)GO TO 4
       GO TO 999
14     WRITE(*,1)
       WRITE(*,*)'---->  You have two choices to key in your data. '
       WRITE(*,*)' '
       WRITE(*,*)'    ***  From terminal ----> Enter "1" '
       WRITE(*,*)'         ***  From data file (name:INPUT.DAT) ---->',
      &' Enter "2" '
          READ(*,*)NINP
          IF(NINP.EQ.1)GO TO 21
       WRITE(*,1)
       WRITE(*,*)'----> Is your data file (INPUT.DAT) ready in C-drive ?'
       WRITE(*,*)' '
       WRITE(*,*)'      ****  Enter "1" = Yes'
       WRITE(*,*)'           ****  Enter "2" = No '
          READ(*,*)N23
          IF(N23.EQ.2)GO TO 999
       WRITE(*,1)
       WRITE(*,15)
15     FORMAT(//,15X,'***  Please note the format in your data file. ***',
      &//,'----> Before computer starts to read your data file, please',
      &' make sure that',/' the data file is in the right format.',//
      &5X,'****  Data are in right format ----> Enter "1" ',/9X,'****',
      &'  Enter "2" ----> Exiting the program.')
          READ(*,*)N24
          IF(N24.EQ.2) GO TO 999
       READ(10,*)P,TEMP
       DO 16 I=1,NT
         READ(10,17)FORM(I,1),FORM(I,2)
16       READ(10,*)C(I,1),C(I,2)
17       FORMAT(2A5)
       DO 20 I=1,NT
```

```
20        READ(10,*)(A(I,J), J=1,NE)
     GO TO 31
21   WRITE(*,1)
     WRITE(*,*)'-----> Please input the system pressure (atm).'
     READ(*,*)P
     WRITE(*,1)
     WRITE(*,*)'-----> Please input the system temperature (K).'
     READ(*,*)TEMP
     WRITE(*,22)
22   FORMAT(26(/),'*****  Please input C1 (J/mole-K) & C2 (J/mole) val',
    &'ues for each component.'/)
     WRITE(*,*)'          ----> Data could be obtained from JANAF',
    & ' table  <---- '
     WRITE(*,*)' '
     WRITE(*,*)'*****  Please start from gas phase and remember',
    & ' the sequence number of '
     WRITE(*,*)'       each component !!!!'
     DO 26 I=1,NT
       WRITE(*,23)I
23     FORMAT(/,'    ----> Please enter the formula for component # ',
    &          I2)
       READ(*,24)FORM(I,1),FORM(I,2)
24     FORMAT(2A5)
       WRITE(*,25)I
25     FORMAT(/,'         ----> C1 and C2 values for component # ',I2)
       READ(*,*)C(I,1),C(I,2)
26     WRITE(*,1)
     WRITE(*,1)
     WRITE(*,*)'----> Is there any mistake when you input C1 & C2',
    &' values for each component ?'
     WRITE(*,*)'     *****  No mistake ----> Please enter "1" '
     WRITE(*,*)'         *****  Need to correct input ----> Please',
    &          ' enter "2" '
     READ(*,*)N3
     IF(N3.EQ.1)GO TO 31
     WRITE(*,1)
     WRITE(*,*)'----> How many components need to be corrected ?'
     READ(*,*)NC
     WRITE(*,*)' '
     DO 30 I=1,NC
     WRITE(*,1)
     WRITE(*,*)'----> Please enter the sequence number of component i.'
     READ(*,*)NI
     WRITE(*,*)' '
     WRITE(*,*)'----> Please input new C1 & C2 values for this',
    &' component.'
```

```
      READ(*,*)C(NI,1),C(NI,2)
30    WRITE(*,1)
31    WRITE(*,1)
      WRITE(*,*)'****  Please key in the initial mole(s) of each ele',
     &'ment in the system,'
      WRITE(*,*)'      and also remember the sequence number of each',
     &' element.'
      DO 34 I=1,NE
      WRITE(*,32)I
32    FORMAT(/3X,'---->  Please key in the formula of element # ',I2,
     &       '.')
      READ(*,33)ELEM(I)
33    FORMAT(A2)
      WRITE(*,36)I
36    FORMAT(/7X,'----> Initial mole(s) of this element b-',I2,' = ?')
      READ(*,*)B(I)
34    WRITE(*,1)
      WRITE(*,*)' ****  No mistake on your input  ----> Enter "1" '
      WRITE(*,*)' '
      WRITE(*,*)'       ****  Need to correct ----> Enter "2" '
      READ(*,*)N4
      IF (N4.EQ.2)GO TO 31
35    WRITE(*,1)
      WRITE(*,40)
40    FORMAT(//,5X,'According to your initial mole(s) of each element',
     &', please enter',/' the initial mole(s) of reactant component.'//,
     &'-----> How many reactant components are in your system ?')
      READ(*,*)NR
      WRITE(*,*)' '
      DO 43 I=1,NR
        WRITE(*,41)I
41      FORMAT(/'-----> Please enter the formula of reactant compo',
     &          'nent # ',I2)
        READ(*,42)REAC(I,1),REAC(I,2)
42      FORMAT(2A5)
        WRITE(*,*)' '
        WRITE(*,*)'    ----> Initial mole of this reactant compo',
     &          'nent = ?'
        READ(*,*)COMP(I)
43      WRITE(*,1)
      WRITE(*,44)
44    FORMAT(//'----> Any mistake for your inputs ?'//10X,'*****  No ',
     &'mistake ----> Enter "1" '/15X,'*****  Need to correct',
     &' ----> Enter "2" '//)
      READ(*,*)N5
      IF(N5.EQ.2)GO TO 35
```

```
      WRITE(*,1)
      WRITE(*,*)'----> Please key in your initial guess for component',
     &          ' i.'
      WRITE(*,*)'          **********  Only gas phase **********'
      WRITE(*,*)' '
      DO 46 I=1,N
      WRITE(*,*)' '
      WRITE(*,45)I
 45   FORMAT(/5X,3('*'),' component # ',I2,' : initial guess = ?')
 46   READ(*,*)Y(I)
C
C
      CALL AMTRX(A,NE,NT,NINP)
C
      WRITE(*,1)
      LK=0
      WRITE(*,50)
 50    FORMAT(//,'      Before computer starts to run your program,',
     & ' please enter the required'/,'  accuracy for your results.',/)
      WRITE(*,*)'-----> Tolerable Error less than or equal to  ?'
      READ(*,*)TOLERR
C
 51    CALL SETMX(A,B,F,Y,G,C,TRX,NE,N,NT,NN,P,TEMP,NCASE)
      CALL GUASS(TRX,NN)
      CALL SOLVE(TRX,W,ERR,A,F,X,Y,NN,NT,N,NE,NTEST,NELI,TOLERR)
C
     IF(NTEST.EQ.N)GO TO 57
       LK=LK+1
       NOUT=0
     DO 52 I=N+1,NT
       NUM=I
       IF(NELI(I).EQ.LK.AND.NELI(I).EQ.1000)NOUT=777
       IF(NELI(I).EQ.LK.AND.NELI(I).EQ.1000)GO TO 57
 52   CONTINUE
       DO 53 I=N+1,NT
         IF(X(I).LT.0.)GO TO 54
 53     CONTINUE
     GO TO 56
 54     NNEGA=N+1
       DO 55 I=N+2,NT
         IF(NELI(I).GT.NELI(NNEGA))NNEGA=I
         NOUT=777
         NUM=NNEGA
 55    CONTINUE
 56   IF(LK.EQ.10000)GO TO 57
     GO TO 51
```

```
57   WRITE(*,60)LK
60   FORMAT(19X,'****  Iteration = ',I5,' (times)  ****')
     GIBBS=0.
     DO 61 I=1,NE
61      GIBBS=GIBBS+W(I)*B(I)
     WRITE(*,*)' '
     DO 62 I=1,NE
62      WRITE(NDATA,63)I,ELEM(I),B(I)
63      FORMAT(/8X,'Initial atom-mole of element #',I2,' (',A2,
    &          ') = ',F11.5,' mole(s)')
     WRITE(NDATA,*)' '
     WRITE(NDATA,64)TEMP,P
64   FORMAT(/,5X,67('-')/15X,5('*'),8X,'Temperature = ',F7.2,' (K)',
    &9X,5('*')//,18X,5('*'),5X,'Pressure =',F10.2,' (atm)',5X,5('*'),
    &/5X,67('-'))
     WRITE(NDATA,65)(EQ(1,J),J=1,12)
65   FORMAT(//,5X,'Reaction : ',12A5)
     WRITE(NDATA,66)(EQ(2,J),J=1,12)
66   FORMAT(20X,12A5//)
     DO 70 I=1,NR
70    WRITE(NDATA,71)REAC(I,1),REAC(I,2),COMP(I)
71    FORMAT(13X,' Initial mole(s) of ',A5,A5,'= ',F11.5,' mole(s)'/)
     WRITE(NDATA,72)LK
72   FORMAT(/19X,'---->  Iteration = ',I5,' (times)  <----'///,
    &5X,3('#'),2X,'At equilibrium conditions, final results are',
    &' as follows:',2X,3('#')/)
     IF(NOUT.EQ.777)GO TO 73
     GO TO 80
73   WRITE(NDATA,74)NUM,FORM(NUM,1),FORM(NUM,2)
74   FORMAT(/24X,'***  Warning !!!!  ***'//,5X,'----> Component #',I2,
    &' ( ',2A5,') shall be eliminated from your system.',//,18X,'****',
    &' It becomes more and more negative !!! ****'//)
     WRITE(*,*)'                    ****  Warning !!!!  ****'
     WRITE(*,*)' '
     WRITE(*,*)' '
     WRITE(*,75)NUM,NDATA
75   FORMAT(5X,'---> Component # ',I2,' shall be eliminated from',
    &' your system.',/15X,'---> It becomes more and more negative',
    &' !!! <----'//'*****  Please eliminate this component and ',
    &'try it again. Good Luck  !!!!  *****'//7X,'----> The results ',
    &'in the " RESULT.0',I1,' " are not correct. <----'/////)
80   DO 81 I=1,NT
81      WRITE(NDATA,82)I,FORM(I,1),FORM(I,2),X(I)
82      FORMAT(/9X,'*** mole(s) of component # ',I2,' : ',2A5,
    &          ' = ',F15.9)
     WRITE(NDATA,83)GIBBS
```

```
 83   FORMAT(///6X,6('#'),5X,'Total dimensionless G/RT = ',F15.8,5X,
     &6('#'))
      IF(NOUT.EQ.777)GO TO 999
      WRITE(*,84)NDATA
 84   FORMAT('      ***** Your results are saved in the " RESULT.0',
     &I1,' " data file. *****')
      WRITE(*,85)
 85   FORMAT(////,13X,'----> Please hit " ENTER " key to continue',
     &' !!!! <----')
      READ(*,86)CONT
 86   FORMAT(A5)
      WRITE(*,1)
      WRITE(*,87)
 87   FORMAT(10(/),3X,'---->    Do you want to change the molar-ratio',
     &' of reactants and <----'/10X,'recalculate the equilibrium com',
     &'positions ?',///3X,'***** Please enter "1" ----> Yes'/10X,
     &'***** Otherwise, please enter "2" ----> No'//)
      READ(*,*)NAD1
      IF(NAD1.EQ.2)GO TO 88
      NDATA=NDATA+1
      GO TO 31
 88   WRITE(*,1)
      WRITE(*,90)
 90   FORMAT(10(/),' ---->      Do you want to add some possible',
     &' condensed products into <----'/7X,' the current system ? '//,
     &' **** Please enter "1" ----> Yes'/'      **** Otherwise,',
     &' enter "2" ----> No'//)
      READ(*,*)NAD2
      IF(NAD2.EQ.2)GO TO 97
C
 91   CALL TESTNEW(A,NT,NE,W,TEMP,NRECAL,FORM,C)
C
      WRITE(*,1)
      IF(NRECAL.EQ.555)GO TO 92
      GO TO 95
 92   WRITE(*,93)FORM(NT+1,1),FORM(NT+1,2)
 93   FORMAT('****      According to the previous results, do you',
     &' want to add ',2A5,'****'/5X,'into the system and recalculate',
     &' the equilibrium compositions ?'//10X,'**** Please enter "1" ',
     &' ----> Yes'/14X,'**** Please enter "2" ----> No')
      READ(*,*)NAD3
      IF(NAD3.EQ.2)GO TO 95
      NT=NT+1
      NDATA=NDATA+1
      WRITE(*,1)
      WRITE(*,*)' -----> Please key in your new reaction equation.'
```

```
      DO 94 I=1,2
 94         READ(*,941)(EQ(I,J),J=1,12)
 941        FORMAT(12A5)
      LK=0
      GO TO 51
 95   WRITE(*,1)
      WRITE(*,96)
 96   FORMAT('    ----> Do you still want to test another condensed',
     &' product ? <----'///11X,'****  Please enter "1" ----> Yes'/,
     &14X,' ****  Please enter "2" ----> No')
      READ(*,*)NAD4
      IF(NAD4.EQ.1)GO TO 91
 97   WRITE(*,98)
 98   FORMAT(////)
 999  STOP
      END
C
C
C
C
      SUBROUTINE AMTRX(A,NE,NT,NINP)
      DOUBLE PRECISION A
      DIMENSION A(50,20)
C
      IF(NINP.EQ.2)GO TO 130
      WRITE(*,888)
      WRITE(*,*)'*** Please recall the sequence numbers of each',
     &' element and component.'
      WRITE(*,*)' '
      WRITE(*,*)'*** Define Aij: number of atoms of the j-th element',
     &' in the i-th component.'
      WRITE(*,*)'*** You have to input #(element) x #(component) Aij',
     &' values.'
      WRITE(*,*)' '
      DO 100 I=1,NT
        WRITE(*,110)NE,I,I,I,NE
 110    FORMAT(/5X,'*** number of atoms of 1-th to ',I2,'-th element',
     &       ' in # ',I2,' component :'/,20X,' A(',I2,', 1) ----> A(',
     &       I2,',',I2,')')
      READ(*,*)(A(I,J),J=1,NE)
 100  WRITE(*,888)
      WRITE(*,105)
 105  FORMAT(10X,'----> Do you need to correct your Aij inputs ? <---',
     &'-'//17X,'****  No mistake ---> Enter  "1" ',/,21X,'****  Need ',
     &'to correct ---> Entern "2" ')
      READ(*,*)N4
```

```
      WRITE(*,888)
  888 FORMAT(24(/))
      IF(N4.EQ.1)GO TO 130
  120 WRITE(*,*)'*** Please enter i & j values for Aij which will',
     &' be corrected.'
      READ(*,*)IK,JK
      WRITE(*,*)'*** Please input correct value for this Aij.'
      READ(*,*)A(IK,JK)
      WRITE(*,*)'All done ?  Yes ---> Enter "1"  ;  No ---> Enter "2" '
      READ(*,*)N5
      IF(N5.EQ.1)GO TO 130
      GO TO 120
  130 WRITE(11,135)
  135 FORMAT(5X,70('#')//16X,3('*'),5X,'The A(i,j) matrix is as',
     &' follows:',5X,3('*'),//5X,70('#')/)
      DO 140 I=1,NT
  140       WRITE(11,150)(A(I,J),J=1,NE)
  150       FORMAT(/,5X,'   ***',20(3X,F4.1),'   ***')
      WRITE(11,160)
  160 FORMAT(/)
      RETURN
      END
C
C
C
C
      SUBROUTINE SETMX(A,B,F,Y,G,C,TRX,NE,N,NT,NN,P,TEMP,NCASE)
      DOUBLE PRECISION A,B,F,Y,G,C,TRX,TOTY,TP,TF,TK,TS,SS
      DIMENSION A(50,20),B(20),F(50),D(20),Y(50),G(50),C(50,2),
     &          TRX(50,50)
C
        DO 200 I=1,NT
  200       G(I)=C(I,1)/8.314+C(I,2)/(8.314*TEMP)
      TOTY=0.0
        DO 210 I=1,N
  210       TOTY=TOTY+Y(I)
        DO 220 I=1,N
  220       F(I)=Y(I)*(G(I)+DLOG(P*Y(I)/TOTY))
      NN=NE+NT-N+2
        DO 230 I=1,NN-1
          DO 230 J=1,NN
  230         TRX(I,J)=0.0
      IF(NCASE.EQ.1)GO TO 245
        DO 240 I=1,NT-N
          DO 240 J=1,NE
            TRX(I,J)=A(N+I,J)
```

```
240           TRX(I,NN)=G(N+I)
245       DO 250 I=1,NE
            TF=0.0
            TK=0.0
            DO 260 J=1,N
              TK=TK+A(J,I)*Y(J)
260            TF=TF+F(J)
            TRX(NT-N+1,I)=TK
250          TRX(NT-N+1,NN)=TF
          DO 270 I=1,NE
            TP=0.0
            DO 280 J=1,N
280           TP=TP+A(J,I)*Y(J)
270         D(I)=TP-B(I)
          DO 290 J=1,NE
            JJ=NT-N+J+1
            TK=0.0
            TF=0.0
            DO 300 K=1,NE
              TS=0.0
              DO 293 L=1,N
293             TS=TS+A(L,J)*A(L,K)*Y(L)
300             TRX(JJ,K)=TS
            DO 310 I=1,N
              TK=TK+Y(I)*A(I,J)
310            TF=TF+F(I)*A(I,J)
          TRX(JJ,NE+1)=TK
          TRX(JJ,NN)=TF-D(J)+TK
          IF(NCASE.EQ.1)GO TO 290
            DO 320 M=1,NT-N
320           TRX(JJ,NE+M+1)=A(N+M,J)
290       CONTINUE
      DO 350 I=1,NN-2
        NJ=I
        JK=I
330          JK=JK+1
          IF(JK.EQ.NN)GO TO 340
          IF(ABS(TRX(JK,I)).GT.ABS(TRX(NJ,I)))NJ=JK
          GO TO 330
340           DO 360 J=1,NN
                SS=TRX(I,J)
                TRX(I,J)=TRX(NJ,J)
360              TRX(NJ,J)=SS
350   CONTINUE
      RETURN
      END
```

```
C
C
C
C
      SUBROUTINE GUASS(TRX,NN)
      DOUBLE PRECISION TRX,RATIO
      DIMENSION TRX(50,50)
C
      DO 400 I=1,NN-2
        DO 400 J=I+1,NN-1
          TRX(J,NN)=TRX(J,NN)-TRX(I,NN)*TRX(J,I)/TRX(I,I)
        RATIO=TRX(J,I)/TRX(I,I)
          DO 400 K=1,NN-1
 400        TRX(J,K)=TRX(J,K)-TRX(I,K)*RATIO
      WRITE(*,*)' '
      DO 410 I=NN-1,2,-1
        DO 410 J=I-1,1,-1
          TRX(J,NN)=TRX(J,NN)-TRX(I,NN)*TRX(J,I)/TRX(I,I)
          DO 410 K=1,NN-1
 410          TRX(J,K)=TRX(J,K)-TRX(I,K)*TRX(J,I)/TRX(I,I)
      RETURN
      END
C
C
C
C
      SUBROUTINE SOLVE(TRX,W,ERR,A,F,X,Y,NN,NT,N,NE,NTEST,NELI,
     &            TOLERR)
      DOUBLE PRECISION TRX,W,ERR,X,Y,TOTWA,A,F,TOLERR
      DIMENSION TRX(50,50),ERR(50),A(50,20),W(20),F(50),X(50),Y(50),
     &        XY(50),NELI(50)
C
      DO 500 I=1,NE+1
 500      W(I)=TRX(I,NN)/TRX(I,I)
      DO 510 K=1,NT-N
        L=N+K
        J=NE+K+1
        X(L)=TRX(J,NN)/TRX(J,J)
        IF(X(L).LT.0.AND.ABS(X(L)).GT.XY(L))NELI(L)=NELI(L)+1
 510    XY(L)=X(L)
      L=0
      J=0
      DO 520 I=1,N
        TOTWA=0.0
        DO 530 J=1,NE
 530      TOTWA=TOTWA+A(I,J)*W(J)
```

```
520         X(I)=-F(I)+Y(I)*(W(NE+1)+TOTWA)
      DO 540 I=1,N
        ERR(I)=ABS((X(I)-Y(I))/Y(I))
        Y(I)=X(I)
540     IF(X(I).EQ.0.0.OR.X(I).LT.0.0)Y(I)=0.00000000000000001
      NTEST=0
      DO 550 I=1,N
550     IF(ERR(I).LE.TOLERR)NTEST=NTEST+1
      RETURN
      END
C
C
C
C
      SUBROUTINE TESTNEW(A,NT,NE,W,TEMP,NRECAL,FORM,C)
      DOUBLE PRECISION A,W,MU,SUMNEW,FORM,C
      DIMENSION A(50,20),W(20),B(20),FORM(50,2),C(50,2)
C
      NEWT=NT+1
      WRITE(*,620)
      WRITE(*,*)'      ----> New Compound Name = ?'
      READ(*,605)FORM(NEWT,1),FORM(NEWT,2)
605   FORMAT(2A5)
      WRITE(*,620)
      WRITE(*,610)
610   FORMAT(////,' ****      Please key in the C1 (J/mole-K) and C2',
     &' (J/mole) values ****'/'      of the condensed component ',
     &'which you want to add.'//)
      READ(*,*)C(NEWT,1),C(NEWT,2)
      WRITE(*,620)
620   FORMAT(24(/))
      NEWT=NT+1
      WRITE(*,625)NEWT,NEWT,NE
625   FORMAT(3X,'----> Please enter the Aij values of this new compon',
     &'ents. <----'//15X'****  A(',I2,', 1 ) ----> A(',I2,' , ',I2,')',
     &' = ?')
      READ(*,*)(A(NEWT,I),I=1,NE)
      WRITE(*,620)
      MU=C(NEWT,1)/8.314+C(NEWT,2)/(8.314*TEMP)
      SUMNEW=0.0
        DO 630 I=1,NE
          SUMNEW=SUMNEW+A(NEWT,I)*W(I)
630   CONTINUE
      NRECAL=0
      IF(MU.LT.SUMNEW)GO TO 650
      WRITE(*,640)FORM(NEWT,1),FORM(NEWT,2)
```

```
640  FORMAT(' ----> The condensed component ( ',2A5,') you are ',
     &'currently considering  <----'/5X,'should not be added into',
     &' the system.')
      GO TO 670
650  WRITE(*,660)FORM(NEWT,1),FORM(NEWT,2)
660  FORMAT(' ----> The condensed component ( ',2A5,') you are ',
     &'currently considering  <----'/5X,'should be added into the',
     &' system.')
      NRECAL=555
670  WRITE(*,665)
665  FORMAT(///,13X,'----> Please hit " ENTER " key to continue',
     &' !!!!  <----')
      READ(*,675)CONT
675  FORMAT(A5)
      RETURN
      END
```

APPENDIX B

The following program is written in Fortran language. The integral term and rate constant *k* shown in Table 4.7 (page 67) was calculated by this program.

```
      DOUBLE PRECISION PM,DX,F1,F2,AREA,C,X,CK
      DIMENSION TEMP(7),P(7),FA0(7),XF(7),C(7),CK(7)
      OPEN (UNIT=1,FILE='K.01',STATUS='UNKNOWN')
      OPEN (UNIT=2,FILE='DATA',STATUS='OLD')
      DO 5 I=1,5
5     READ(2,*)TEMP(I),P(I),FA0(I),XF(I)
      PM=1./3.
40    DO 10 I=1,5
      DX=XF(I)/10.0
      AREA=0.
      X=0.0
      DO 20 K=1,10
            F1=((1+X)/(1-X))**PM
            F2=((1+(X+DX))/(1-(X+DX)))**PM
            AREA=AREA+(F1+F2)*DX/2.0
        X=K*DX
20    CONTINUE
      WRITE(1,*)'TEMP = ',TEMP(I),'      Area = ',AREA
      C(I)=P(I)/(14.7*82.05*(TEMP(I)+273))
      WRITE(1,*)' '
      WRITE(1,*)'CAO =    ',C(I)
10    CK(I)=FA0(I)*AREA*1.238/(298*82.05)/(7.51712*C(I)**PM)*10000./60.
      WRITE(1,*)' '
      WRITE(1,30)PM,(CK(I),I=1,5)
30    FORMAT(//5X,'*****  Power = ',F7.4,'  *****'/'---> K values = ',
     &2(E15.10,3X)/2(2X,E15.10)/3(2X,E15.10))
999   STOP
      END
```

APPENDIX C

On the basis of Equations (4.11) and (4.13), the following program has been used to estimate the remaining amount of NH_3 at the outlet of Al_2O_3 feeder. The molar ratios of NH_3/SiO, shown in Table 4.10 on page 74, are also calculated by this program.

```
      DOUBLE PRECISION F1,F2,A,CK,VOL,TERML,AREA
      DIMENSION A(1000)
      WRITE(*,*)'---->  Heating Length ? (in inch)'
      READ(*,*)CL
      WRITE(*,*)'---->  Reaction Temperature ? (in C)'
      READ(*,*)TEMP
      WRITE(*,*)'---->  System Pressure ? (in psi)'
      READ(*,*)PI
      WRITE(*,*)'---->  Volume Expansion Factor ? (= 1 for pure NH3)'
      READ(*,*)EA
      WRITE(*,*)'---->  Ammonia Inlet Flow Rate ? (in cc/min)'
      READ(*,*)FAO
      WRITE(*,*)'---->  SiO Generation Rate ? (in g/min)'
      READ(*,*)SIO
      DX=0.001
      P=PI/14.7
      X=0.0
      DO 10 I=1,1000
            F1=((1.+EA*X)/(1-X))**(1./3.)
            F2=((1.+EA*(X+DX))/(1-X-DX))**(1./3.)
            A(I)=(F1+F2)*DX/2.0
            X=X+DX
10     CONTINUE
      CK=5.236E10*EXP(-278000/8.314/(TEMP+273.0))
      CAO=P/(8.205E-5*(273.+TEMP))
      VOL=0.123312*CL*2.54/1.0E6
      TERML=CK*VOL*CAO**(1./3.)/(FAO/60.0*P/(82.05*298))
      AREA=0.0
      K=1
20      AREA=AREA+A(K)
       IF(AREA.GE.TERML)GO TO 30
        K=K+1
      GO TO 20
```

```
30     XAF=DX*K
       IF(XAF.GE.1.0)XAF=1.0
       FAF=FAO*(1.-XAF)
       AMO=FAF*P/(82.05*298.)
       RATIO=AMO*44.0855/SIO
       WRITE(*,*)' '
       WRITE(*,*)' '
       WRITE(*,*)'---->  Rate constant (k) at this temperature = ', CK
       WRITE(*,*)' '
       WRITE(*,*)'---->  Final conversion XA = ',XAF
       WRITE(*,*)' '
       WRITE(*,*)'---->  Ammonia left (cc/min) = ',FAF
       WRITE(*,*)' '
       WRITE(*,*)'---->  Molar Ratio (NH3/SiO) = ', RATIO
       WRITE(*,*)' '
       STOP
       END
```